

**DESIGN AND SYNTHESIS OF HIV-1 PROTEASE INHIBITORS
FEATURING A BICYCLIC HEXAHYDROPYRROLOFURAN SCAFFOLD**

by

Joseph D. Bungard

A Dissertation

Submitted to the Faculty of Purdue University

In Partial Fulfillment of the Requirements for the degree of

Doctor of Philosophy



Department of Chemistry

West Lafayette, Indiana

May 2020

THE PURDUE UNIVERSITY GRADUATE SCHOOL
STATEMENT OF COMMITTEE APPROVAL

Dr. Arun K. Ghosh, Chair

Department of Chemistry

Dr. Christopher Uyeda

Department of Chemistry

Dr. Kavita Shah

Department of Chemistry

Dr. Elizabeth Parkinson

Department of Chemistry

Approved by:

Dr. Christine Hrycyna

Dedicated to my family, friends, Stella, and Riley for their love and endless support.

ACKNOWLEDGMENTS

First, and foremost, I would like to sincerely thank Professor Arun K. Ghosh for his mentorship and guidance throughout my career at Purdue University. His enthusiasm and dedication towards chemistry has developed an exceptional lab environment to continually grow as a scientist. I am grateful to have had the opportunity to learn under such a brilliant mind and hope to utilize these experiences to help others grow in the field of science as well.

I would like to thank my committee members, Professor Chris Uyeda, Professor Kavita Shah, and Professor Elizabeth Parkinson for their time, support, and guidance throughout my graduate school career. Additionally, I would like to thank the Department of Chemistry at Purdue for a supportive environment and the Prep Lab Staff for their help in teaching the Undergraduates.

To my mentors, Dr. Luke Kassekert and Dr. Anthony Tomaine, I sincerely appreciate your time, constructive interaction, and assistance during my graduate school career. To my current colleagues, Amartyo Basu, Daniel Lee, Josh Born, Miranda Belcher, Hannah Simpson, Monika Yadav, Jennifer Mishevich, Abhijith Anil Kumar, Will Robinson, John Gulliver, Abdulkhaliq Alawaed, Caesar Gomez, Dr. Satish Kovala, Dr. Zilei Xia, Dr. Raghavaiah Jakka, Dr. Srinivasa Rao Allu, Dr. Shivaji Markad, Dr. Dana Shahabi, Dr. Jingei Yang, and Dr. Che-Sheng Hsu, thank you all for your wonderful discussions and support. I could not have asked for better lab mates. You all have made this experience an unforgettable one and I truly wish nothing but the best for each and every one of you as you proceed with your post-graduate career.

Lastly, I want to thank my parents, David and Cherie, for all of their love and helping me become the man I am today. Words are not enough to appreciate all that you have done for me. I want to thank my sisters, Brooke and Becca, for their utmost support and making the holiday breaks enjoyable. I want to show my appreciation for my wife, Becky, for being by my side every step of the way of graduate school. It has truly been a blessing having you, Stella, and Riley out here in Indiana and all the memories we have made over the years. To my family and friends in Virginia, thank you all for your constant support and encouragement.

TABLE OF CONTENTS

LIST OF TABLES	7
LIST OF FIGURES	8
LIST OF SCHEMES.....	10
LIST OF ABBREVIATIONS.....	11
ABSTRACT.....	14
CHAPTER 1. DESIGN AND SYNTHESIS OF HIV-1 PROTEASE INHIBITORS FEATURING A BICYCLIC HEXAHYDROPYRROLOFURAN SCAFFOLD	15
1.1 The Human Immunodeficiency Virus and Acquired Immunodeficiency Syndrome	15
1.2 Epidemiology of HIV	16
1.3 The HIV Life Cycle	17
1.4 Therapeutic Treatment for HIV/AIDS.....	20
1.4.1 Entry and Fusion Inhibitors	22
1.4.2 Reverse Transcriptase Inhibitors	24
1.4.2.1 Nucleoside Reverse Transcriptase Inhibitors	26
1.4.2.2 Non-Nucleoside Reverse Transcriptase Inhibitors	27
1.4.3 Integrase Inhibitors	28
1.5 HIV Protease.....	31
1.6 HIV Protease Inhibitor Design Strategies.....	34
1.6.1 First Generation HIV Protease Inhibitors	35
1.6.1.1 Saquinavir	35
1.6.1.2 Ritonavir.....	37
1.6.1.3 Indinavir	40
1.6.1.4 Nelfinavir	41
1.6.1.5 Amprenavir	43
1.6.2 Second Generation HIV Protease Inhibitors.....	44
1.6.2.1 Lopinavir.....	44
1.6.2.2 Atazanavir	45
1.6.2.3 Tipranavir.....	46
1.6.2.4 Darunavir	48

1.7	Combatting Drug Resistance	52
1.8	Design, Synthesis, and Biological Evaluation of HIV-1 Protease Inhibitors featuring a Novel Hexahydropyrrolofuran (HPF) Scaffold as the P2 Ligand	55
1.8.1	Introduction.....	55
1.8.2	Design of HIV-1 Protease Inhibitors with HPF P2 Ligand	56
1.8.3	Synthetic Strategy	60
1.8.4	Results.....	62
1.8.4.1	Synthesis of HIV-1 Protease Inhibitors	62
1.8.4.2	Biological Evaluation and Discussion	74
1.8.5	Conclusion	80
1.8.6	Experimental.....	82
CHAPTER 2. SYNTHESIS OF CALLYSPONGIOLIDE FRAGMENTS		99
2.1	Introduction.....	99
2.2	Isolation and Biological Activity of Callyspongiolide	100
2.3	Mechanism of Action.....	101
2.4	First Reported Total Synthesis of Callyspongiolide	101
2.5	Total Synthesis Reported by Ghosh Group	106
2.6	Synthesis of Callyspongiolide Fragments.....	110
2.7	Conclusion	115
2.8	Experimental	116
APPENDIX A: NMR SPECTRA		122
APPENDIX B: HPLC ANALYSIS OF LIPASE RESOLUTION		151
REFERENCES		154
VITA.....		166
PUBLICATIONS.....		167

LIST OF TABLES

Table 1.1 FDA Approved Treatments for HIV/AIDS	21
Table 1.2 Optimization for the Preparation of <i>ene</i> -carbamate 22	63
Table 1.3 Optimization of Cbz Deprotection.....	69
Table 1.4 Biological Evaluation of Carbamate-based HIV-1 Protease Inhibitors.....	75
Table 1.5 Biological Evaluation of Amide-based HIV-1 Protease Inhibitors	77
Table 1.6 Biological Evaluation of Sulfonamide-based HIV-1 Protease Inhibitors.....	78
Table 1.7 Calculated logp Values of Selected Inhibitors.....	80
Table 2.1 Optical Rotation Reported by Ye.....	106
Table 2.2 Optical Rotation Reported by Ghosh.....	110
Table 2.3 Optical Rotation of Callyspongiolide Isomers From Second Synthesis	115

LIST OF FIGURES

Figure 1.1 Representative Structure of HIV Virion.....	18
Figure 1.2 HIV Life Cycle	19
Figure 1.3 Structures of FDA Approved Entry and Fusion Inhibitors Enfuvirtide and Maraviroc	23
Figure 1.4 Mechanism of Action of CCR5 Antagonist Maraviroc.....	24
Figure 1.5 X-ray Crystal Structure of HIV-1 Reverse Transcriptase (PDB: 1REV).....	25
Figure 1.6 Structures of FDA Approved Nucleoside Reverse Transcriptase Inhibitors.....	27
Figure 1.7 Structures of FDA Approved Non-Nucleoside Reverse Transcriptase Inhibitors	28
Figure 1.8 X-ray Crystal Structure of HIV-1 Integrase CCD (PDB: 1BIS) ⁵⁶	29
Figure 1.9 Structures of FDA Approved Integrase Inhibitors	30
Figure 1.10 Schematic Binding Mode of Dolutegravir with Highlighted Mg ²⁺ Interactions ⁶³	31
Figure 1.11 X-ray Crystal Structure of HIV-1 Protease (PDB: 4LL3).....	32
Figure 1.12 Proteolytic Mechanism of HIV-1 Protease.....	33
Figure 1.13 Standard Nomenclature of Active Site of HIV-1 Protease.....	34
Figure 1.14 Non-hydrolyzable Transition State Isosteres for HIV-1 Protease Inhibitors ⁷⁰	35
Figure 1.15 Development of Saquinavir Based on Substrate Sequence ⁷⁴	36
Figure 1.16 Crystal Structure of SQV-Bound HIV Protease ^{73,75}	37
Figure 1.17 Development of Ritonavir from Lead Compound A-77003	39
Figure 1.18 Development of Indinavir from Lead Compound L-682,679	41
Figure 1.19 Development of Nelfinavir from Lead Compound LY289612	42
Figure 1.20 Structure of Amprenavir.....	43
Figure 1.21 Development of Lopinavir from Ritonavir.....	45
Figure 1.22 Conceptual Design of Atazanavir.....	46
Figure 1.23 Identification of Tipranavir from Phenprocoumon Lead Compound.....	47
Figure 1.24 Development of <i>bis</i> -THF P ₂ Ligand ^{105,110}	49
Figure 1.25 Structure of TMC-126 with <i>bis</i> -THF P ₂ Ligand.....	50
Figure 1.26 Crystal Structure of TMC-126-Bound to HIV-1 Protease ¹¹²	50
Figure 1.27 Structure of Darunavir with <i>bis</i> -THF P ₂ Ligand	51

Figure 1.28 Crystal Structure of Darunavir-Bound HIV-1 Protease ¹¹³	52
Figure 1.29 HIV-1 Protease Inhibitors Developed from Backbone Binding Concept	54
Figure 1.30 Representative Binding Mode of HIV-1 Protease Inhibitors Modeled with Inhibitor 10 ²⁸	55
Figure 1.31 Structure of GRL-0519A Featuring <i>tris</i> -THF P2 Ligand.....	56
Figure 1.32 Crystal Structure of GRL-0519A-Bound HIV-1 Protease ¹²⁰	57
Figure 1.33 Fused Tricyclic HIV-1 Protease Inhibitors.....	58
Figure 1.34 Crystal Structure of 13 -bound HIV-1 Protease Inhibitors ¹²²	58
Figure 1.35 Structure of Designed HIV-1 Protease Inhibitor Featuring HPF Scaffold.....	59
Figure 1.36 Proposed Hydrogen Bond Interactions of HPF P ₂ Ligand	60
Figure 1.37 X-ray Crystal Structure of 30	66
Figure 1.38 HIV-1 Protease Inhibitors Featuring Carbamate Functionality.....	72
Figure 1.39 HIV-1 Protease Inhibitors Featuring Carboxamide Functionality	73
Figure 1.40 HIV-1 Protease Inhibitors Featuring Sulfonamide Functionality	73
Figure 2.1 Synthetic Modifications of Penicillin G	99
Figure 2.2 Anticancer Marine Natural Products	100
Figure 2.3 Reported Isolated Structure of Callyspongiolide	101
Figure 2.4 Potential Callyspongiolide Structural Assignment.....	106
Figure 2.5 Synthetic Callyspongiolide Isomers Completed by Ghosh	110
Figure 2.6 Callyspongiolide Isomers Generated From Second Synthesis	114

LIST OF SCHEMES

Scheme 1.1 Retrosynthetic Analysis for the Construction of HPF Core	61
Scheme 1.2 Initial Synthesis of <i>ene</i> -carbamate 22	62
Scheme 1.3 Alternative Synthesis of <i>ene</i> -carbamate 22	64
Scheme 1.4 Preparation of Racemic Alcohol 17	64
Scheme 1.5 Enzymatic Resolution of Racemic Alcohol 17	66
Scheme 1.6 Preparation of Activated Carbonate Species (-)- 31 and (+)- 31	67
Scheme 1.7 Synthesis of Hydroxyethylamine Isostere Ligand 18	68
Scheme 1.8 Carbamate Coupling for Preparation of Final Inhibitors 16a and 16b	68
Scheme 1.9 Hydrogenolysis of Cbz Protecting Group and Derivatization Sequence	71
Scheme 2.1 Ye's Retrosynthetic Analysis of Callyspongiolide	102
Scheme 2.2 Synthetic Route to Di-silyl ether 40	103
Scheme 2.3 Synthesis of Vinyl Iodide 50	104
Scheme 2.4 Synthesis Towards Enyne 38	105
Scheme 2.5 Ghosh's Retrosynthetic Analysis of Callyspongiolide.....	107
Scheme 2.6 Synthesis of Lactone 64	108
Scheme 2.7 Chiral Reduction Method to Acquire C-21 Epimers (<i>S</i>)- 66 and (<i>R</i>)- 66	109
Scheme 2.8 Retrosynthetic Analysis with Synthesized Fragments Highlighted	111
Scheme 2.9 Synthesis of Diol 69	112
Scheme 2.10 Synthesis of Enyne (<i>S</i>)- 55	113
Scheme 2.11 Synthesis of Enyne (<i>R</i>)- 55	114

LIST OF ABBREVIATIONS

10 ⁸	100,000,000
10 ⁹	1,000,000,000
¹³ C	Carbon
1D	One Dimensional
¹ H	Proton
2D	Two Dimensional
9-BBN	9-Borabicyclo(3.3.1)nonane
Å	Angstrom
Ac	Acetyl
Ac ₂ O	Acetic Anhydride
AcCl	Acetyl Chloride
AIBN	Azobisisobutyronitrile
Arg	Arginine
Asn	Asparagine
Asp	Aspartic Acid
atm	Atmosphere
BMS	Borane dimethylsulfide
Boc	<i>Tert</i> -butyloxycarbonyl
CBS	Corey-Bakshi-Shibata
Cbz	Benzyloxycarbonyl
CDCl ₃	Chloroform- <i>d</i>
DCM	Dichloromethane
DDQ	2,3-Dichloro-5,6-dicyano-1,4-benzoquinone
DIBAL-H	Diisobutylaluminum hydride
DIPEA	N,N-Diisopropylethylamine
DMF	Dimethylformamide
DNA	Deoxyribonucleic acid
dr	Diastereomeric ratio
EC ₅₀	Effective Concentration, 50%
EC ₉₀	Effective Concentration, 90%
<i>ee</i>	Enantiomeric excess
Et ₂ O	Diethyl ether
Et ₃ N	Triethylamine
EtOAc	Ethyl Acetate
EtOH	Ethanol
Glu	Glutamic Acid
Gly	Glycine
HPLC	High Performance Liquid Chromatography
HRMS	High Resolution Mass Spectrometry
HX	Hexanes
Hz	Hertz
I ₂	Iodine
IC ₅₀	Inhibitory Concentration, 50%

IC ₉₀	Inhibitory Concentration, 90%
Ile	Isoleucine
IPA	Isopropyl Alcohol
KHMDS	Potassium bis(trimethylsilyl)amide
K _i	Kinetic Inhibitor
LAH	Lithium Aluminum Hydride
Leu	Leucine
LHMDS	Lithium bis(trimethylsilyl)amide
LRMS	Low Resolution Mass Spectrometry
MeCN	Acetonitrile
MeI	Methyl Iodide
MeOH	Methanol
Mg ²⁺	Magnesium(II)
MHz	Megahertz
μM	Micromolar
Mn ²⁺	Manganese(II)
mRNA	Messenger RNA
MS	Molecular Sieves
Na ₂ S ₂ O ₃	Sodium Thiosulfate
NaHMDS	Sodium bis(trimethylsilyl)amide
nBu ₃ SnH	Tributyltin hydride
nBuLi	<i>n</i> -Butyllithium
ND	Not Determined
NIS	N-Iodosuccinimide
nm	Nanometers
nM	Nanomolar
NMO	N-Methylmorpholine N-Oxide
NMR	Nuclear Magnetic Resonance
O ₃	Ozone
OH	Alcohol
PCC	Pyridinium Chlorochromate
Phe	Phenylalanine
PhI(OAc) ₂	(Diacetoxyiodo)benzene
PhMe	Toluene
pM	Picomolar
PMB	p-Methoxybenzyl
PN	Pentanes
PPTS	Pyridinium p-toluenesulfonate
Pro	Proline
pTSA	p-Toluenesulfonic acid
RNA	Ribonucleic Acid
RT	Room Temperature
SAR	Structure Activity Relationship
t _{1/2}	Half life
TBAF	Tetrabutylammonium Fluoride
TBAI	Tetrabutylammonium Iodide

TBDPS	<i>tert</i> -Butyldiphenylsilyl
TBS	<i>tert</i> -Butyldimethylsilyl
TBSOTf	<i>tert</i> -Butyldimethylsilyl trifluoromethanesulfonate
TEMPO	2,2,6,6-Tetramethyl-1-piperidinyloxy
TES	Triethylsilyl
TESOTf	Triethylsilyl trifluoromethanesulfonate
TFA	Trifluoroacetic acid
TFAA	Trifluoroacetic anhydride
Thr	Threonine
TLC	Thin Layer Chromatography
TMS	Trimethylsilyl
TMSOTf	Trimethylsilyl trifluoromethanesulfonate
Trp	Tryptophan
Tyr	Tyrosine
UV	Ultraviolet
Val	Valine
XRC	X-Ray Crystallography

ABSTRACT

Since 1981, HIV/AIDS has affected over 70 million individuals worldwide. Due to the incorporation of Combination Antiretroviral Therapy (cART), this deadly virus has now become a manageable chronic illness with a reduction in mortality and morbidity rates. Combination therapy targets multiple stages of the HIV replication cycle including fusion, entry, reverse transcription, integration, and maturation. The HIV-1 protease enzyme is responsible for cleavage and processing of viral polyproteins into mature enzymes and is a common therapeutic target for inhibition of HIV. To date, there have been many protease inhibitors approved by the FDA and introduced into the market. However, mutations within the protease enzyme has rendered some of these inhibitors ineffective. This has led to an ever-growing need to develop novel protease inhibitors to combat drug resistance through mutations. Described herein is the design, synthesis, and biological evaluation of HIV-1 protease inhibitors featuring a novel hexahydropyrrolofuran (HPF) bicyclic scaffold as a P₂ ligand to target binding interactions with Asp29 and Asp30. The HPF ligand provides a molecular handle that allows for further structure-activity discoveries within the enzyme. The HIV-1 protease inhibitors discussed feature carbamate, carboxamide, and sulfonamide derivatives which displayed good to excellent activity.

CHAPTER 1. DESIGN AND SYNTHESIS OF HIV-1 PROTEASE INHIBITORS FEATURING A BICYCLIC HEXAHYDROPYRROLOFURAN SCAFFOLD

1.1 The Human Immunodeficiency Virus and Acquired Immunodeficiency Syndrome

The detection, isolation, and characterization of the first human retrovirus in 1980 was a significant discovery within the science community. This virus, known as human T cell lymphotropic virus (HTLV), was disclosed through the work of Robert Gallo.¹ HTLV was isolated from two separate patients; one with cutaneous T-cell lymphoma and the other with cutaneous T-cell leukemia.² While retrovirus infection had resulted in immune deficiencies in animals, it was uncertain how this newly identified retrovirus would impact the immune system of humans. Coincidentally, cases of a rare infection *Pneumocystis carinii pneumonia* (PCP) and an aggressive cancer named *Kaposi's Sarcoma* began to arise in healthy individuals that eventually led to death from severe immune deficiency.^{3,4} Scientists were left to wonder if HTLV played a role in these immune deficiency cases. The United States Centers for Disease Control and Prevention coined this phenomenon as acquired immune deficiency syndrome (AIDS).⁵

While the number of reported cases of AIDS continued to increase, the direct cause of this deadly disease was still unknown. In 1983, Françoise Barré-Sinoussi and Luc Montagnier, from the Pasteur Institute in France, isolated a new retrovirus believed to belong to the HTLV family. The new isolate presented itself in a patient who showed signs and symptoms that often preceded AIDS. Barré-Sinoussi and Montagnier collected these isolates from the lymph nodes of the patient and named this new retrovirus as lymphadenopathy-associated virus (LAV).⁶ However, the correlation between LAV and AIDS was still unknown. A year later, Gallo identified a third subgroup of HTLV, labeled HTLV-III, and its prevalence in patients with immune deficiency disorders. Utilizing the same characterization techniques for HTLV-I, it was determined that HTLV-III was the causative agent for AIDS.⁷ However, results corroborated that HTLV-III was the same virus as the previously reported LAV and was eventually renamed by the International Committee on the Taxonomy of Viruses to human immunodeficiency virus (HIV).⁸ In 2008, Françoise Barré-Sinoussi and Luc Montagnier received the Nobel Prize in Medicine for the isolation and identification of the HIV virus.

Since the beginning of the AIDS epidemic in 1981, approximately 70 million individuals have become infected with HIV while 32 million have died from AIDS-related illnesses. Research efforts have provided treatment options for this deadly disease to assist in keeping viral levels low and improving the overall lifestyle of individuals affected. While a strategy to fully combat this virus remains to be seen, today's therapeutic options have made HIV a manageable disease in today's society.

1.2 Epidemiology of HIV

HIV can be classified into two separate types; HIV-1 and HIV-2. HIV-1 and HIV-2 have both been shown to cause AIDS and share similar intracellular mechanisms of replication and modes of transmission. However, HIV-1 and HIV-2 are very different in terms of mortality and possess structural anomalies to one another. For HIV-1, the progression to AIDS occurs much more rapidly than HIV-2; hence HIV-1 is a more appealing therapeutic target.⁹ Both HIV-1 and HIV-2 exhibit major differences within their nucleotide and amino acid sequences; with an estimated 55% genetic variance.¹⁰ The origins of HIV-1 and HIV-2 are a result of the recombination of various strains of zoonotic infectious diseases, particularly the simian immunodeficiency virus (SIV). Recombination is the process in which two distinctly different viral genomes co-infect the same host cell and exchange genetic material during the replication process.¹¹ Reports indicate the precursor for HIV-1 is SIVcpz and the precursor for HIV-2 is SIVsm.^{12,13} The recombination to produce SIVcpz and SIVsm can be explained through exposure of infected blood through hunting practices or injuries occurred by infected species.

Despite the early theories of initial cross-species transmission, HIV can be transmitted through numerous avenues. These avenues include the human genital tract, intestinal tract, placenta, and the bloodstream. HIV infection occurs when infected bodily fluid such as blood, semen, and even breast milk come into contact at the mucosal surfaces of these sites.^{14,15} Upon initial infection, HIV targets vital cells in the immune system with CD4 surface receptors including CD4⁺ T cells, macrophages, monocytes and dendritic cells.¹⁶ Once a cell is infected with HIV, the virus cannot be eradicated, instead the cell must die in order to prevent replication of HIV. Both HIV-infected and uninfected CD4⁺ T cells die during infection through a variety of plausible mechanisms.¹⁷ The decline in the number of immune cells ultimately leads to immunosuppression and opportunistic infections.

1.3 The HIV Life Cycle

HIV is a member of the *Retroviridae* family and of the lentivirus subgroup. A retrovirus is an RNA virus that possesses the reverse transcriptase (RT) enzyme.¹⁸ In the case of HIV, the RNA is reverse transcribed into its resultant complementary DNA and further incorporated into the DNA of the host cell during the replication process.

A mature HIV-1 virion is a spherical particle that contains an array of outer-layer glycoproteins (gp120 and gp41) and measures roughly 100 nm in diameter. Inside the core, HIV has two single-stranded RNA genomes that are responsible for encoding structural and regulatory proteins. Each protein produced from this genome plays an integral role in the survival and replication of HIV. The three major structural genes include *gag*, *pol*, and *env*. The *gag* gene encodes the matrix (MA) proteins essential for virion assembly, the capsid (CA) proteins which form the hydrophobic core, and the nucleocapsid (NC) proteins which bind tightly to the single-stranded RNA to protect the genome. The *pol* sequence contains the genetic code for the protease (PR), reverse transcriptase (RT), and the integrase (IN) enzymes necessary for viral replication. The *env* gene encodes the membrane surface glycoprotein gp160 from which the two crucial glycoproteins gp120 and gp41 are derived during viral maturation. The regulatory proteins encoded in the RNA genome include *tat* (transactivator protein) and *rev* (RNA splicing-regulator). These proteins are responsible for the initiation of HIV replication.^{19–21}

The HIV life cycle is initiated when the envelop glycoprotein gp120 of the mature HIV particle attaches to the CD4 receptor of the host cell. Upon attachment, gp120 undergoes a conformational change to expose the co-receptor binding site. The type of host cell infected will determine the corresponding binding co-receptor; T-lymphocytes contain the CXCR4 receptor while monocytes contain the CCR5 receptor.²² Once the CD4 receptor and co-receptors are fully engaged with the virion, the hydrophobic fusion peptide located at gp41 is released and inserted into the membrane of the target cell, thus creating an entry point into the host cell.²³ Once the viral capsid enters the cytoplasm of the cell, the uncoating process initiates to expose the viral RNA. The viral RNA is reverse transcribed into viral complementary DNA by the reverse transcriptase (RT) enzyme. The resulting DNA is then transported to the nucleus of the host cell where the viral DNA is integrated into the host DNA via the integrase (IN) enzyme. Using the host cell machinery, transcription and translation proceeds to produce viral proteins as long polyprotein strands containing the same genetic material as a mature HIV virion. These components gather around

the inner membrane and begin to bud from the host cell. The protease (PR) enzyme cleaves the polyproteins into mature proteins.

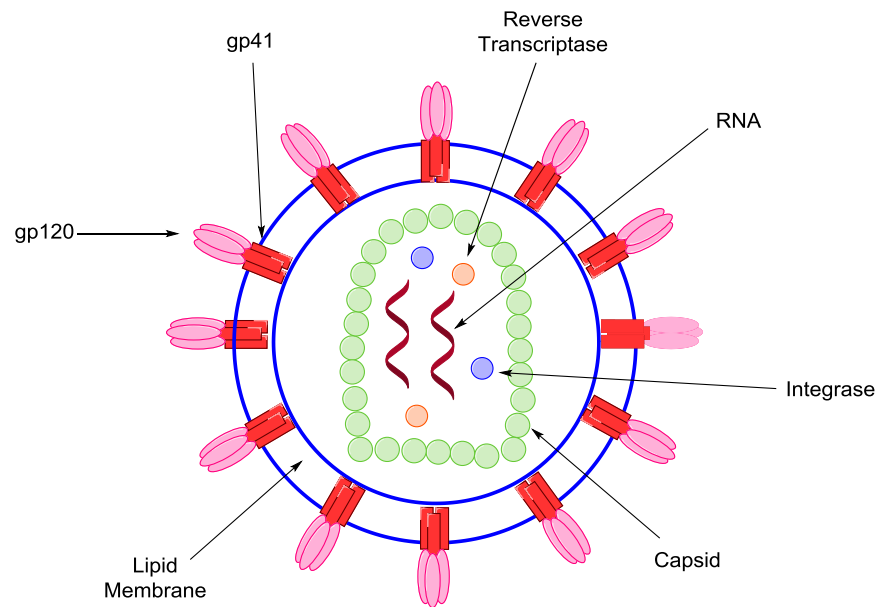


Figure 1.1 Representative Structure of HIV Virion

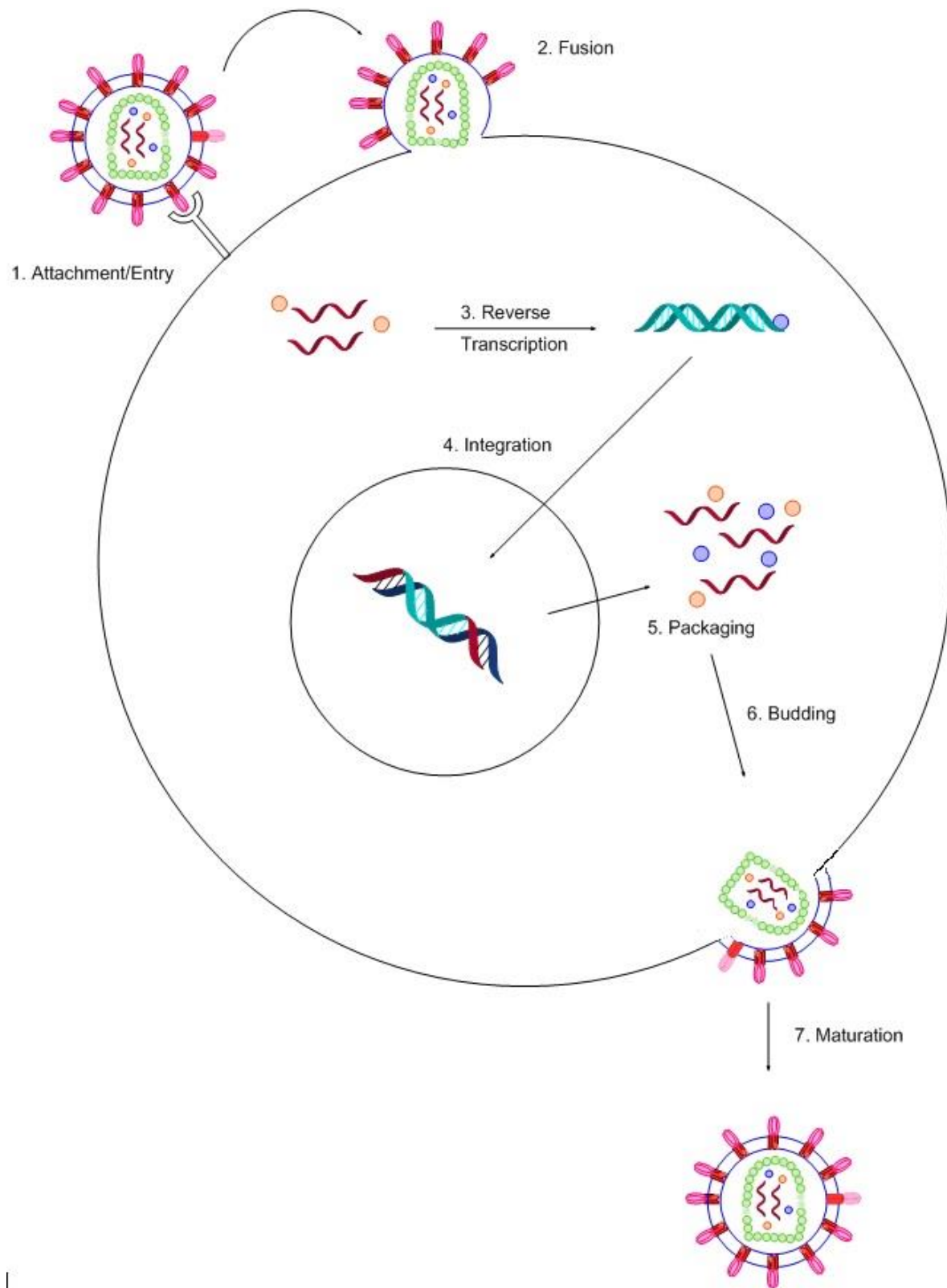


Figure 1.2 HIV Life Cycle

1.4 Therapeutic Treatment for HIV/AIDS

When HIV/AIDS was first introduced, the ability to combat this deadly virus was essentially non-existent as there was a lack of effective antiviral drugs at the time. In 1964, a drug by the name of zidovudine (ZDV), otherwise known as 3'-azido-3'-deoxythymidine (azidothymidine, AZT), was synthesized as a potential anti-cancer drug.²⁴ Due to lack of anti-cancer activity, this drug candidate was placed on hold. It wasn't until 1987, when ZDV was approved by the U.S. Food and Drug Association (FDA) as a HIV-1 nucleoside reverse transcriptase inhibitor (NRTI), AIDS-infected patients were starting to improve in terms of their condition. Unfortunately, viral resistance quickly emerged and the need for new therapeutic options became apparent.²⁵ Soon after the approval of ZDV, three other NRTI's were approved for the treatment of HIV; didanosine, zalcitabine, and stavudine. These NRTI's were initially used as monotherapy, but later reports indicated that combination antiretroviral therapy (cART) of two or more NRTI's improved outcomes in comparison to monotherapy.^{26,27}

The improved efficacy of cART is evident through the development of inhibitors targeting multiple stages of the HIV replication cycle. Inhibitor classes include entry, fusion, reverse transcriptase (RT), integrase (IN), and protease inhibitors (PI). The first protease inhibitor to be approved was Saquinavir in 1995. The incorporation of Saquinavir, in combination with a reverse transcriptase inhibitor, marked the beginning of highly active antiretroviral therapy (HAART). The advent of HAART has significantly improved treatment options for HIV/AIDS by suppressing viral replication, reducing HIV-1 viral loads, and increasing overall life expectancy.²⁸ Scientific advancements in HAART have provided numerous FDA-approved drugs for the treatment of HIV/AIDS (Table 1.1).

While incorporation of cART has set the stage for treatment of HIV/AIDS, there remains a method to completely eradicate this deadly virus from an infected individual. HAART has assisted in turning this deadly disease into a manageable illness, but the issue of drug resistance through mutations will continue to exist. Therefore, there will continue to be an ever-growing need for the development of new and effective inhibitors, regardless of class.

Table 1.1 FDA Approved Treatments for HIV/AIDS

Drug Class	Generic Name	Brand Name	Approval Date
Entry and Fusion Inhibitors	Enfuvirtide	Fuzeon	March 13, 2003
	Maraviroc	Selzentry	August 6, 2007
	Ibalizumabuiyk	Trogarzo	March 6, 2018
Reverse Transcriptase Inhibitors	Zidovudine	Retrovir	March 19, 1987
	Didanosine	Videx	October 9, 1991
	Zalcitabine	Hivid	June 19, 1992
	Stavudine	Zerit	June 27, 1994
	Lamivudine	Epivir	November 17, 1995
	Abacavir	Ziagen	December 17, 1998
	Tenofovir	Viread	October 26, 2001
	Adefovir	Hepsera	September 20, 2002
	Emtricitabine	Emtriva	July 2, 2003
	Nevirapine	Viramune	June 21, 1996
	Delavirdine	Rescriptor	June 12, 1997
	Efavirenz	Sustiva	September 17, 1998
	Etravirine	Intelence	January 18, 2008
	Rilpivirine	Edurant	May 20, 2011
	Doravirine	Pifeltro	August 30, 2018
Integrase Inhibitors	Raltegravir	Isentress	October 12, 2007
	Dolutegravir	Tivicay	August 13, 2013
	Elvitegravir	Vitekta	September 24, 2014
Protease Inhibitors	Saquinavir	Invirase	December 6, 1995
	Ritonavir	Norvir	March 1, 1996
	Indinavir	Crixivan	March 13, 1996
	Nelfinavir	Viracept	March 14, 1997
	Amprenavir	Agenerase	April 15, 1999
	Lopinavir	Kaletra	September 15, 2000
	Atazanavir	Reyataz	June 20, 2003
	Fosamprenavir	Lexiva	October 20, 2003
	Tipranavir	Aptivus	June 22, 2005
	Darunavir	Prezista	June 23, 2006
Pharmacokinetic Enhancers	Cobicistat	Tybost	September 24, 2014

1.4.1 Entry and Fusion Inhibitors

The process of entry into the host cell by a HIV virion traditionally involves three key stages: (i) attachment to the host cell mediated by CD4 receptor binding, (ii) co-receptor binding with either CCR5 or CXCR4, and (iii) fusion of the virion to the host cell membrane.²⁹ The first stage of attachment involves the interaction of the gp120 and gp41 spikes located on the outer membrane of the HIV particle with the host cell's CD4 receptor. These spikes are composed of trimeric units of gp120 and gp41 to form a heterotrimeric unit.³⁰ Once gp120 binds to the CD4 cell, there is a conformational shift that exposes the co-receptor binding site and allows for interaction with the chemokine co-receptor of the host cell. After complete attachment of gp120 to CD4 and the chemokine receptor, gp41 undergoes a conformational change to expose, and release, the fusion peptide into the membrane to initiate the fusion process.³¹ Insertion of the hydrophobic fusion peptide into the host cell leads to the formation of a six-helix bundle, from the gp41 subunits, forming the heptad repeat (HR) regions HR1 and HR2.³² The result of the formation of this six-helix bundle is the fusion of the viral and cellular membranes where the viral capsid can be expelled into the host cell. Each stage has been the target for the development of entry and fusion inhibitors.

The first FDA approved inhibitor of this class was Enfuvirtide in 2003 to be used as a fusion inhibitor (Figure 1.3). Enfuvirtide is a 36-amino-acid synthetic peptide designed to mimic the HR2 region of gp41.^{31,33} Reports show that Enfuvirtide competitively binds to the HR1 domain of gp41 thus preventing the development of the six-helix bundle conformation that is essential to the fusion process. Drawbacks of this inhibitor includes administration by injection, low genetic barrier for resistance, insomnia, depression, and weak pharmacokinetic properties.³⁴

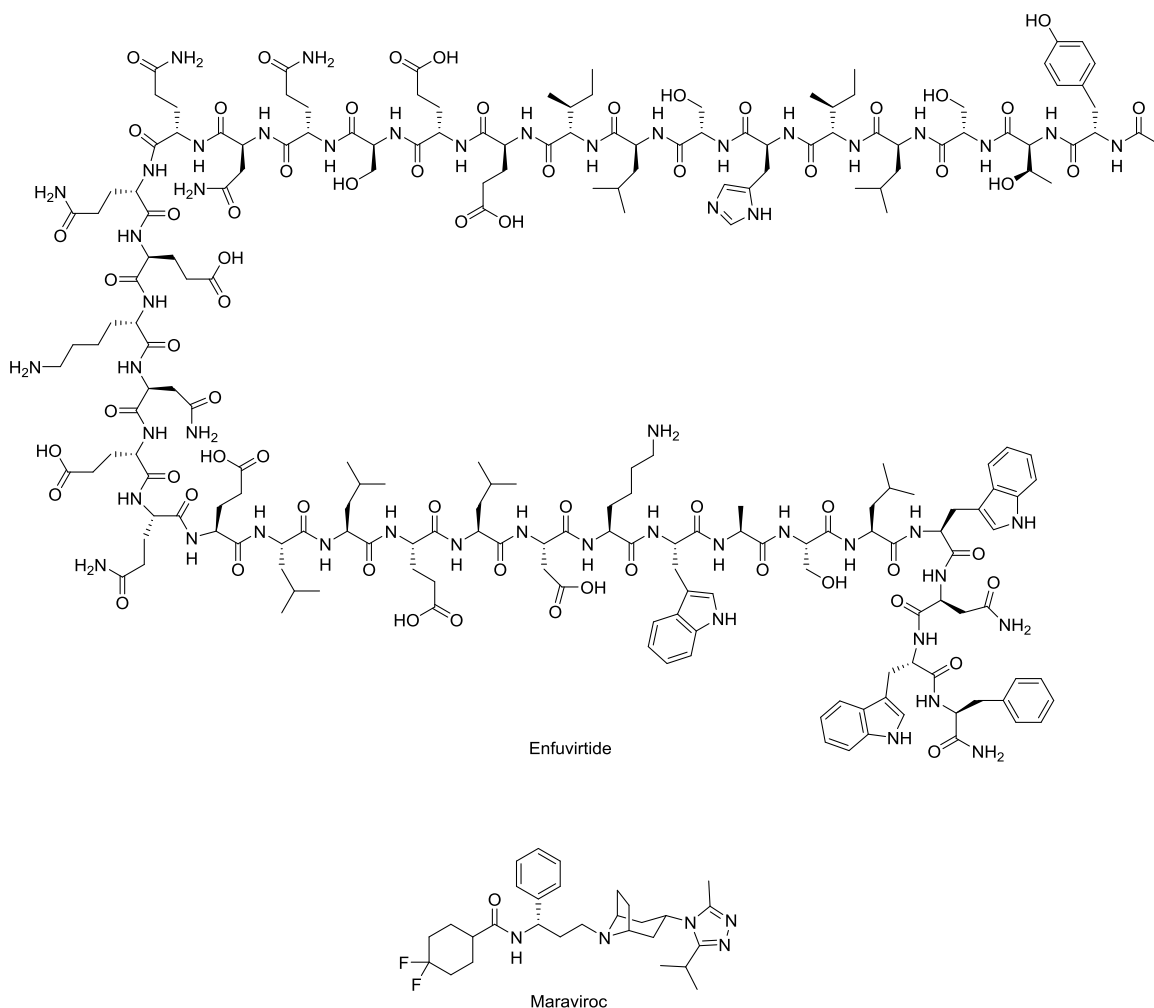


Figure 1.3 Structures of FDA Approved Entry and Fusion Inhibitors Enfuvirtide and Maraviroc

The second FDA approved inhibitor of this class was Maraviroc in 2007 (Figure 1.3). Maraviroc is a selective CCR5 antagonist to prevent the HIV-1 entry process. It is believed that Maraviroc selectively binds to the hydrophobic cavity formed by the transmembrane helices of the CCR5 receptor.^{35,36} This interaction prevents the CCR5 co-receptor from interaction with gp120 and inhibits the entry and fusion process of HIV to the host cell. However, this inhibitor is only effective with CCR5 receptors and does not affect the binding affinity in the presence of CXCR4 co-receptors (Figure 1.4).

Overall, strategizing the inhibition of HIV attachment, entry, and fusion processes has numerous advantages. Since the active site of this inhibitor class is mainly extracellular, these sites of inhibition are readily accessible and could limit cell toxicity profiles.

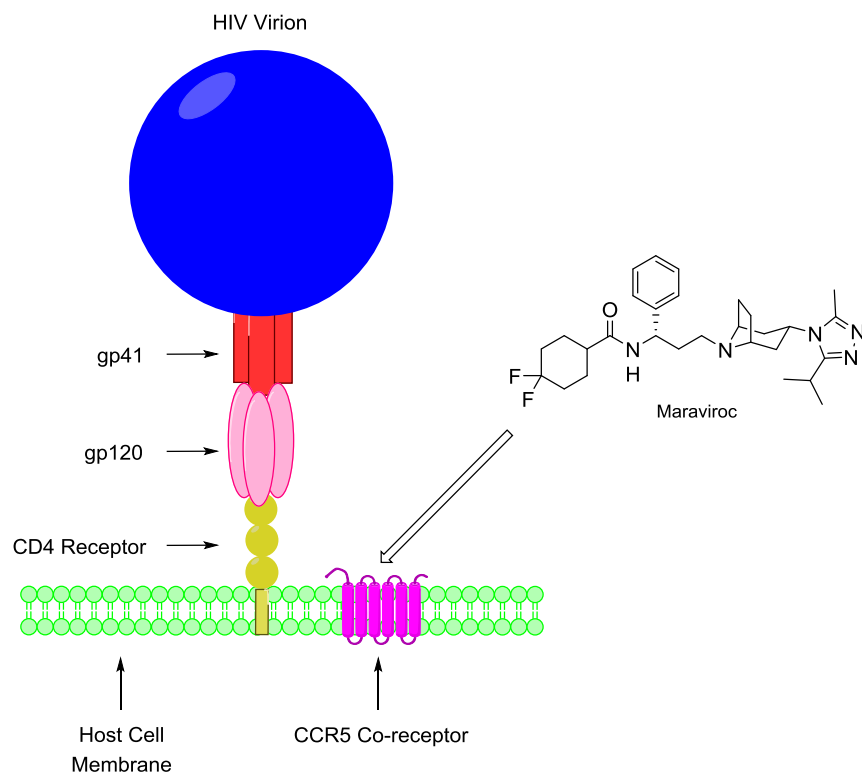


Figure 1.4 Mechanism of Action of CCR5 Antagonist Maraviroc

1.4.2 Reverse Transcriptase Inhibitors

Reverse transcriptase (RT) inhibitors are categorized into two different classes: Nucleoside Reverse Transcriptase Inhibitors (NRTI) and Non-nucleoside Reverse Transcriptase Inhibitors (NNRTI). Each class of reverse transcriptase inhibitors has a distinct mechanism of action to prevent the synthesis of viral DNA from the viral single-stranded RNA. Reverse transcriptase is a unique heterodimer consisting of two related subunits, p66 and p51 (Figure 1.5). The larger p66 subunit contains two significant domains, polymerase and ribonuclease H (RNase H). These domains are responsible for the enzymatic activity of RT and are essential for copying the single-stranded RNA into the double-stranded DNA. Furthermore, the polymerase domain is composed of four subdomains labeled fingers, palm, thumb, and connection. The p51 subunit is believed to provide structural support to the RT enzyme, but is not inert during the reverse transcription process.^{37,38}

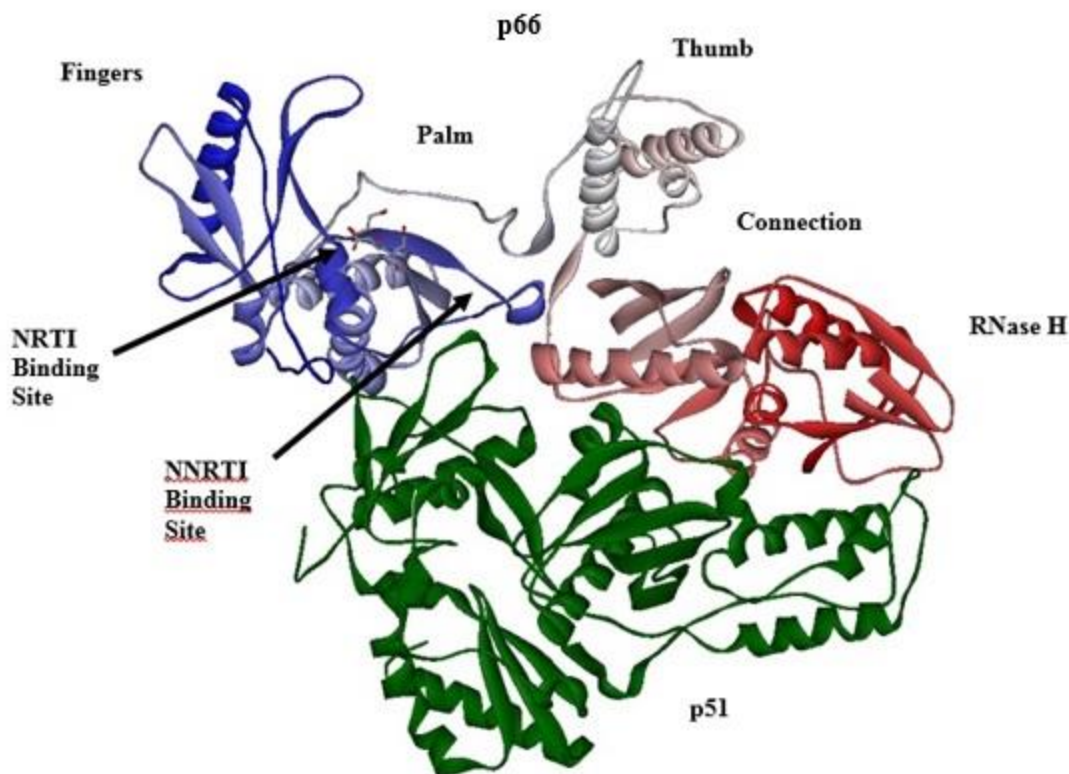


Figure 1.5 X-ray Crystal Structure of HIV-1 Reverse Transcriptase (PDB: 1REV)

During the reverse transcription process, the viral RNA first binds to the polymerase active site where the polymerization reaction is initiated. This binding results in a conformational shift of the p66 thumb from a closed to an open orientation.³⁹ This conformation allows the first step of nucleotide incorporation to begin. The incoming deoxyribonucleoside triphosphate (dNTP) binds at the nucleotide binding site to form a ternary complex.⁴⁰ The p66 fingers subdomain then closes down on the dNTP to align the 3'-OH of the RNA, the α -phosphate of the dNTP, and the polymerase active site.³⁹⁻⁴¹ The catalytic activity of the polymerase domain can be attributed to three main aspartic acid residues located in the palm subdomain of p66, Asp 110, Asp185, and Asp186.^{42,43} The carboxylate groups of the catalytic residues are responsible for coordinating with divalent metal ions (Mg^{2+} or Mn^{2+}) to facilitate the attack of the 3'-OH on the α -phosphate of the incoming dNTP.^{39,44,45} Completion of the polymerization sequence produces a RNA-DNA double-strand complex that is then processed further in the RNase H domain.

The RNase H domain is responsible for the degradation of the RNA strand of the RNA-DNA complex and removal of the primers engaged in initiating the reverse transcription process.

The catalytic residues in the active site of RNase H are Asp443, Glu478, Asp498, and Asp549.^{46,47} In a similar mechanism to the active site of the polymerase domain, the catalytic residues of RNase H form a complex with two divalent metal ions along with the phosphate of the base pairs. The RNase H selectively cleaves the RNA sequence to produce a single strand of viral DNA. The single-stranded viral DNA is then processed through the polymerase once more to undergo an additional polymerization sequence to produce the desired double-stranded viral DNA, also known as complementary DNA (cDNA). The catalytic activity induced by the polymerase and RNase H domains make these attractive targets for antiretroviral therapy.

1.4.2.1 Nucleoside Reverse Transcriptase Inhibitors

The first type of reverse transcriptase inhibitors are the NRTI's (Figure 1.6). This class of inhibitors are structurally designed to mimic the natural substrates of DNA synthesis. During DNA synthesis, these inhibitors can be read as a naturally occurring triphosphate to be incorporated into the polymerization sequence. However, in order for the NRTI's to be effective reverse transcriptase inhibitors, they must be phosphorylated to the triphosphate.^{48,49} The triphosphate derivatives then act as competitive inhibitors with the naturally occurring deoxynucleotide triphosphates. The NRTI's all lack the 3'-OH group which allow them to act as chain terminators once incorporated into the viral DNA.⁵⁰

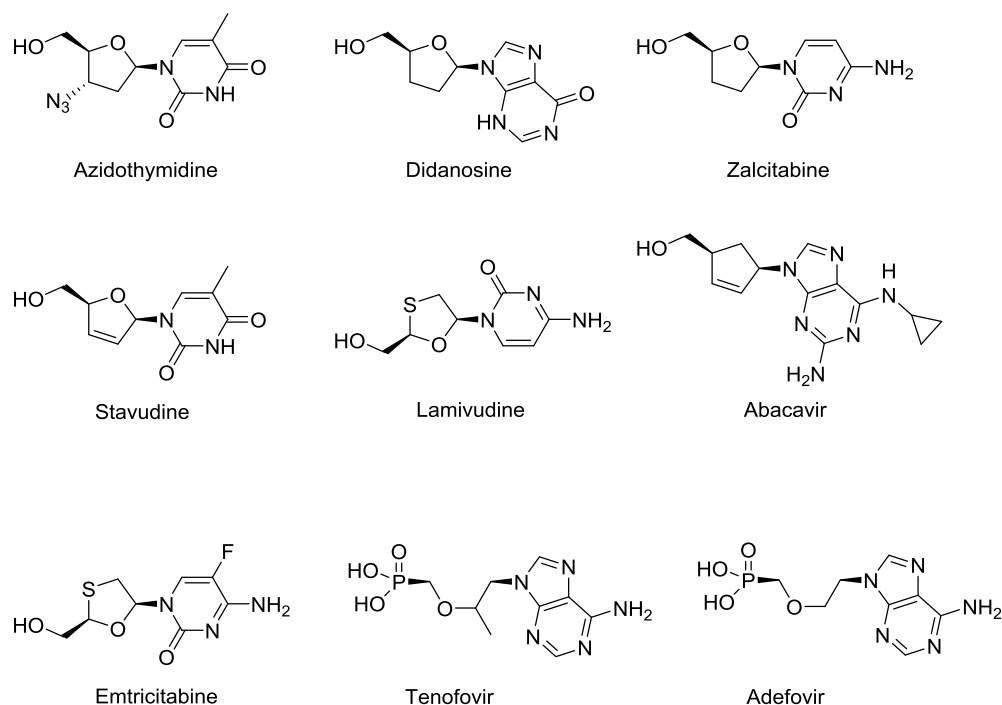


Figure 1.6 Structures of FDA Approved Nucleoside Reverse Transcriptase Inhibitors

1.4.2.2 Non-Nucleoside Reverse Transcriptase Inhibitors

The second type of reverse transcriptase inhibitors are the NNRTI's (Figure 1.7). NNRTI's are not designed as analogs of nucleotides making them noncompetitive inhibitors. These inhibitors have a unique hydrophobic binding site next to the polymerase active site known as the NNRTI-binding pocket (NNIBP). Structural data suggests that NNRTI-binding changes the conformation of the catalytic residues that bind to the divalent metal ions leading to reduced activity of the polymerase and interference with viral DNA synthesis.⁵¹ In the absence of an inhibitor bound to RT, the NNIBP is nonexistent and is therefore created upon entry of the NNRTI. The binding mode of the NNRTI's can be described as either "butterfly" or "horseshoe" with a central scaffold and two "wings" attached.⁵² Design of these inhibitors features π -electron systems that can interact with the aromatic amino acids within the NNIBP, specifically Tyr181, Tyr188, Trp229, and Tyr318.^{51,53}

The first generation of inhibitors were Nevirapine, Delavirdine, and Efavirenz. This generation adopted the butterfly conformation. However, this generation of inhibitors had a low genetic barrier and a single-point mutation led to resistance. The resulting mutations from the error-prone reverse transcription process led to the development of second generation NNRTI's to

overcome this genetic barrier and combat drug resistance. The second generation of inhibitors consists of Etravirine, Rilpivirine, and Dapivirine. Unlike the first generation, the second generation inhibitors adopt a horseshoe conformation and are better equipped to combat drug resistance caused by mutations.

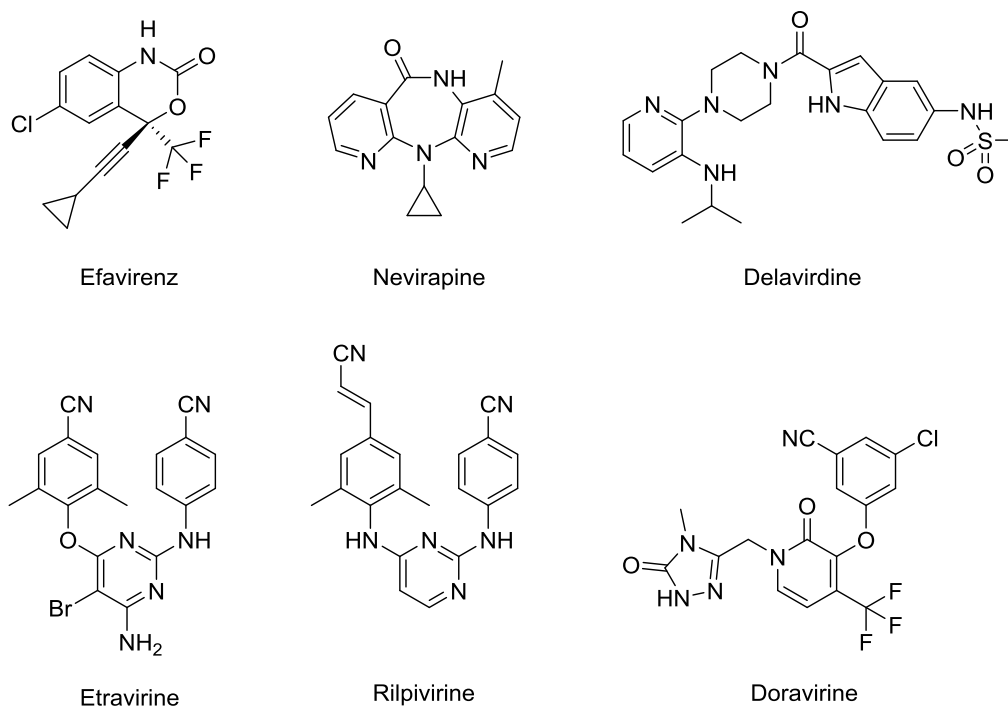


Figure 1.7 Structures of FDA Approved Non-Nucleoside Reverse Transcriptase Inhibitors

1.4.3 Integrase Inhibitors

Integrase inhibitors have been developed to terminate the process of viral DNA (cDNA) inserting into the host cell DNA and further inhibit the replication cycle. The integrase enzyme is a 288-amino acid protein that contains three structural domains: (i) N-terminal domain (NTD), (ii) a highly conserved catalytic domain (CCD), and (iii) the C-terminal domain (CTD). The N-terminal domain contains a zinc-binding HHCC motif consisting of histidine and cysteine residues. This domain is responsible for the arrangement of the active form of the enzyme by promoting tetramer formation.^{54,55} The central catalytic domain active site is comprised of three amino acid residues; Asp64, Asp116, and Glu152 (Figure 1.8). These particular amino acids bind to the

divalent metal ions (Mg^{2+} or Mn^{2+}) during the nucleophilic substitution of the strand transfer (ST) reaction.⁵⁶

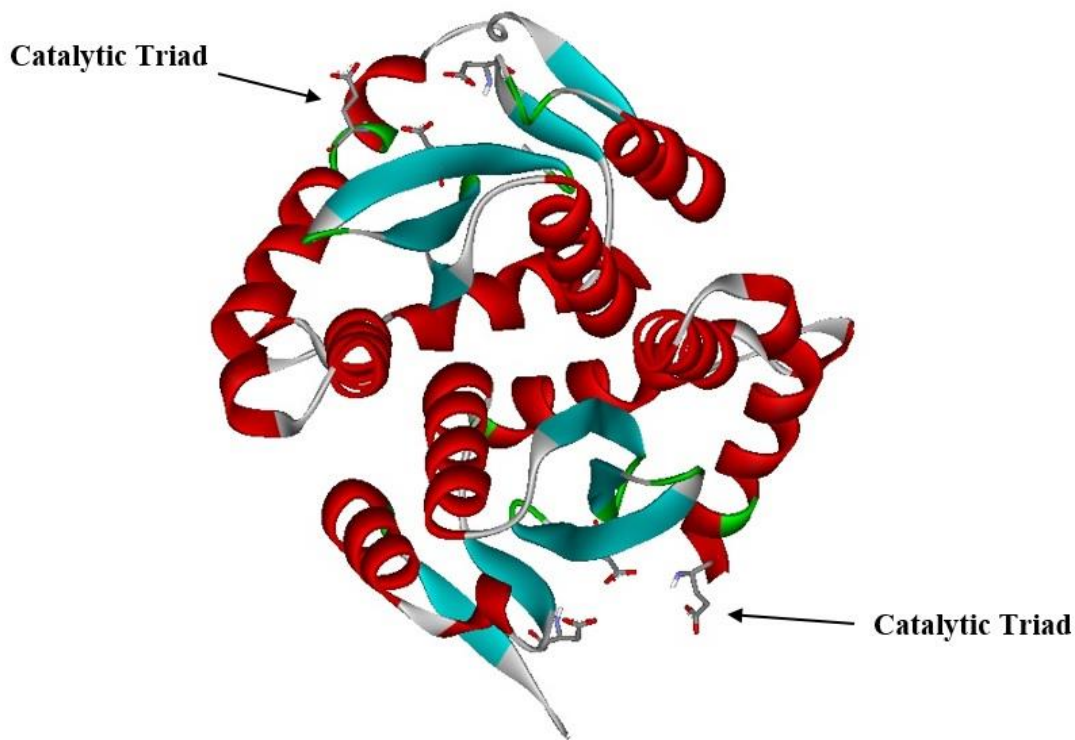


Figure 1.8 X-ray Crystal Structure of HIV-1 Integrase CCD (PDB: 1BIS)⁵⁶

Integrase facilitates two catalytic steps during the process of integration. The first catalytic step is a 3'-processing (3'-P) event that transpires in the cytoplasm. The CAGT tetranucleotide at the 3'-end of the cDNA is hydrolyzed, by nucleophilic attack of a water molecule on the phosphodiester bond, resulting in the cleavage of the GT nucleotides and exposure of the CA nucleotides at the 5'-end.⁵⁷ After hydrolysis, the IN remains bound to the cDNA forming a preintegration complex (PIC). This complex is carried into the nucleus of the cell where it binds to the host DNA through the intermediacy of the host protein lens epithelium-derived growth factor/p75 (LEDGF/p75). LEDGF/p75 acts as a bridge to tether HIV integrase to the cellular genome.^{58,59} Once bound to the host DNA, the second catalytic step is initiated; strand transfer. The strand transfer reaction is a phosphodiester transesterification reaction mediated by a divalent metal ion. During this process, the 3'-OH groups perform a nucleophilic attack on the phosphodiester bond of the complementary strand thus making the 5'-end of the host DNA the

leaving group. The resulting gaps in the DNA strands are repaired through the host cell's DNA polymerases.⁶⁰

The divalent metal ions are critical assets for catalytic activity. They assist in stabilizing the enzyme-DNA complex and promote the charge flow from the viral 3'-OH group to the 3'-OH group of the host DNA.^{61,62} Without this stabilization effect, the integration process will not proceed. This unique effect has brought about inspiration in the design of HIV integrase inhibitors. Since 2007, the FDA has approved three HIV integrase inhibitors. Raltegravir (2007), Dolutegravir (2013), and Elvitegravir (2014) are classified as strand transfer inhibitors and share a common structural motif that explains the mechanism of action for each (Figure 1.9). Structural similarities include the incorporation of a metal-chelating scaffold (orange), a hydrophobic region for enzyme binding (red), and a linker (black). The metal-chelating groups are oxygenated moieties that coordinate to the divalent metal ions present and inhibit the binding of host DNA to the viral integrase (Figure 1.10).⁶³⁻⁶⁵

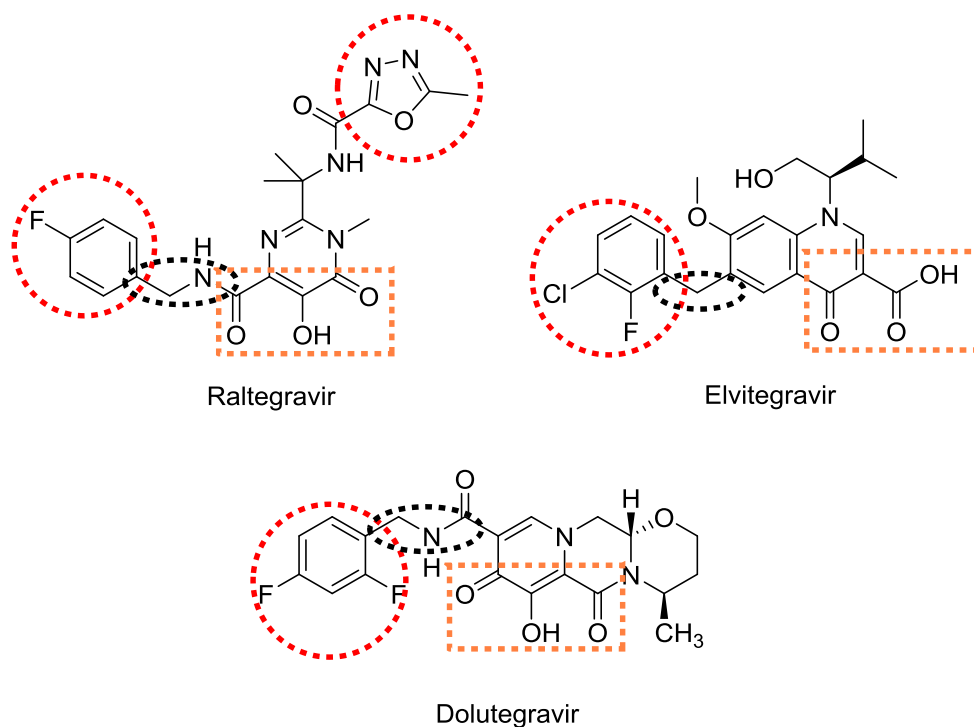


Figure 1.9 Structures of FDA Approved Integrase Inhibitors

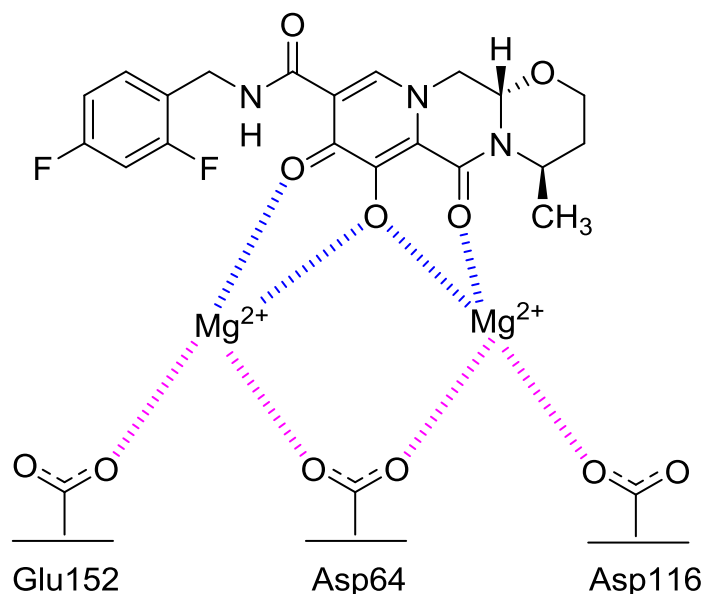


Figure 1.10 Schematic Binding Mode of Dolutegravir with Highlighted Mg^{2+} Interactions⁶³

1.5 HIV Protease

After integration into the host cell DNA, HIV then exploits the cellular mechanisms to transcribe the viral DNA into mRNA. Furthermore, the viral mRNA is translated to produce the *gag* and *gag-pol* polyproteins. The viral RNA, *gag*, *gag-pol* polyprotein precursors and accessory proteins compile near the cell surface. The mature protease, released via autoprocessing, is responsible for the proteolytic cleavage of the *gag* and *gag-pol* polyproteins to assemble the structural proteins and functional enzymes.⁶⁶ These include the glycoproteins, matrix, capsid, reverse transcriptase, integrase, and protease for newly formed virions. Inhibition or disruption of the viral PR activity results in defective viral particles, reduced infectivity, and is an attractive target for treatment of HIV and AIDS.⁶⁷

X-ray structural studies of HIV PR provided more insight into the structure and catalytic activity of the enzyme. The first crystal structure was obtained by Merck Laboratories in 1989 and was subsequently followed with another crystal structure from the collaborative efforts of NCI-Frederick Cancer Research Facility and California Institute of Technology (Figure 1.11).^{68,69} PR is a homodimer with two 99 amino acid subunits. Each monomer contributes a glycine-rich β -sheet region that acts as an entry point of the native substrate, or inhibitor, into the active site. This is known as the flap region. The flap region will have an open conformation in the absence of a substrate in the active site, but will undergo a conformational shift to fold down in the presence of

a substrate. Additionally, the catalytic active site resides in the base of the cavity at the dimer interface.

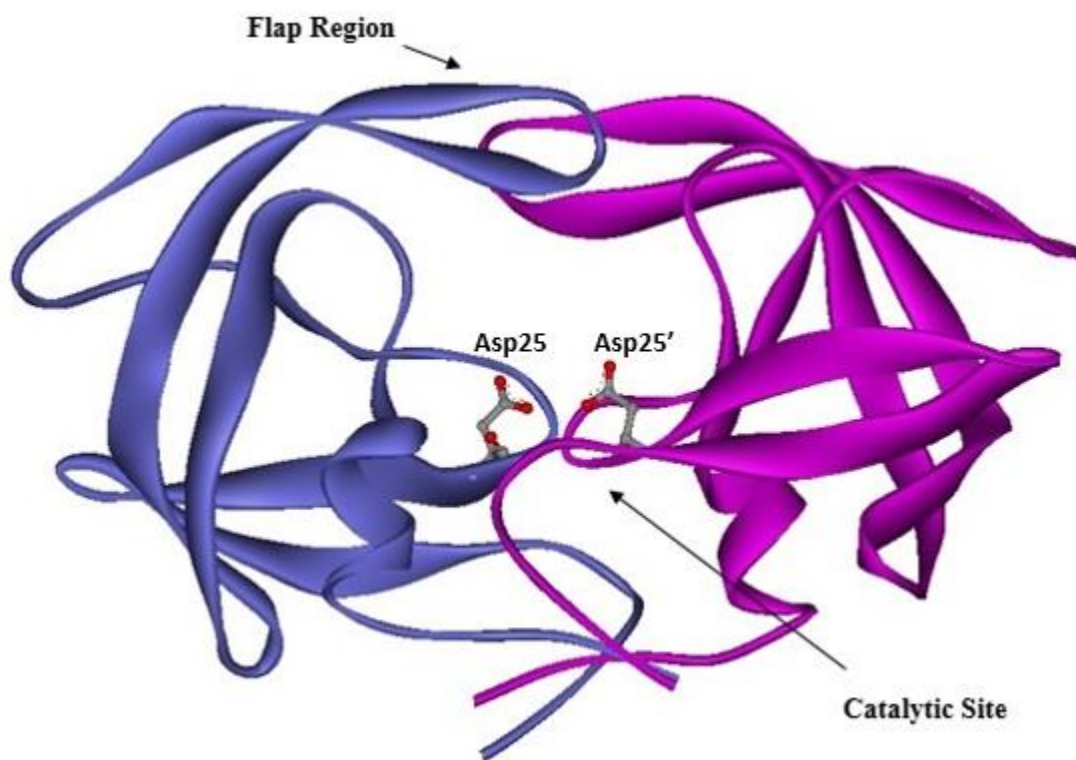


Figure 1.11 X-ray Crystal Structure of HIV-1 Protease (PDB: 4LL3)

The active site consists of Asp25-Thr26-Gly27 and Asp25'-Thr26'-Gly27' residues provided from each subunit. The catalytic aspartic acid residues Asp25 and Asp25' are important for the proteolytic activity of the enzyme. In the presence of a substrate, Asp25 and Asp25' activates a water molecule for nucleophilic addition to the carbonyl of the scissile bond. The resulting tetrahedral intermediate further collapses to yield the corresponding carboxylic acid and amine (Figure 1.12).⁷⁰

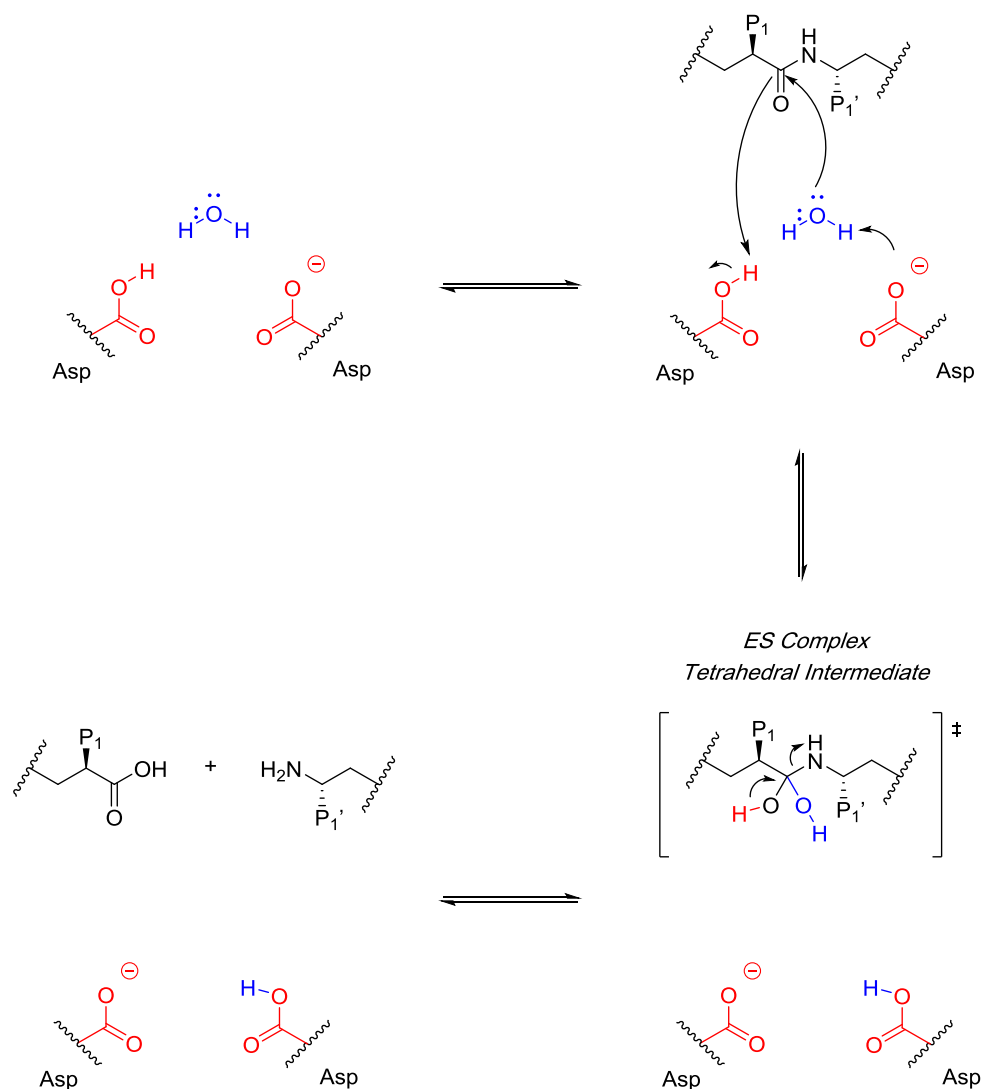


Figure 1.12 Proteolytic Mechanism of HIV-1 Protease

As mentioned previously, the peptide bond that undergoes proteolytic cleavage is denoted as the scissile bond. From the scissile bond, each region of the native substrate, or inhibitor, can be categorized. The subunits located to the left of the scissile bond are denoted as “P” subunits and are labeled as P_1 , P_2 , P_3 , and so forth. On the right side of the scissile bond, the subunits are labeled as P_1' , P_2' , P_3' and so on. These subunits lie within a certain subsite which is denoted as “S”. For example, the P_2 subunit would accommodate the S_2 subsite and the P_1' subunit would be housed within the S_1' subsite. The standard nomenclature is depicted below where the scissile bond is highlighted in red.^{28,70}

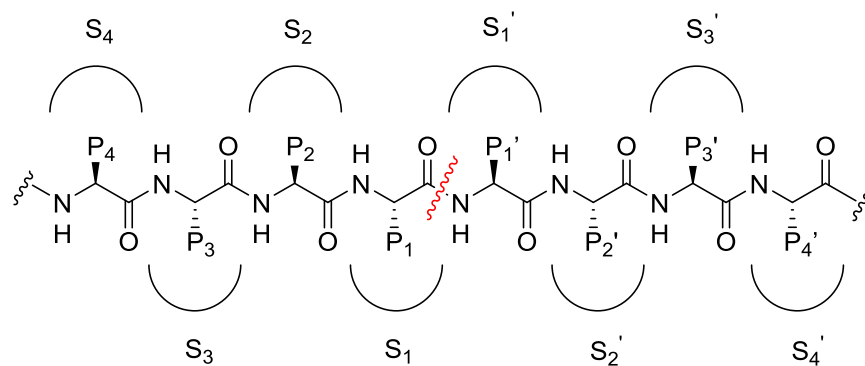


Figure 1.13 Standard Nomenclature of Active Site of HIV-1 Protease

1.6 HIV Protease Inhibitor Design Strategies

The efficacy of a protease inhibitor is reliant on the structural design of the drug candidate. The structural features of the inhibitor should promote strong interactions with the enzyme to reduce the protease activity and assist in maintaining stability in physiological conditions. Experiments have confirmed the formation of the tetrahedral diol intermediate which rapidly breaks down to the corresponding amine and carboxylic acid. Preventing the formation of the diol intermediate halts the progression of the proteolytic activity. Therefore, incorporating a scaffold which mimics this transition state could prevent the hydrolysis from occurring.

Initially, HIV PR inhibitors were designed after other aspartic acid protease inhibitors, such as renin. These results promote the design and incorporation of a non-hydrolyzable isostere which mimics the tetrahedral transition state (Figure 1.14).⁷¹ The isostere cores such as hydroxyethylamine, hydroxyethylene, and silanediol each have an alcohol functional group which the catalytic aspartic acids will interact with via hydrogen bonding. The reduced amide isostere lacks the carbonyl and will not undergo hydrolysis, thus preventing the proteolytic activity of the enzyme and maintaining the integrity of the ligand. Strategic incorporation of these isosteres are observed in the first and second generations of HIV protease inhibitors.

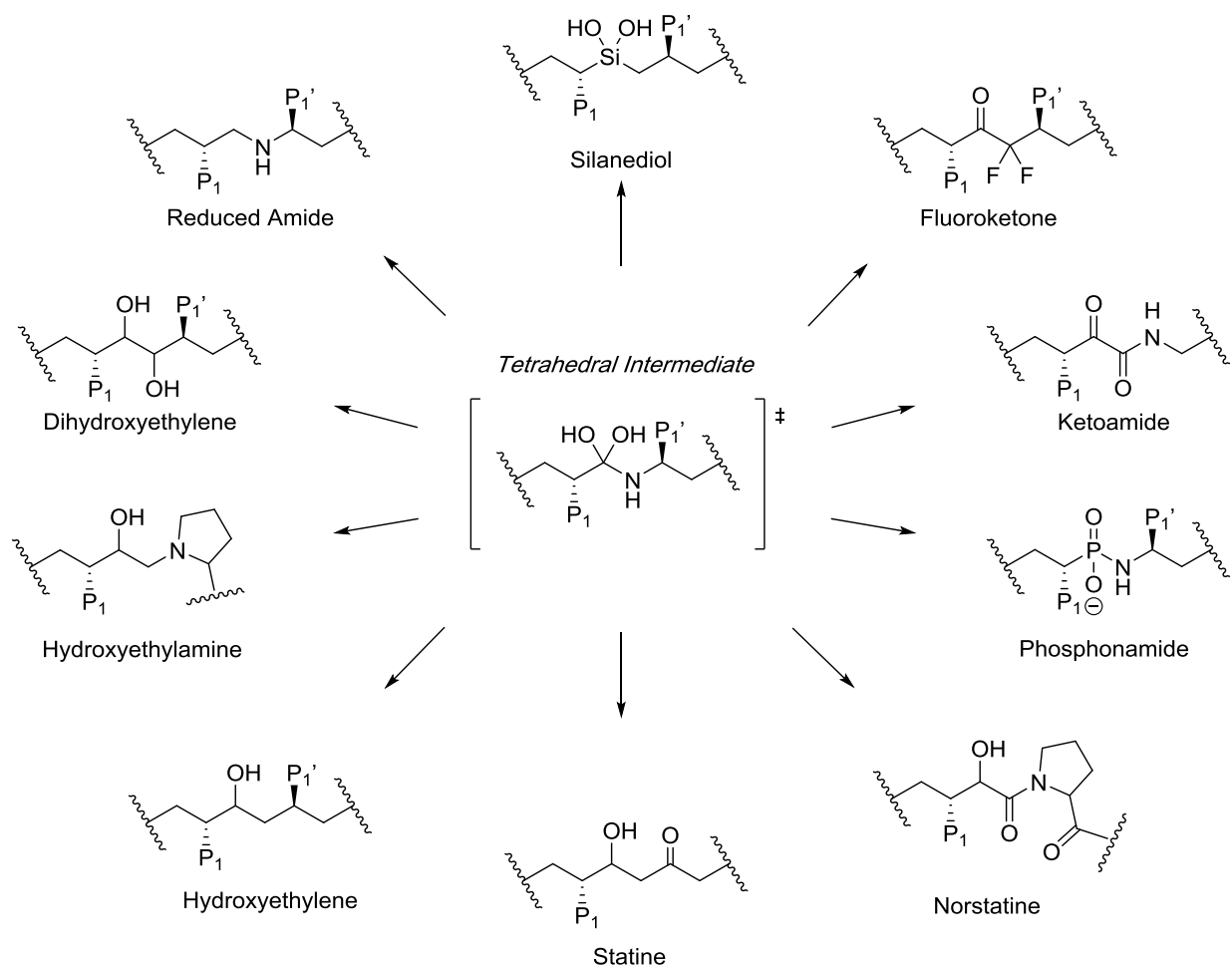


Figure 1.14 Non-hydrolyzable Transition State Isosteres for HIV-1 Protease Inhibitors⁷⁰

1.6.1 First Generation HIV Protease Inhibitors

1.6.1.1 Saquinavir

Saquinavir (SQV) was the first FDA-approved HIV-1 protease inhibitor and marked the incorporation of highly active antiretroviral therapy (HAART). Developed by Hoffman-La Roche in 1990, this protease inhibitor was officially approved for therapeutic use in 1995. Hoffman-La Roche had comprised a team of scientists to develop protease inhibitors through rational design which originally began with transition-state peptidomimetics. Based upon the observation that HIV PR tends to cleave Phe-Pro and Tyr-Pro peptide bonds, it was believed the incorporation of this dipeptide sequence within the inhibitor would promote selectivity for the viral enzyme (Figure

1.15).⁷² To accommodate these structural features, an acceptable transition-state isostere was investigated. The transition-state isostere with the (*R*)-hydroxyethylamine isostere was incorporated into **1** and exhibited an IC₅₀ value of 750 nM. The stereochemistry of the central hydroxyl group was important for potency within the active site, as discovered through crystal structure analysis.⁷³ Inhibitor **1** extended into the S₃ subsite which initiated optimization efforts to reduce the overall size of the inhibitor while maintaining key binding interactions. With the transition-state isostere intact, the overall size of the backbone of the inhibitor was reduced to occupy subsites S₃ – S₂' and resulted in the identification of inhibitor **2** with an IC₅₀ value of 18 nM. Further structural modifications led to the design of SQV which utilizes a (*S,S,S*)-decahydro-isoquiniline-3-carbonyl (DIQ) moiety as a key P₁' subunit.

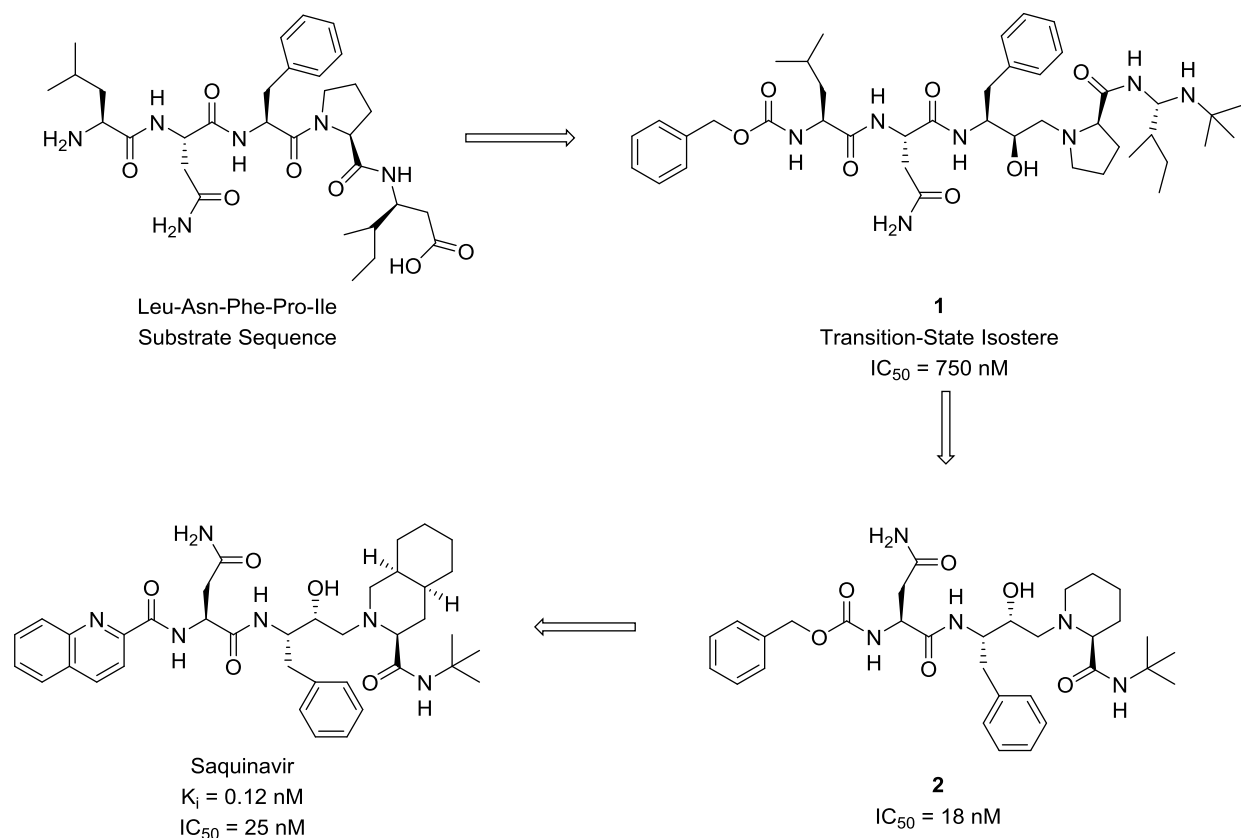


Figure 1.15 Development of Saquinavir Based on Substrate Sequence⁷⁴

Saquinavir is a very potent HIV-1 protease inhibitor with a K_i value of 0.12 nM and an IC_{50} value of 25 nM. The potency of SQV can be explained through the crystal structure of the inhibitor bound to the active site of the enzyme (Figure 1.16). SQV binds to the protease enzyme in an extended fashion where the central hydroxyl group interacts tightly with the catalytic Asp25 and Asp25' residues. The carbonyls of the *tert*-butyl amide and the central amide participate in water-mediated hydrogen bonding with the Ile50 and Ile50' residues of the flap region. The carbonyl of the quinoline amide picks up an interaction with Asp29 and the terminal amide interacts with Asp29 and Asp30 in the S_2 subsite.

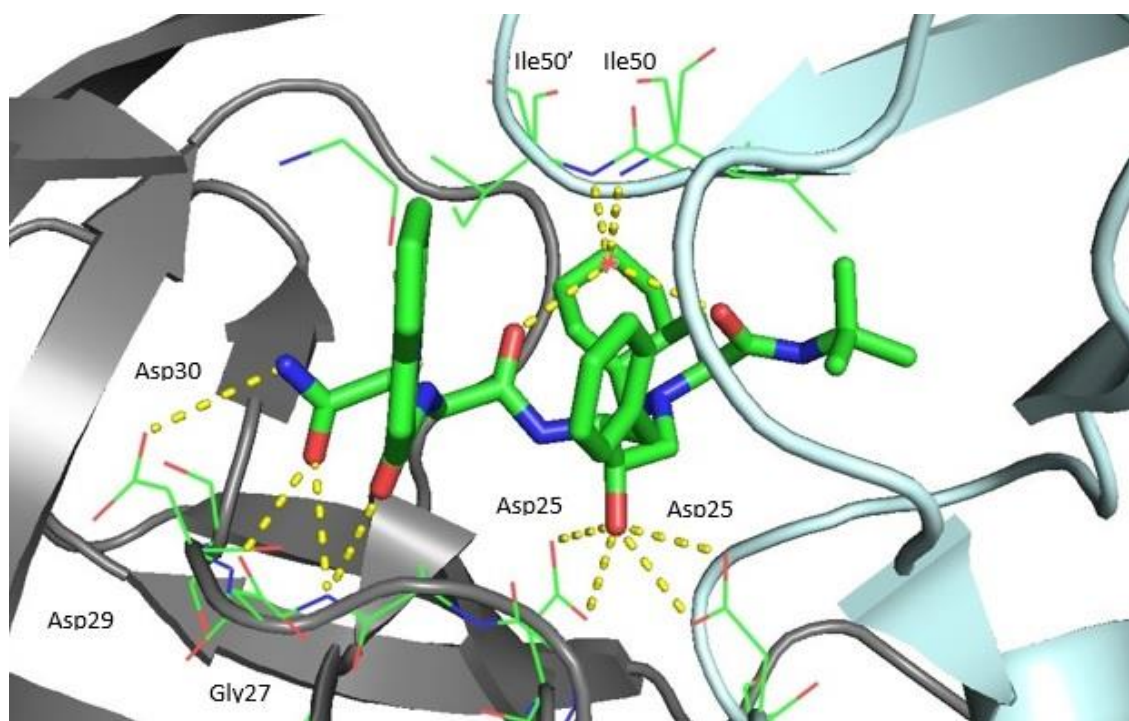


Figure 1.16 Crystal Structure of SQV-Bound HIV Protease^{73,75}
(Recreated based upon literature)

1.6.1.2 Ritonavir

Ritonavir, developed by Abbott Laboratories, was the second FDA-approved HIV-1 protease inhibitor. The design of this protease inhibitor was based upon the structural feature of the HIV protease enzyme. Since the PR is a homodimer, it was theorized the active site should

exhibit C_2 symmetry and the subsites S_1 and S_1' should be indistinguishable.⁷⁶ This led to the design and development of C_2 symmetry-based inhibitors in which the transition state of the peptide hydrolysis is also considered. The peptide bond, which would normally be proteolytically cleaved, was replaced with either a 1,2-diol or a central secondary alcohol, as shown in A-77003 and A-80987 (Figure 1.17).⁷⁷ The exploratory results of A-77003 were less than desirable as this inhibitor presented poor oral bioavailability, but promising enzymatic inhibition.⁷⁸ Efforts focusing on improving oral bioavailability resulted in the identification of A-80987. Unfortunately, A-80987 exhibited high metabolic clearance due to the presence of the pyridinyl substituents. Metabolic experiments determined the by-products observed were the resulting N-oxides of the pyridinyl amines.⁷⁹ To effectively combat the metabolic issue, the pyridinyl groups were replaced with thiazole heterocycles. Introduction of the thiazole groups not only enhanced metabolic stability, but enhanced potency, aqueous solubility, and pioneered the development of Ritonavir ($K_i = 0.015$ nM). The large improvement of potency of Ritonavir, compared to A-80987, can be explained through XRC analysis. The isopropyl substituent of the thiazole heterocycle presents an additional hydrophobic interaction with Pro81 and Val82.⁷⁹

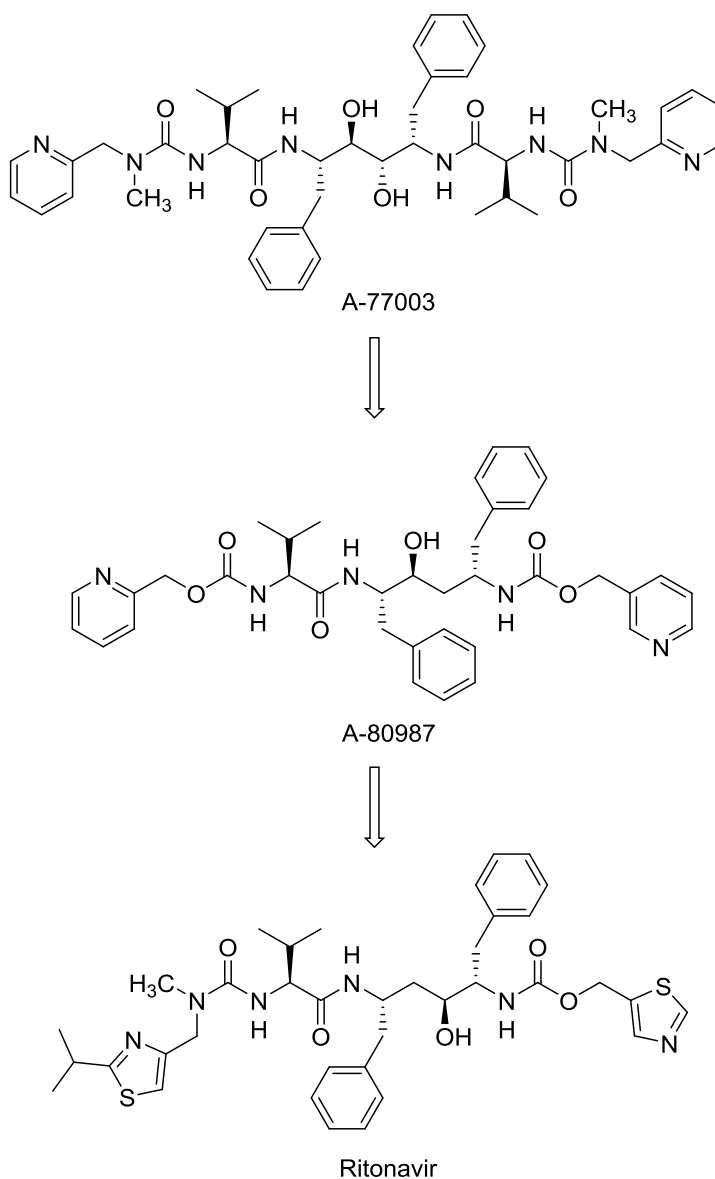


Figure 1.17 Development of Ritonavir from Lead Compound A-77003

The discovery of Ritonavir led to a unique observation in terms of potential medical uses. Although a potent inhibitor for HIV PR, it was soon discovered that Ritonavir was also an inhibitor of a common metabolic enzyme, cytochrome P4503A4 (CYP450). Metabolization of Ritonavir has been documented to occur through several possible sequences: demethylation of the nitrogen, oxidation and cleavage of the isopropyl thiazole moiety, and hydroxylation of the isopropyl side chain.^{80,81} Structural analysis indicates the nitrogen of the thiazole heterocycle binds to the heme center of the cytochrome enzyme resulting in affinity for the inhibitor.⁸² From these observations,

Ritonavir has been utilized as a pharmacokinetic booster to assist in maintaining higher levels of other protease inhibitors.

1.6.1.3 Indinavir

Indinavir was developed by Merck Laboratories using the transition-state mimetic concept established from the experience of renin inhibitors. From this concept, Merck identified a lead compound, L-682,679 (Figure 1.18).⁸³ This inhibitor was extremely peptidic in nature and led to the incorporation of the hydroxyethylene isostere to improve metabolic stability. Further structural modifications identified a 2-hydroxyindan P₂' ligand substitute for the C-terminal dipeptide unit of the lead compound L-682,679 and introduced inhibitor L-685,434.⁸⁴ Regardless of potency, L-685,434 was poorly soluble in aqueous media and lacked an ideal pharmacokinetic profile. Using SQV as inspiration, researchers at Merck hypothesized that by incorporating a basic amine into the backbone of the inhibitor, the solubility and bioavailability of the inhibitor could be improved.⁸⁵ Cyclic amines were investigated because of the limited conformational change that would occur within the active site of the enzyme. Of the cyclic amine family units, the piperazine moiety was more potent than proline, DIQ, and piperidine analogs. Conceivably, the attendance of two nitrogens in the piperazine ring, as shown in L-732,747, could significantly enhance solubility and provide an additional nitrogen as a molecular handle for further modification if necessary. Optimization of the piperazine subunit in ligand L-732,747 led to the development of Indinavir which features a 3-pyridylmethyl unit as a P₂ ligand and exhibits a K_i of 0.36 nM.⁸⁶

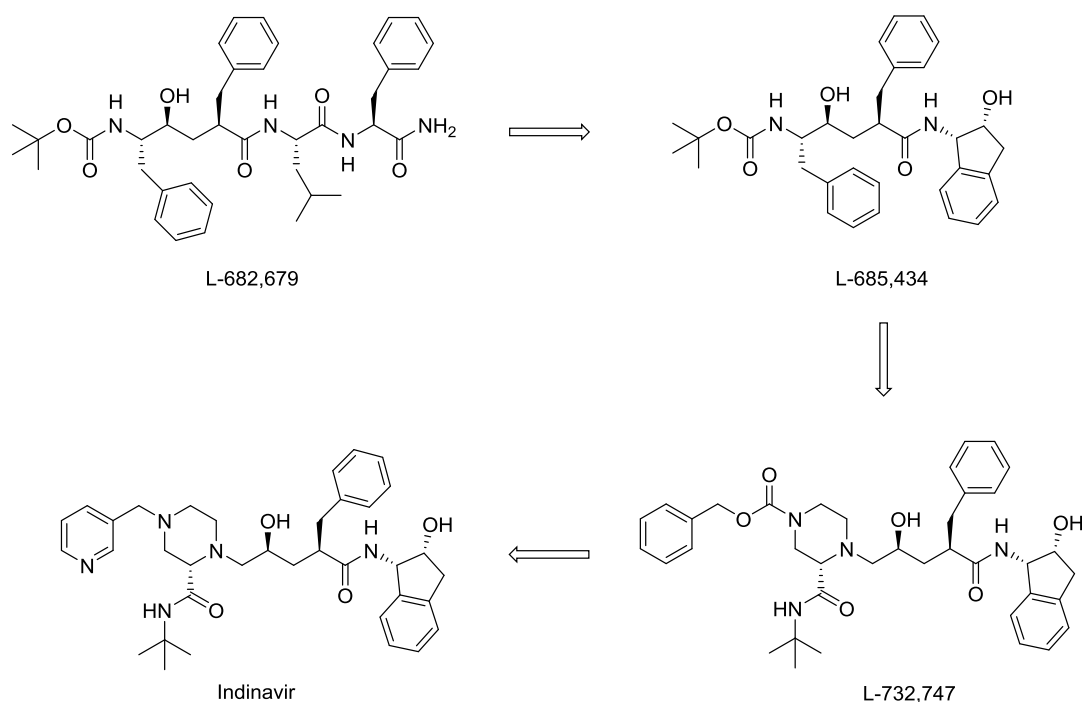


Figure 1.18 Development of Indinavir from Lead Compound L-682,679

1.6.1.4 Nelfinavir

The approach to the identification and development of Nelfinavir was unique compared to previously approved protease inhibitors. Rather than designing inhibitors based upon the transition-state, Agouron Pharmaceuticals and Eli Lilly decided to investigate potential inhibitors through iterative crystal structure analysis of the enzyme with previously developed peptidomimetic inhibitors (Figure 1.19).⁸⁷ In conjunction with the crystal structures obtained, a program known as the Monte Carlo De Novo Ligand Generator assisted in identifying potential hydrophobic groups to incorporate into the correct subsites.⁸⁸ Investigation into novel protease inhibitors were initiated by designing ligands to mimic the Phe-Pro substrate sequence, similar to SQV. The proline sequence was replaced with substituted benzamide subunits to reduce the structural complexity while experimenting with various substitutions on the phenyl ring. Based upon known HIV-1 protease – inhibitor crystal structures, placement of the *tert*-butyl amide on the ortho position should participate in hydrogen bonding with a water molecule residing in the flap region.⁸⁹ Early SAR data of various substituted benzamide subunits identified compound LY289612 as the lead compound with an initial K_i value of 1.5 nM.

Structural analysis indicated the P₃ quinoline and P₁ phenyl groups were extremely close in nature. Optimization efforts of LY289612 were focused on modifying the P₁ subunit to occupy the S₁ and S₃ subsite while replacing the quinoline moiety with a smaller subunit. Ultimately, the phenyl group was replaced with a thio-naphthyl group, where the sulfur enhanced the hydrophobic interaction within the S₁ subsite, and the quinoline group was replaced with an acetamide subunit. These modifications are observed in LY297135 with an IC₅₀ value of 1.1 nM.⁹⁰

Inhibitors LY289612 and LY297135 presented potent antiviral activity, but lacked proper bioavailability due to the highly peptidic nature of these inhibitors. The P₂ subunit was modified to incorporate a substituted phenol ring that would enhance solubility while maintaining potency within the enzyme and produced AG1254.⁹¹ In an effort to further improve the bioavailability properties, inspiration was drawn from SQV to include the hydroxyethylamine isostere and the DIQ moiety as a P1' ligand. Reducing the size of the naphthyl group to a thio-phenyl group substantially improved enzyme inhibitory activity and provided Nelfinavir.⁹²

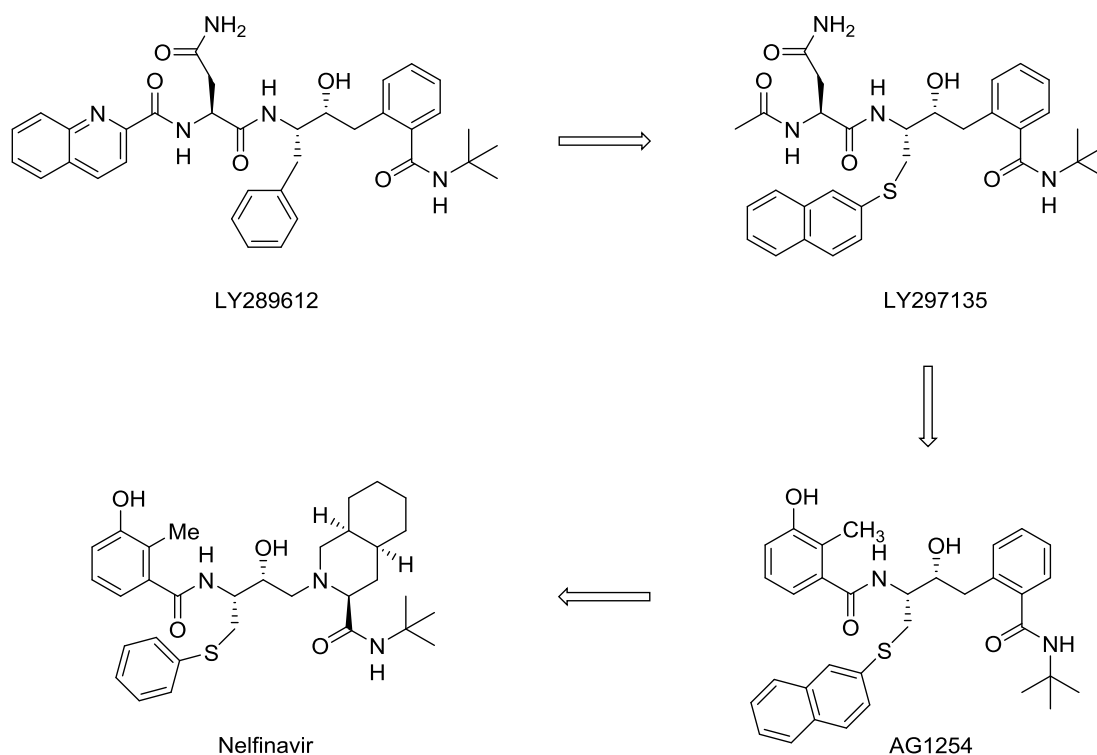


Figure 1.19 Development of Nelfinavir from Lead Compound LY289612

1.6.1.5 Amprenavir

Amprenavir was developed by Vertex Pharmaceuticals and approved by the FDA in 1999 (Figure 1.20). This protease inhibitor was the result of a structure-based design program that sought to apply structural information collected from previous angiotensin converting enzyme inhibitors and previous protease inhibitors thus far. The structure-based design method seeks to incorporate molecular motifs in the inhibitor to interact with specific residues within the active site of the enzyme while maintaining an optimal pharmacological profile. The goal was to promote interactions with the catalytic Asp residues, sustain water-mediated flap interactions, and maintain conformational stability within the protease. The crystal structure of Amprenavir-bound HIV-1 protease revealed the key interactions responsible for the biological profile. The central hydroxyl group interacts with the catalytic Asp25 and Asp25' residues thus positioning the tetrahydrofuranyl (THF) ring into the S_2 subsite causing interactions between the oxygen and residues Asp29 and Asp30. The novel aminobenzenesulfonamide moiety is positioned into the S_2' subsite where one oxygen of the sulfonyl participates in water-mediated hydrogen bonding with the flap region and the second oxygen fits into the hydrophobic pocket between Ile50 and Ile84. Furthermore, there are interactions observed between the amine and Asp30'. Based upon these interactions, Amprenavir was shown to have a K_i of 0.6 nM.⁹³

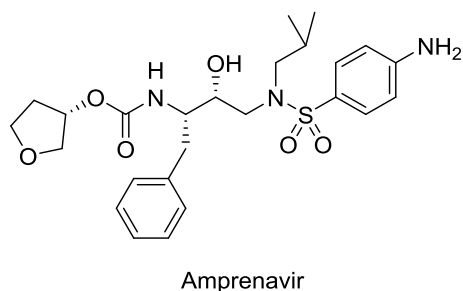


Figure 1.20 Structure of Amprenavir

The first generation protease inhibitors were highly peptidic in their chemical structure. This structural feature resulted in low half-life, high metabolic clearance, poor oral bioavailability, and undesirable side effects. More importantly, drug-resistant strains of HIV began to emerge and rendered these therapies almost ineffective. The focus was shifted to design protease inhibitors

that could tackle the problem of drug-resistant strains while improving overall efficacy. Therefore, a second generation of protease inhibitors erupted.

1.6.2 Second Generation HIV Protease Inhibitors

1.6.2.1 Lopinavir

Lopinavir was developed by Abbott Laboratories and was approved by the FDA in 2000. This protease inhibitor marked the introduction of the second generation of protease inhibitors to overcome the obstacles presented by the first generation. One of the major obstacles observed with the first generation were mutations of the enzyme resulting in loss of activity. Specifically, Lopinavir was developed to combat the mutation of Val82 that led to the resistance of Ritonavir (Figure 1.21). The isopropyl side chain of the thiazole heterocycle exhibited hydrophobic interactions with Val82 where mutations caused disruption.⁹⁴ Initial experiments with Val82A, Val82F, and V82T mutations proved the inhibitory profile of Ritonavir diminished substantially.⁹⁵ The key structural modifications of Lopinavir include the replacement of the isopropylthiazole group with a cyclic urea and the thiazole heterocycle was altered to a phenoxyacetyl group. Structural models indicated the cyclic urea interacts with Asp29 and Asp30 in the S₂ subsite and the smaller nature of Lopinavir prevented hydrophobic interactions with Val82. The reduced interaction with Val82 led to an increase in potency, with a K_i value of 1.3 pM, and the ability to overcome Val82 mutations.

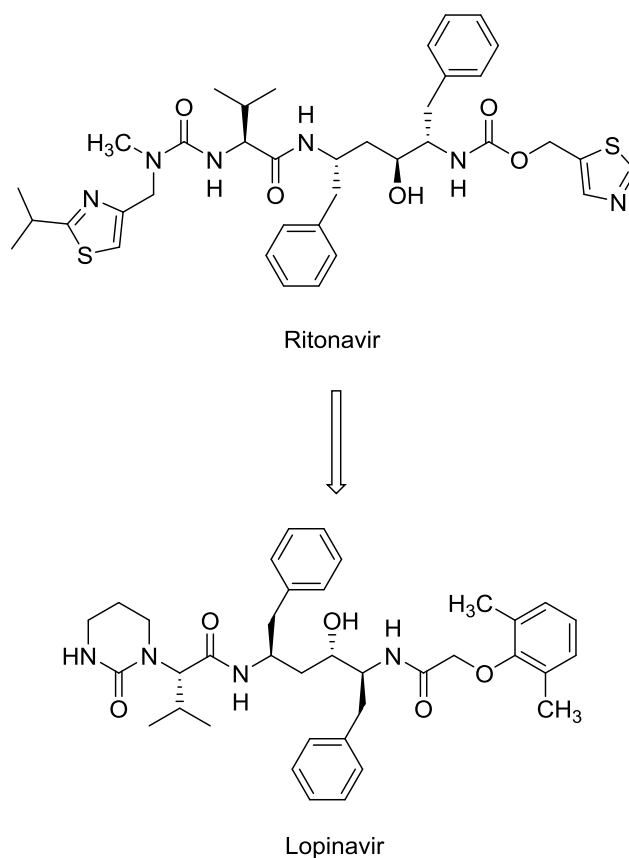


Figure 1.21 Development of Lopinavir from Ritonavir

1.6.2.2 Atazanavir

The purpose behind the development of Atazanavir was to create a protease inhibitor with potent antiviral activity and better bioavailability compared to other PI's at this time. The strategy to accomplish this goal involved synthesizing a novel hydroxyethyl hydrazine dipeptide isostere to replace the traditional hydroxyethylene isostere. In this model, the P_1' subunit would be attached to a nitrogen atom which eliminates a stereogenic center and allows for easy manipulation for SAR studies. Results from the initial screening of inhibitors featuring the hydrazine isostere identified CGP53820 as a very potent inhibitor with an IC_{50} value of 9 nM (Figure 1.22).⁹⁶

Structural analysis of CGP53820 indicated the desired interactions as the P_1 phenyl and P_1' cyclohexyl subunits accommodate the S_1 and S_1' subsites while the central hydroxyl moiety binds tightly to the catalytic Asp25 and Asp25' residues.⁹⁷ Further analysis indicated the S_1 subsite could house larger P_1 ligands, as compared to cyclohexyl, while the P_3 , P_2 , P_2' , and P_3' ligands could be expanded in a parallel fashion. However, the carbonyl of the acyl group was important for antiviral

activity which restricted the functional groups to either an amide or carbamate for SAR studies.⁹⁸ Expansion of the P₁' ligand from a cyclohexyl unit to a pyridylbenzyl group successfully occupied the S₁' – S₃' subsites and led to the development of Atazanavir.⁹⁹ A crystal structure of Atazanavir-bound HIV-1 protease confirms the extensive hydrogen bond network within the active site.¹⁰⁰ Atazanavir displayed potent antiviral activity with an EC₅₀ range of 2.6 to 5.3 nM and EC₉₀ range of 9 to 15 nM and superior bioavailability properties.¹⁰¹

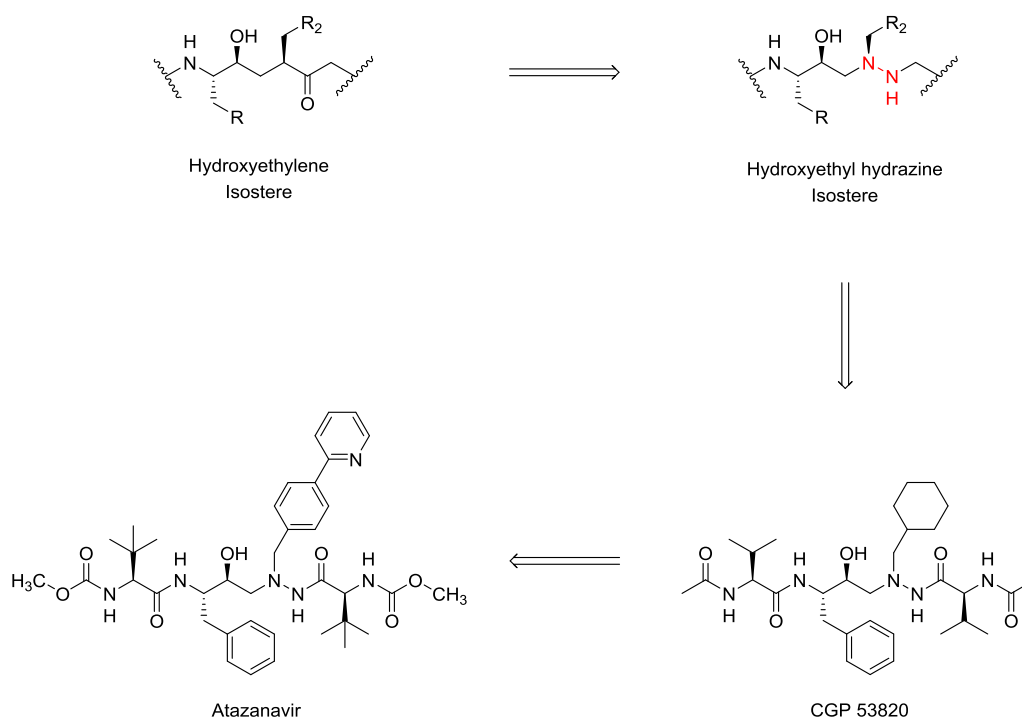


Figure 1.22 Conceptual Design of Atazanavir

1.6.2.3 Tipranavir

Tipranavir, discovered by Pharmacia & Upjohn, is a non-peptidic protease inhibitor in which the traditional transition-state isostere is absent. Instead, this protease inhibitor features a novel 5,6-dihydro-4-hydroxy-2-pyrone scaffold in which the hydroxyl moiety is the central subunit of the inhibitor. The development of this inhibitor began through an initial fluorescence-based screening of a molecular library that identified the phenprocoumon molecule as a potential small-molecule inhibitor for HIV-1 protease; initial K_i value of about 1 μ M (Figure 1.23).¹⁰² Initial crystal structure analysis of phenprocoumon-bound HIV-1 protease revealed the ethyl chain lies

in the S_1 subsite, the phenyl ring resides in the S_2 subsite, and the fused benzene ring is not adequately housed within the S_1' subsite. Expansion of the inhibitor to fill the active site from $S_2 - S_2'$ resulted in the identification of PNU-96988 ($K_i = 38$ nM) where the ethyl subunits lie within S_1 and S_1' while the phenyl rings reside in S_2 and S_2' , respectively.¹⁰²

While the pharmacokinetic profile of phenprocoumon and PNU-96988 was acceptable, the antiviral potency was modest with micromolar IC_{50} values. Optimization efforts were then aimed at significantly enhancing potency through iterative structural analysis of inhibitor-bound HIV-1 protease. Investigation into this process led to the discovery that an improvement in potency could be obtained with the introduction of an amide or carbamate linkage, likely associated with the increase in hydrogen bond donors and acceptors within the inhibitor. Further optimization results indicated an increase in potency with the presence of a sulfonamide group and expansion of the inhibitor ligand with the cyclooctane ring resulting in the development of PNU10317 ($K_i = 0.8$ nM, $IC_{50} = 1.5$ μ M).¹⁰³ Modifications to PNU-103017 included replacing the cyclooctane ring with two separate alkyl-based moieties and a 5-(trifluoromethyl-2-pyridyl) subunit to replace the 4-cyanophenyl group and provided Tipranavir ($K_i = 8$ pM, $IC_{50} = 100$ nM).^{103,104}

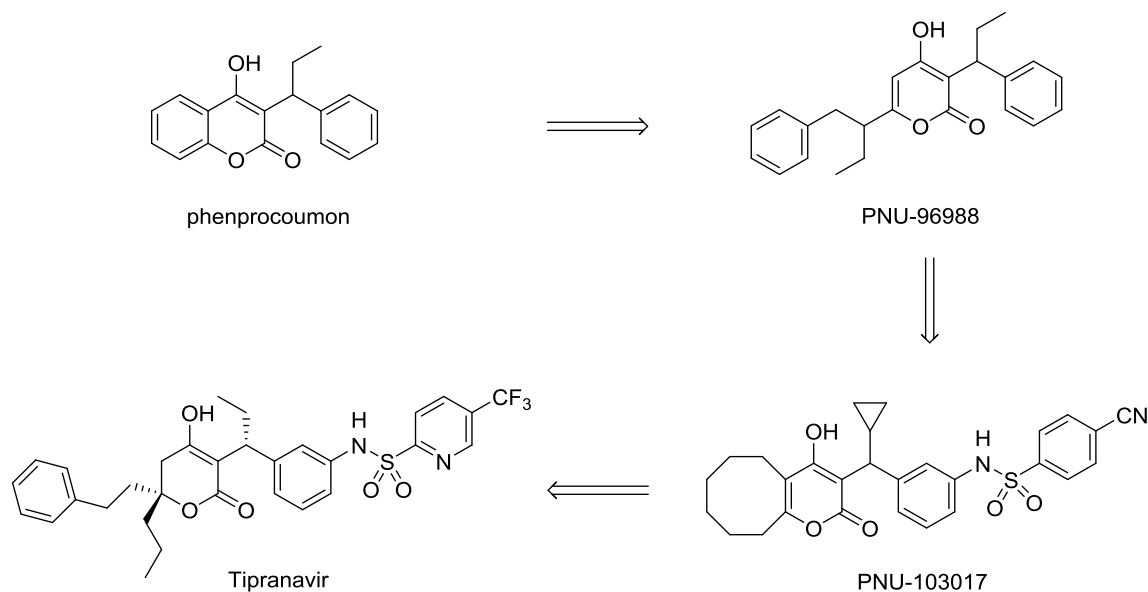


Figure 1.23 Identification of Tipranavir from Phenprocoumon Lead Compound

1.6.2.4 Darunavir

Darunavir (DRV) is the first FDA approved protease inhibitor to be used as a first-line treatment option for those affected by HIV. The superb biological profile of DRV against wild-type and multidrug-resistant HIV strains can be interpreted through the structural features and unique mechanism of action. The development of DRV can be traced back to simple structural modifications of SQV (Figure 1.24). SQV, a very potent inhibitor, suffered from complications with oral bioavailability due to the highly peptidic nature of this compound. To improve upon these properties, the amide functionality was replaced by a configurationally restricted cyclic ether. Cyclic ethers are prominent in biologically active natural products and can serve as amide surrogates to reduce the peptidic nature, provide hydrogen bond accessibility, and improve pharmacokinetic properties.¹⁰⁵

Investigation into the biological properties of cyclic ether units was initiated by replacing the carbonyl that binds to Asp29 with a THF moiety to target interactions within the S₂ subsite and provided inhibitor **3**. Results of the THF unit demonstrated a higher potency than SQV.¹⁰⁶ To further study the influence of the cyclic ether, the P₃ quinoline subunit of SQV was completely removed to provide inhibitor **4**. Interestingly enough, this inhibitor still exhibited potent activity and provided sufficient reasoning to explore the cyclic ether scaffold further. The THF scaffold was then incorporated into a hydroxyethylene isostere, as presented in Indinavir, to produce inhibitor **5** and displayed a significant increase in potency from inhibitor **4**.¹⁰⁷ Based upon ligand-enzyme structural analysis, the oxygen of the THF subunit consistently showed interactions with the Asp29 and Asp30 backbone residues. However, details of these structural studies revealed the chemical space available within the S₂ subsite. Optimization efforts were then focused towards developing a cyclic ether in which the chemical space of the S₂ subsite could effectively be filled while improving upon the backbone interactions displayed from inhibitor **5**.

From these efforts, a stereochemically defined bicyclic *bis*-tetrahydrofuranyl (*bis*-THF) P₂ ligand was generated.¹⁰⁸ The utility of this novel P₂ ligand was discovered upon incorporation with the hydroxyethylene isostere in **4** to provide inhibitor **6**. Inhibitor **6** presented higher potency, better oral bioavailability, and smaller molecular weight compared to the SQV counterpart. Structural analysis confirm both oxygens are participating in interactions with Asp29 and Asp30 residues.¹⁰⁹ Biological activity was dependent upon the placement, and presence, of the oxygen atoms as the removal of either oxygen resulted in a decrease in activity, as displayed by inhibitors

7 and 8. These results confirm the *bis*-THF P₂ ligand is a promising scaffold for future protease inhibitors.

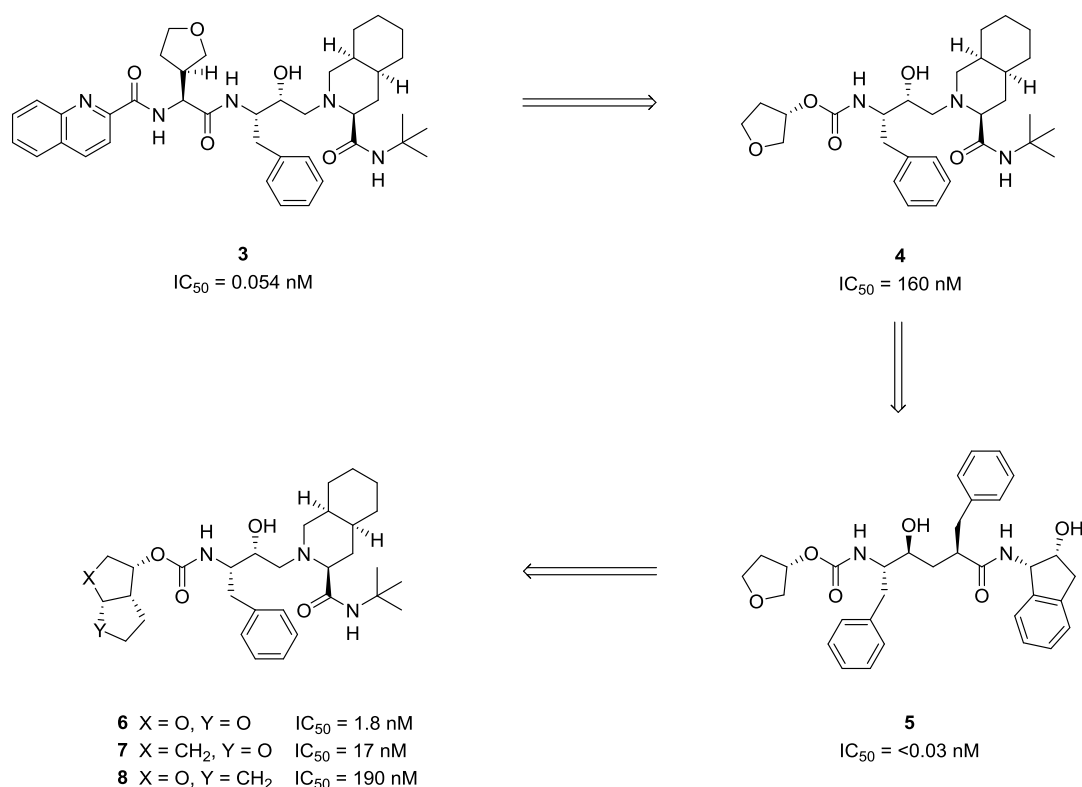
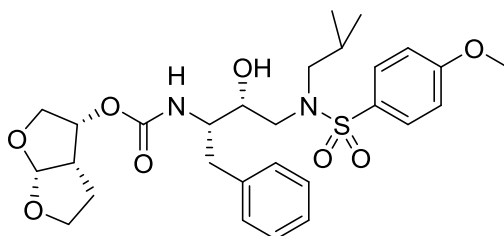


Figure 1.24 Development of *bis*-THF P₂ Ligand^{105,110}

After the discovery of the *bis*-THF ligand, attention was then turned to optimization efforts of the non-hydrolyzable transition-state isostere. The choice of isostere was important as the purpose was to not only mimic the transition state of the proteolysis, but to improve upon the potency and bioavailability of previously approved protease inhibitors. This could be accomplished by incorporating a bioisostere in which extensive hydrogen bonding with the backbone residues of the protease could occur.

The first isostere to be invoked was a (hydroxyethylamine)sulfonamide with a methoxy substitution at the *para* position, as shown in TMC-126 (Figure 1.25). This inhibitor exhibited a remarkable enzyme inhibitory profile with a *K_i* of 14 pM and an IC₉₀ of 1.4 nM.¹¹¹ Insight into the biological activity profile can be explained from its crystal structure bound to HVI-1 protease (Figure 1.26). The oxygens of the *bis*-THF P₂ ligand are interacting with Asp29 and Asp30

while the central hydroxyl group is hydrogen bonding to the catalytic Asp25 and Asp25' residues. The carbonyl oxygen of the carbamate and an oxygen from the sulfonyl participate in water-mediated hydrogen bonding with Ile50 and Ile50' of the flap region. The methoxy substituent fills the S_2' subsite effectively and binds with Asp30'. The phenyl P_1 subunit and isopropyl P_1' subunit are housed within the S_1 and S_1' subsites, respectively.¹¹²



TMC-126
 $K_i = 14 \text{ pM}$
 $IC_{90} = 1.4 \text{ nM}$

Figure 1.25 Structure of TMC-126 with *bis*-THF P_2 Ligand

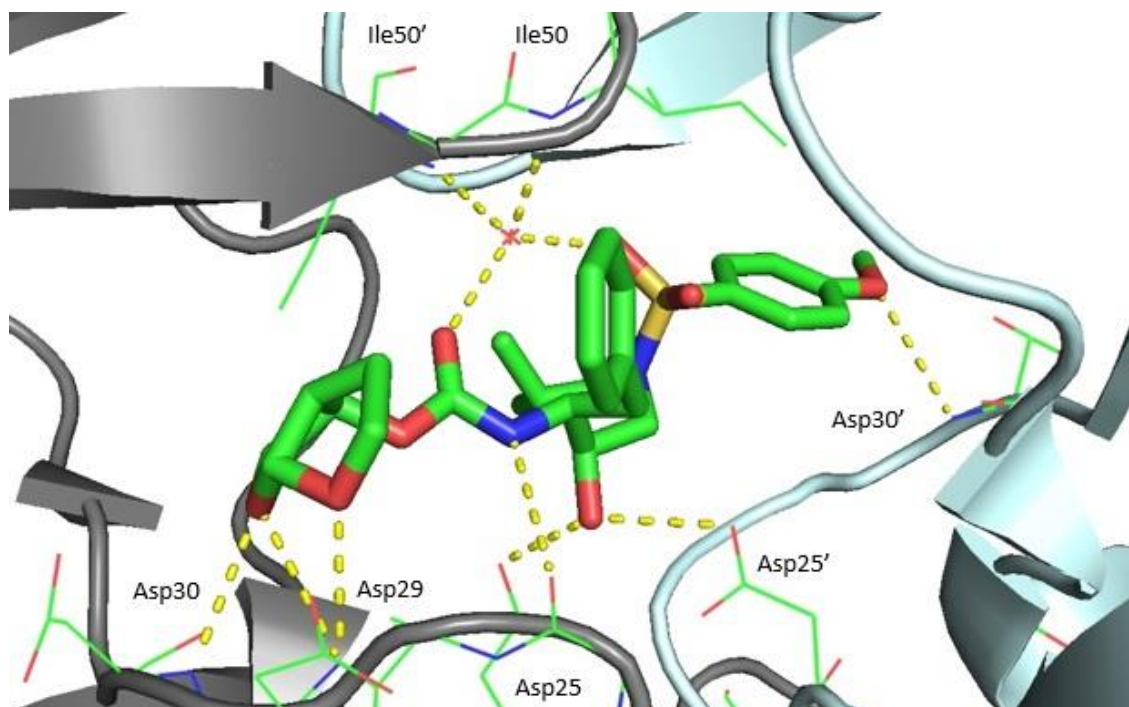
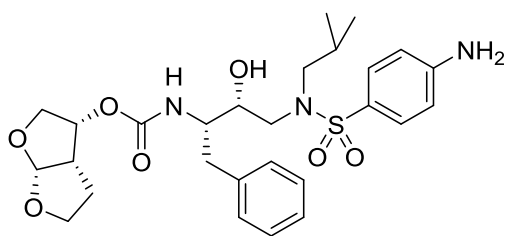


Figure 1.26 Crystal Structure of TMC-126-Bound to HIV-1 Protease¹¹²
 (Recreated based upon literature)

The second isostere to be studied was a similar (hydroxyethylamine)sulfonamide isostere as TMC-126, but the methoxy substituent was replaced with an amine to provide Darunavir (Figure 1.27). In comparison to TMC-126, Darunavir exhibited a similar biological profile ($K_i = 16$ pM, $IC_{90} = 4.1$ nM) while maintaining similar interactions within the active site. Crystal structure of Darunavir-bound HIV-1 protease shows the *bis*-THF interactions with Asp29 and Asp30 while the hydroxyl group continues to interact with Asp25 and Asp25' (Figure 1.28). Other backbone interactions include those with Gly27, Ile50, Ile50', and the terminal amine interacts with Asp30' similar to the methoxy subunit.²⁸



Darunavir
 $K_i = 16$ pM
 $IC_{90} = 4.1$ nM

Figure 1.27 Structure of Darunavir with *bis*-THF P₂ Ligand

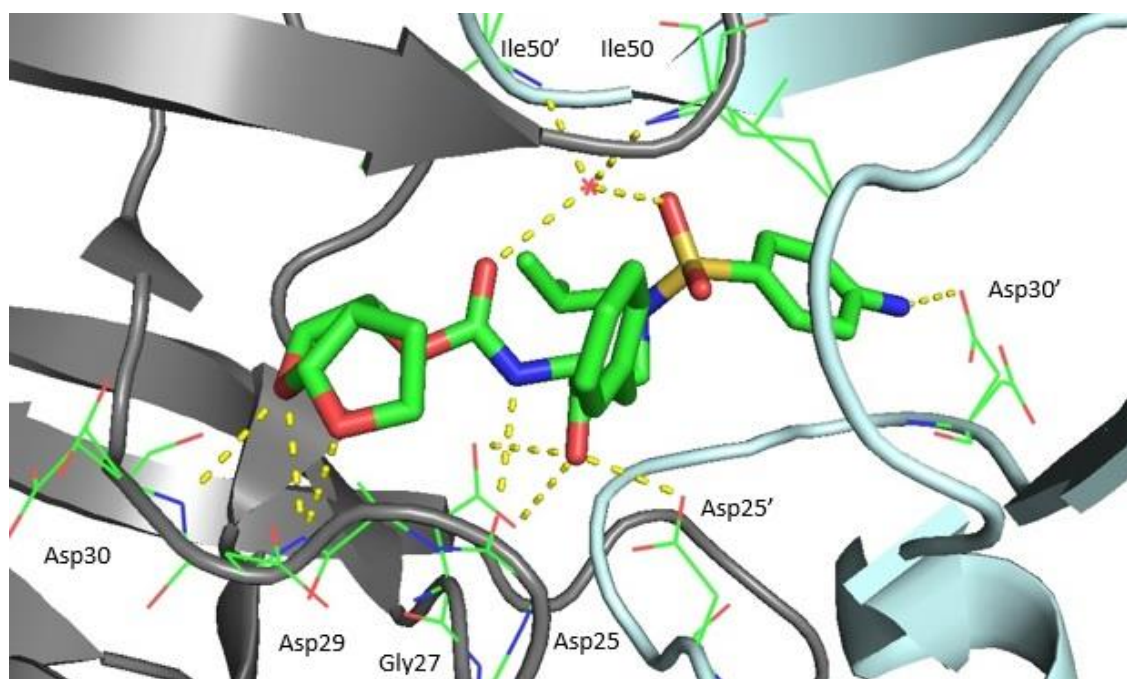


Figure 1.28 Crystal Structure of Darunavir-Bound HIV-1 Protease¹¹³

(Recreated based upon literature)

While DRV is extremely potent, the mode of action and biological profile are just as intriguing. It has been shown that DRV has two mechanisms of action: DRV inhibits the dimerization process of HIV-1 protease while also inhibiting dimeric, fully functional HIV-1 protease activity.¹¹⁴ Further structural analysis of Darunavir with several mutant proteases revealed consistent hydrogen bond interactions with the backbone residues among the various mutant strains. As determined from TMC-126 and DRV, these interactions are important for biological activity. Therefore, targeting interactions between the inhibitor and the backbone residues has led to the development of the backbone binding concept.

1.7 Combatting Drug Resistance

While the evolution of the protease inhibitor class from SQV to DRV has certainly been remarkable, it is of interest to divulge the persistent problem of drug resistance. Both first and second generation protease inhibitors currently have mutant variant HIV-1 strains in which these therapies are ineffective. Introduction of mutant viral strains can be rationalized through the HIV

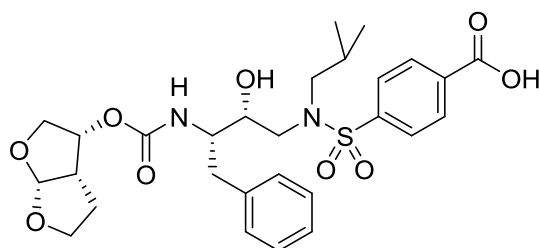
replication cycle. HIV has a high viral replication rate of $10^8 - 10^9$ virions per day and the reverse transcription process is extremely error prone due to the lack of a proofreading mechanism.^{70,115} This leads to an error rate of about 1 in 10,000 bases and increases the probability of genetic mutants being introduced into the system.¹¹⁶ The resulting mutations can affect the ability of an inhibitor to effectively stop the viral replication.

Mutations of HIV-1 PR can be classified into primary and secondary subsets. Primary mutations are observed within the active site of the enzyme, specifically with residues responsible for substrate binding. While these mutations typically alter the enzyme-substrate binding capacity, the catalytic residues remain natural as mutations of the Asp25 and Asp25' residues result in impaired proteolytic activity.¹¹⁷ Secondary mutations are observed away from the active site and do not affect the catalytic activity of the enzyme.

The observation of these particular mutations has led to numerous design strategies to combat the problem of drug resistance through mutation. In particular, when comparing the wild-type HIV-1 PR crystal structure to that of various mutant strains there is a unique structural pattern observed. The backbone conformation of the wild-type HIV-1 PR, along with the mutant variants, remains largely unchanged.^{118,119} It was hypothesized that by designing a protease inhibitor in which the interactions with the backbone residues are maximized, then the ability of the inhibitor to combat drug-resistant mutant strains may be promising. This has led to the development of the “backbone binding” strategy as a means to design and develop effective protease inhibitors.^{110,113}

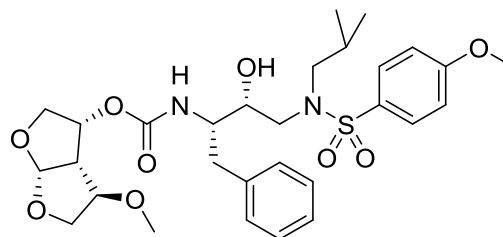
Application of the backbone binding concept has led to the development of novel protease inhibitors demonstrating exceptional binding affinity for the HIV protease. Examples of these inhibitors are shown below (Figure 1.29).²⁸ From the inhibitors presented, there have been structural changes in different regions of the molecule. Some variations include the size and atomic nature of the P₂ ligand to investigate a fused bicyclic system with two oxygens in comparison to a single ring system with the same number of oxygens in similar locales. Other modifications include variance in the aromatic substituent to provide an additional hydrogen bond interaction. However, the backbone binding concept provides unique insight into how the newly designed inhibitor may bind within the active site. A representative model for the binding mode of these inhibitors is demonstrated below (Figure 1.30). The targeted key residues include Asp29, Asp30, Gly27, Gly48, Asp25, Ile50, Asp25', Ile50', Asp29', and Asp30'. On the basis of structural modification, the backbone binding concept allows us to design a diverse array of

inhibitors that target the conserved backbone residues of the active site to combat HIV/AIDS while overcoming drug-resistant mutations.



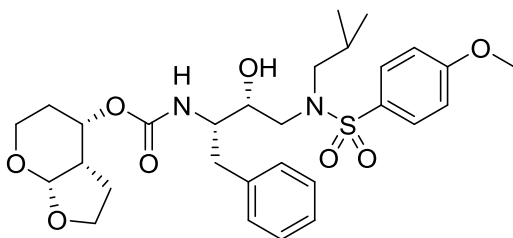
9

$K_i = 12.7 \text{ pM}$
 $EC_{50} = >10 \text{ }\mu\text{M}$



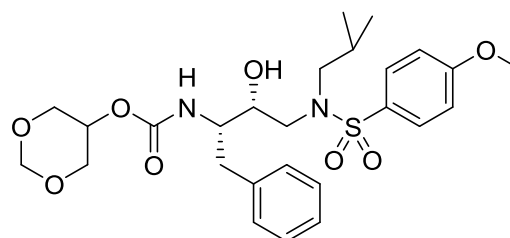
10

$K_i = 0.0029 \text{ nM}$
 $IC_{50} = 2.4 \text{ nM}$



11

$K_i = 0.0027 \text{ nM}$
 $IC_{50} = 0.0005 \text{ }\mu\text{M}$



12

$K_i = 41 \text{ pM}$
 $IC_{50} = 3.4 \text{ nM}$

Figure 1.29 HIV-1 Protease Inhibitors Developed from Backbone Binding Concept

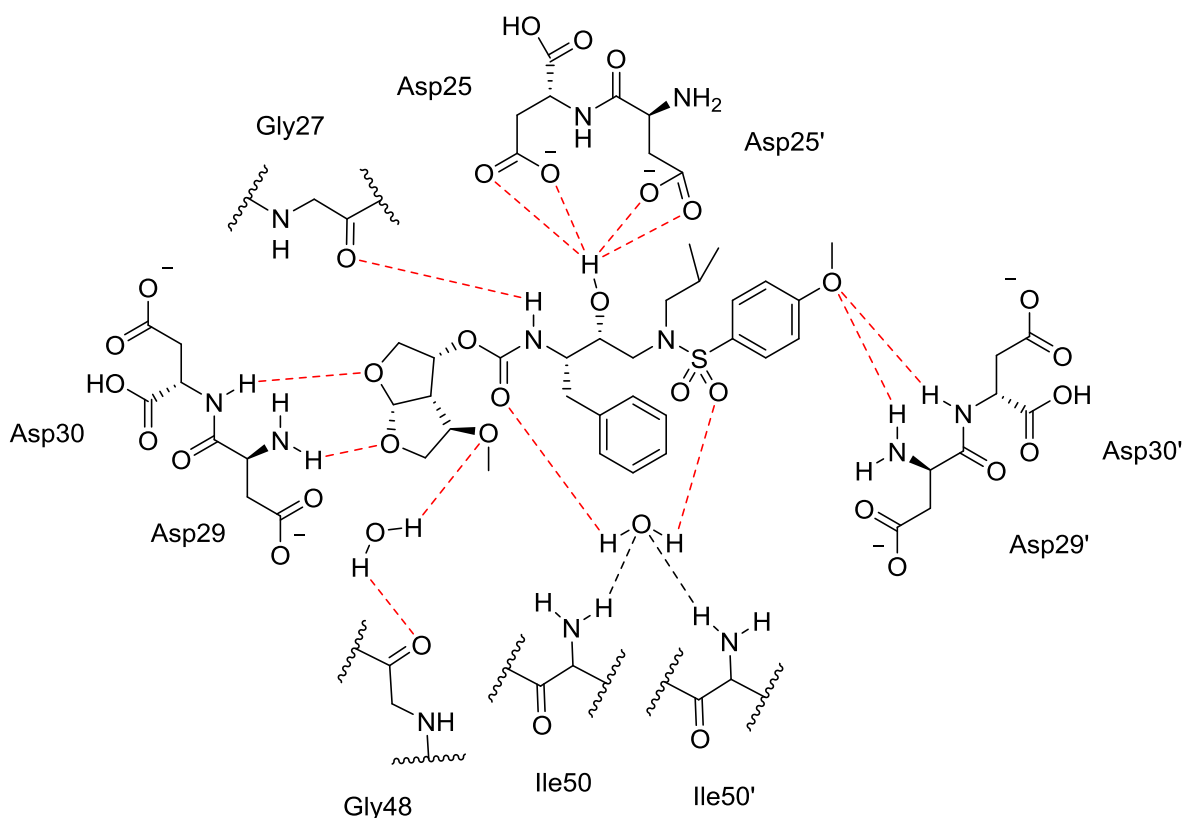


Figure 1.30 Representative Binding Mode of HIV-1 Protease Inhibitors Modeled with Inhibitor **10²⁸**
(Recreated based upon literature)

1.8 Design, Synthesis, and Biological Evaluation of HIV-1 Protease Inhibitors featuring a Novel Hexahydropyrrolofuran (HPF) Scaffold as the P2 Ligand

1.8.1 Introduction

Since the introduction of HAART to combat HIV/AIDS, the resultant combination therapy has dramatically improved the overall lifestyle of individuals affected. In the presence of multiple treatment options and therapeutic targets, there still lacks a treatment to completely eradicate this virus. The resulting HIV-1 mutant variants, from the replication process, possess the ability to overcome the most successful of HAART regimens. This evolutionary feature leads to the ever-growing issue of drug resistance. The development of more effective HIV-1 protease inhibitors is required to appropriately combat drug resistance and improve HAART regimens.

1.8.2 Design of HIV-1 Protease Inhibitors with HPF P2 Ligand

While DRV was an exceptionally potent inhibitor, there was a desire to improve upon the established biological profile. Referring back to the outlined interactions between DRV and the backbone residues of the active site, the *bis*-THF P₂ ligand partially fills the hydrophobic void at the S₂ subsite. In an effort to expand upon these interactions, an additional tetrahydrofuran ring was incorporated to better fill this particular hydrophobic pocket and produce a 5/5/5 tricyclic P₂ ligand. This P₂ ligand became known as *tris*-THF. Application of this P₂ ligand led to the development of GRL-0519A, a very potent inhibitor with a K_i of 5.9 pM and an IC₅₀ value of 1.8 nM (Figure 1.31).^{120,121} Structural analysis of GRL-0519A confirms a similar network of hydrogen bonding within the active site relative to DRV (Figure 1.32). However, the oxygen of the third tetrahydrofuran ring of the P₂ ligand displays water-mediated hydrogen bonding interactions with Arg8' and exhibits a unique CH – O interaction with Gly48 located in the flap region of the protease.

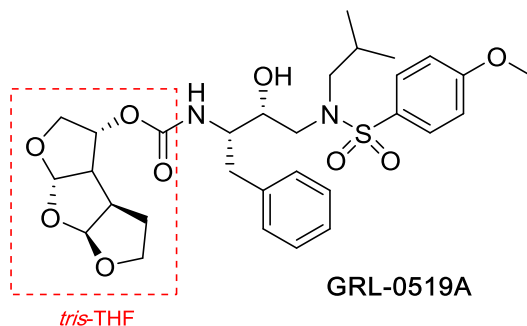


Figure 1.31 Structure of GRL-0519A Featuring *tris*-THF P₂ Ligand

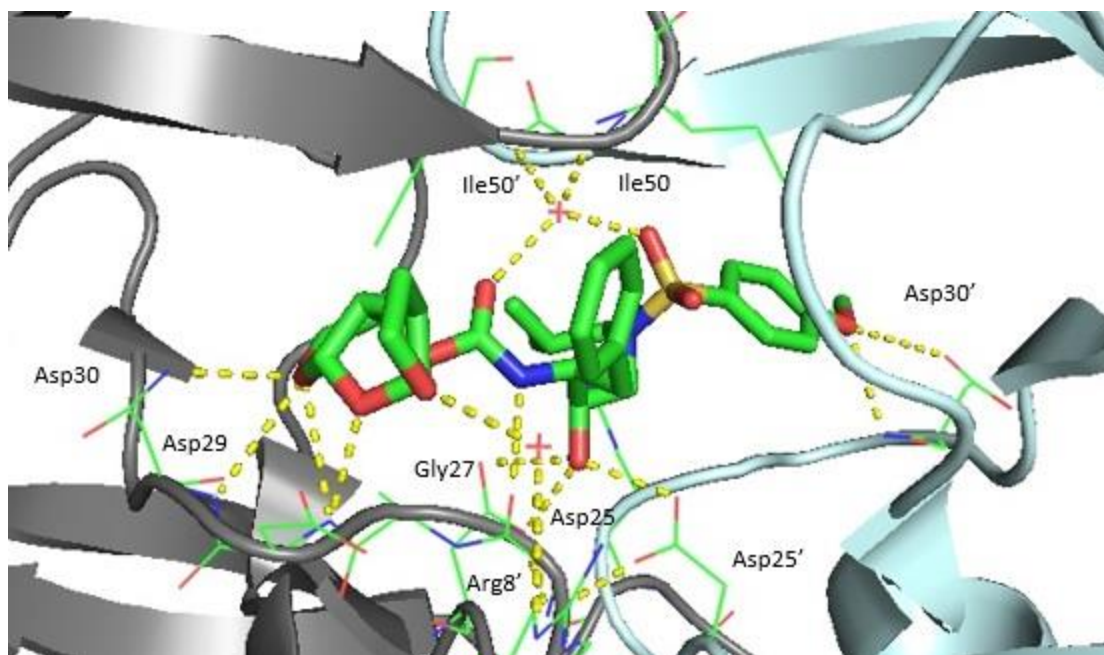


Figure 1.32 Crystal Structure of GRL-0519A-Bound HIV-1 Protease¹²⁰
(Recreated based upon literature)

The molecular insight of *tris*-THF led to the development of other tricyclic P₂ ligands of various ring combinations. The 6/5/5 tricyclic inhibitors **13**, **14**, and **15** were prepared on the basis of the desired *syn-anti-syn* stereochemistry for inhibitory activity (Figure 1.33).¹²² Structural analysis of inhibitor **13** displays the cyclohexane ring's ability to fill in the hydrophobic pocket (Figure 1.34). In addition, the oxygen of the middle furan ring connects with the amide NH of the Asp29 residue. The oxygen of the second tetrahydrofuran ring creates a water-mediated hydrogen bond with Gly27. Overall, these interactions with the conserved backbone residues explain the potency of these particular fused ring systems and fill the S₂ subsite effectively.

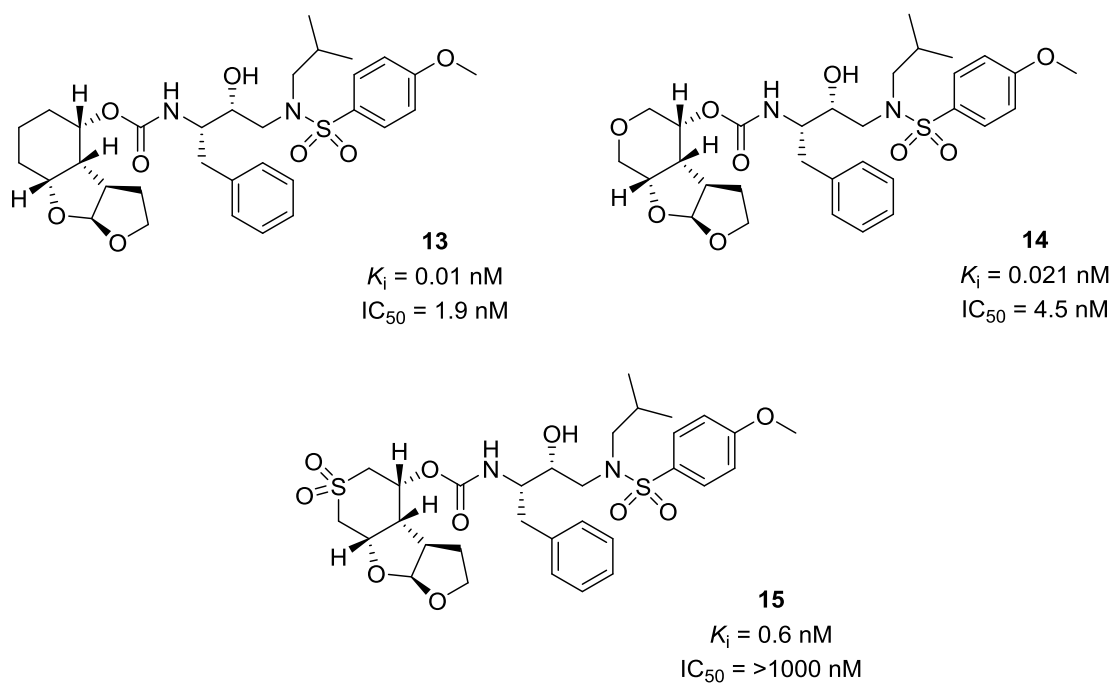


Figure 1.33 Fused Tricyclic HIV-1 Protease Inhibitors

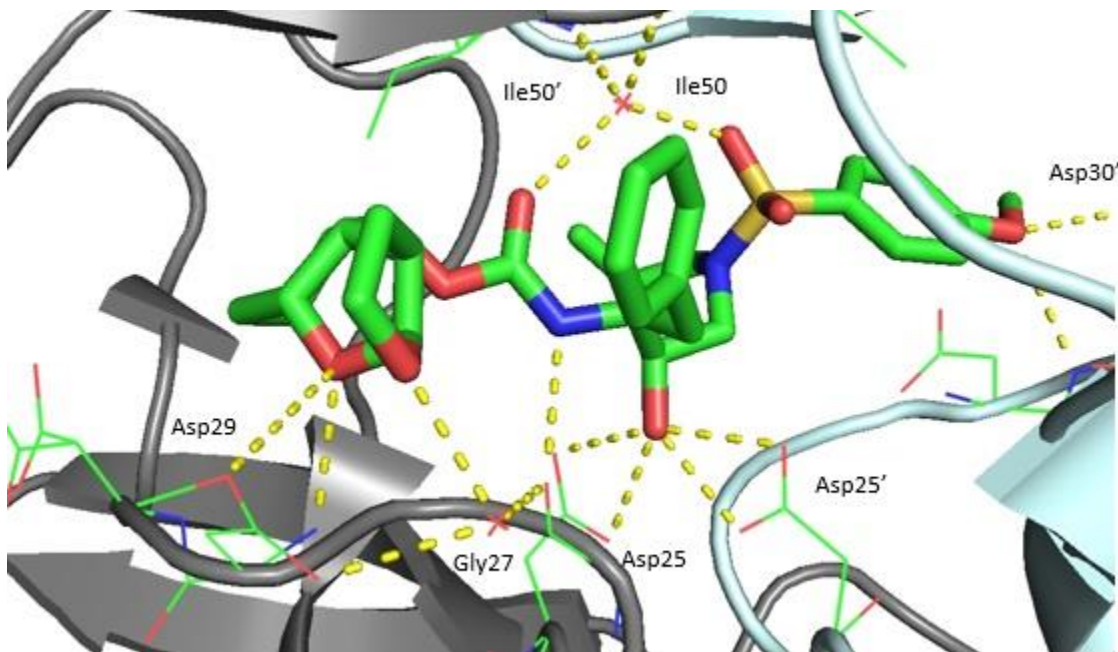


Figure 1.34 Crystal Structure of **13**-bound HIV-1 Protease Inhibitors¹²²
 (Recreated based upon literature)

In an effort to expound upon the observations presented by DRV, *tris*-THF, and **13**, a new class of HIV-1 protease inhibitors was developed to accommodate features of the previously described potent inhibitors. This novel 5/5 bicyclic scaffold has been termed hexahydropyrrolofuran (HPF) (Figure 1.35). The purpose of this P₂ ligand was to utilize the nitrogen as a molecular handle to induce additional hydrogen bond interactions with featured functional groups while simultaneously filling the hydrophobic pocket with various hydrocarbon substituents. A brief overlay of the highlighted interactions of DRV with Asp29 and Asp30 provide insight into the potential spatial orientation of the HPF P₂ ligand. If the carbonyl oxygen of the HPF scaffold continues to interact with the amide NH of Asp30, the corresponding nitrogen-based functional group could interact with the amide NH of Asp29 resulting in the hydrophobic alkyl group occupying the S₂ hydrophobic pocket, thus maintaining potency. However, if a tetrahedral-based sulfonamide subunit is present, this may allow two potential hydrogen bond interactions causing the alkyl group to occupy the same hydrophobic pocket (Figure 1.36).

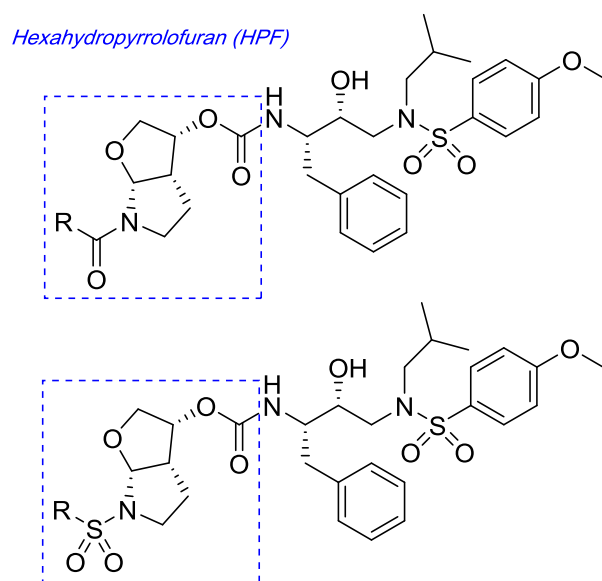


Figure 1.35 Structure of Designed HIV-1 Protease Inhibitor Featuring HPF Scaffold

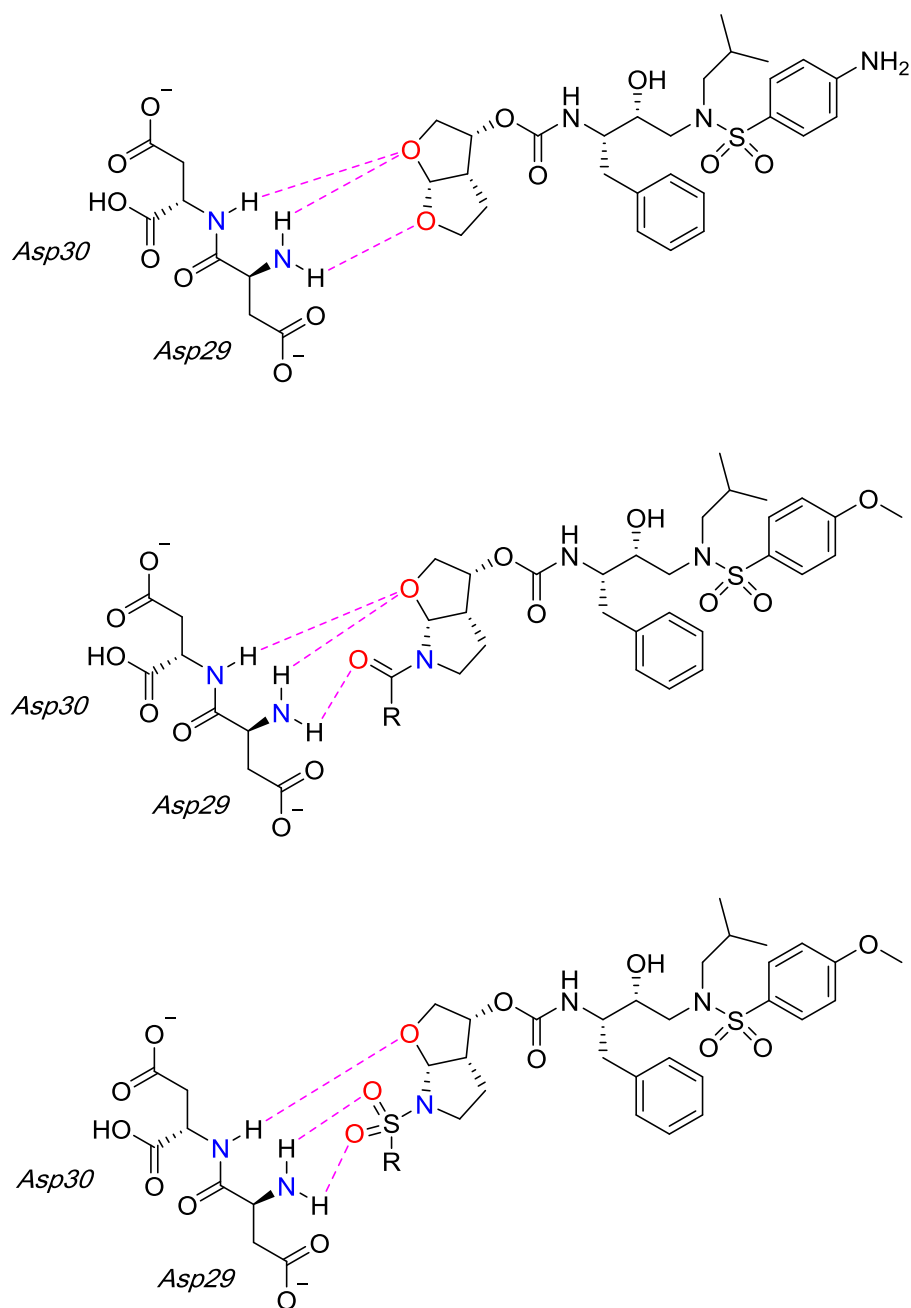
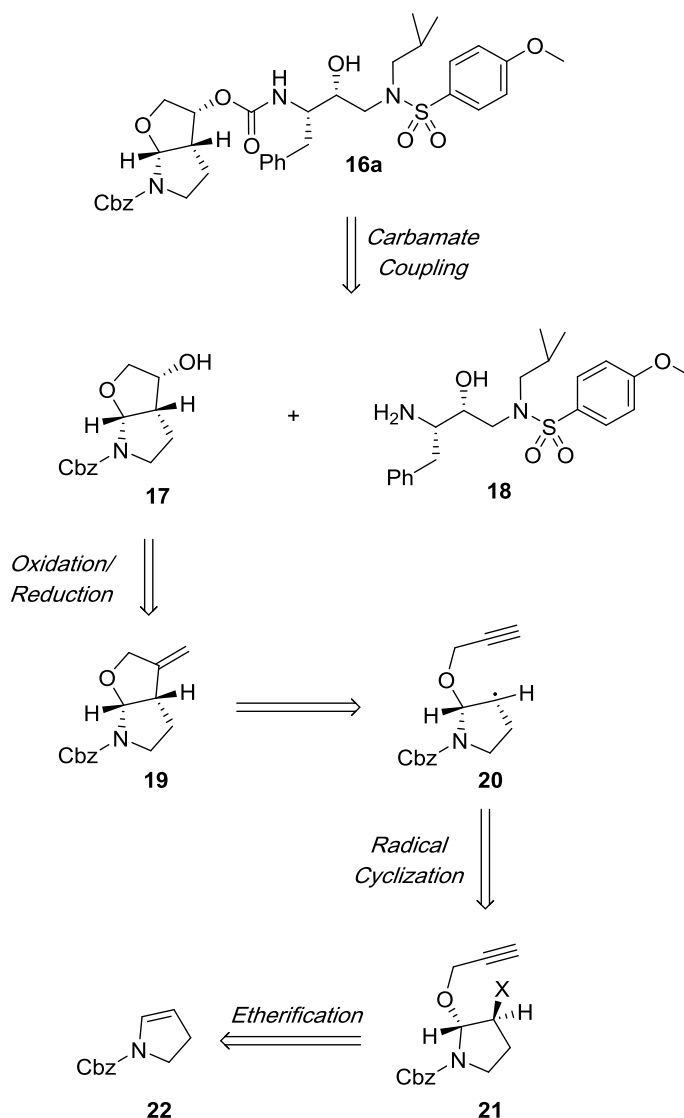


Figure 1.36 Proposed Hydrogen Bond Interactions of HPF P₂ Ligand

1.8.3 Synthetic Strategy

The general strategy for the synthesis of the novel HPF scaffold as a P₂ ligand is outlined in the scheme below (Scheme 1.1). It was envisaged to synthesize an inhibitor, **16**, through a late-stage carbamate coupling with the desired hydroxyethylamine bioisostere **18** and the corresponding activated carbonate derived from the enantiopure alcohol **17**. The alcohol could be

furnished through an oxidative cleavage of the *exo*-olefin in **19** to the resulting ketone and further reduced. The *exo*-olefin could be achieved through a radical-induced annulation, presumably through the radical intermediate **20**. The radical intermediate **20** could be readily prepared from a halogenated hemiaminal ether **21**. The propargyl ether substituent can be synthesized from the *ene*-carbamate **22**.

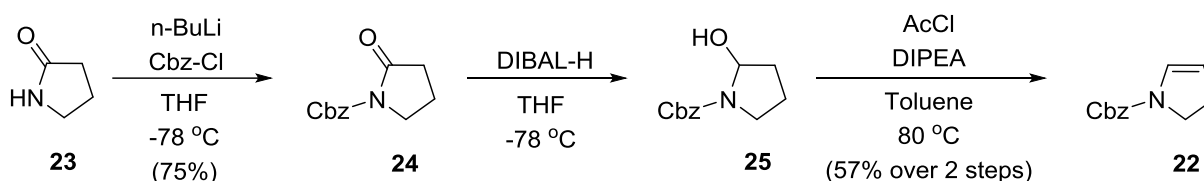


Scheme 1.1 Retrosynthetic Analysis for the Construction of HPF Core

1.8.4 Results

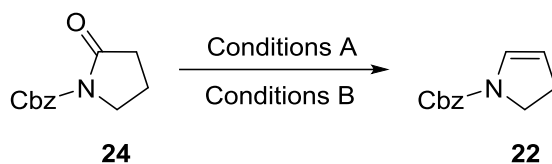
1.8.4.1 Synthesis of HIV-1 Protease Inhibitors

The forward synthetic plan was carried out to obtain the versatile *ene*-carbamate **22** (Scheme 1.2). This intermediate, along with cyclic derivatives of various sizes, has the capacity to provide a variety of fused bicyclic P₂ ligands including 5/5, 5/6, and 6/6 fused ring systems. Beginning with 2-pyrrolidinone **23**, Cbz protection was accomplished by treatment with *n*-BuLi and Cbz-Cl to afford the protected lactam **24**. Reduction of the lactam with DIBAL-H provided the lactamol intermediate **25**. Unfortunately, attempts to purify this intermediate were unfruitful and the crude product was moved forward. The lactamol was added to a heated mixture of AcCl and DIPEA in toluene to furnish the desired *ene*-carbamate **22**.



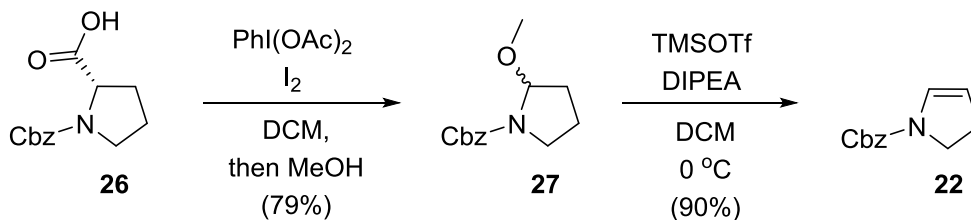
Scheme 1.2 Initial Synthesis of *ene*-carbamate **22**

While the reaction and purification proceeded smoothly, the resulting yields were inconsistent. Therefore, an optimal method to obtain **22** was necessary. These attempts are outlined in the table below (Table 1.2). While the acetate is not a great leaving group, even at elevated temperatures, it was believed that introduction of a better leaving group could facilitate a more facile elimination and promote formation of the *ene*-carbamate. Therefore, the lactamol was treated with TFAA at -78 °C followed by addition of 2,6-lutidine. Interestingly, the result of these conditions were formation of an inseparable by-product and an elevated yield. Investigating further, the lactamol was treated with 20 mol% of PPTS and refluxed with a Dean-Stark apparatus. These conditions were promising in terms of purification, but the yield was low. Increasing equivalents of PPTS did not lead to an increase of the *ene*-carbamate. Switching from PPTS to pTSA proved ineffective. The lactam was treated with KHMDS to form the enol triflate and subsequently subjected to Pd-catalyzed Stille coupling conditions only to provide a complex mixture of products.

Table 1.2 Optimization for the Preparation of *ene*-carbamate **22**

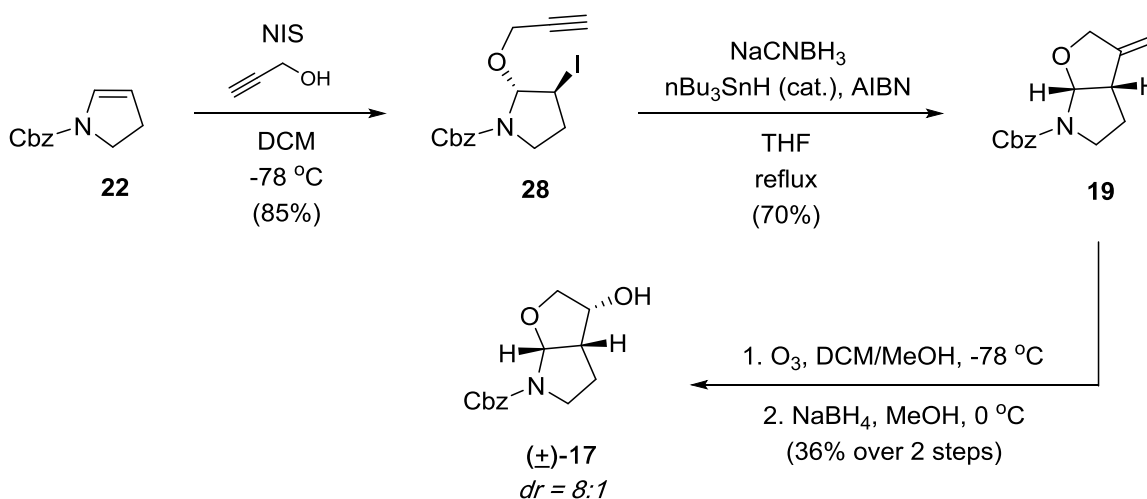
Entry	Conditions A	Conditions B	Result
1	DIBAL-H THF, -78 °C	AcCl, DIPEA Toluene, 80 °C	41%
2	DIBAL-H THF, -78 °C	AcCl, DIPEA Toluene, 80 °C	57%
3	DIBAL-H THF, -78 °C	AcCl, DIPEA Toluene, 80 °C	34%
4	DIBAL-H THF, -78 °C	AcCl, DIPEA Toluene, 80 °C	17%
5	DIBAL-H THF, -78 °C	TFAA, 2,6-lutidine Toluene, -78 °C to RT	74%, Inseparable mixture of by-pdts
6	DIBAL-H THF, -78 °C	PPTS (0.2 mol %) Toluene, reflux	22%
7	DIBAL-H THF, -78 °C	PPTS (1 equiv.)	27%
8	DIBAL-H THF, -78 °C	pTSA	Complex mixture
9	KHMDS, N-Phenyl- bis(trifluoromethanesulfonamide) THF, -78 °C	Pd(PPh ₃) ₄ , LiCl nBu ₃ SnH THF, -78 °C to RT	Complex mixture

Based upon these results, it was necessary to seek an alternative synthetic strategy that would yield consistently high results. Commercially available Z-Pro-OH **26** was converted into the corresponding hemiaminal methyl ether **27** through a decarboxylative etherification with PhI(OAc)₂ followed by quenching with MeOH (Scheme 1.3). Elimination of the methoxy substituent was facilitated by TMSOTf and DIPEA to afford *ene*-carbamate **22** in 90%. This method has two distinct advantages: (i) the experiments provided consistently high yields on multigram scale and (ii) is more cost efficient than the previously attempted experiments.



Scheme 1.3 Alternative Synthesis of *ene*-carbamate **22**

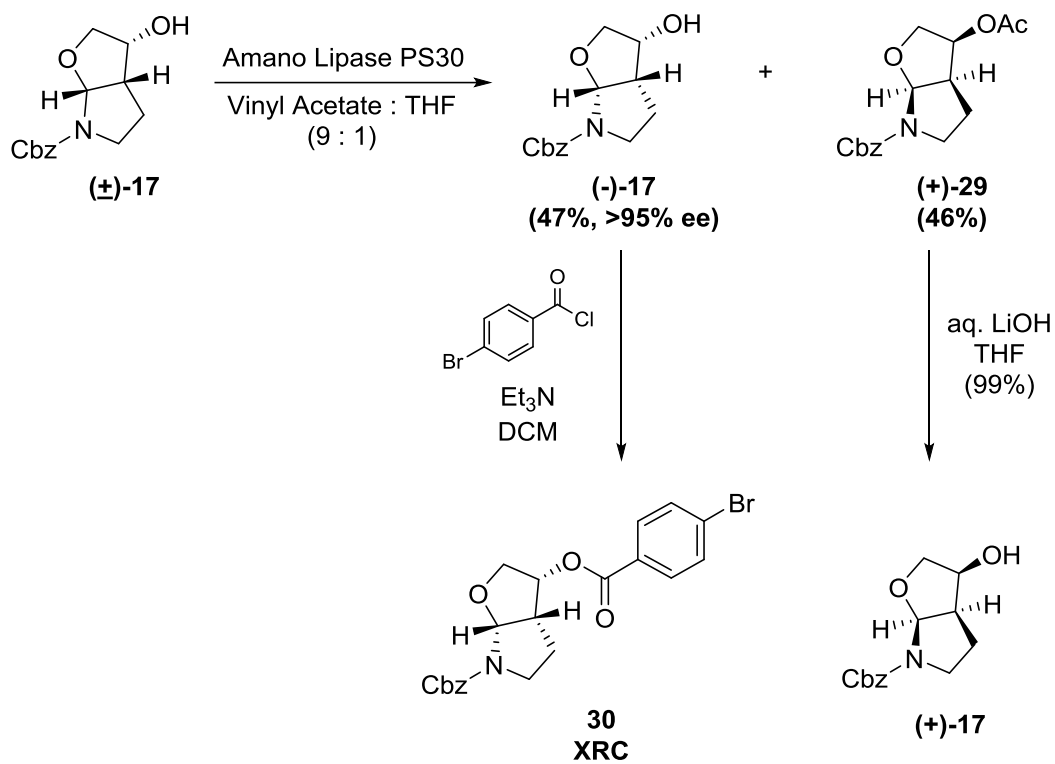
After optimizing the production of the *ene*-carbamate, attention was focused on the preparation of the fused bicyclic ring system. Following Batey's literature procedure, iodoetherification of the *ene*-carbamate with N-Iodosuccinimide and propargyl alcohol at $-78\text{ }^\circ\text{C}$ successfully installed the propargyl ether side chain to provide **28** (Scheme 1.4). Free-radical annulation was induced with NaCNBH_3 , AIBN, and a catalytic amount of nBu_3SnH and refluxed in THF to provide the *exo*-olefin intermediate **19** and construct the HFP core framework.¹²³ Treatment of the olefin with O_3 in a DCM/MeOH solvent system at $-78\text{ }^\circ\text{C}$ afforded the crude ketone which was readily reduced with NaBH_4 , in MeOH, to the racemic secondary alcohol **17** in a diastereomeric ratio of 8:1 in 36% yield over 2 steps.



Scheme 1.4 Preparation of Racemic Alcohol **17**

As evidenced by the structural studies of DRV and *tris*-THF, the active site of the HIV-1 PR is stereospecific. To achieve optimal enzyme inhibition, the correct stereochemical orientation of the fused ring system is crucial for the hydrogen bond network. Since this is the first hemiaminal

ether scaffold to be tested against HIV-1 PR, the preferential orientation of the HPF scaffold relative to the active site is unknown. Methods have been previously developed to enzymatically resolve racemic alcohols into corresponding enantiomers. Employing similar conditions to resolve the *bis*-THF P₂ ligand of DRV, the secondary alcohol was treated with Amano Lipase PS30 and Ac₂O in THF.¹⁰⁸ Although the acetate was achieved, roughly 30% of starting material was converted in the span of 2 days, based on recovered starting material. Altering the solvent system to a vinyl acetate and THF mixture in a 9:1 ratio, with the same enzyme, resulted in complete resolution to provide the enantiopure alcohol (-)-**17** in 47% yield (>95% ee) and acetate (+)-**29** in 46% yield (Scheme 1.5). Identification of the absolute stereochemistry was accomplished by XRC of the analogous *p*-bromobenzoate ester (Figure 1.37). As a control experiment, the racemic alcohol was introduced to the same conditions in the absence of the active enzyme which resulted in complete recovery of the racemic alcohol starting material. Therefore, the resolution occurred enzymatically. Furthermore, the enantiopure acetate underwent standard hydrolysis conditions with aqueous LiOH to produce the enantiomeric alcohol (+)-**17**. The presence of enantiomers were confirmed through chiral HPLC and optical rotation. Alcohol (-)-**17** presented an optical rotation of $[\alpha]_D^{20}$ -95.3 (*c* 0.513, CHCl₃) and acetate (+)-**29** displayed an optical rotation of $[\alpha]_D^{20}$ +121.2 (*c* 1.45, CHCl₃). Alcohol (+)-**17** presented an optical rotation of $[\alpha]_D^{20}$ +86.8 (*c* 0.35, CHCl₃) and confirmed the success of the enzymatic resolution.



Scheme 1.5 Enzymatic Resolution of Racemic Alcohol **17**

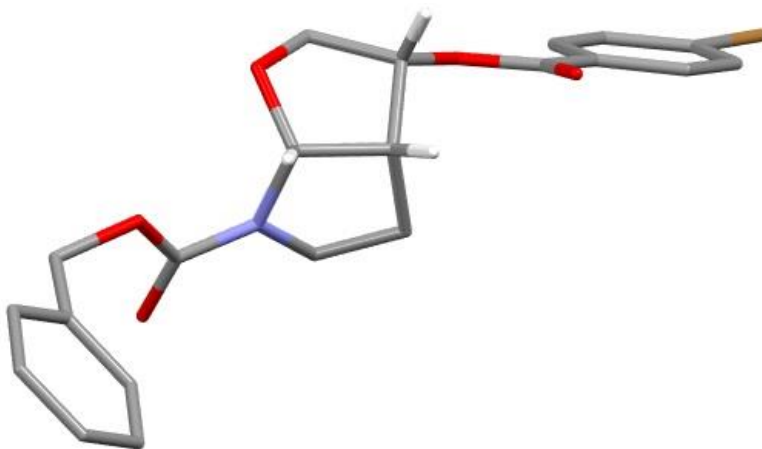
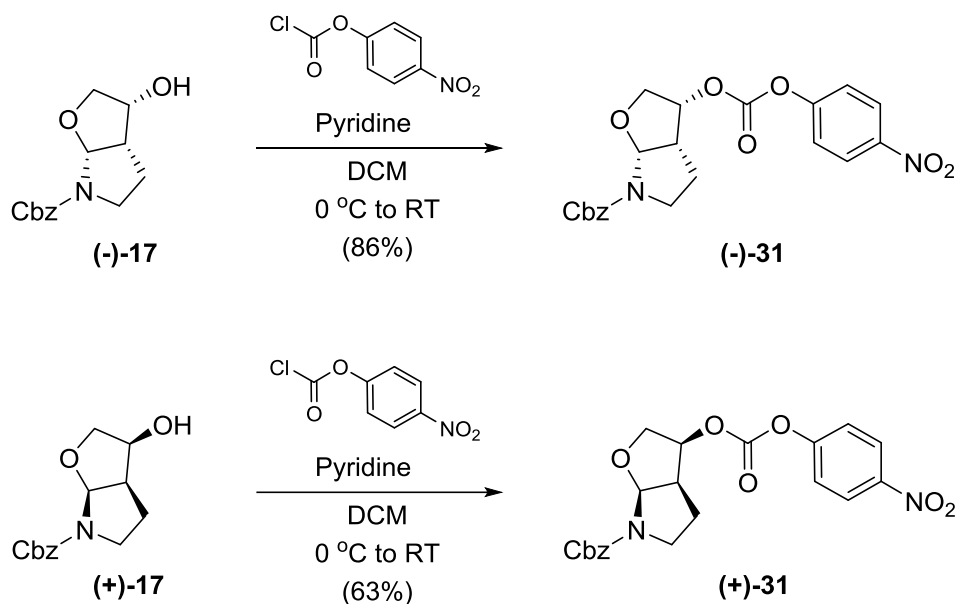


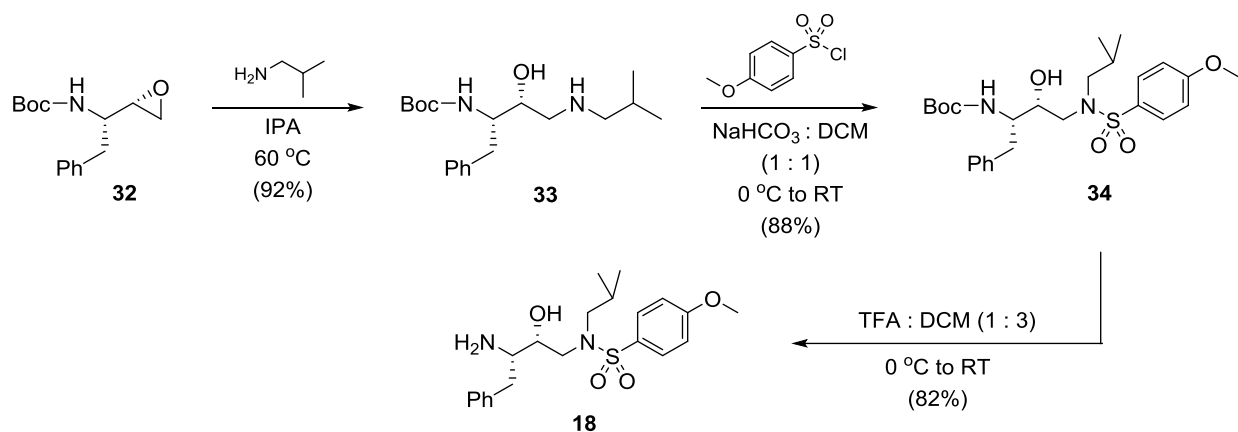
Figure 1.37 X-ray Crystal Structure of **30**

After completion of the enzymatic resolution, the stage was then set to synthesize the final inhibitor. The enantiopure alcohols were converted into their respective nitrophenyl carbonates as a precursor for the carbamate coupling (Scheme 1.6). This strategy has been applied extensively in literature for the preparation of other HIV-1 protease inhibitors.^{124,125}



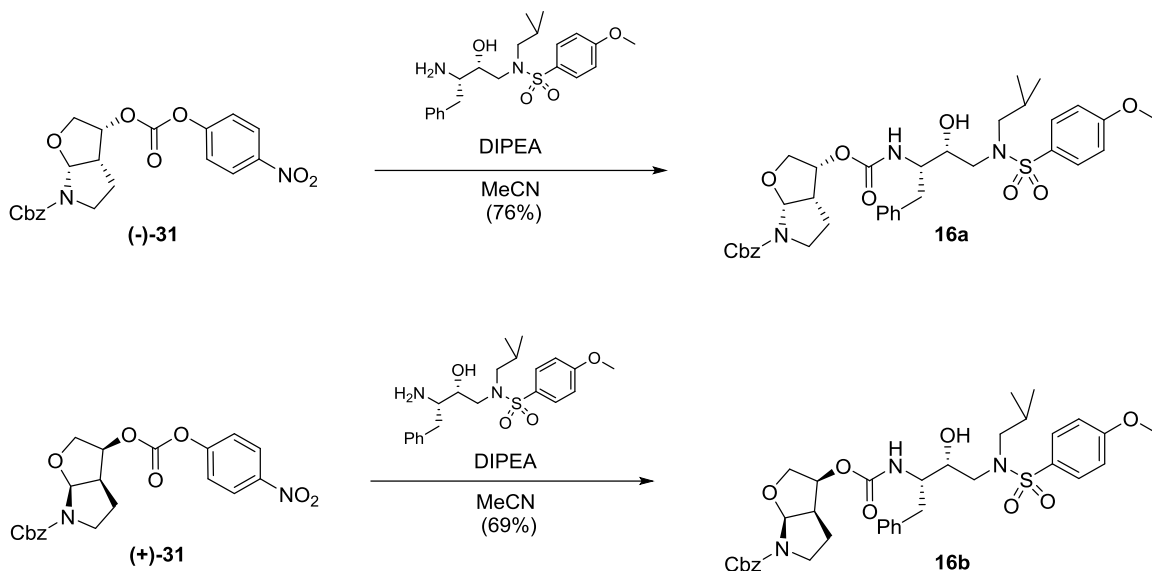
Scheme 1.6 Preparation of Activated Carbonate Species **(-)-31** and **(+)-31**

After preparation of the activated carbonate species, a variety of hydroxyethylamine isosteres could be effectively coupled to produce the final inhibitor featuring a stable carbamate linkage. For this particular project, the hydroxyethylamine isostere **18** incorporated a *para*-methoxybenzenesulfonamide P₂' ligand. This isostere could be prepared in 3 steps from commercially available starting material (Scheme 1.7).¹²⁶ Epoxide **32** was treated with isobutylamine in IPA for 18 hours to acquire the hydroxyethylamine core **33**. The isobutyl group is designed to fit into the hydrophobic S₁' subsite. Progressing further, the hydroxyethylamine isostere was completed with the addition of *p*-methoxybenzenesulfonyl chloride and subjected to acidic media to remove the Boc protecting group.



Scheme 1.7 Synthesis of Hydroxyethylamine Isostere Ligand **18**

The final inhibitors were furnished through upon treatment of the activated carbonate and the isostere with DIPEA in MeCN (Scheme 1.8). The final inhibitors **16a** and **16b** were isolated in moderate yields of 76% and 69%, respectively.

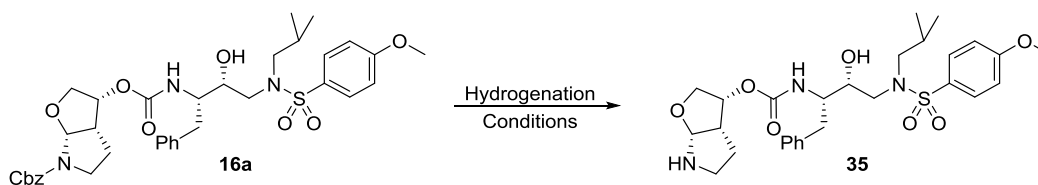


Scheme 1.8 Carbamate Coupling for Preparation of Final Inhibitors **16a** and **16b**

The Cbz-protected final inhibitors were used as initial substrates for biological evaluation to provide insight into the HPF scaffold as a P₂ ligand. In order to evaluate other nitrogen-based functional groups, a common intermediate needed to be identified for this divergent method. Based on the structural features of the final inhibitor, it was theorized the Cbz protecting group

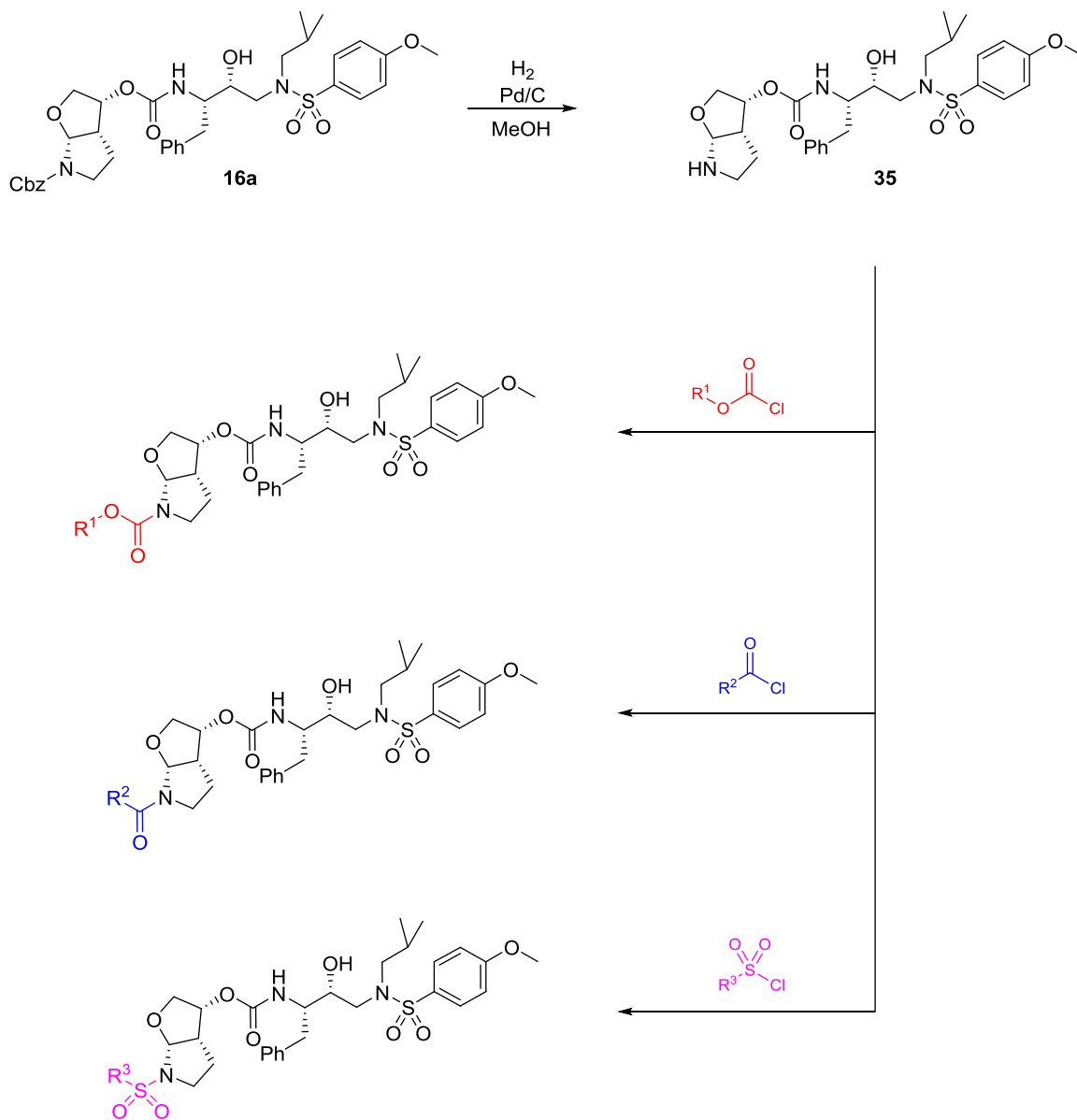
could be removed under mild conditions, since strong acids or bases could decompose the substrate. Exploration for the removal of this group was initiated with standard hydrogenolysis conditions (Table 1.3). The first catalyst examined was Pd(OH)₂/C under 1 atmosphere of hydrogen. In the presence of MeOH, the carbamate linkage was cleaved and resulted in reisolation of the hydroxyethylamine isostere. Utilizing EtOAc to weaken the catalytic system was ineffective. The isostere was recovered and believed to result from the long reaction time and extended exposure to the palladium catalyst. Focusing on the catalyst itself, attention was turned to Pd/C. In the presence of MeOH, the isostere was collected, but the liberated free amine had been observed. Additionally, the reaction proceeded in 2 hours and achieved 100% conversion. To inhibit the carbamate linkage from cleaving, the milder solvent system of EtOAc was tested. The isostere and liberated amine were both observed, but the reaction rate was slow as roughly 20% of the starting material was converted. Opting to investigate an alternative sequence, a transfer hydrogenation experiment was performed with Pd/C as the catalyst and cyclohexadiene as the hydrogen source. This strategy provided similar results as the carbamate linkage was cleaved. Therefore, Pd/C in MeOH would be used to synthesize the desired protease inhibitors.

Table 1.3 Optimization of Cbz Deprotection



Entry	Conditions	Result
1	Pd(OH) ₂ /C (20 mol%), H ₂ (1 atm) MeOH, 1 Hour	Carbamate Cleavage
2	Pd(OH) ₂ /C (20 mol%), H ₂ (1 atm) EtOAc, 20 Hours	Carbamate Cleavage
3	Pd/C (10 mol%), H ₂ (1 atm) MeOH, 2 Hours	Liberated Amine Observed with Carbamate Cleavage; 100% conv.
4	Pd/C (10 mol%), H ₂ (1 atm) EtOAc, 24 Hours	Liberated Amine Observed with Carbamate Cleavage; ~20% conv.
5	Pd/C, Cyclohexadiene EtOH, 24 Hours	Carbamate Cleavage

Due to the sensitive nature of the liberated amine, the hemiaminal ether intermediate could not be isolated effectively and the crude material was carried forward. Treatment of the crude amine with an acceptable electrophile led to the formation of the desired nitrogen-based functional group which included carbamates, carboxamides, and sulfonamides (Scheme 1.9). During isolation of the final inhibitors, the hydroxyethylamine isostere was recovered, both as the free amine and the product of the resulting derivatization sequence. The collected isosteres could be recycled and resubjected to the standard coupling conditions to conserve material.



Scheme 1.9 Hydrogenolysis of Cbz Protecting Group and Derivatization Sequence

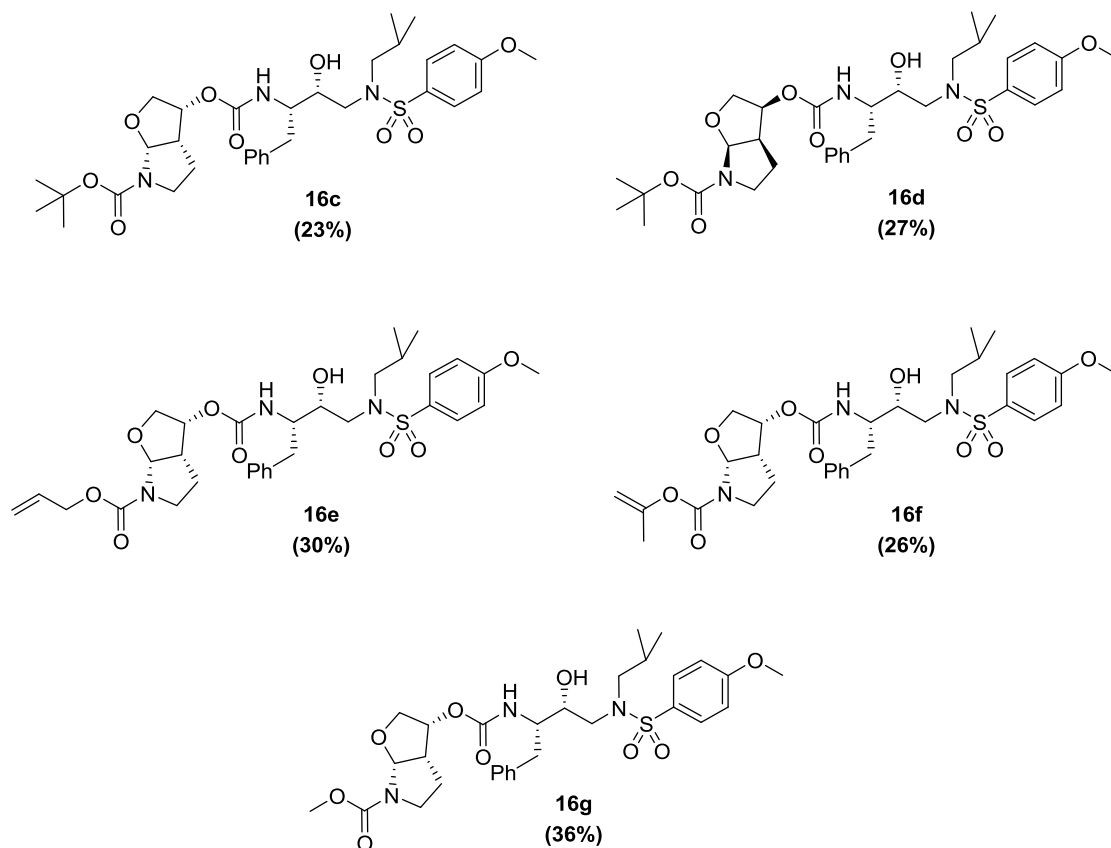


Figure 1.38 HIV-1 Protease Inhibitors Featuring Carbamate Functionality

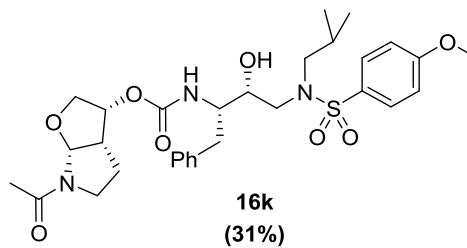
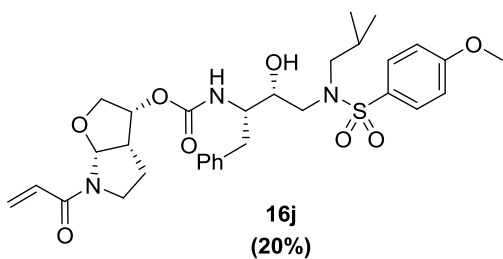
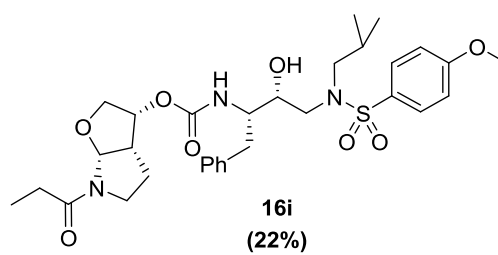
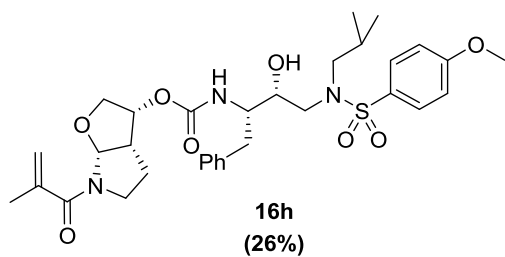


Figure 1.39 HIV-1 Protease Inhibitors Featuring Carboxamide Functionality

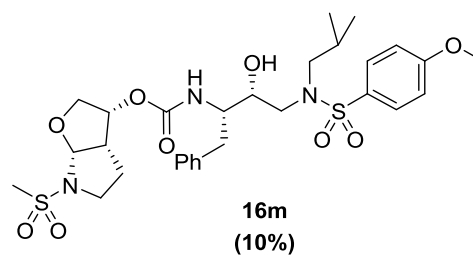
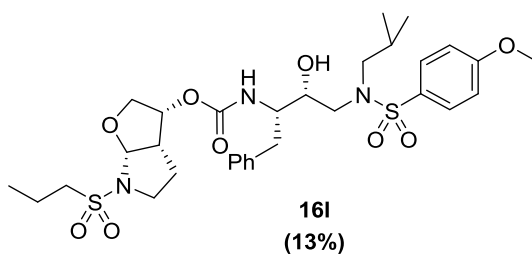


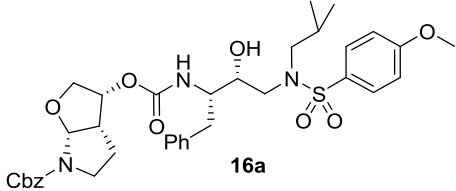
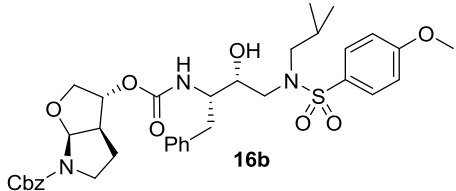
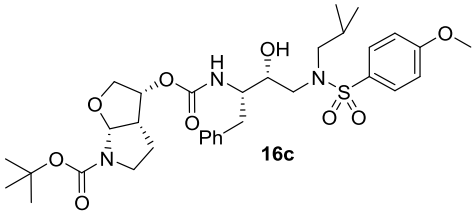
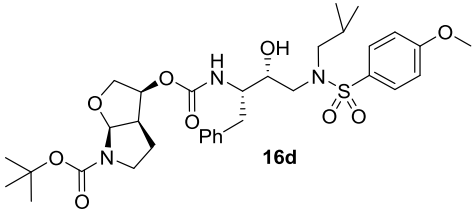
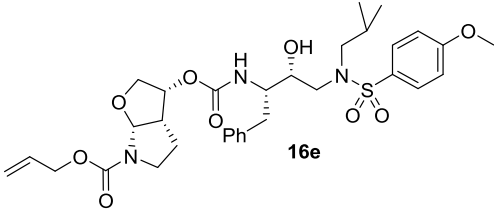
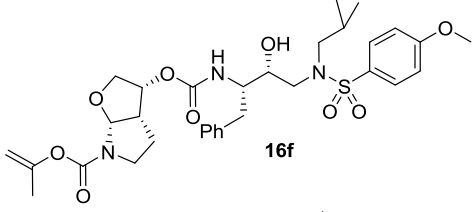
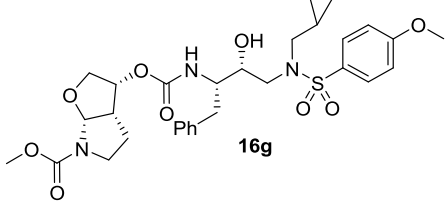
Figure 1.40 HIV-1 Protease Inhibitors Featuring Sulfonamide Functionality

1.8.4.2 Biological Evaluation and Discussion

Biological evaluation of the HPF scaffold as a P₂ ligand for HIV-1 protease inhibitors was divided amongst three classes of compounds; carbamate, carboxamide, and sulfonamide. The carbamate moiety contains two oxygen atoms that have the potential to interact with the desired backbone residues Asp29 and Asp30 while the alkyl group fills the hydrophobic pocket. The Cbz-protected inhibitor **16a** was evaluated to obtain an initial enzyme inhibitory value and provide a gateway for the remainder of the structure-activity relationship (SAR) study (Table 1.4). The Cbz inhibitor **16a** presented an enzyme inhibition value of 15.6 nM. While this initial result was promising, the specificity of the active site was probed further. To better understand the orientation of the HPF core within the enzyme, the Cbz inhibitor **16b**, containing the alternate stereochemistry across the ring junction, was evaluated and returned a K_i value of 81.4 nM. The enzyme inhibition values, relative to the defined stereochemistry, were consistent with previously reported HIV-1 protease inhibitors.

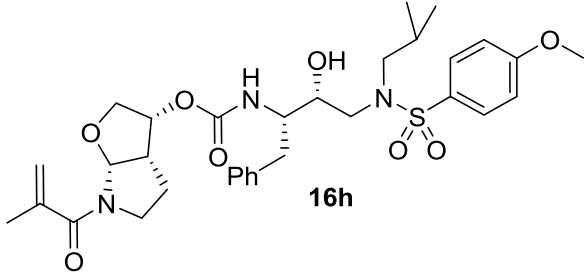
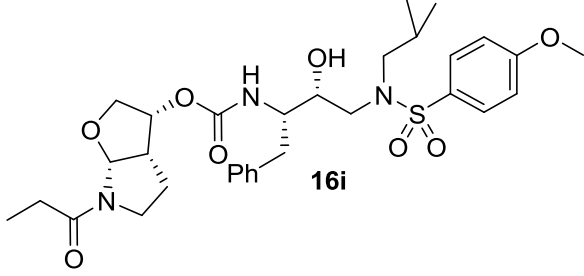
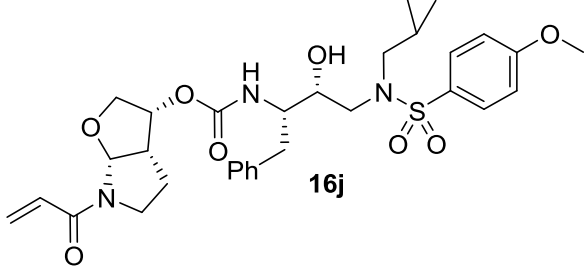
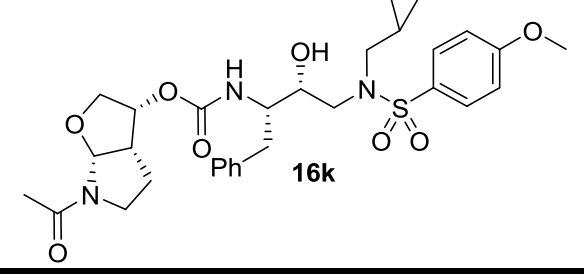
Considering the large steric bias of the phenyl ring in inhibitor **16a**, the alkyl group was reduced to better fill the void set by the hydrophobic pocket of S₂. Replacing the Cbz group with a Boc group for inhibitor **16c** led to an increase in enzyme inhibition slightly (K_i = 7.0 nM). Diverting back to the Boc diastereomeric partner, inhibitor **16d** produced a K_i value of 104.7 nM. This 14-fold decrease in activity confirmed the preferential orientation of the HPF scaffold within the active site of the enzyme to achieve maximal inhibition. From the results of the Cbz and Boc groups, the carbamate functionality was then linearized by attaching an allyl carbamate group to prepare inhibitor **16e**. The resulting effect of linearization was a decrease in K_i from 7.0 nM to 3.1 nM. It is reasonable to suggest the increase in activity is caused by the flexible nature of the hydrocarbon chain. Attempting to maintain the flexible feature of the carbamate group, the olefin was relocated to provide inhibitor **16f** with isopropenyl chloroformate and resulted in a K_i of 0.15 nM. The increase in inhibition can be attributed to the smaller hydrocarbon chain length and suggests the depth of the S₂ subsite may be limited. Reducing the carbon chain to the simplest of form, inhibitor **16g** was obtained from methyl chloroformate. This was the smallest carbamate ligand evaluated and presented a K_i of 0.42 nM. The slight decrease in inhibition suggests the presence of a hydrocarbon chain of reasonable size is important to maintain potency and fill the hydrophobic pocket.

Table 1.4 Biological Evaluation of Carbamate-based HIV-1 Protease Inhibitors

Entry	Inhibitor	K_i (nM)	IC_{50}
1	 16a	15.6	ND
2	 16b	81.4	ND
3	 16c	7.0	>1000 nM
4	 16d	104.7	>1000 nM
5	 16e	3.1	777 nM
6	 16f	0.15	>1000 nM
7	 16g	0.42	267 nM

While the protease inhibitors featuring the carbamate functionality were reasonably potent, it was believed that only one of the oxygens present in the carbamate connectivity was participating in hydrogen bonding with the conserved Asp29/30 residues. To better rationalize this theory, one of the oxygens was removed to promote hydrogen bonding with the carbonyl more effectively, thus resulting in the rise of the carboxamide class of inhibitors (Table 1.5). The first inhibitor of the carboxamide class was the methacrylamide inhibitor **16h** and presented a K_i value of 17.2 nM. Comparing inhibitor **16h** to that of the corresponding carbamate inhibitor **16f**, there is a 115-fold loss of enzyme inhibition. This drastic loss in activity indicates the additional oxygen of the carbamate group is directly interacting within the active site. Understanding the size of the functional group has an effect on the inhibitory activity, smaller amide-based ligands were prepared. Removal of a methylene unit to prepare the propionamide inhibitor **16i** presented an increase in enzyme inhibition with a K_i value of 3.69 nM. Exploring further, the acrylamide inhibitor **16j** displayed similar activity relative to **16i**. The slight loss in activity could be explained through the sp^2 character of the olefin. The olefin has a shorter bond length and is less flexible than the propionamide inhibitor which indicates the acrylamide is not adequately housed in the S_2 subsite. The smallest functional group examined was the acetamide, featured in inhibitor **16k**. As expected, inhibitor **16k** displays the best enzyme inhibition activity with a K_i of 2.14 nM. Biological evaluation of this class presented protease inhibitors with moderate activity, however these particular inhibitors did not display promising IC_{50} results. Presumably, the inhibitors are not penetrating the cellular membrane and the activity may be attributed to a solubility issue as these molecules are extremely polar. Therefore, a third class of inhibitors were designed to overcome this issue.

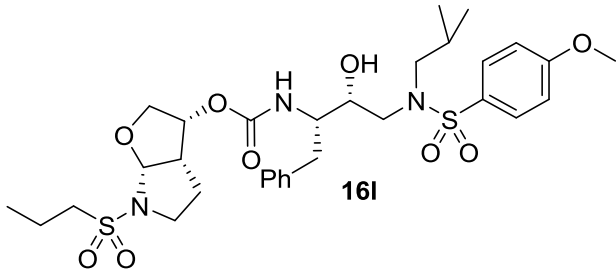
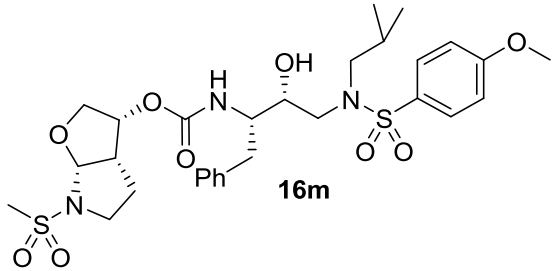
Table 1.5 Biological Evaluation of Amide-based HIV-1 Protease Inhibitors

Entry	Inhibitor	K_i (nM)	IC_{50}
1	 16h	17.2	>1000 nM
2	 16i	3.69	>1000 nM
3	 16j	3.76	953 nM
4	 16k	2.14	>1000 nM

The carbamate and amide-based protease inhibitors explored were planar, rotameric, sp^2 -hybridized ligands. These geometrical attributes may result in a limited spatial orientation within the active site and potentially restricts the desired hydrogen bond interactions from occurring. To better understand the acceptable spatial geometry of the HPF scaffold, the sulfonamide-based inhibitor class was prepared (Table 1.6). The sulfonamide functional group features sp^3 -hybridization and leads to a tetrahedral orientation. Additionally, the tetrahedral orientation could increase the interactions between Asp29 and Asp30 with the fully-exposed oxygens. To further investigate, the propylsulfonamide inhibitor **16l** was synthesized. Considering the small,

flexible nature of the propyl chain, the initial K_i value of 0.57 nM was promising. Shortening the carbon chain further, the methanesulfonamide moiety was prepared. When inhibitor **16m** was evaluated against HIV-1 protease, the result was a stellar enzyme inhibition value of 0.027 nM. In the absence of a crystal structure, the increase in activity suggests the tetrahedral spatial geometry is promoting additional hydrogen bond interactions with the conserved residues of the backbone.

Table 1.6 Biological Evaluation of Sulfonamide-based HIV-1 Protease Inhibitors

Entry	Inhibitor	K_i (nM)	IC ₅₀
1	 16l	0.57	ND
2	 16m	0.027	ND

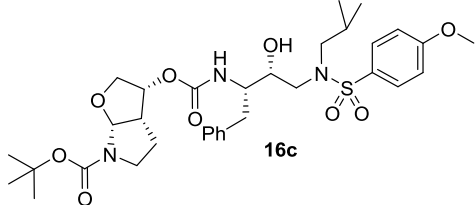
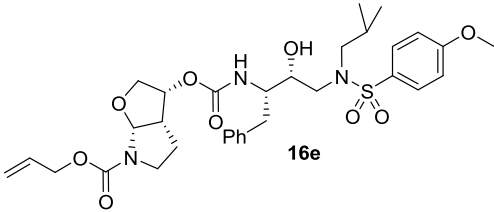
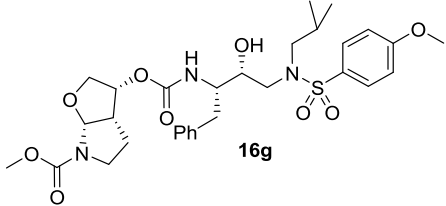
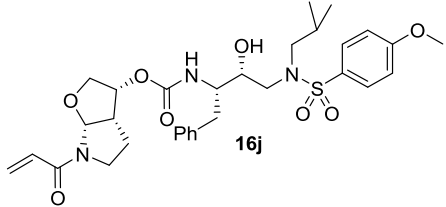
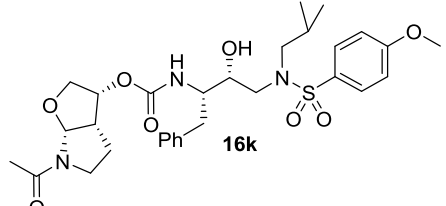
Based upon the biological data collected from the HIV protease inhibitors, there are significant discrepancies between the observed enzyme inhibitory activity and the resulting IC₅₀ values. To better understand this observation, further exploration into the chemical properties of the inhibitors was required. One particular chemical property that can be investigated is the partition coefficient (log_p) of the inhibitor. The partition coefficient is a measure of a compound's hydrophilicity, lipophilicity, and plays a crucial role as it relates to the compound's ADMET (absorption, distribution, metabolism, excretion, and toxicity) profile. It has been well established that a log_p value below 5 indicates a molecule possesses drug-like properties and the capacity to be an effective drug molecule. Molecules with a value higher than 5 indicate the compound is highly lipophilic and may not pass through the cell membrane effectively. Therefore, the discrepancy between the K_i and IC₅₀ values might be explained through analysis of the calculated

partition coefficient (clogp) to determine if the inhibitor possesses the ability to pass through the cellular membrane to become an effective HIV-1 protease inhibitor.

The clogp value was calculated for five different protease inhibitors and is outlined below (Table 1.7). From the calculations, there is an observed trend between the relationship of the clogp value and the corresponding IC₅₀ value for the carbamate class of compounds. While the clogp value never exceeds 5, it appears the lower clogp value correlates to a lower IC₅₀ value. Initial analysis of the boc inhibitor **16c** depicts the largest clogp value of 4.41 along with the highest IC₅₀ of the carbamate class at >1000 nM. It is plausible to conclude the boc inhibitor is too lipophilic and results in a higher concentration of the inhibitor residing in the cellular membrane, rather than permeating into the cell to function appropriately, and leads to a larger IC₅₀ value. The allyl carbamate inhibitor **16e** provided an IC₅₀ value of 777 nM and a clogp value of 4.23. With respect to the data recorded from inhibitor **16c**, inhibitor **16e** is not as lipophilic, however there may still remain a large concentration of the inhibitor in the cellular membrane. Lastly, the calculated logp value of the methyl carbamate inhibitor **16g** is 3.53 and correlates to an IC₅₀ of 267 nM, the lowest in the carbamate class. While the IC₅₀ value is still within a large contrast to that of the K_i value, the methyl carbamate inhibitor may be more cell permeable than the other carbamate inhibitors, but the lipophilicity of the inhibitor should be reduced to determine the absolute relationship between the clogp and IC₅₀ results.

While this trend is observed in the carbamate class of compounds, this same trend is not presented for the amide class of compounds. The acrylamide inhibitor **16j** has a clogp value of 3.63 and an IC₅₀ of 953 nM while the acetamide inhibitor **16k** was calculated at 2.95 with an IC₅₀ of >1000 nM. The absence of a trend, as presented by the carbamates, indicates there may be alternative reasons as to the discrepancies in the enzyme inhibitory activity and the IC₅₀ concentrations. The amide inhibitors may exhibit issues related to solubility or stability within the cellular environment. However, further SAR analysis is required to determine the absolute relationship between the partition coefficient and the resulting IC₅₀ values. Chemical modifications would be necessary to reduce the clogp value to observe the resulting bioactivity of the inhibitor.

Table 1.7 Calculated logp Values of Selected Inhibitors

Entry	Inhibitor	IC ₅₀	clogp*
1	 16c	>1000 nM	4.41
2	 16e	777 nM	4.23
3	 16g	267 nM	3.53
4	 16j	953 nM	3.63
5	 16k	>1000 nM	2.95

*Calculated using ChemDraw version 17.0

1.8.5 Conclusion

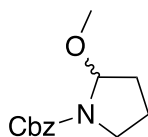
The sustained development of potent HIV-1 protease inhibitors exemplifies the applicable nature of the “backbone binding” concept and led to the development of a new class of protease inhibitors. The novel bicyclic hexahydropyrrolofuran scaffold incorporates a hemiaminal ether linkage. Batey’s iodoetherification was utilized to install the ether side chain and an enzymatic resolution allowed for the separation of optically active enantiomers. This P2 ligand was designed to expose a molecular handle to induce short-path hydrogen bonding while simultaneously filling

the hydrophobic pocket of the S₂ subsite with various hydrocarbon systems. Selected functional groups include carbamate, carboxamide, and sulfonamide. Sulfonamide Inhibitor **16m** was the most potent with a K_i of 0.027 nM. These rudimentary results are leading further optimization efforts to improve biological efficacy of HIV-1 protease inhibitors featuring this novel scaffold.

1.8.6 Experimental

All chemical and reagents were purchased from commercial suppliers and used without further purification unless otherwise noted. All reactions were performed in oven-dried round-bottom flasks. The flasks were fitted with rubber septa and kept under a positive pressure of argon. Cannula were used in the transfer of moisture-sensitive liquids. Heated reactions were ran using an oil bath on a hot plate equipped with a temperature probe. TLC analysis was conducted using glass-backed thin-layer silica gel chromatography plates (60 Å, 250 µm thickness, F-254 indicator). Flash chromatography was done using a 230–400 mesh, a 60 Å pore diameter silica gel. Organic solutions were concentrated at 30–35 °C on rotary evaporators capable of achieving a minimum pressure of ~25 Torr and further concentrated on a Hi-vacuum pump capable of achieving a minimum pressure of ~4 Torr. ¹H NMR spectra were recorded on 400 and 800 MHz spectrometers. ¹³C NMR spectra were recorded at 100 and 200 MHz on the respective NMRs. Chemical shifts are reported in parts per million and referenced to the deuterated residual solvent peak (CDCl₃, 7.26 ppm for ¹H and 77.16 ppm for ¹³C). NMR data are reported as δ value (chemical shift), J-value (Hz), and integration, where s = singlet, bs = broad singlet, d = doublet, t = triplet, q = quartet, p = quintet, m = multiplet, dd = doublet doublets, and so on. Optical rotations were recorded on a digital polarimeter. Low resolution mass spectra (LRMS) spectra were recorded using a quadrupole LCMS under positive electrospray ionization (ESI+). High-resolution mass spectrometry (HRMS) spectra were recorded at the Purdue University Department of Chemistry Mass Spectrometry Center. These experiments were performed under ESI+ and positive atmospheric pressure chemical ionization (APCI+) conditions using an Orbitrap XL Instrument.

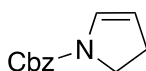
benzyl 2-methoxypyrrolidine-1-carboxylate



To a solution of Z-Pro-OH (11.6110 g, 46.574 mmol) in DCM (300 mL) was added PhI(OAc)₂ (30.0901 g, 93.419 mmol) and I₂ (6.1527 g, 24.241 mmol) sequentially. After stirring for 6 hours, anhydrous MeOH was added and allowed to stir for an additional 2 hours. After this time, the reaction was quenched with saturated Na₂S₂O₃. The crude product was extracted with DCM

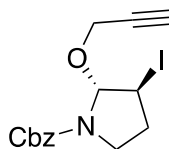
(x3), washed with brine, dried over anhydrous MgSO_4 , and concentrated under reduced pressure. Product was purified via silica gel chromatography (15% EtOAc/Hexanes) to provide 8.65 g (79%) of hemiaminal ether product as a clear oil. ^1H NMR (400 MHz, CDCl_3) δ 7.40 – 7.27 (m, 5H), 5.26 – 5.11 (m, 3H), 3.52 (ddd, $J = 10.9, 8.7, 2.0$ Hz, 1H), 3.39 (m, 3H), 3.26 (s, 1H), 2.11 – 2.01 (m, 1H), 1.95 – 1.84 (m, 2H), 1.79 – 1.72 (m, 1H); ^{13}C NMR (100 MHz, CDCl_3) δ (ppm): 155.7, 154.8, 136.5, 128.3, 127.9, 127.7, 89.0, 88.4, 67.0, 66.7, 55.8, 55.3, 45.8, 45.6, 32.4, 31.8, 22.5, 21.6; LRMS-ESI (+) m/z : 258.1 $[\text{M} + \text{Na}]^+$

benzyl 2,3-dihydro-1*H*-pyrrole-1-carboxylate



To a solution of hemiaminal ether (8.65 g, 36.765 mmol) in DCM (180 mL) at 0 °C was added DIPEA (13 mL, 74.636 mmol) followed by TMSOTf (10 mL, 55.251 mmol). After stirring for 1 hour, the reaction was quenched with saturated NaHCO_3 . The crude product was extracted with DCM (x3), washed with brine, dried over anhydrous MgSO_4 , and concentrated under reduced pressure. Product was purified via silica gel chromatography (10% EtOAc/Hexanes) to afford 6.83 g (91%) of enecarbamate product as a yellow oil. ^1H NMR (400 MHz, CDCl_3) δ (ppm): 7.39 – 7.30 (m, 5H), 6.65 – 6.54 (m, 2H), 5.18 (s, 2H), 5.09 – 5.02 (m, 1H), 3.78 (dt, $J = 12.9, 9.1$ Hz, 2H), 2.69 – 2.60 (m, 2H); ^{13}C NMR (100 MHz, CDCl_3) δ (ppm): 152.7, 151.9, 136.5, 129.6, 128.9, 128.4, 127.9, 127.9, 127.8, 108.6, 108.5, 66.9, 66.76, 45.1, 44.9, 29.6, 28.5; LRMS-ESI (+) m/z : 204.1 $[\text{M} + \text{H}]^+$

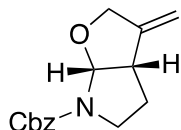
benzyl 3-iodo-2-(prop-2-yn-1-yloxy)pyrrolidine-1-carboxylate



To a light pink solution of N-iodosuccinimide (9.6853 g, 43.050 mmol) and propargyl alcohol (3 mL, 51.534 mmol) in DCM (250 mL) at -78 °C was added a solution of enecarbamate (6.83 g, 33.606 mmol) in DCM (50 mL) dropwise via addition funnel. After 1 hour, the reaction was quenched with saturated $\text{Na}_2\text{S}_2\text{O}_3$ and slowly warmed to room temperature. Once at room

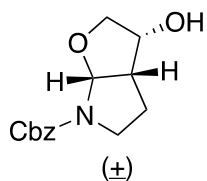
temperature, the crude product was extracted with DCM (x3), washed with brine, dried over anhydrous MgSO_4 , and concentrated under reduced pressure. Product was purified via silica gel chromatography (10% EtOAc/Hexanes) to provide 11.06 g (85%) of iodoether product as a yellow oil. ^1H NMR (400 MHz, CDCl_3) δ (ppm): 7.38 – 7.31 (m, 5H), 5.58 (d, $J = 36.4$ Hz, 1H), 5.21 – 5.14 (m, 2H), 4.33 (d, $J = 5.0$ Hz, 2H), 4.12 (s, 1H), 3.76 – 3.66 (m, 1H), 3.56 – 3.51 (m, 1H), 2.58 – 2.51 (m, 1H), 2.42 (d, $J = 35.9$ Hz, 1H), 2.16 – 2.09 (m, 1H); ^{13}C NMR (100 MHz, CDCl_3) δ (ppm): 155.5, 154.5, 136.1, 135.9, 128.4, 128.0, 127.6, 95.1, 94.4, 79.6, 79.2, 74.3, 67.5, 67.2, 56.5, 55.8, 44.8, 44.7, 33.6, 32.7, 26.6, 25.9; LRMS-ESI (+) m/z : 408.0 $[\text{M} + \text{Na}]^+$

benzyl 3-methylenehexahydro-6*H*-furo[2,3-*b*]pyrrole-6-carboxylate



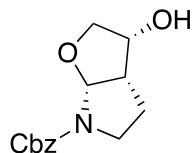
A solution of NaCNBH_3 (1.8333 g, 29.174 mmol), $n\text{Bu}_3\text{SnH}$ (300 μL , 1.132 mmol), and AIBN (374.1 mg, 2.278 mmol) was dissolved in THF (100 mL) and heated to reflux. Upon refluxing for approximately 45 minutes, a solution of iodoether (8.4640 g, 21.973 mmol) in THF (75 mL) was added dropwise. After refluxing the solution for 18 hours, the reaction was cooled to room temperature and concentrated under reduced pressure. The crude product was purified via silica gel chromatography (20% EtOAc/Hexanes) to provide 4.08 g (71%) of the *exo*-olefin product as a yellow oil. ^1H NMR (400 MHz, CDCl_3) δ (ppm): 7.39 – 7.30 (m, 5H), 5.89 (dd, $J = 21.0, 5.9$ Hz, 1H), 5.32 – 5.03 (m, 4H), 4.42 (dt, $J = 5.2, 2.4$ Hz, 2H), 3.70 – 3.63 (m, 1H), 3.40 – 3.31 (m, 2H), 2.13 – 2.04 (m, 1H), 1.93 – 1.89 (m, 1H); ^{13}C NMR (100 MHz, CDCl_3) δ (ppm): 154.3, 149.6, 136.6, 128.4, 128.3, 127.9, 127.7, 127.6, 105.6, 92.9, 92.3, 71.1, 66.8, 47.4, 46.5, 45.5, 45.3, 31.0, 30.6; LRMS-ESI (+) m/z : 260.1 $[\text{M} + \text{H}]^+$

benzyl 3-hydroxyhexahydro-6*H*-furo[2,3-*b*]pyrrole-6-carboxylate



To a solution of *exo*-olefin (7.5000g, 28.923 mmol) in MeOH:DCM (1:1) at -78 °C was bubbled ozone (O₃) gas through solution. Mixture was kept at this temperature until a faint blue color appeared. Upon observation of this color, oxygen (O₂) was bubbled through solution to remove excess ozone present and was further quenched with dimethyl sulfide (40 mL, 20 equiv.) and slowly warmed to room temperature. The quenching process continued overnight where volatiles were then removed under reduced pressure and the crude mixture was used for the NaBH₄ reduction in the next step. To a solution of crude ketone in MeOH at 0 °C was added NaBH₄ (1.3203g, 34.901 mmol) in one portion slowly. After 2 hours, reaction was quenched with saturated NH₄Cl and slowly warmed to room temperature. The crude product was extracted with ethyl acetate (3x), washed with brine, dried over anhydrous Na₂SO₄, and concentrated under reduced pressure. Product was purified via silica gel chromatography (50% EtOAc/Hexanes) to provide 2.64 g (36% over 2 steps) as a colorless oil. ¹H NMR (400 MHz, CDCl₃) δ(ppm): 7.36 – 7.30 (m, 5H), 5.76 – 5.72 (m, 1H), 5.29 – 5.09 (m, 2H), 4.39 (d, *J* = 7.0 Hz, 1H), 3.93 (dd, *J* = 9.4, 5.9 Hz, 1H), 3.62 (dd, *J* = 9.4, 6.3 Hz, 2H), 3.49 – 3.45 (m, 1H), 2.86 (brs, 1H), 2.55 (brs, 1H), 2.26 – 2.20 (m, 1H), 1.86 – 1.80 (m, 1H); ¹³C NMR (100 MHz, CDCl₃) δ(ppm): 154.5, 136.7, 128.5, 128.0, 127.9, 92.7, 92.1, 72.9, 71.3, 67.1, 47.7, 47.5, 46.8, 45.9, 23.3, 22.8; LRMS-ESI (+) *m/z*: 264.1 [M + H]⁺; HRMS (ESI) *m/z*: [M + Na]⁺ calcd C₁₄H₁₇NO₄Na 286.1050; found 286.1053.

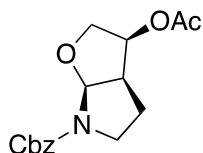
benzyl (3*R*,3*aS*,6*aR*)-3-hydroxyhexahydro-6*H*-furo[2,3-*b*]pyrrole-6-carboxylate



To a solution of racemic alcohol (2.64 g, 10.027 mmol) in a 9:1 solution of vinyl acetate (90 mL) and THF (10 mL) was added Amano Lipase PS 30 (1.3695 g, 50 wt. %) and stirred for 24 hours. Upon completion of the enzymatic resolution (as determined by NMR), the mixture was filtered

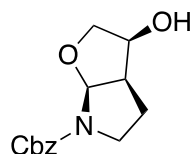
through celite and concentrated under reduced pressure. The product was purified via silica gel chromatography (30% EtOAc/Hexanes) to provide 1.2544 g (47%) of enantiopure alcohol as a colorless oil. ^1H NMR (400 MHz, CDCl_3) δ (ppm): 7.38 – 7.28 (m, 5H), 5.77 – 5.72 (m, 1H), 5.28 – 5.09 (m, 2H), 4.42 – 4.36 (m, 1H), 3.93 (dd, $J = 9.4, 5.9$ Hz, 1H), 3.62 (dd, $J = 9.4, 6.3$ Hz, 2H), 3.49 – 3.43 (m, 1H), 3.11 (brs, 1H), 2.83 (brs, 1H), 2.26 – 2.20 (m, 1H), 1.87 – 1.78 (m, 1H); ^{13}C NMR (100 MHz, CDCl_3) δ (ppm): 154.3, 136.5, 128.3, 127.8, 127.7, 92.5, 91.9, 72.7, 71.0, 66.9, 47.5, 47.2, 46.6, 45.6, 23.1, 22.5; LRMS-ESI (+) m/z : 264.1 $[\text{M} + \text{H}]^+$; $[\alpha]_D^{20}$ -95.3 (c 0.513, CHCl_3).

benzyl (3*S*,3*aR*,6*aS*)-3-acetoxylhexahydro-6*H*-furo[2,3-*b*]pyrrole-6-carboxylate



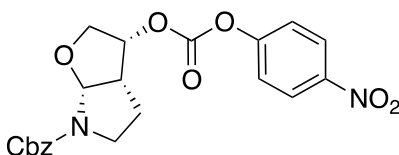
To a solution of racemic alcohol (2.64 g, 10.027 mmol) in a 9:1 solution of vinyl acetate (90 mL) and THF (10 mL) was added Amano Lipase PS 30 (1.3695 g, 50 wt. %) and stirred for 24 hours. Upon completion of the enzymatic resolution, the mixture was filtered through celite and concentrated under reduced pressure. The product was purified via silica gel chromatography (30% EtOAc/Hexanes) to provide 1.4547 g (47%) of enantiopure acetate as a colorless oil. ^1H NMR (400 MHz, CDCl_3) δ (ppm): 7.36 – 7.26 (m, 5H), 5.81 – 5.76 (m, 1H), 5.27 – 5.09 (m, 3H), 4.04 (dd, $J = 10.0, 5.9$ Hz, 1H), 3.77 (dd, $J = 10.0, 5.6$ Hz, 1H), 3.69 – 3.63 (m, 1H), 3.47 (ddd, $J = 10.7, 8.9, 7.1$ Hz, 1H), 3.06 (brs, 1H), 2.08 (s, 3H), 1.99 – 1.81 (m, 2H); ^{13}C NMR (100 MHz, CDCl_3) δ (ppm): 170.2, 154.5, 154.1, 136.4, 128.3, 127.9, 127.7, 92.3, 91.6, 73.2, 70.6, 67.0, 47.2, 46.9, 45.0, 44.1, 24.0, 23.4, 20.7; LRMS-ESI (+) m/z : 306.1 $[\text{M} + \text{H}]^+$; HRMS (ESI) m/z : $[\text{M} + \text{Na}]^+$ calcd $\text{C}_{16}\text{H}_{19}\text{NO}_5\text{Na}$ 328.1155; found 328.1159; $[\alpha]_D^{20}$ +121.2 (c 1.45, CHCl_3).

benzyl (3*S*,3*aR*,6*aS*)-3-hydroxyhexahydro-6*H*-furo[2,3-*b*]pyrrole-6-carboxylate



To a solution of enantiopure acetate (1.4547 g, 4.764 mmol) in THF (40 mL) was added aq. LiOH solution (20 mL, 0.2M) and stirred vigorously for 3 hours. After that time, the crude product was extracted with EtOAc (x3), washed with brine, dried over anhydrous Na₂SO₄, and concentrated under reduced pressure to provide 1.2539 g (99%) of enantiopure alcohol as a colorless oil without further purification. ¹H NMR (400 MHz, CDCl₃) δ (ppm): 7.35 – 7.28 (m, 5H), 5.74 – 5.71 (m, 1H), 5.26 – 5.07 (m, 2H), 4.39 – 4.33 (m, 1H), 3.91 (dd, *J* = 9.3, 5.9 Hz, 1H), 3.59 (dd, *J* = 9.3, 6.5 Hz, 2H), 3.48 – 3.42 (m, 1H), 3.08 (brs, 1H), 2.83 (brs, 1H), 2.26 – 2.19 (m, 1H), 1.85 – 1.75 (m, 1H); ¹³C NMR (100 MHz, CDCl₃) δ (ppm): 154.8, 154.4, 136.4, 128.3, 127.8, 127.6, 92.5, 91.9, 72.6, 70.8, 66.9, 47.5, 47.2, 46.5, 45.5, 23.1, 22.5; LRMS-ESI (+) *m/z*: 264.1 [M + H]⁺; [α]_D²⁰ +86.8 (*c* 0.35, CHCl₃).

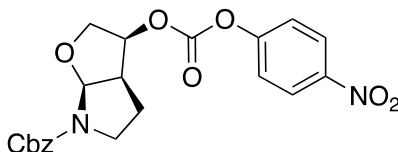
benzyl (3*R*,3*aS*,6*aR*)-3-(((4-nitrophenoxy)carbonyl)oxy)hexahydro-6*H*-furo[2,3-*b*]pyrrole-6-carboxylate



To a solution of enantiopure alcohol (1.009 g, 3.836 mmol) in DCM (40 mL) at 0 °C was added pyridine (620 μ L, 7.672 mmol) and *p*-Nitrophenyl chloroformate (1.1782 g, 5.844 mmol) sequentially. Solution remained at 0 °C for 1 hour and then slowly warmed to room temperature with the flask covered by aluminum foil. After stirring for 16 hours, reaction was concentrated under reduced pressure and purified via silica gel chromatography (40% EtOAc/Hexanes) to provide 1.2678 g (77%) of desired carbonate as an amorphous, white solid. ¹H NMR (400 MHz,

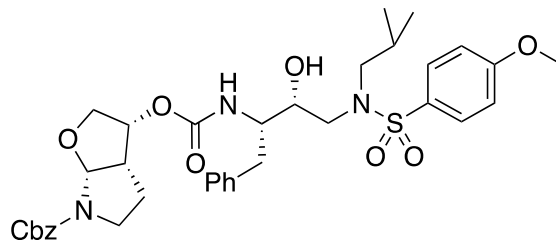
CDCl₃) δ (ppm): 8.30 – 8.26 (m, 1H), 7.40 – 7.30 (m, 7H), 5.90 – 5.82 (m, 1H), 5.31 – 5.12 (m, 3H), 4.14 (dd, J = 10.4, 5.6 Hz, 1H), 4.00 – 3.96 (m, 1H), 3.76 – 3.70 (m, 1H), 3.61 – 3.52 (m, 1H), 3.20 (brs, 1H), 2.16 – 2.11 (m, 1H), 2.04 – 1.96 (m, 1H); ¹³C NMR (100 MHz, CDCl₃) δ (ppm): 155.0, 152.0, 145.4, 136.3, 128.4, 128.0, 127.8, 125.3, 121.5, 92.4, 91.7, 78.1, 77.9, 70.4, 67.1, 47.2, 46.9, 45.2, 44.3, 24.0, 23.4; LRMS-ESI (+) m/z : 429.1 [M + H]⁺; [α]_D²⁰ -79.3 (c 0.99, CHCl₃).

benzyl (3*S*,3*aR*,6*aS*)-3-(((4-nitrophenoxy)carbonyl)oxy)hexahydro-6*H*-furo[2,3-*b*]pyrrole-6-carboxylate



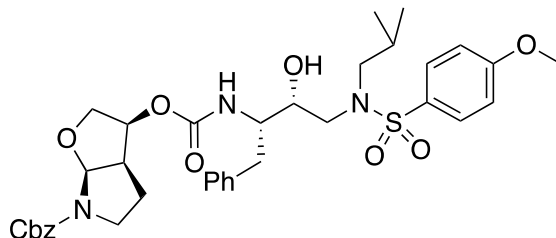
To a solution of enantiopure alcohol (0.920 g, 3.494 mmol) in DCM (40 mL) at 0 °C was added pyridine (565 μ L, 6.988 mmol) and *p*-Nitrophenyl chloroformate (1.1623 g, 5.765 mmol) sequentially. Solution remained at 0 °C for 1 hour and then slowly warmed to room temperature with the flask covered by aluminum foil. After stirring for 16 hours, reaction was concentrated under reduced pressure and purified via silica gel chromatography (40% EtOAc/Hexanes) to provide 939.8 mg (63%) of desired carbonate as an amorphous, white solid. ¹H NMR (400 MHz, CDCl₃) δ (ppm): 8.30 – 8.26 (m, 2H), 7.40 – 7.30 (m, 7H), 5.89 – 5.82 (m, 1H), 5.31 – 5.12 (m, 3H), 4.14 (dd, J = 10.4, 5.6 Hz, 1H), 4.00 – 3.96 (m, 1H), 3.76 – 3.70 (m, 1H), 3.59 – 3.52 (m, 1H), 3.19 (brs, 1H), 2.17 – 2.10 (m, 1H), 2.04 – 1.96 (m, 1H); ¹³C NMR (100 MHz, CDCl₃) δ (ppm): 155.0, 152.0, 145.4, 136.4, 128.4, 128.0, 127.8, 125.3, 121.5, 92.4, 91.7, 78.1, 77.9, 70.4, 67.1, 47.2, 46.9, 45.3, 44.2, 24.0, 23.4; LRMS-ESI (+) m/z : 429.1 [M + H]⁺; [α]_D²⁰ +93.9 (c 1.21, CHCl₃).

benzyl (3*R*,3*aS*,6*aR*)-3-((((2*S*,3*R*)-3-hydroxy-4-((*N*-isobutyl-4-methoxyphenyl)sulfonamido)-1-phenylbutan-2-yl)carbamoyl)oxy)hexahydro-6*H*-furo[2,3-*b*]pyrrole-6-carboxylate



To a solution of *p*-Nitrocarbonate (577.3 mg, 1.348 mmol) in MeCN (15 mL) was added the corresponding isostere (552.8 mg, 1.360 mmol) followed by DIPEA (1 mL, 5.741 mmol) and stirred until the reaction was completed based on TLC. After completion, the reaction mixture was concentrated under reduced pressure and purified via silica gel chromatography (40% EtOAc/Hexanes) to afford 710.1 mg (76%) of Cbz-protected inhibitor as a white solid. ¹H NMR (400 MHz, CDCl₃) δ (ppm): 7.71 (d, *J* = 8.8 Hz, 2H), 7.37 – 7.19 (m, 10H), 6.98 (d, *J* = 8.9 Hz, 2H), 5.73 – 5.68 (m, 1H), 5.25 – 4.97 (m, 4H), 3.92 – 3.84 (m, 6H), 3.71 – 3.67 (m, 2H), 3.56 – 3.46 (m, 1H), 3.21 – 3.07 (m, 3H), 3.01 – 2.94 (m, 3H), 2.79 (dd, *J* = 13.4, 6.7 Hz, 2H), 1.86 – 1.78 (m, 1H), 1.69 – 1.54 (m, 2H), 0.90 (dd, *J* = 19.6, 6.6 Hz, 6H). ¹³C NMR (200 MHz, CDCl₃) δ (ppm): 163.0, 155.4, 154.6, 154.2, 137.5, 136.5, 136.3, 129.6, 129.4, 129.2, 128.5, 128.4, 128.0, 127.9, 127.7, 126.5, 126.0, 115.5, 114.3, 92.4, 91.7, 73.9, 73.7, 72.7, 70.9, 70.8, 67.0, 60.3, 58.7, 55.5, 55.1, 53.6, 47.3, 47.0, 45.6, 44.7, 35.6, 27.2, 23.7, 23.1, 20.9, 20.1, 19.8, 14.1; LRMS-ESI (+) *m/z*: 696.3 [M + H]⁺; HRMS (ESI) *m/z*: [M + Na]⁺ calcd C₃₆H₄₅N₃O₉SNa 718.2769; found 718.2762.

benzyl (3*S*,3*aR*,6*aS*)-3-(((2*S*,3*R*)-3-hydroxy-4-((*N*-isobutyl-4-methoxyphenyl)sulfonamido)-1-phenylbutan-2-yl)carbamoyloxy)hexahydro-6*H*-furo[2,3-*b*]pyrrole-6-carboxylate



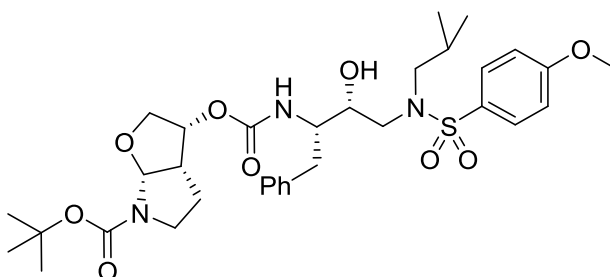
To a solution of *p*-Nitrocarbonate (600 mg, 1.401 mmol) in MeCN (14 mL) was added the corresponding isostere (573.8 mg, 1.411 mmol) followed by DIPEA (1 mL, 5.741 mmol) and stirred until the reaction was completed based on TLC. After completion, the reaction mixture was concentrated under reduced pressure and purified via silica gel chromatography (40% EtOAc/Hexanes) to afford 669.5 mg (69%) of Cbz-protected inhibitor as a white solid. ¹H NMR (400 MHz, CDCl₃) δ (ppm): 7.70 (d, *J* = 8.7 Hz, 2H), 7.37 – 7.20 (m, 10H), 6.98 (d, *J* = 8.8 Hz, 2H), 5.78 – 5.73 (m, 1H), 5.30 – 4.94 (m, 4H), 3.95 – 3.78 (m, 7H), 3.65 – 3.58 (m, 2H), 3.39 (m, 1H), 3.13 (dd, *J* = 15.1, 8.6 Hz, 1H), 3.02 – 2.89 (m, 5H), 2.77 (dd, *J* = 13.4, 6.6 Hz, 1H), 1.91 – 1.77 (m, 3H), 0.88 (dd, *J* = 20.1, 6.6 Hz, 6H). ¹³C NMR (200 MHz, CDCl₃) δ (ppm): 163.0, 155.6, 154.6, 154.2, 137.4, 136.5, 136.3, 129.7, 129.4, 129.3, 128.5, 128.4, 128.0, 127.9, 127.8, 126.6, 126.0, 115.5, 114.3, 92.3, 91.6, 73.7, 73.6, 72.4, 70.7, 67.0, 58.7, 55.5, 55.2, 55.5, 53.3, 47.2, 46.9, 45.3, 44.4, 35.2, 35.1, 27.2, 23.9, 23.3, 20.0, 19.8, 14.1; LRMS-ESI (+) *m/z*: 696.3 [M + H]⁺; HRMS (ESI) *m/z*: [M + Na]⁺ calcd C₃₆H₄₅N₃O₉SNa 718.2769; found 718.2772.

General Procedure for Carbamation and Acylation Reactions

To a solution of Cbz-protected inhibitor (1 equiv.) in MeOH (0.05 M solution) was added 10% Pd/C (5 mol %) and stirred under H₂ atmosphere. Upon completion, the mixture was filtered through celite and concentrated under reduced pressure to provide the crude amine. The crude amine was then dissolved in DCM (0.05 M solution) along with triethylamine (1.5 equiv.) and cooled to 0 °C. The corresponding electrophile (0.8 – 1.0 equiv.) was then added at this temperature and slowly warmed to room temperature. Upon completion of the reaction, the crude

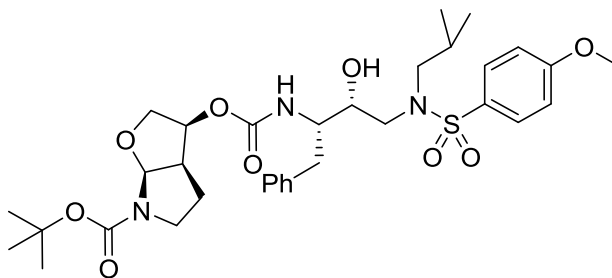
mixture was concentrated down and purified directly via silica gel chromatography to provide the resulting carbamate, carboxamide, or sulfonamide inhibitor.

tert-butyl-(3R,3aS,6aR)-3-((((2S,3R)-3-hydroxy-4-((N-isobutyl-4-methoxyphenyl)sulfonamido)-1-phenylbutan-2-yl)carbamoyl)oxy)hexahydro-6H-furo[2,3-b]pyrrole-6-carboxylate



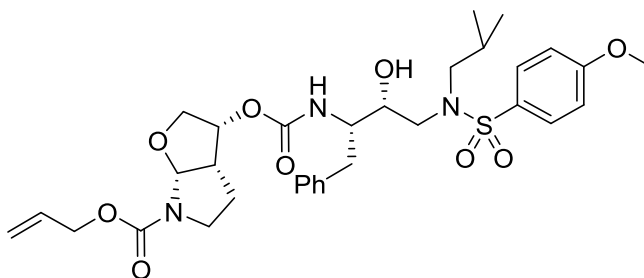
^1H NMR (400 MHz, CDCl_3) δ (ppm): 7.71 (d, J = 8.9 Hz, 2H), 7.28 – 7.20 (m, 5H), 6.98 (d, J = 8.9 Hz, 2H), 5.68 – 5.59 (m, 1H), 5.01 (brs, 1H), 4.88 (d, J = 8.9 Hz, 1H), 3.90 – 3.83 (m, 6H), 3.75 – 3.66 (m, 2H), 3.50 – 3.39 (m, 2H), 3.19 – 3.05 (m, 3H), 3.01 – 2.87 (m, 3H), 2.78 (dd, J = 13.4, 6.6 Hz, 2H), 1.88 – 1.76 (m, 1H), 1.47 (s, 9H), 1.37 – 1.28 (m, 1H), 0.90 (dd, J = 21.6, 6.6 Hz, 6H). ^{13}C NMR (200 MHz, CDCl_3) δ (ppm): 163.2, 155.7, 154.2, 153.9, 137.7, 129.8, 129.6, 129.5, 128.7, 126.7, 114.5, 92.2, 80.3, 74.2, 74.0, 72.9, 70.8, 70.6, 59.0, 55.7, 55.2, 53.9, 53.5, 47.3, 46.9, 45.7, 44.9, 35.9, 34.8, 31.7, 29.8, 28.5, 27.4, 25.4, 23.8, 23.3, 22.79, 20.8, 20.3, 20.0, 14.2; LRMS-ESI (+) m/z : 684.2 $[\text{M} + \text{Na}]^+$; HRMS (ESI) m/z : $[\text{M} + \text{Na}]^+$ calcd $\text{C}_{33}\text{H}_{47}\text{N}_3\text{O}_9\text{SNa}$ 684.2925; found 684.2929.

tert-butyl-(3S,3aR,6aS)-3-((((2S,3R)-3-hydroxy-4-((N-isobutyl-4-methoxyphenyl)sulfonamido)-1-phenylbutan-2-yl)carbamoyl)oxy)hexahydro-6H-furo[2,3-b]pyrrole-6-carboxylate



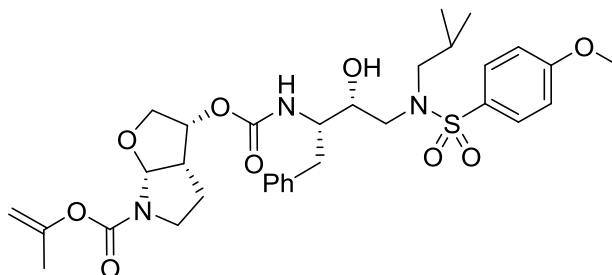
^1H NMR (800 MHz, CDCl_3) δ (ppm): 7.71 (d, J = 8.5 Hz, 2H), 7.30 – 7.22 (m, 5H), 6.98 (d, J = 8.5 Hz, 2H), 5.68 (d, J = 67.4 Hz, 1H), 5.08 – 5.02 (m, 2H), 3.91 – 3.85 (m, 7H), 3.59 – 3.49 (m, 2H), 3.31 (brs, 1H), 3.14 – 3.11 (m, 1H), 3.01 – 2.94 (m, 4H), 2.90 – 2.87 (m, 1H), 2.80 (dd, J = 13.4, 6.8 Hz, 1H), 1.88 – 1.76 (m, 3H), 1.48 (s, 9H), 0.89 (dd, J = 34.1, 6.7 Hz, 7H). ^{13}C NMR (200 MHz, CDCl_3) δ (ppm): 163.1, 155.8, 154.1, 153.8, 137.6, 129.9, 129.55, 129.51, 128.6, 126.7, 114.4, 92.1, 92.0, 80.3, 74.0, 73.8, 72.6, 70.7, 70.5, 68.0, 58.8, 55.7, 55.3, 53.6, 47.2, 46.8, 45.3, 44.5, 35.3, 29.7, 28.4, 28.3, 27.3, 24.0, 23.4, 20.2, 19.9, 14.2; LRMS-ESI (+) m/z : 84.3 [$\text{M} + \text{Na}$] $^+$; HRMS (ESI) m/z : [$\text{M} + \text{Na}$] $^+$ calcd $\text{C}_{33}\text{H}_{47}\text{N}_3\text{O}_9\text{SNa}$ 684.2925; found 684.2920.

allyl (3R,3aS,6aR)-3-((((2S,3R)-3-hydroxy-4-((N-isobutyl-4-methoxyphenyl)sulfonamido)-1-phenylbutan-2-yl)carbamoyl)oxy)hexahydro-6H-furo[2,3-b]pyrrole-6-carboxylate



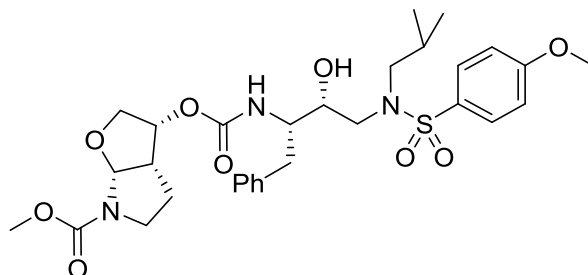
^1H NMR (400 MHz, CDCl_3) δ (ppm): 7.71 (d, J = 8.9 Hz, 2H), 7.30 – 7.20 (m, 5H), 6.98 (d, J = 8.9 Hz, 2H), 5.99 – 5.89 (m, 1H), 5.72 – 5.68 (m, 1H), 5.32 (d, J = 17.1 Hz, 1H), 5.21 (d, J = 10.5 Hz, 1H), 5.03 (q, J = 6.0 Hz, 1H), 4.90 (d, J = 9.0 Hz, 1H), 4.62 (m, 2H), 3.95 – 3.84 (m, 6H), 3.73 – 3.65 (m, 2H), 3.54 – 3.51 (m, 1H), 3.20 – 3.06 (m, 3H), 3.02 – 2.95 (m, 3H), 2.79 (dd, J = 13.4, 6.6 Hz, 2H), 1.88 – 1.77 (m, 1H), 1.45 – 1.38 (m, 1H), 0.90 (dd, J = 21.8, 6.6 Hz, 6H). ^{13}C NMR (200 MHz, CDCl_3) δ (ppm): 163.2, 155.6, 154.6, 154.2, 137.7, 132.8, 129.8, 129.6, 129.4, 128.6, 126.7, 117.8, 114.5, 92.6, 91.9, 73.9, 72.9, 71.0, 66.2, 58.9, 55.7, 55.2, 53.8, 47.5, 47.1, 45.8, 44.8, 35.8, 34.7, 31.7, 29.8, 29.1, 27.4, 25.4, 23.9, 23.3, 22.77, 22.74, 20.8, 20.2, 20.0, 14.2, 11.5; LRMS-ESI (+) m/z : 668.2 $[\text{M} + \text{Na}]^+$; HRMS (ESI) m/z : $[\text{M} + \text{Na}]^+$ calcd $\text{C}_{32}\text{H}_{43}\text{N}_3\text{O}_9\text{SNa}$ 668.2612; found 668.2608.

prop-1-en-2-yl (3R,3aS,6aR)-3-(((2S,3R)-3-hydroxy-4-((N-isobutyl-4-methoxyphenyl)sulfonamido)-1-phenylbutan-2-yl)carbamoyl)oxy)hexahydro-6H-furo[2,3-b]pyrrole-6-carboxylate



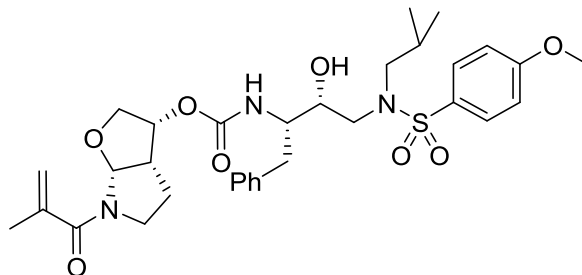
^1H NMR (800 MHz, CDCl_3) δ (ppm): 7.71 (d, J = 8.6 Hz, 2H), 7.29 – 7.19 (m, 5H), 6.98 (d, J = 8.4 Hz, 2H), 5.72 – 5.66 (m, 1H), 5.06 – 4.99 (m, 2H), 4.73 – 4.65 (m, 2H), 3.94 – 3.87 (m, 7H), 3.74 – 3.67 (m, 2H), 3.55 – 3.42 (m, 1H), 3.27 – 3.15 (m, 2H), 3.09 (dd, J = 14.4, 4.7 Hz, 1H), 3.01 – 2.96 (m, 3H), 2.82 – 2.75 (m, 2H), 1.95 (s, 3H), 1.85 – 1.80 (m, 1H), 1.70 (brs, 1H), 1.44 – 1.35 (m, 1H), 0.90 (dd, J = 38.1, 6.5 Hz, 6H). ^{13}C NMR (200 MHz, CDCl_3) δ (ppm): 163.2, 155.6, 153.1, 152.7, 152.3, 137.7, 129.8, 129.6, 129.6, 129.5, 128.7, 128.6, 126.7, 114.5, 101.9, 92.5, 92.1, 74.0, 73.9, 72.9, 71.2, 71.1, 67.2, 58.9, 55.7, 55.2, 53.8, 47.5, 47.4, 46.0, 44.9, 35.8, 34.7, 31.7, 29.8, 29.1, 27.4, 25.4, 23.9, 23.3, 22.7, 20.8, 20.2, 20.1, 20.0, 19.9, 14.2, 11.5; LRMS-ESI (+) m/z : 668.2 $[\text{M} + \text{Na}]^+$; HRMS (ESI) m/z : $[\text{M} + \text{Na}]^+$ calcd $\text{C}_{32}\text{H}_{43}\text{N}_3\text{O}_9\text{SNa}$ 668.2612; found 668.2609.

methyl-(3R,3aS,6aR)-3-((((2S,3R)-3-hydroxy-4-((N-isobutyl-4-methoxyphenyl)sulfonamido)-1-phenylbutan-2-yl)carbamoyl)oxy)hexahydro-6H-furo[2,3-b]pyrrole-6-carboxylate



^1H NMR (800 MHz, CDCl_3) δ (ppm): 7.73 (d, J = 8.4 Hz, 2H), 7.30 – 7.21 (m, 5H), 7.00 (d, J = 8.4 Hz, 2H), 5.74 – 5.64 (m, 1H), 5.05 (q, J = 6.0 Hz, 1H), 4.96 (d, J = 9.2 Hz, 1H), 3.95 – 3.87 (m, 6H), 3.76 – 3.68 (m, 5H), 3.56 – 3.45 (m, 1H), 3.21 – 3.17 (m, 2H), 3.10 (dd, J = 14.2, 4.5 Hz, 1H), 3.01 – 2.96 (m, 3H), 2.82 – 2.78 (m, 2H), 1.86 – 2.83 (m, 1H), 1.44 – 1.25 (m, 2H), 0.92 (dd, J = 41.4, 6.3 Hz, 6H). ^{13}C NMR (200 MHz, CDCl_3) δ (ppm): 163.2, 155.6, 155.0, 137.7, 129.8, 129.6, 129.5, 128.7, 126.7, 114.5, 92.6, 91.9, 74.1, 73.9, 72.9, 71.0, 58.9, 55.7, 55.2, 53.8, 53.0, 52.7, 47.5, 47.1, 45.9, 44.8, 35.8, 34.8, 34.6, 31.7, 29.8, 29.1, 27.4, 25.4, 23.9, 23.3, 22.7, 20.8, 20.2, 20.0, 18.8, 14.2, 11.5; LRMS-ESI (+) m/z : 642.2 $[\text{M} + \text{Na}]^+$; HRMS (ESI) m/z : $[\text{M} + \text{Na}]^+$ calcd $\text{C}_{30}\text{H}_{41}\text{N}_3\text{O}_9\text{SNa}$ 642.2456; found 642.2450.

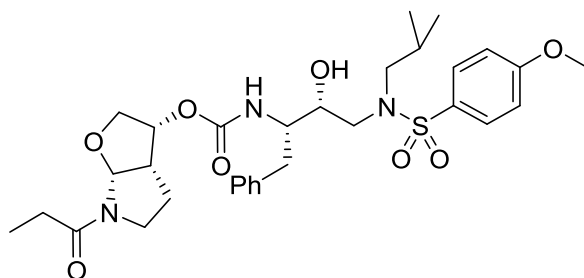
(3R,3aS,6aR)-6-methacryloylhexahydro-2H-furo[2,3-b]pyrrol-3-yl (((2S,3R)-3-hydroxy-4-((N-isobutyl-4-methoxyphenyl)sulfonamido)-1-phenylbutan-2-yl)carbamate



^1H NMR (800 MHz, CDCl_3) δ (ppm): 7.73 (d, J = 8.8 Hz, 2H), 7.32 – 7.18 (m, 5H), 7.00 (d, J = 8.5 Hz, 2H), 5.61 (brs, 0.7H), 5.40-5.31 (m, 2H), 5.09 – 5.04 (m, 2H), 3.93 – 3.75 (m, 7H), 3.69 (brs, 1H), 3.19 – 3.17 (m, 2H), 3.10 (dd, J = 14.2, 4.6 Hz, 1H), 3.02 – 2.96 (m, 3H), 2.83 – 2.79

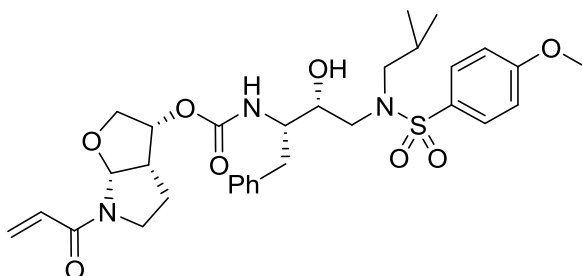
(m, 2H), 1.98 (s, 3H), 1.86 – 1.83 (m, 1H), 1.42 (brs, 1H), 1.32 – 1.29 (m, 1H), 0.92 (dd, $J = 38.6, 6.7$ Hz, 6H). ^{13}C NMR (200 MHz, CDCl_3) δ (ppm): 171.8, 163.2, 155.6, 140.4, 137.7, 129.8, 129.6, 129.5, 128.7, 126.7, 117.9, 114.5, 93.2, 74.2, 72.9, 71.0, 58.9, 55.8, 55.3, 53.8, 46.2, 46.0, 35.8, 34.8, 31.7, 29.8, 29.2, 27.4, 25.4, 23.1, 22.7, 20.8, 20.6, 20.3, 20.1, 20.0, 14.2, 11.5; LRMS-ESI (+) m/z : 630.3 $[\text{M} + \text{H}]^+$; HRMS (ESI) m/z : $[\text{M} + \text{Na}]^+$ calcd $\text{C}_{32}\text{H}_{43}\text{N}_3\text{O}_8\text{SNa}$ 652.2663; found 652.2667.

(3R,3aS,6aR)-6-propionylhexahydro-2H-furo[2,3-b]pyrrol-3-yl ((2S,3R)-3-hydroxy-4-((N-isobutyl-4-methoxyphenyl)sulfonamido)-1-phenylbutan-2-yl)carbamate



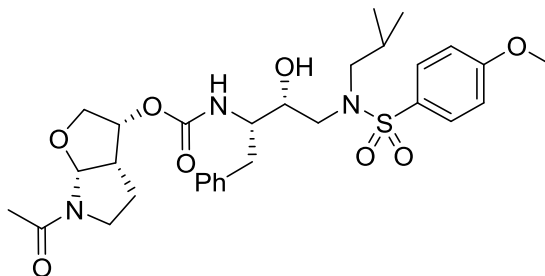
^1H NMR (800 MHz, CDCl_3) δ (ppm): 7.74 (d, $J = 8.8$ Hz, 2H), 7.32 – 7.20 (m, 5H), 7.00 (d, $J = 8.4$ Hz, 2H), 5.90 (d, 0.17H, $J = 6.4$ Hz), 5.61 (d, $J = 6.3$ Hz, 0.8H), 5.10 – 5.05 (m, 1H), 4.99 – 4.97 (m, 1H), 3.97 – 3.87 (m, 6H), 3.71 – 3.65 (m, 2H), 3.21 – 3.15 (m, 2H), 3.10 (dd, $J = 14.1, 4.7$ Hz, 1H), 3.03 – 2.93 (m, 3H), 2.84 – 2.77 (m, 2H), 2.55 – 2.51 (m, 0.8H), 2.41 – 2.36 (m, 0.9H), 1.87 – 1.82 (m, 1H), 1.66 – 1.50 (m, 2H), 1.37 – 1.33 (m, 1H), 1.16 (t, $J = 7.4$ Hz, 3H), 0.92 (dd, $J = 44.6, 6.8$ Hz, 6H). ^{13}C NMR (200 MHz, CDCl_3) δ (ppm): 174.0, 163.2, 155.5, 137.6, 129.9, 129.6, 129.54, 129.5, 128.7, 128.6, 126.7, 114.56, 114.54, 92.1, 91.1, 74.4, 73.8, 73.0, 72.9, 71.3, 71.0, 59.0, 55.8, 55.3, 55.2, 53.8, 47.5, 46.7, 46.4, 44.4, 35.8, 29.8, 28.4, 27.4, 27.2, 24.2, 22.5, 20.3, 20.0, 14.27, 9.2, 8.8; LRMS-ESI (+) m/z : 640.3 $[\text{M} + \text{Na}]^+$; HRMS (ESI) m/z : $[\text{M} + \text{Na}]^+$ calcd $\text{C}_{31}\text{H}_{44}\text{N}_3\text{O}_8\text{SNa}$ 618.2844; found 618.2853.

(3R,3aS,6aR)-6-acryloylhexahydro-2H-furo[2,3-b]pyrrol-3-yl ((2S,3R)-3-hydroxy-4-((N-isobutyl-4-methoxyphenyl)sulfonamido)-1-phenylbutan-2-yl)carbamate



^1H NMR (800 MHz, CDCl_3) δ (ppm): 7.73 (d, J = 8.5 Hz, 2H), 7.31 – 7.21 (m, 5H), 7.00 (d, J = 8.5 Hz, 2H), 6.64 (dd, J = 16.9, 10.4 Hz, 1H), 6.41 (d, J = 16.5 Hz, 1H), 5.72 – 5.70 (m, 2H), 5.13 – 5.03 (m, 2H), 4.00 – 3.97 (m, 1H), 3.93 – 3.87 (m, 5H), 3.75 – 3.68 (m, 2H), 3.27 (q, J = 10.9, 9.9 Hz, 1H), 3.19 (dd, J = 15.2, 9.0 Hz, 1H), 3.10 (dd, J = 14.2, 4.4 Hz, 1H), 3.04 – 2.99 (m, 3H), 2.83 – 2.77 (m, 2H), 1.88 – 1.83 (m, 1H), 1.59 – 1.53 (m, 1H), 1.40 – 1.37 (m, 1H), 0.96 – 0.88 (m, 6H). ^{13}C NMR (200 MHz, CDCl_3) δ (ppm): 165.5, 163.2, 155.5, 137.7, 129.9, 129.6, 129.5, 128.7, 128.6, 128.3, 126.7, 114.5, 92.0, 73.8, 72.9, 71.3, 58.9, 55.7, 55.3, 53.8, 46.9, 46.4, 35.8, 34.8, 31.7, 29.8, 27.4, 25.4, 24.2, 22.7, 22.5, 20.8, 20.3, 20.0, 14.2, 11.5; LRMS-ESI (+) m/z : 616.2 $[\text{M} + \text{H}]^+$; HRMS (ESI) m/z : $[\text{M} + \text{Na}]^+$ calcd $\text{C}_{31}\text{H}_{41}\text{N}_3\text{O}_8\text{SNa}$ 638.2507; found 638.2502.

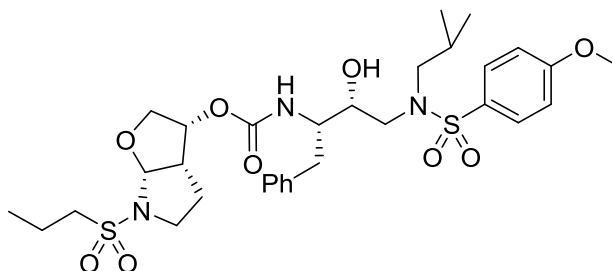
(3R,3aS,6aR)-6-acetylhexahydro-2H-furo[2,3-b]pyrrol-3-yl ((2S,3R)-3-hydroxy-4-((N-isobutyl-4-methoxyphenyl)sulfonamido)-1-phenylbutan-2-yl)carbamate



^1H NMR (800 MHz, CDCl_3) δ (ppm): 7.73 (d, J = 8.9 Hz, 2H), 7.30 – 7.20 (m, 5H), 7.00 (d, J = 9.0 Hz, 2H), 5.58 (d, J = 6.3 Hz, 0.8H), 5.09 – 5.00 (m, 2H), 3.99 – 3.89 (m, 6H), 3.71 – 3.63 (m, 2H), 3.20 – 3.15 (m, 2H), 3.11 – 3.09 (m, 1H), 3.02 – 2.99 (m, 3H), 2.80 (m, 2H), 2.16 (s, 2.35H), 2.07 (s, 0.49H), 1.87 – 1.82 (m, 1H), 1.56 – 1.51 (m, 1H), 1.35 – 1.32 (m, 1H), 0.92 (dd,

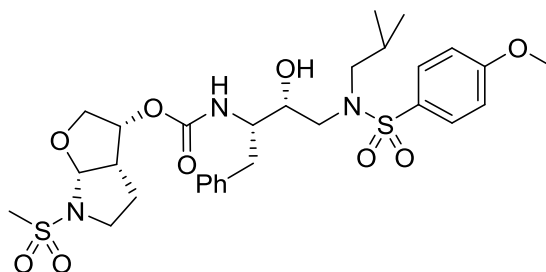
$J = 41.8, 6.5$ Hz, 6H). ^{13}C NMR (200 MHz, CDCl_3) δ (ppm): 170.6, 170.2, 163.28, 163.24, 137.7, 129.9, 129.6, 129.53, 129.50, 128.7, 128.6, 126.7, 114.55, 114.52, 92.8, 90.9, 74.3, 73.7, 73.0, 72.9, 71.5, 71.1, 59.0, 58.9, 55.7, 55.3, 55.2, 53.8, 48.5, 46.7, 46.3, 44.7, 35.8, 34.8, 31.7, 29.8, 27.4, 25.4, 24.2, 23.0, 22.7, 22.6, 21.9, 20.3, 20.06, 20.03, 14.26; LRMS-ESI (+) m/z : 604.3 $[\text{M} + \text{H}]^+$; HRMS (ESI) m/z : $[\text{M} + \text{Na}]^+$ calcd $\text{C}_{30}\text{H}_{41}\text{N}_3\text{O}_8\text{SNa}$ 626.2507; found 626.2503.

(3R,3aS,6aR)-6-(propylsulfonyl)hexahydro-2H-furo[2,3-b]pyrrol-3-yl ((2S,3R)-3-hydroxy-4-((N-isobutyl-4-methoxyphenyl)sulfonamido)-1-phenylbutan-2-yl)carbamate



^1H NMR (800 MHz, CDCl_3) δ (ppm): 7.74 (d, $J = 8.8$ Hz, 2H), 7.31 – 7.22 (m, 5H), 7.01 (d, $J = 8.8$ Hz, 2H), 5.67 (d, $J = 6.2$ Hz, 1H), 5.05 (dt, $J = 8.1, 5.3$ Hz, 1H), 5.00 (d, $J = 8.9$ Hz, 1H), 3.94 – 3.90 (m, 6H), 3.74 (dd, $J = 10.0, 4.9$ Hz, 1H), 3.67 (brs, 1H), 3.54 (td, $J = 8.9, 2.4$ Hz, 1H), 3.20 (dd, $J = 15.1, 8.6$ Hz, 1H), 3.13 – 3.10 (m, 1H), 3.09 – 3.06 (m, 3H), 3.04 – 3.00 (m, 3H), 2.84 – 2.80 (m, 2H), 1.95 – 1.90 (m, 1H), 1.89 – 1.83 (m, 2H), 1.69 – 1.64 (m, 1H), 1.38 – 1.33 (m, 1H), 1.08 (t, $J = 7.4$ Hz, 3H), 0.93 (dd, $J = 6.3$ Hz, 6H). ^{13}C NMR (200 MHz, CDCl_3) δ (ppm): 163.3, 155.4, 137.7, 129.8, 129.6, 129.4, 128.7, 128.6, 126.8, 114.5, 93.6, 73.8, 73.0, 71.2, 67.1, 59.0, 55.8, 55.6, 55.2, 53.8, 48.8, 46.2, 35.5, 31.7, 29.8, 27.4, 24.9, 22.8, 20.3, 20.0, 16.9, 14.2, 13.2; LRMS-ESI (+) m/z : 690.2 $[\text{M} + \text{Na}]^+$; HRMS (ESI) m/z : $[\text{M} + \text{Na}]^+$ calcd $\text{C}_{31}\text{H}_{45}\text{N}_3\text{O}_9\text{S}_2\text{Na}$ 690.2489; found 690.2484.

(3R,3aS,6aR)-6-(methylsulfonyl)hexahydro-2H-furo[2,3-b]pyrrol-3-yl ((2S,3R)-3-hydroxy-4-((N-isobutyl-4-methoxyphenyl)sulfonamido)-1-phenylbutan-2-yl)carbamate



^1H NMR (800 MHz, CDCl_3) δ (ppm): 7.73 (d, J = 8.9 Hz, 2H), 7.31 – 7.22 (m, 5H), 7.01 (d, J = 8.4 Hz, 2H), 5.63 (d, J = 6.2 Hz, 1H), 5.06 (d, J = 6.7 Hz, 1H), 5.00 (d, J = 8.9 Hz, 1H), 3.94 – 3.89 (m, 6H), 3.75 (dd, J = 10.2, 4.5 Hz, 1H), 3.67 (brs, 1H), 3.49 (t, J = 8.6 Hz, 1H), 3.22 – 3.19 (m, 1H), 3.10 – 2.99 (m, 8H), 2.83 – 2.80 (m, 2H), 1.89 – 1.84 (m, 1H), 1.72 – 1.67 (m, 1H), 1.35 (dd, J = 13.2, 5.9 Hz, 1H), 0.93 (dd, J = 42.2, 6.6 Hz, 6H). ^{13}C NMR (200 MHz, CDCl_3) δ (ppm): 163.3, 155.4, 137.7, 129.8, 129.6, 129.4, 128.7, 126.8, 114.5, 94.0, 73.8, 73.0, 71.5, 59.0, 55.8, 55.2, 53.8, 48.5, 46.2, 40.3, 35.5, 29.8, 27.4, 24.6, 20.3, 20.0, 14.2; LRMS-ESI (+) m/z : 662.2 [$\text{M} + \text{Na}$] $^+$; HRMS (ESI) m/z : [$\text{M} + \text{Na}$] $^+$ calcd $\text{C}_{29}\text{H}_{41}\text{N}_3\text{O}_9\text{SNa}$ 662.2176; found 662.2183.

CHAPTER 2. SYNTHESIS OF CALLYSPONGIOLIDE FRAGMENTS

2.1 Introduction

Natural products (NPs) have vastly contributed to the success of research and development programs in the pharmaceutical industry to treat various diseases and illnesses.¹²⁷ The biological activity of these natural products can be attributed to their chemical architecture. In some cases, natural products do not exhibit potent cytotoxicity or prove to be unstable in physiological conditions. However, their core scaffold makes for a positive starting point to investigate structural motifs responsible for biological activity. Simple structural modifications can lead to an increase in solubility, a decrease in toxicity, and improve binding affinity to the respective target.¹²⁸ This has led researchers to synthesize natural product derivatives and has resulted in numerous FDA-approved drugs; i.e. Amoxicillin. In 1928, Alexander Fleming discovered a novel antibiotic from a penicillium mould, known as Penicillin G.¹²⁹ Upon further investigation, Penicillin G was shown to have a narrow spectrum of activity with poor oral absorption. Synthetic modifications led to the first aminopenicillin derivative, Ampicillin. This modification improved oral absorption, increased half-life, and broadened the spectrum of treatable bacterial infections compared to that of Penicillin G. Further structural alterations led to the discovery of Amoxicillin, a more commonly used antibiotic to date. Amoxicillin is superior to Ampicillin in terms of oral absorption and is effective against similar strains of bacteria.¹³⁰

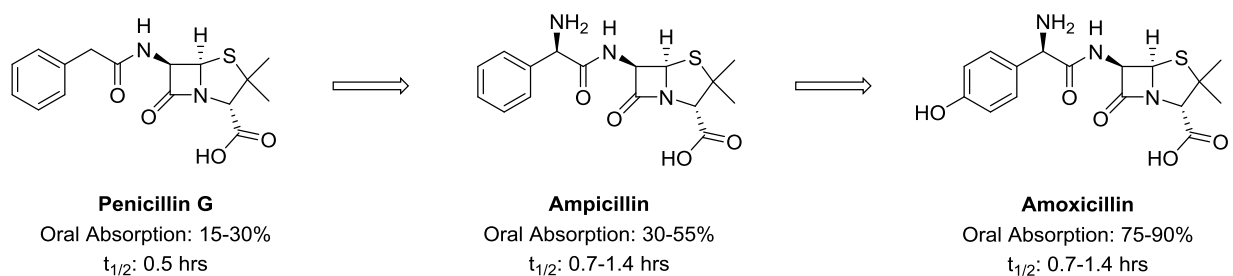


Figure 2.1 Synthetic Modifications of Penicillin G

While derivatization of natural products has significantly enhanced strategies to combat diseases, one of the more desirable ailments to cure has been cancer. Of the current anticancer drugs, over 60% of them have been derived from natural sources and present issues such as poor

Callyspongiolide exhibited inhibitory activity against human Jurkat J16 T ($IC_{50} = 70$ nM) and Ramos B lymphocytes ($IC_{50} = 60$ nM).

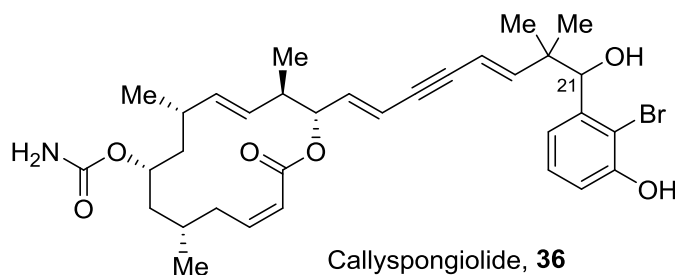


Figure 2.3 Reported Isolated Structure of Callyspongiolide

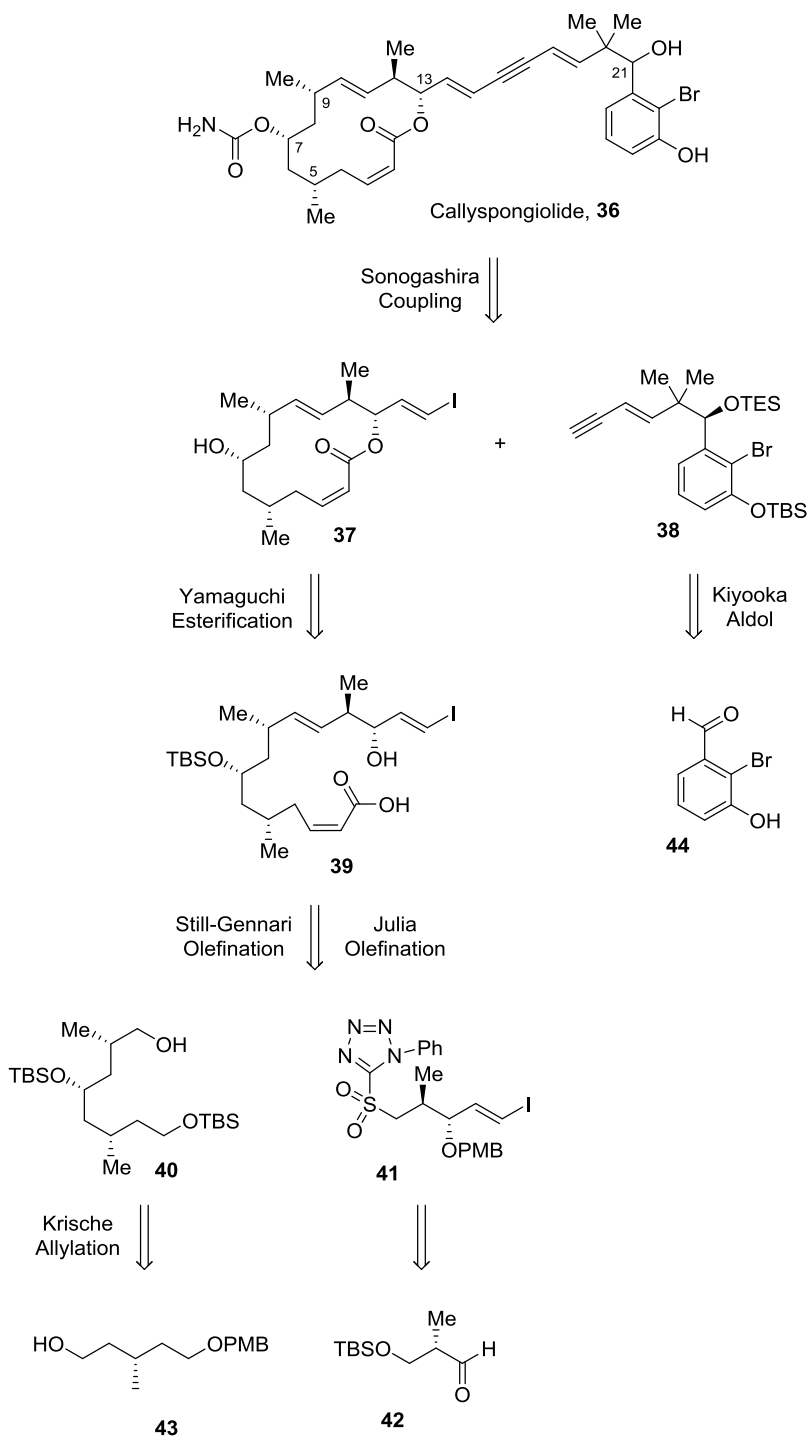
2.3 Mechanism of Action

Callyspongiolide is a very potent natural product with promising ability as an anticancer agent. However, the direct mechanism of action of Callyspongiolide is unknown. While this property is still to be determined, a plausible mechanism of action can be proposed based upon natural products with similar scaffolds. One anticancer natural product that can be compared to Callyspongiolide is Laulimalide. Laulimalide is an 18-membered *cis*-macrolactone whereas Callyspongiolide is a 14-membered *cis*-macrolactone. The potent activity of Laulimalide can be explained as this natural product is a microtubule stabilizing agent.¹³³ During the continuous process of microtubule assembly and disassembly, Laulimalide binds to the β -tubulin of the tubulin dimer, prevents the disassembly process and further leads to mitotic arrest.¹³⁴ Therefore, it is possible Callyspongiolide exhibits a similar mechanism of action, but further experimentation is necessary to divulge the complete process.

2.4 First Reported Total Synthesis of Callyspongiolide

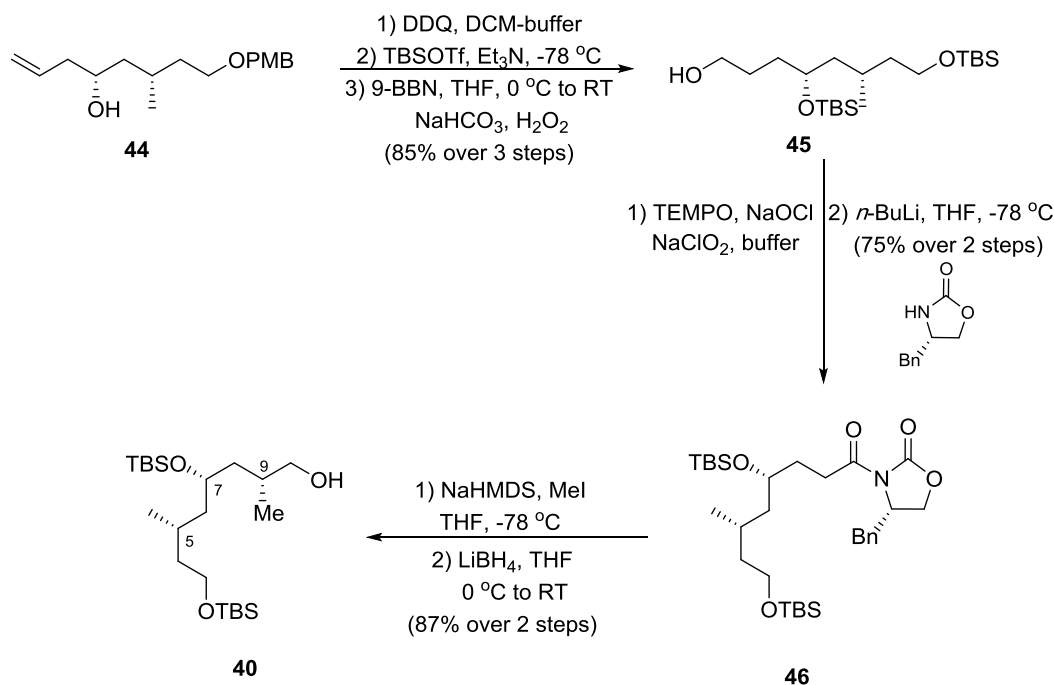
The first total synthesis of Callyspongiolide, along with 3 stereoisomers, was reported by Xu and Ye.¹³⁵ Their retrosynthetic analysis for the construction of this complex natural product is shown below. A late-stage Sonogashira coupling was envisioned to furnish the natural product from vinyl iodide **37** and the enyne **38** fragment. The macrocyclic core of **37** would come from an intramolecular Yamaguchi esterification from the carboxylic acid precursor **39**. A Kocienski-Julia olefination between silyl ether **40** and sulfone **41** would provide the desired *trans*-alkene in

39. Sulfone **41** could be prepared from aldehyde **42** and silyl ether **40** could be furnished from a Krische allylation sequence involving mono-protected alcohol **43**.



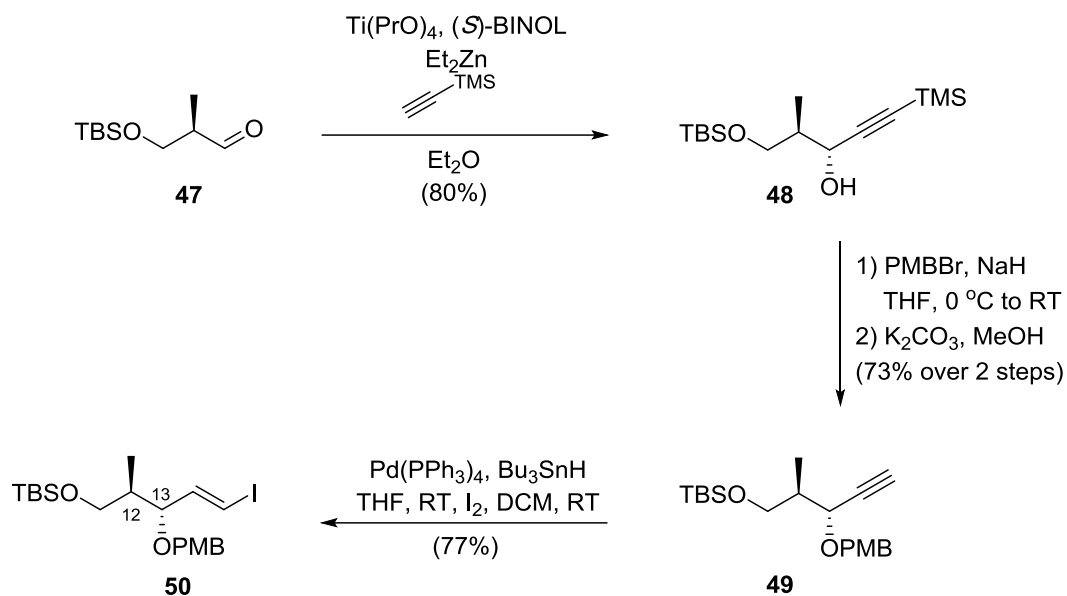
Scheme 2.1 Ye's Retrosynthetic Analysis of Callyspongiolide

Following a diastereoselective Krische allylation, resulting in the desired stereochemistry of the resulting alcohol at C-7, the terminal olefin was oxidized under hydroboration conditions with 9-BBN providing **45** (Scheme 2.2). The alcohol was oxidized to the aldehyde and further treated with *n*-BuLi followed by Evans' chiral auxiliary to afford **46**. Use of this auxiliary permitted the induction of the desired stereochemistry at C-9 from the resulting methylation with NaHMDS and MeI. Removal of the auxiliary with LiBH₄ afforded primary alcohol **40**.



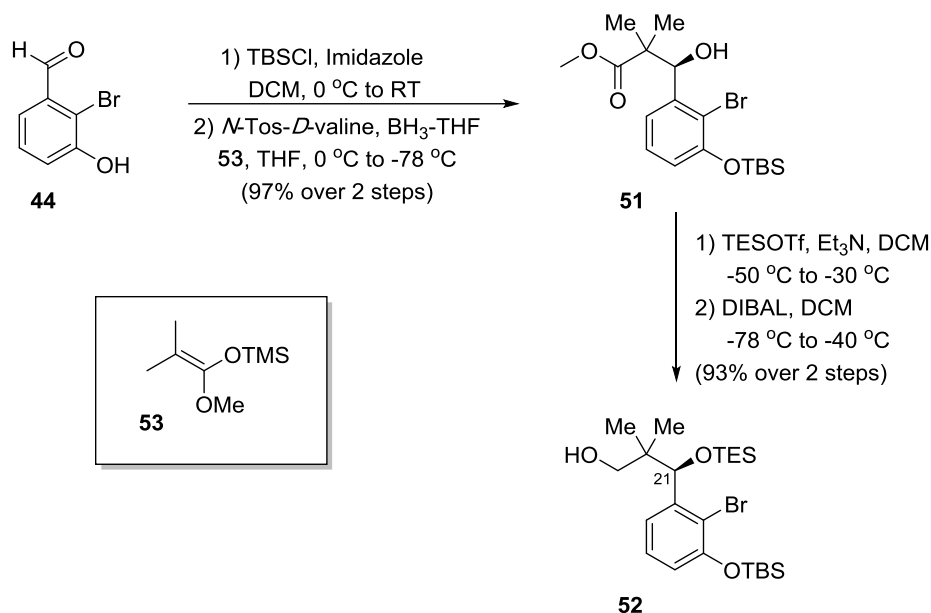
Scheme 2.2 Synthetic Route to Di-silyl ether **40**

To prepare the vinyl iodide side chain, aldehyde **47** was treated with Ti(O^{*i*}Pr)₄, (*S*)-BINOL, Et₂Zn, and TMS-acetylene resulting in the propargylic alcohol **48** (Scheme 2.3). Due to the chirality of the BINOL ligand, the resulting stereochemistry was set at C-13. Progressing further, the secondary alcohol was protected as a PMB ether and the silyl group was removed under the mild conditions of K₂CO₃ in MeOH providing alkyne **49**. The terminal alkyne underwent hydrostannylation with Pd(PPh₃)₄ and Bu₃SnH where the resulting stannane was treated with iodine affording the vinyl iodide intermediate **50**.



Scheme 2.3 Synthesis of Vinyl Iodide **50**

Synthesis of the enyne side chain **38** was accomplished from aldehyde **44** (Scheme 2.4). After silyl protection with TBSCl, a Kiyooka aldol reaction with methyl trimethylsilyl ketene **53** and oxazaborolidine (prepared *in situ*) provided the β-hydroxy methyl ester **51**. Incorporation of the enantiomeric valine unit provided the enantiomer of **51** to allow structural determination of the natural product at this carbon center.



Scheme 2.4 Synthesis Towards Enyne **38**

From the chemistry design outlined above, Ye and co-workers were able to synthesize four potential stereoisomers of Callyspongiolide (Figure 2.4). Synthesis and characterization of each isomer allowed for full structural assignment of the natural product, including the unambiguous assignment of the C-21 carbon center that was elusive during the isolation of this molecule. Based upon their collected ¹H NMR, ¹³C NMR, and optical rotation, Ye and coworkers concluded **36c** is the naturally occurring Callyspongiolide natural product (Table 2.1).

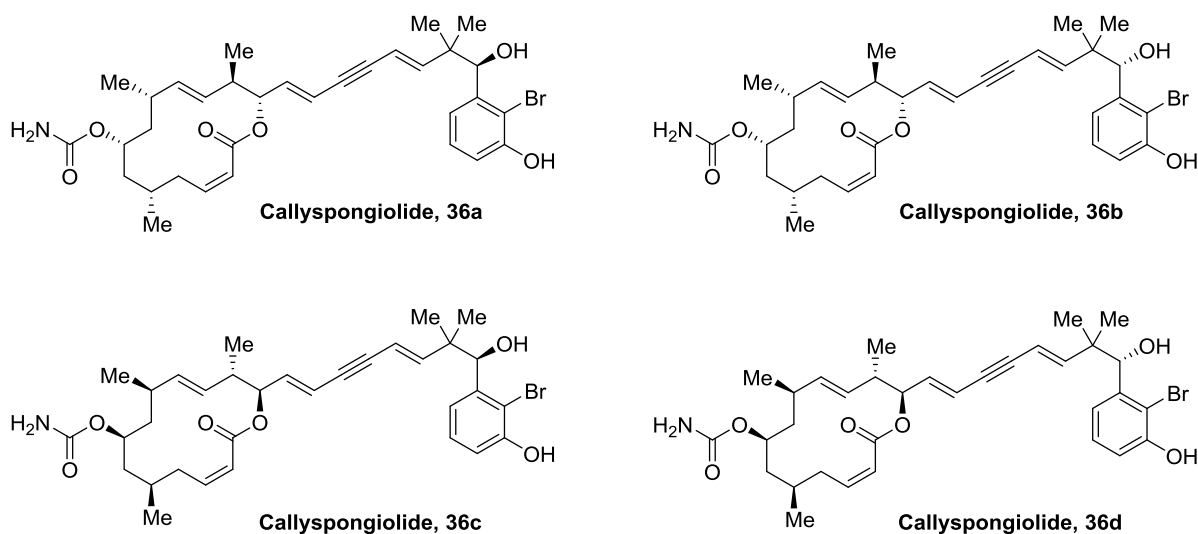


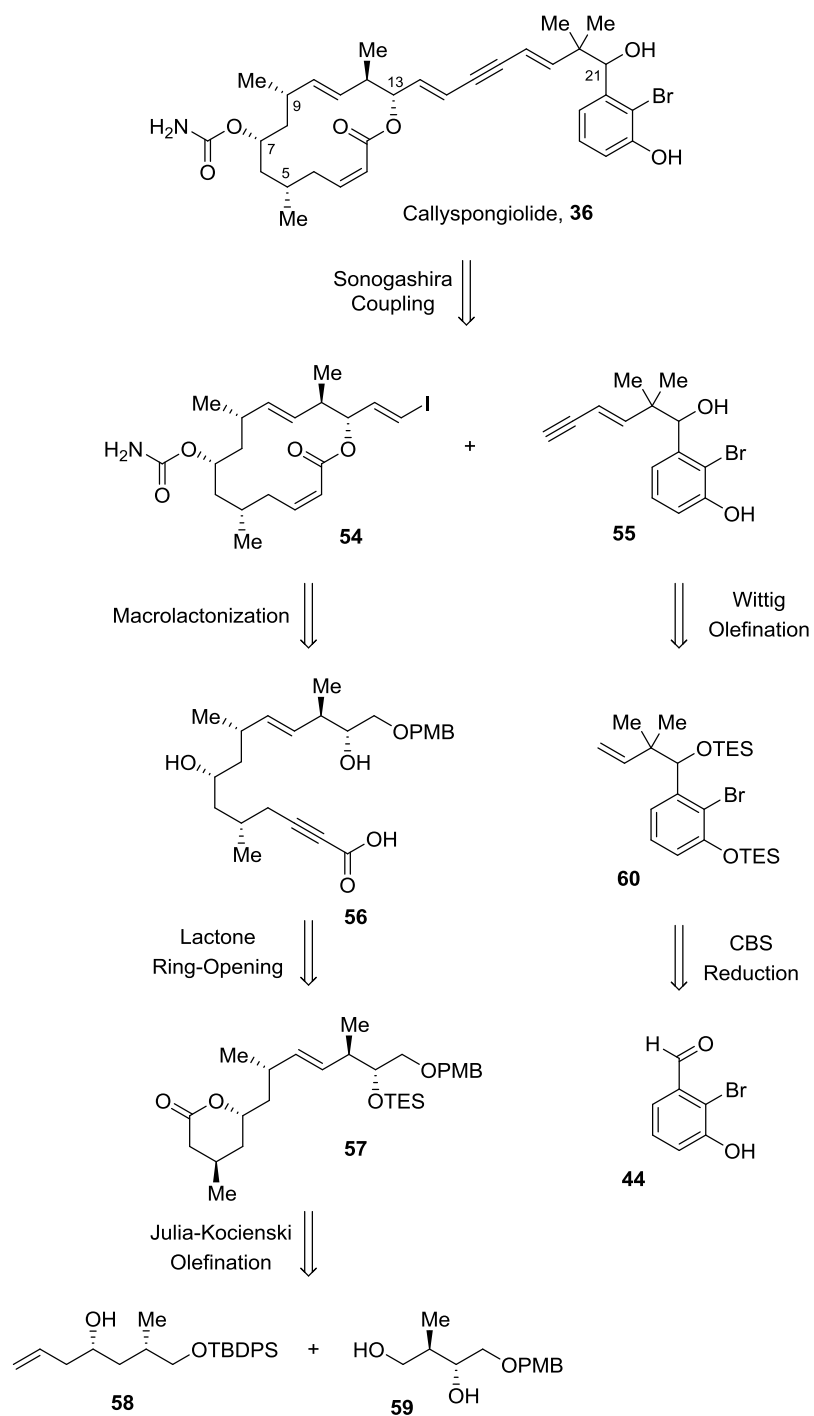
Figure 2.4 Potential Callyspongiolide Structural Assignment

Table 2.1 Optical Rotation Reported by Ye

Stereoisomer	$[\alpha]_D^{20}$ (c 0.1, MeOH)
Isolated Natural Product	-12.5
36a	+66.0
36b	+12.0
36c	-13.0
36d	-62.9

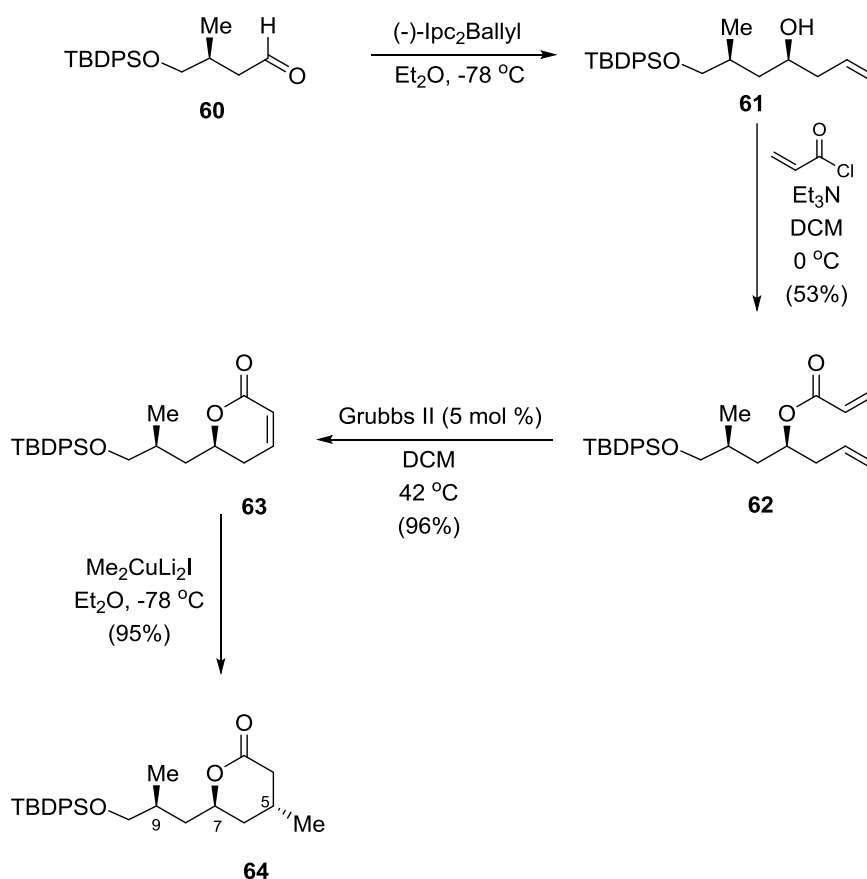
2.5 Total Synthesis Reported by Ghosh Group

The second total synthesis of Callyspongiolide, and identification of the correct C-21 epimer, was accomplished by Ghosh.¹³⁶ The retrosynthetic analysis is presented below. Similar to the Ye synthesis, a Sonogashira coupling between vinyl iodide **54** and enyne **55** could furnish Callyspongiolide. The macrocyclic core of vinyl iodide **54** could be constructed through a macrocyclization/reduction sequence. Acid **56** could be obtained through ring-opening of lactone **57**. The olefin in **57** can be achieved from a Julia-Kocienski olefination from the corresponding aldehyde of allyl alcohol **58** and the sulfone prepared from diol **59**. The enyne coupling partner would be furnished through a Wittig olefination to install the terminal alkyne with the aldehyde derived from alkene **60**. A chiral reduction utilizing a CBS catalyst could afford either of the desired C-21 epimers from the ketone precursor.



Scheme 2.5 Ghosh's Retrosynthetic Analysis of Callyspongiolide

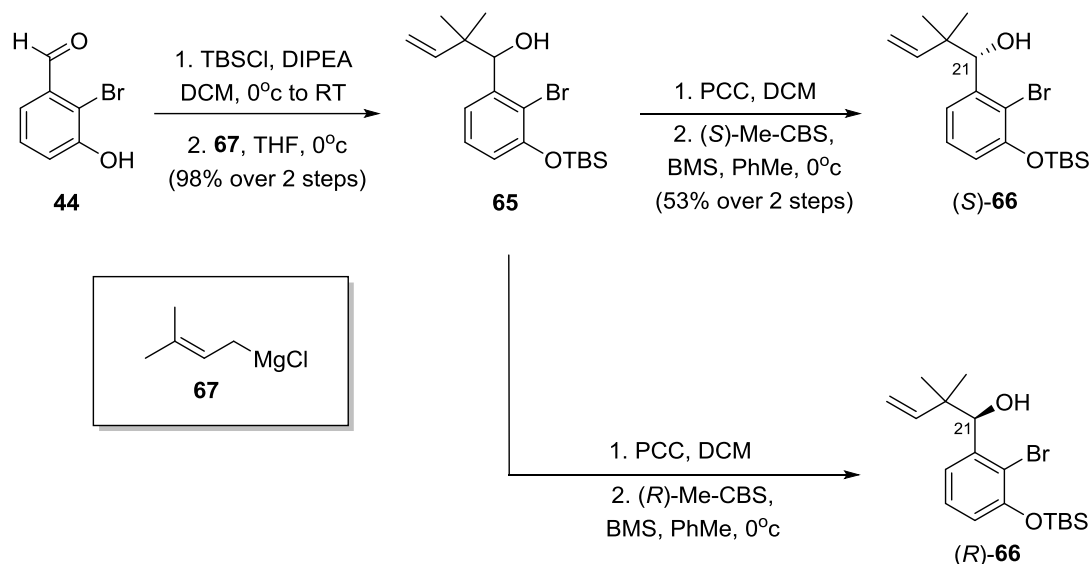
The Ghosh synthesis utilizes several key transformations to install the appropriate stereochemistry at C-5, C-7, C-9, and C-21. These transformations are independent of the Ye synthesis and are highlighted below (Scheme 2.6). Aldehyde **60** underwent Brown allylation with (-)-Ipc₂Ballyl to provide allyl alcohol **61** with the desired stereochemistry at C-7. Allyl alcohol **61** was then converted to an acrylate ester with acryloyl chloride and subsequently treated with Grubbs II catalyst to facilitate a ring-closing metathesis to produce lactone **62**. A stereoselective methyl 1,4-addition was accomplished with Me₂CuLi₂I to afford lactone **64** with the desired C-5 stereochemistry.



Scheme 2.6 Synthesis of Lactone **64**

To identify the correct stereochemistry at C-21, Ghosh utilized a chiral reduction method with Corey's CBS-catalyst (Scheme 2.7). Alteration of this catalyst would provide the desired enantiomer to be processed further in the synthetic scheme. Starting with aldehyde **44**, reverse prenylation with 3-methyl-2-butenylmagnesium chloride proceeded smoothly to provide racemic

alcohol **65**. The alcohol was oxidized with PCC and the resulting ketone was subsequently reduced with the desired Me-CBS catalyst. The (*S*) catalyst provided (*S*)-**66** and the (*R*)-Me-CBS catalyst produced (*R*)-**66**.



Scheme 2.7 Chiral Reduction Method to Acquire C-21 Epimers (*S*)-**66** and (*R*)-**66**

The synthetic design outlined above provided an efficient avenue to prepare Callyspongiolide isomers **36a** and **36b** (Figure 2.5). While the reported structure of Callyspongiolide included the assigned stereochemistry of the macrocyclic core, investigation into the stereochemistry at C-21 was important to identify the conformation of the natural product. However, upon further investigation into the synthetic ^1H NMR, ^{13}C NMR, and optical rotation values, the absolute stereochemistry of the natural product was difficult to deduce. Anomalies between the synthetic data and the literature reported values led to the belief the reported structure from the isolation was incorrect (Table 2.2). To confirm this theory, the stereochemistry of the macrocyclic core was investigated and resulted in the synthesis of two additional Callyspongiolide isomers.

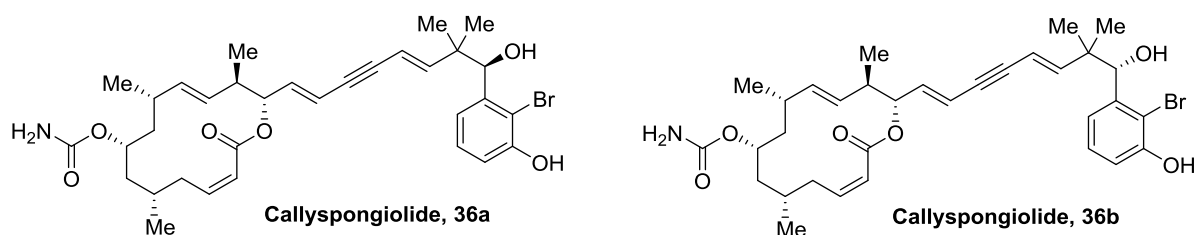


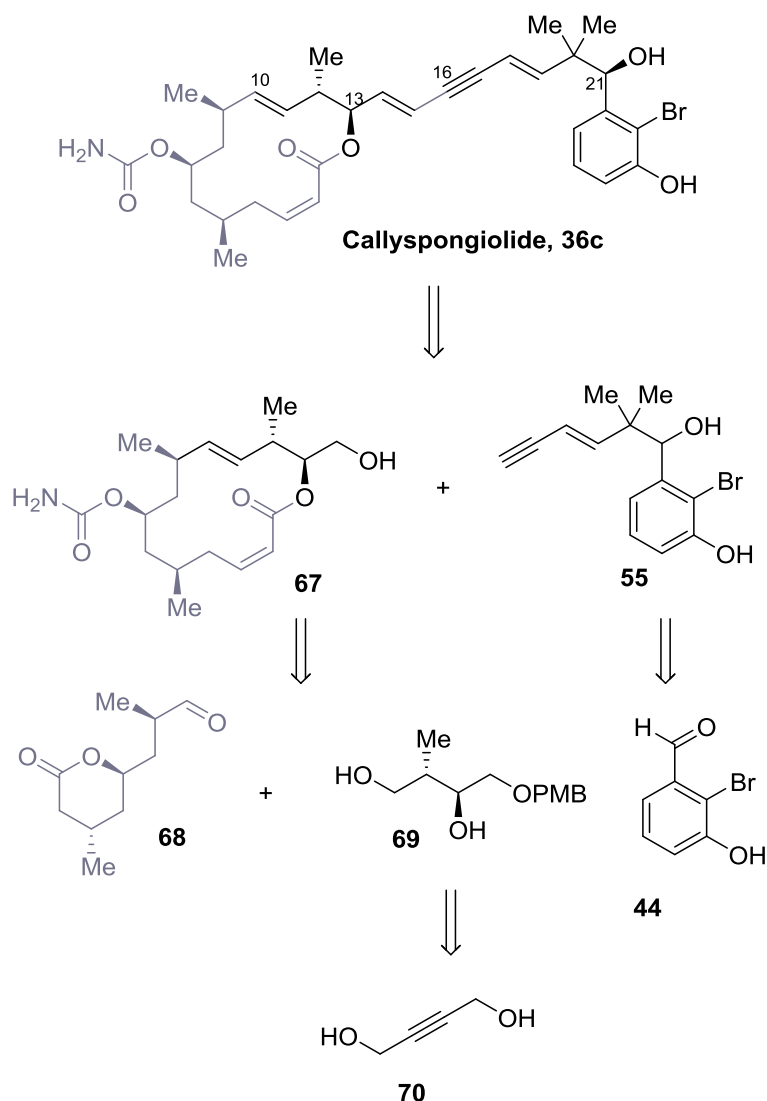
Figure 2.5 Synthetic Callyspongiolide Isomers Completed by Ghosh

Table 2.2 Optical Rotation Reported by Ghosh

Stereoisomer	$[\alpha]_D^{20}$ (c 0.1, MeOH)
Isolated Natural Product	-12.5
36a	+159
36b	+24.5

2.6 Synthesis of Callyspongiolide Fragments

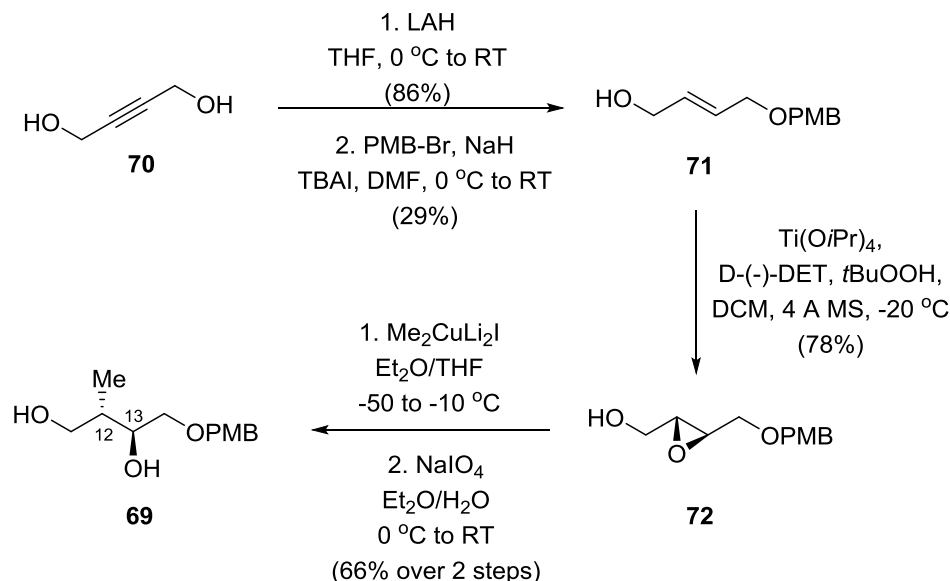
The retrosynthetic analysis of Callyspongiolide can be seen below, with specified synthetic targets bolded (Scheme 2.8). We envisioned a convergent synthesis with a late-stage Sonogashira coupling between alcohol precursor **67** and enyne **55** to furnish the natural product. Alcohol **67** would be prepared from a Julia – Kocienski olefination with aldehyde **69** and the sulfone originating from diol **70**. Diol **70** can be achieved from commercially available 1,4-butanediol. Enyne **55** could be synthesized from aldehyde **44** using similar transformations outlined from the first synthesis of Callyspongiolide by Ghosh.^{136,137}



Scheme 2.8 Retrosynthetic Analysis with Synthesized Fragments Highlighted

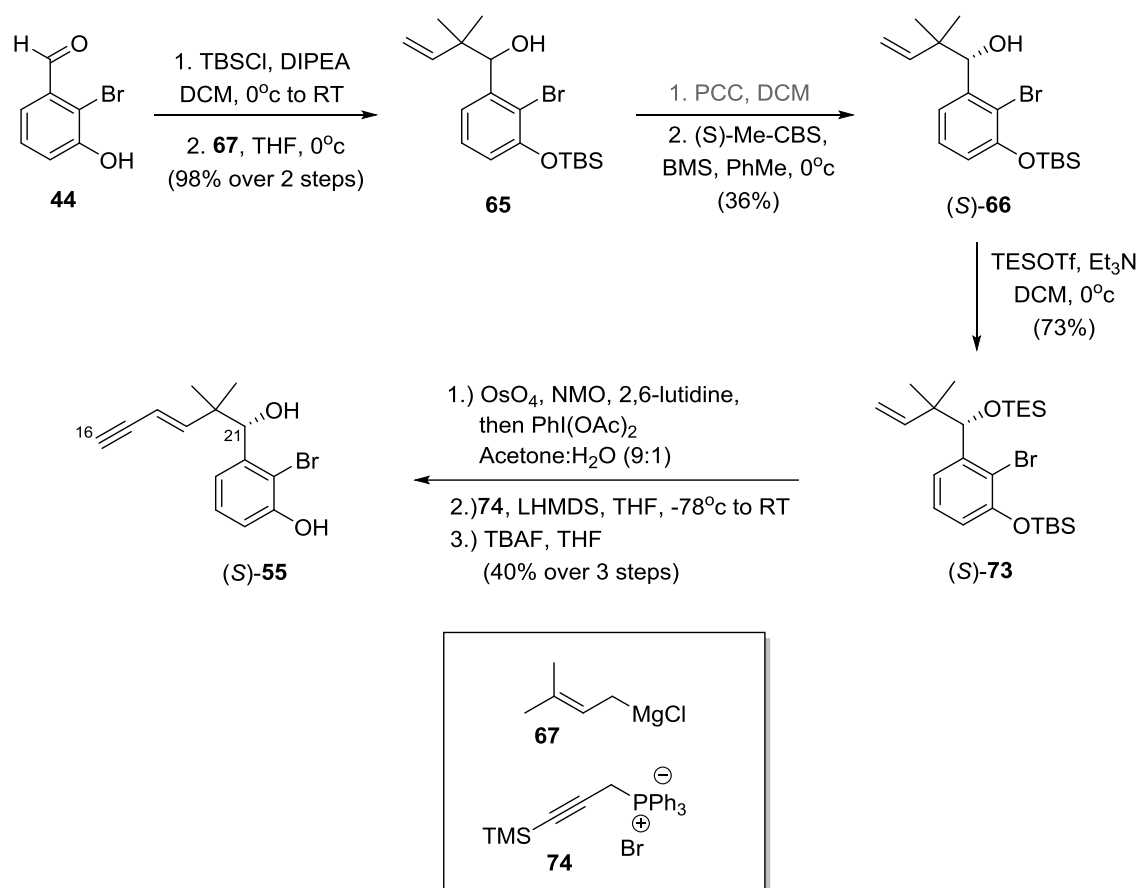
The synthesis of the macrolactone **67** coupling partner was the starting point for the construction of the remaining Callyspongiolide isomers. Beginning with 1,4-butyne-1,4-diol **70**, LAH reduction in THF provided the desired *trans*-alkene in 86% yield. The resulting diol underwent mono-protection with PMB-Br to provide PMB-ether **71** in 29% yield. To establish the correct stereochemistry at C-13, allylic alcohol **71** underwent enantioselective Sharpless epoxidation with D-(-)-DET and Ti(OiPr)₄ to afford enantiopure epoxide **72** in 78% yield. Under the conditions described by Crimmins and co-workers, treatment of the epoxide with Me₂CuLi₂I resulted in regio-

and diastereoselective methyl cuprate addition.¹³⁸ The 1,2-diol by-product was oxidatively cleaved with NaIO₄ to provide the desired diol **69** in 66% yield over two steps.



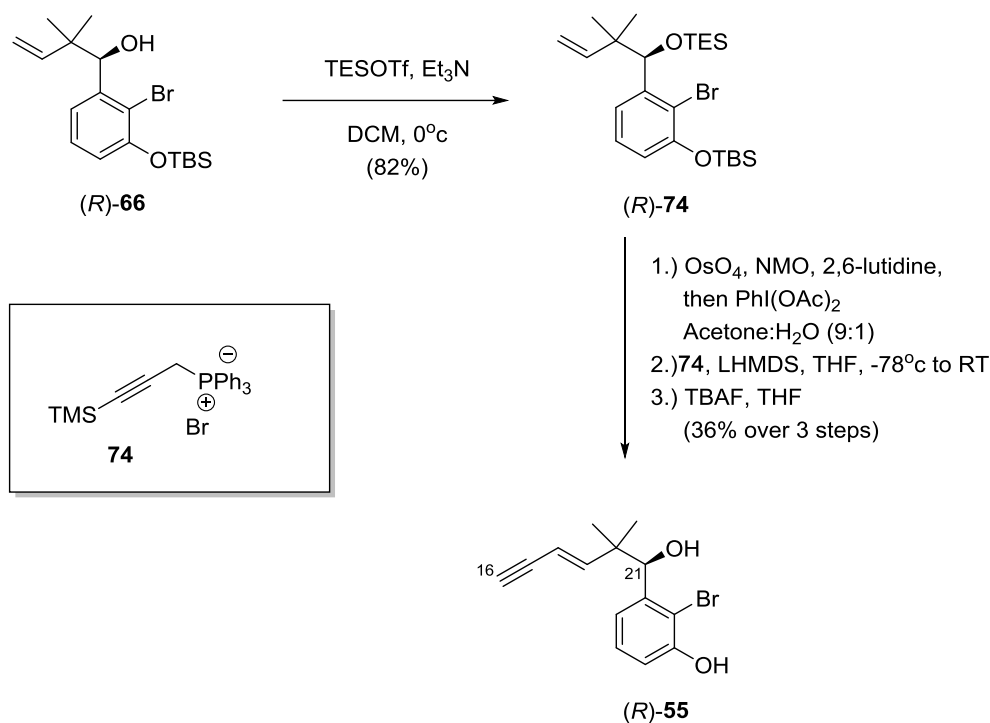
Scheme 2.9 Synthesis of Diol **69**

After successful construction of the macrolactone **67**, the focus shifted to the synthesis of enyne **55** to perform the Sonogashira coupling (Scheme 2.10). Beginning from commercially available aldehyde **44**, the alcohol was protected as a silyl ether with TBSCl. Reverse prenylation with 3-methyl-2-butenylmagnesium chloride successfully afforded racemic alcohol **65** in 98% yield over two steps. Oxidation of the secondary alcohol to the ketone was accomplished with pyridinium chlorochromate (PCC). The desired stereochemistry at C-21 could be set under chiral reduction conditions. Enantioselective Corey-Bakshi-Shibata reduction using (*S*)-Me-CBS catalyst provided alcohol (*S*)-**66** in 36% yield. Alternatively, alcohol (*R*)-**66** was obtained with (*R*)-Me-CBS catalyst. Protection of the secondary alcohol was successful with TESOTf and DIPEA. Using Nicolaou's conditions, the terminal olefin underwent oxidative cleavage to furnish the aldehyde precursor.¹³⁹ Wittig olefination was accomplished through treatment of the aldehyde with LHMDs followed by phosphonium bromide **74** providing TMS-protected enyne. Finally, a global deprotection of the silyl ethers with standard TBAF conditions produced the Sonogashira coupling component enyne (*S*)-**55** in 40% yield over 3 steps.



Scheme 2.10 Synthesis of Enyne (*S*)-**55**

To achieve the corresponding C-21 enantiomer, a similar process was followed (Scheme 2.11). After PCC oxidation of racemic alcohol **65**, the (*R*)-Me-CBS catalyst was used to achieve (*R*)-**66** in an enantioselective fashion. The same protocols to prepare (*S*)-**55** was followed for the preparation of (*R*)-**55**.



Scheme 2.11 Synthesis of Enyne (R) -**55**

The synthesis of the remaining Callyspongiolide isomers **36c** and **36d** was successful in assigning complete stereochemistry of the natural product. Based upon the collected data, we were able to deduce the natural product of Callyspongiolide is **36c**.

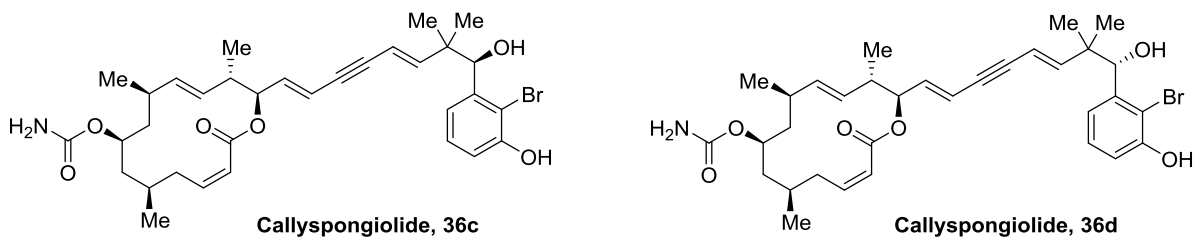


Figure 2.6 Callyspongiolide Isomers Generated From Second Synthesis

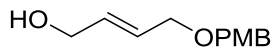
Table 2.3 Optical Rotation of Callyspongiolide Isomers From Second Synthesis

Stereoisomer	$[\alpha]_D^{20}$ (c 0.1, MeOH)
Isolated Natural Product	-12.5
36c	-25.5
36d	-182

2.7 Conclusion

In conclusion, Callyspongiolide is a very potent cytotoxic macrolide with useful potential as an anti-cancer agent. After isolation, the stereochemistry at C-21 could not be determined. The first total synthesis by the Ghosh group accomplished a novel protocol for developing the natural product core. Unfortunately, the synthesis of the first two isomers were unable to provide a conclusion into the structure of the natural product and led to the synthesis of two additional stereoisomers. Upon synthetic completion of all possible stereoisomers, we were able to unambiguously determine the stereochemistry and label Callyspongiolide **36c** as the natural product.

2.8 Experimental

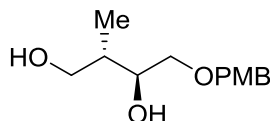


A yellow solution of 2-butyne-1,4-diol (16.1308 g, 187 mmol) in THF (600 mL) was added dropwise to a grey suspension of LAH (8.5773 g, 224 mmol, 1.2 equiv) in THF (150 mL) at 0 °C and the flask was warmed to rt. After 2 hrs, the flask was cooled to 0 °C, reaction quenched with sat. NH_4Cl , and flask warmed to rt. The crude mixture was filtered through celite and washed thoroughly with EA. The crude product was purified via Kugelrohr distillation (bp ~200 °C, ~10mm Hg) to give diol which was used directly in the next step. To a grey suspension of NaH (60% oil, 3.63 g, 90.78 mmol, 1.2 equiv) in DMF (250 mL) at 0 °C was added diol (9.9977 g, 113.47 mmol, 1.5 equiv) in DMF (50 mL). After stirring for 30 mins, TBAI (2.79 g, 7.565 mmol, 0.1 equiv.) and PMB-Br (10.62 mL, 75.65 mmol, 1.0 equiv.) were added. Solution was warmed to rt and stirred overnight. After 12 hrs, the reaction was quenched with H_2O . The crude product was then extracted with EA (x3), washed in brine, and dried over Na_2SO_4 . The crude product was purified by column chromatography (40% EA/HX) to give 5.0976 g of allylic alcohol (29% yield over 2-steps) as a light-yellow oil. ^1H NMR (400 MHz, CDCl_3) δ (ppm): 7.32 – 7.23 (m, 3H), 6.94 – 6.82 (m, 2H), 5.96 – 5.79 (m, 2H), 4.46 (s, 2H), 4.17 (t, J = 4.9 Hz, 2H), 4.03 – 4.00 (m, 2H), 3.81 (s, 3H).

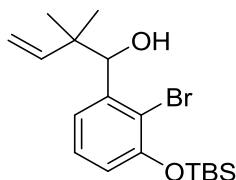


To a white slurry of flame-dried, powdered 4 ÅMS (7.82 g) in DCM (115 mL) at –20 °C was added $\text{Ti}(\text{O}^i\text{Pr})_4$ (745 μL , 2.51 mmol, 0.1 equiv) and D-(-)-DET (650 μL , 3.77 mmol, 0.15 equiv) sequentially. After stirring 20 min, $t\text{BuOOH}$ (5-6M decane, 12.5 mL, 62.83 mmol, 2.5 equiv) was added slowly and left stirring 30 min. A clear solution of allylic alcohol (5.0976 g, 25.13 mmol, 1.0 equiv.) in DCM (15 mL) was then added slowly via cannula and the resulting tan mixture placed in a –20 °C chiller. After 16 hrs, the reaction was quenched with a solution of NaOH in brine (2.6 g in 26 mL) and stirred for 1 hr at rt. The crude mixture was filtered through celite and thoroughly washed with DCM. The crude product was purified by column chromatography (40% EA/HX) to give 4.4126 g of epoxy alcohol (78% yield) as a white solid. ^1H NMR (400 MHz,

CDCl₃) δ (ppm): 7.29 – 7.24 (m, 1H), 6.91 – 6.86 (m, 1H), 4.56 – 4.46 (m, 1H), 3.81 (s, 2H), 3.74 (dd, J = 11.5, 3.1 Hz, 1H), 3.65 (dd, J = 12.7, 4.1 Hz, 1H), 3.50 (dd, J = 11.5, 5.5 Hz, 1H), 1.76 – 1.54 (m, 1H).

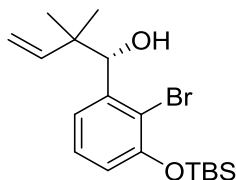


MeLi (3.1M DEM, 62.3 mL, 192.8 mmol, 6.0 equiv) was added slowly to a tan suspension of CuI (8.3432 g, 43.8 mmol, 2.2 equiv) in Et₂O (70 mL) at 0 °C. After stirring 30 mins, the flask was cooled to –50 °C and a clear solution of epoxy alcohol (4.4126 g, 19.7 mmol, 1.0 equiv.) in THF (30 mL) was added dropwise via cannula. The flask was slowly warmed to rt. After 4 hrs, the reaction mixture was filtered through celite, thoroughly washed with Et₂O, and concentrated. The crude product was dissolved in EA, washed with NH₄OH (x2), and back-extracted with EA (x5). The organic layers were combined and dried over Na₂SO₄ and concentrated in vacuo to give a mixture of diols which was used directly in the next step. To a light-yellow, biphasic mixture of diols (4.7339 g, 19.7 mmol, 1.0 equiv.) in Et₂O/H₂O (2:1, 40 mL) at 0 °C was added NaIO₄ (2.1124 g, 9.87 mmol, 0.5 equiv) in one portion. The flask was warmed to rt after 1 hr and left stirring overnight. After 12 hrs, the layers were separated and aqueous phase extracted with EA (x3), washed in brine, and dried over Na₂SO₄. The crude product was purified by column chromatography (50% EA/HX) to give 3.1243 g of diol (66% yield over 2-steps) as a clear oil. R_f = 0.39 (75% EA/HX); ¹H NMR (400 MHz, CDCl₃) δ (ppm): 7.29 – 7.23 (m, 3H), 6.91 – 6.87 (m, 2H), 4.54 – 4.45 (m, 2H), 3.81 (s, 3H), 3.73 (td, J = 7.7, 3.1 Hz, 1H), 3.66 (d, J = 5.5 Hz, 2H), 3.58 (dd, J = 9.5, 3.1 Hz, 1H), 3.42 (dd, J = 9.5, 7.5 Hz, 1H), 2.36 (brs, 2H), 1.85 – 1.76 (m, 1H), 0.86 (d, J = 7.0 Hz, 3H); $[\alpha]_D^{24}$ +9.3 (*c* 1.82, CH₂Cl₂).

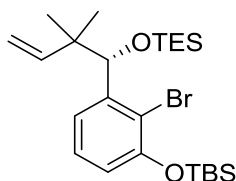


To a grey mixture of phenol (2.0044 g, 9.97 mmol) in DCM (50 mL) at 0 °C was added DIPEA (3.5 mL, 19.9 mmol, 2.0 equiv) and TBSCl (1.9431 g, 12.94 mmol, 1.3 equiv) sequentially. After

6 hrs, the yellow solution was quenched with sat. NH_4Cl . The crude product was extracted with EA (x3), washed with brine, and dried over Na_2SO_4 . The crude product was passed through a short plug of silica gel and used directly in the next step. To a clear solution of aldehyde (3.0526 g, 9.68 mmol) in THF (50 mL) at 0 °C was added a grey solution of 3-methyl-2-butenylmagnesium chloride (1M THF, 15 mL, 15.0 mmol, 1.5 equiv) slowly. After 45 mins, the reaction was quenched with sat. NH_4Cl . The crude product was extracted with EA (x3), washed in brine, and dried over Na_2SO_4 . Purification by flash chromatography (3% EA/HX) gave 3.8306 g of alcohol (98% yield over 2-steps) as a clear oil. ^1H NMR (500 MHz, CDCl_3) δ (ppm): 7.17 – 7.13 (m, 1H), 7.08 (dd, J = 7.8, 1.6 Hz, 1H), 6.81 (dd, J = 7.9, 1.6 Hz, 1H), 6.03 (dd, J = 17.5, 10.8 Hz, 1H), 5.16 – 5.12 (m, 2H), 5.07 (dd, J = 17.6, 1.3 Hz, 1H), 1.99 (brs, 1H), 1.12 (s, 3H), 1.05 (s, 9H), 1.03 (s, 3H), 0.25 (s, 3H), 0.23 (s, 3H); ^{13}C NMR (125 MHz, CDCl_3) δ (ppm): 152.3, 144.9, 142.4, 127.0, 122.2, 119.1, 118.2, 114.0, 78.0, 43.6, 26.0, 24.8, 21.5, 18.6, –4.0, –4.1.

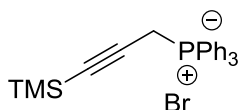


To a faint-yellow solution of ketone (50.1 mg, 0.131 mmol) and (*S*)-Me-CBS (36.5 mg, 0.131 mmol, 1.0 equiv) in PhMe (2 mL) at 0 °C was added BMS (40 μL , 0.275 mmol, 2.0 equiv) dropwise. After 2 h, the reaction was quenched with MeOH dropwise, flask warmed to room temperature, and concentrated via rotary evaporation. Purification by flash chromatography (3% EA/HX) gave 18.1764 mg of alcohol (36% yield) as a clear oil. $[\alpha]_{\text{D}}^{20}$ –46.7 (*c* 2.10, CHCl_3); Chiral HPLC: Chiralpak IC-3 semi-prep, 5% IPA/HX, flow = 6 mL/min, T = 25 °C, UV = 254 nm.

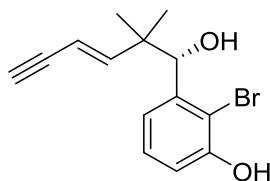


To a clear solution of alcohol (1.8 g, 4.67 mmol, 1.0 equiv.) in DCM (40 mL) at 0 °C was added Et_3N (2 mL, 14.48 mmol, 3.1 equiv) and TESOTf (2 mL, 8.406 mmol, 1.8 equiv) sequentially.

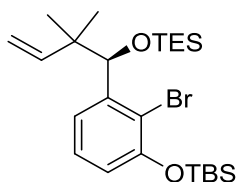
After 30 min, the reaction was quenched with sat. NaHCO_3 and flask warmed to room temperature. The crude product was extracted with DCM (x3), washed in brine, and dried over MgSO_4 . Purification by flash chromatography (2% EA/HX) gave 1.7092 g of TES ether (73% yield) as a clear oil. $R_f = 0.68$ (5% EA/HX); ^1H NMR (500 MHz, CDCl_3) δ (ppm): 7.12 – 7.06 (m, 2H), 6.81 – 6.75 (m, 1H), 6.08 (dd, $J = 17.6, 10.8$ Hz, 1H), 5.06 (s, 1H), 4.94 (dd, $J = 10.8, 1.6$ Hz, 1H), 4.84 (dd, $J = 17.6, 1.6$ Hz, 1H), 1.08 (s, 3H), 1.05 (s, 9H), 1.01 (s, 3H), 0.83 (t, $J = 8.0$ Hz, 9H), 0.54 – 0.39 (m, 6H), 0.23 (s, 3H), 0.22 (s, 3H); ^{13}C NMR (125 MHz, CDCl_3) δ (ppm): 151.8, 145.1, 143.9, 126.5, 123.5, 119.0, 117.9, 112.1, 79.1, 43.8, 26.1, 24.3, 22.6, 18.6, 6.9, 4.9, –4.0, –4.1. $[\alpha]_D^{20} -18.6$ (c 1.03, CHCl_3).



To a yellow solution of propargyl alcohol (5.0 mL, 85.9 mmol) in THF (100 mL) at -78°C was added $n\text{-BuLi}$ (1.6M HX, 113 mL, 181 mmol, 2.1 equiv) slowly. After 2 hr, TMSCl (23.0 mL, 181 mmol, 2.1 equiv) was added dropwise and the flask warmed to rt after 5 min. Following 30 min, the reaction was quenched slowly with 2M HCl and left stirring 1 hr. The crude product was then extracted with Et_2O (x3), washed in brine, and dried over MgSO_4 to give a yellow liquid that was used directly in the next step. PBr_3 (3.3 mL, 35.1 mmol, 0.4 equiv) was added slowly to a yellow solution of alcohol (11.0154 g, 85.9 mmol) in Et_2O (100 mL) at 0°C . After 2 hr, the reaction was carefully quenched with sat. NaHCO_3 and flask warmed to rt. The crude product was then extracted with Et_2O (x3), washed in brine, and dried over MgSO_4 . The crude product was passed through a short plug of silica gel and used directly in the next step. To a clear solution of bromide (16.4170 g, 85.9 mmol) in PhMe (45 mL) was added PPh_3 (25.0289 g, 95.4 mmol, 1.1 equiv) slowly in 5 portions. After 12 hr, the mixture was filtered and washed thoroughly with cold HX to give 11.0040 g of phosphonium bromide (28% yield over 3-steps) as a tan solid. $R_f = 0.18$ (100% PN); ^1H NMR (400 MHz, CDCl_3) δ (ppm): 7.95 – 7.86 (m, 7H), 7.83 – 7.76 (m, 4H), 7.71 – 7.64 (m, 6H), 5.20 (d, $J = 15.2$ Hz, 2H), –0.05 (s, 9H).

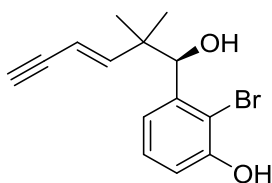


To a clear solution of olefin (972.1 mg, 1.95 mmol) in acetone/H₂O (9:1, 20 mL) was added 2,6-lutidine (500 μ L, 4.29 mmol, 2.2 equiv), NMO (481.3 mg, 4.12 mmol, 2.1 equiv), and OsO₄ (4% H₂O, 2.5 mL, 0.39 mmol, 0.2 equiv) sequentially. The yellow solution was left stirring overnight while covered with aluminum foil. After 12 h, PhI(OAc)₂ (1.0014 g, 3.11 mmol, 1.6 equiv) was added and reaction left stirring additional 30 min. The reaction was quenched with Na₂S₂O₃ and left vigorously stirring 15 min. The crude product was extracted with EA (x3), washed in brine, and dried over Na₂SO₄. The crude product was passed through a short plug of silica gel and used directly in the next step. To a cream-colored suspension of phosphonium bromide (3.2807 g, 7.228 mmol, 4.0 equiv) in THF (45 mL) at -78°C was added LHMDs (1M THF, 7.1 mL, 7.047 mmol, 4.0 equiv) slowly. After 10 min, the flask was warmed to -40°C for an additional 30 min, then recooled to -78°C . A clear solution of aldehyde (906.5 mg, 1.807 mmol, 1.0 equiv.) in THF (15 mL) was then added slowly via cannula. The flask was then slowly warmed to room temperature and left stirring overnight. After 12 h, the reaction was quenched with sat. NH₄Cl. The crude product was extracted with EA (x3), washed in brine, and dried over Na₂SO₄. The crude product was passed through a short plug of silica gel and used directly in the next step. To a clear solution of tri-silyl ether (657.1 mg, 1.133 mmol) in THF (12 mL) was added TBAF (1M THF, 5 mL, 4.532 mmol, 4.0 equiv) slowly. After 20 h, the reaction was quenched with sat. NH₄Cl. The crude product was extracted with EA (x3), washed in brine, and dried over Na₂SO₄. Purification by flash chromatography (15% EA/HX) gave 228.1 mg of enyne (40% yield over 3-steps) as a clear oil. $[\alpha]_{\text{D}}^{20} -98.5$ (*c* 0.33, CHCl₃).



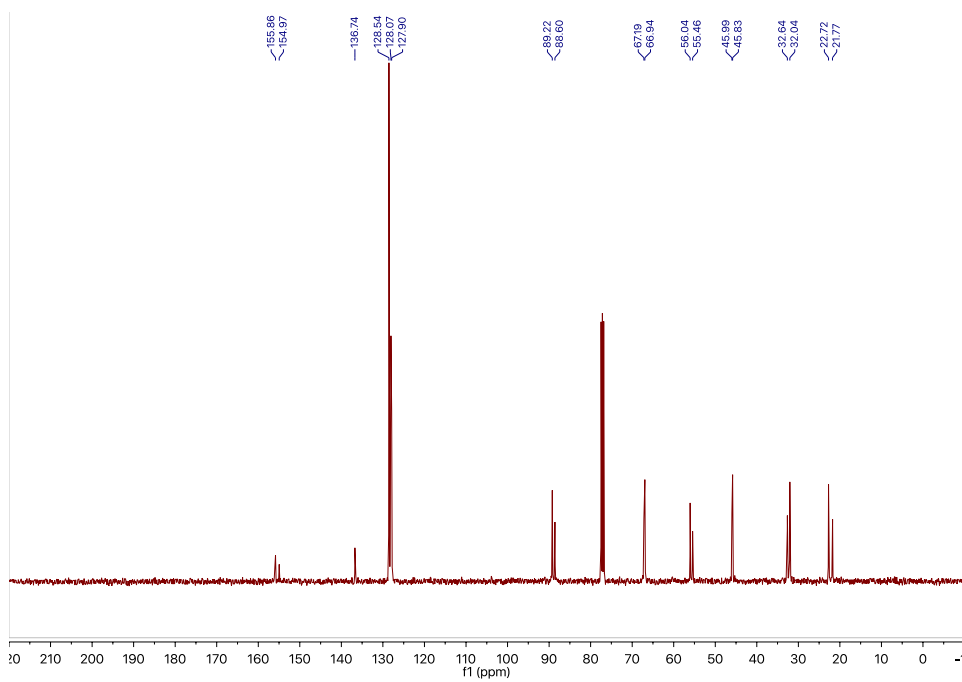
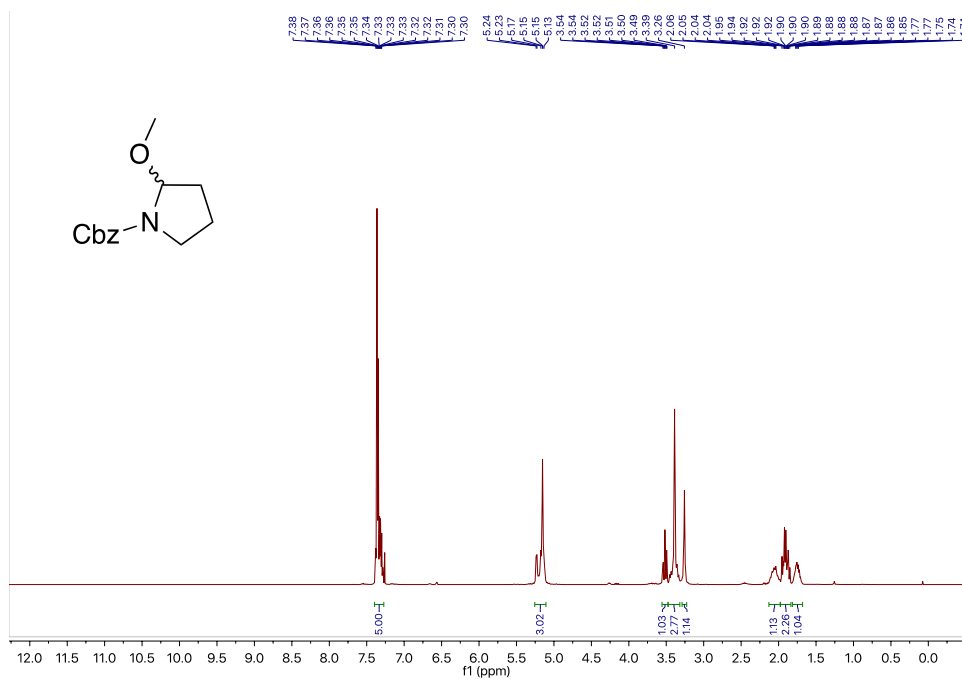
To a clear solution of alcohol (1.8 g, 4.67 mmol, 1.0 equiv.) in DCM (40 mL) at 0°C was added Et₃N (2 mL, 14.48 mmol, 3.1 equiv) and TESOTf (2 mL, 8.406 mmol, 1.8 equiv) sequentially.

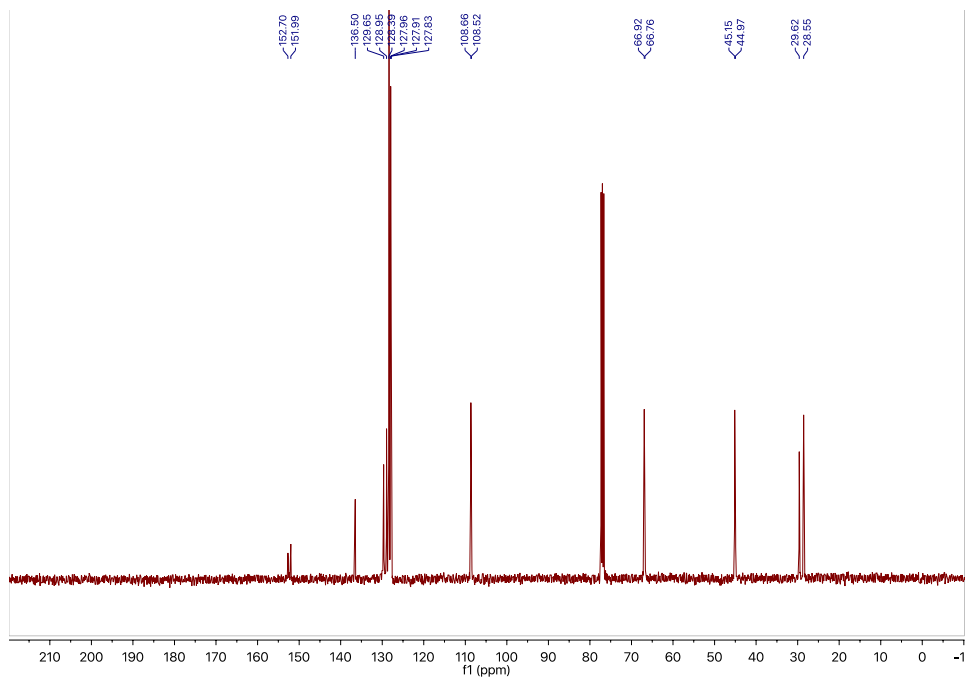
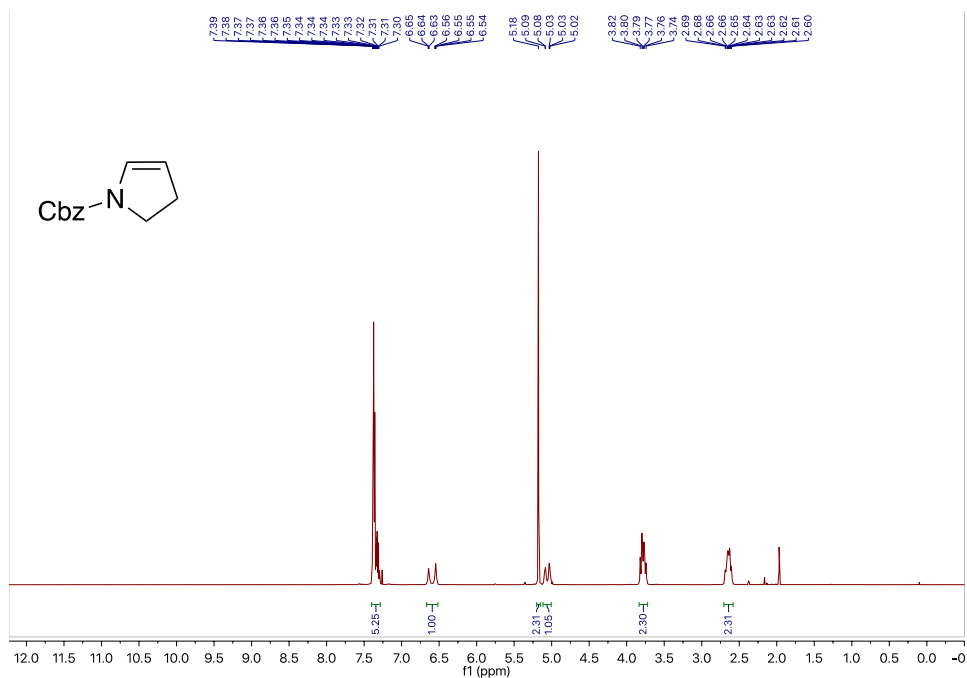
After 30 min, the reaction was quenched with sat. NaHCO_3 and flask warmed to room temperature. The crude product was extracted with DCM (x3), washed in brine, and dried over MgSO_4 . Purification by flash chromatography (2% EA/HX) gave 1.9093 g of TES ether (82% yield) as a clear oil. $R_f = 0.68$ (5% EA/HX); ^1H NMR (500 MHz, CDCl_3) δ (ppm): 7.12 – 7.06 (m, 2H), 6.81 – 6.75 (m, 1H), 6.08 (dd, $J = 17.6, 10.8$ Hz, 1H), 5.06 (s, 1H), 4.94 (dd, $J = 10.8, 1.6$ Hz, 1H), 4.84 (dd, $J = 17.6, 1.6$ Hz, 1H), 1.08 (s, 3H), 1.05 (s, 9H), 1.01 (s, 3H), 0.83 (t, $J = 8.0$ Hz, 9H), 0.54 – 0.39 (m, 6H), 0.23 (s, 3H), 0.22 (s, 3H); ^{13}C NMR (125 MHz, CDCl_3) δ (ppm): 151.8, 145.1, 143.9, 126.5, 123.5, 119.0, 117.9, 112.1, 79.1, 43.8, 26.1, 24.3, 22.6, 18.6, 6.9, 4.9, –4.0, –4.1.

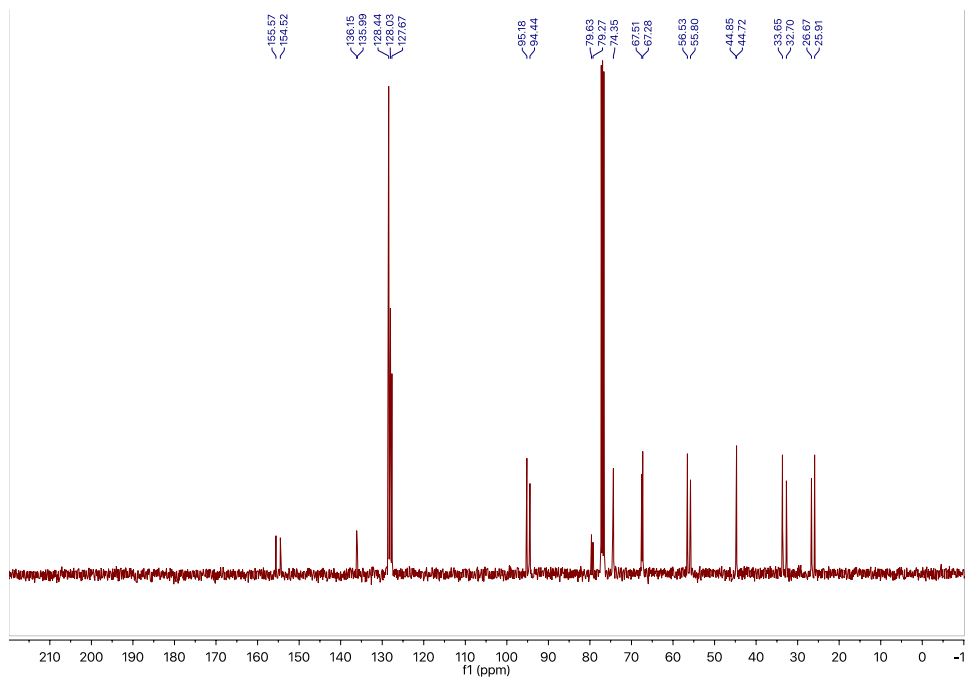
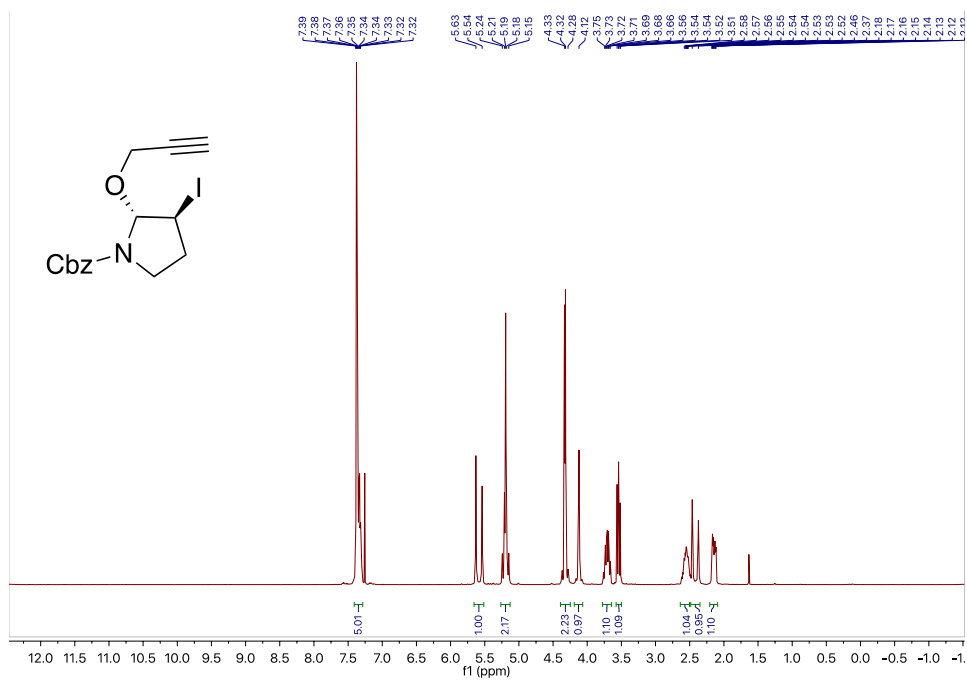


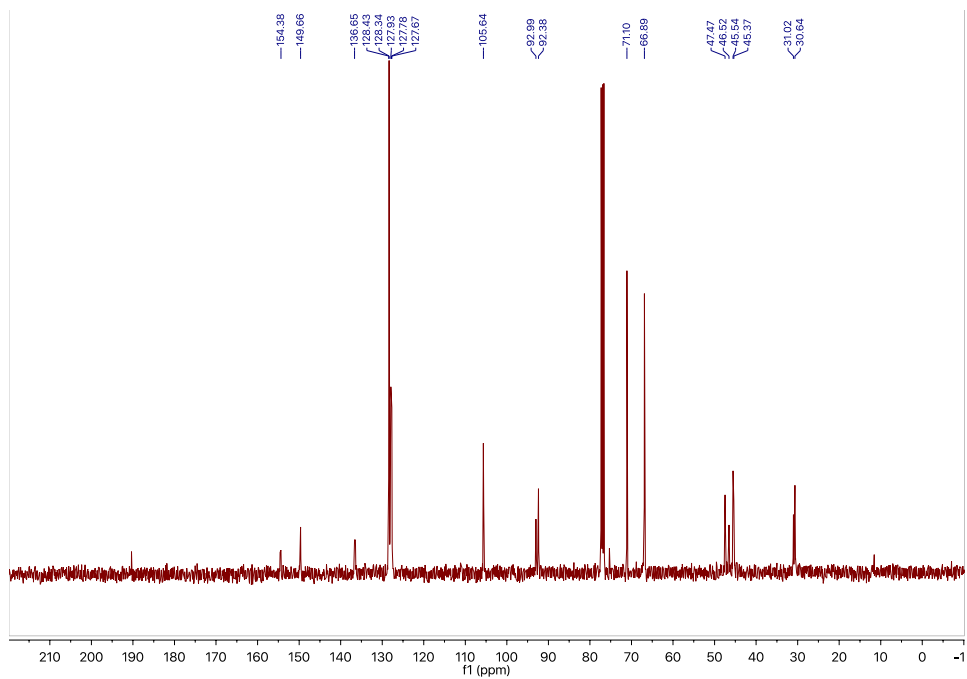
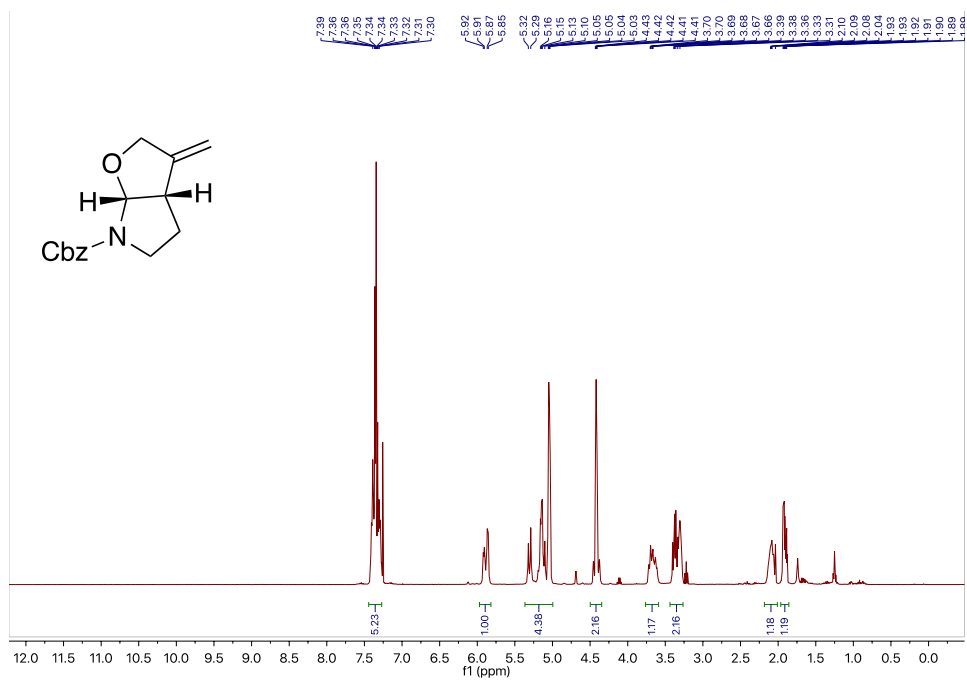
To a clear solution of olefin (975 mg, 1.95 mmol) in acetone/ H_2O (9:1, 20 mL) was added 2,6-lutidine (500 μL , 4.29 mmol, 2.2 equiv), NMO (485.4 mg, 4.14 mmol, 2.1 equiv), and OsO_4 (4% H_2O , 2.5 mL, 0.39 mmol, 0.2 equiv) sequentially. The yellow solution was left stirring overnight while covered with aluminum foil. After 12 h, $\text{PhI}(\text{OAc})_2$ (1.0068 g, 3.13 mmol, 1.6 equiv) was added and reaction left stirring additional 30 min. The reaction was quenched with $\text{Na}_2\text{S}_2\text{O}_3$ and left vigorously stirring 15 min. The crude product was extracted with EA (x3), washed in brine, and dried over Na_2SO_4 . The crude product was passed through a short plug of silica gel and used directly in the next step. To a cream-colored suspension of phosphonium bromide (3.2180 g, 7.044 mmol, 4.0 equiv) in THF (45 mL) at -78°C was added LHMDS (1M THF, 7.0 mL, 7.047 mmol, 4.0 equiv) slowly. After 10 min, the flask was warmed to -40°C for an additional 30 min, then recooled to -78°C . A clear solution of aldehyde (883.6 mg, 1.761 mmol, 1.0 equiv.) in THF (15 mL) was then added slowly via cannula. The flask was then slowly warmed to room temperature and left stirring overnight. After 12 h, the reaction was quenched with sat. NH_4Cl . The crude product was extracted with EA (x3), washed in brine, and dried over Na_2SO_4 . The crude product was passed through a short plug of silica gel and used directly in the next step. To a clear solution of tri-silyl ether (394.8 mg, 0.681 mmol) in THF (7 mL) was added TBAF (1M THF, 3 mL, 3.0 mmol, 4.0 equiv) slowly. After 20 h, the reaction was quenched with sat. NH_4Cl . The crude product was extracted with EA (x3), washed in brine, and dried over Na_2SO_4 . Purification by flash chromatography (15% EA/HX) gave 207.2 mg of enyne (36% yield over 3-steps) as a clear oil.

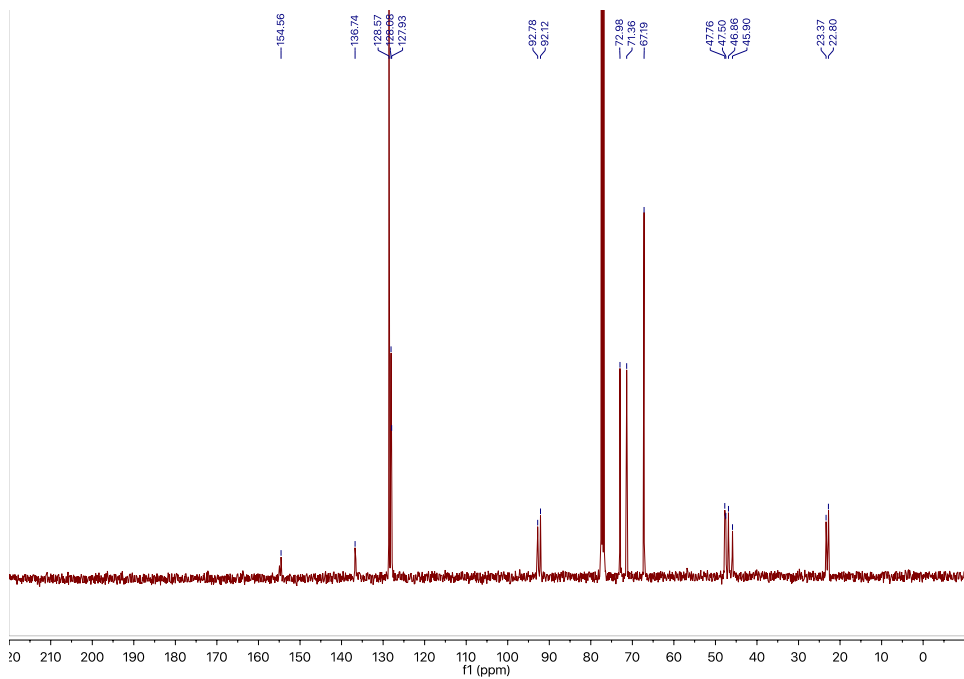
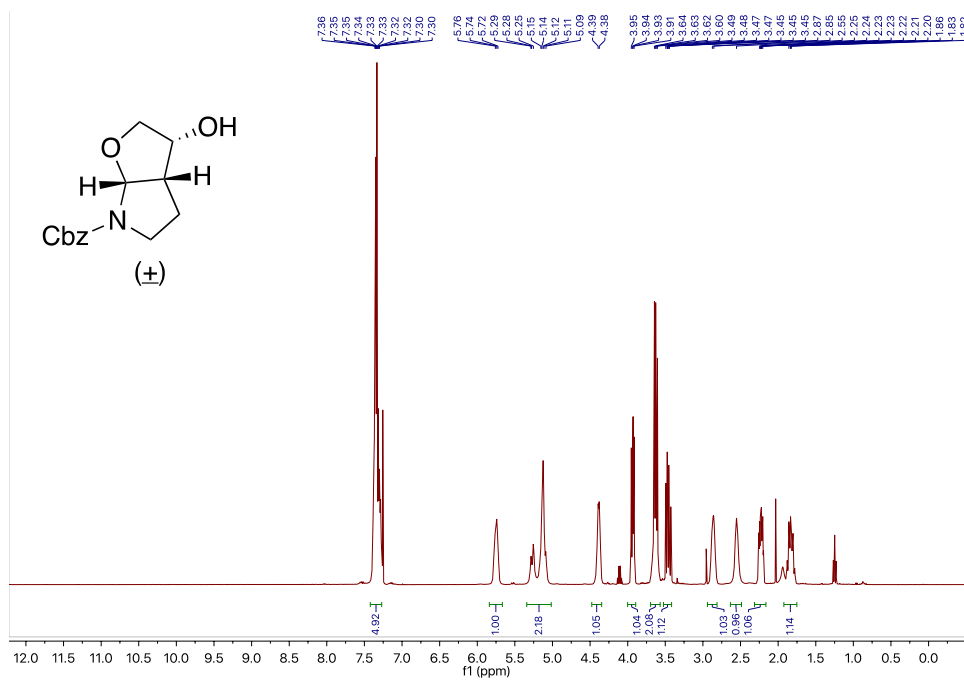
APPENDIX A: NMR SPECTRA

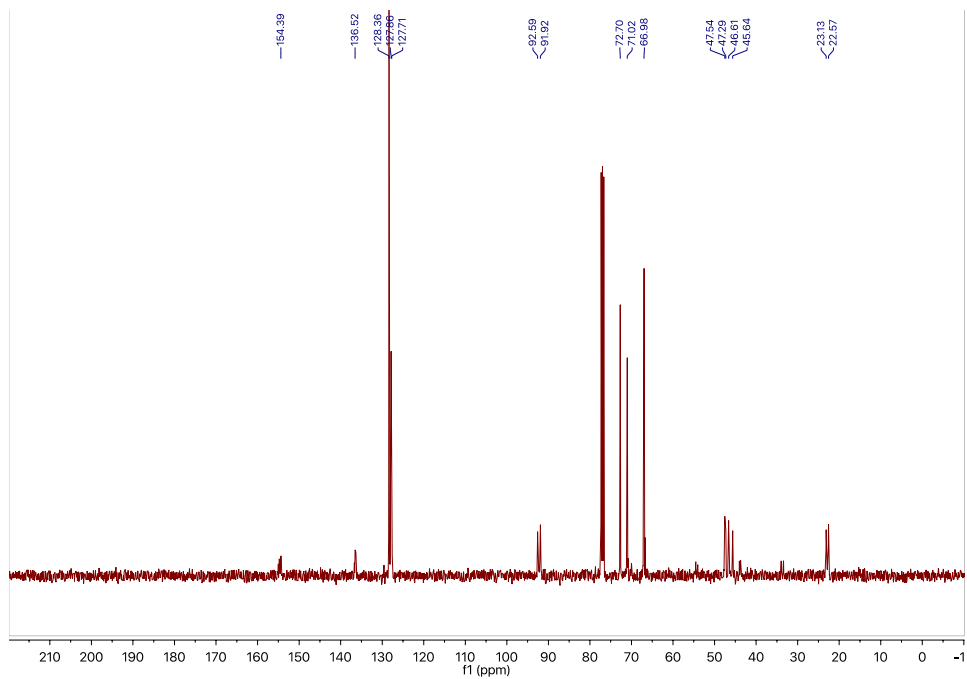
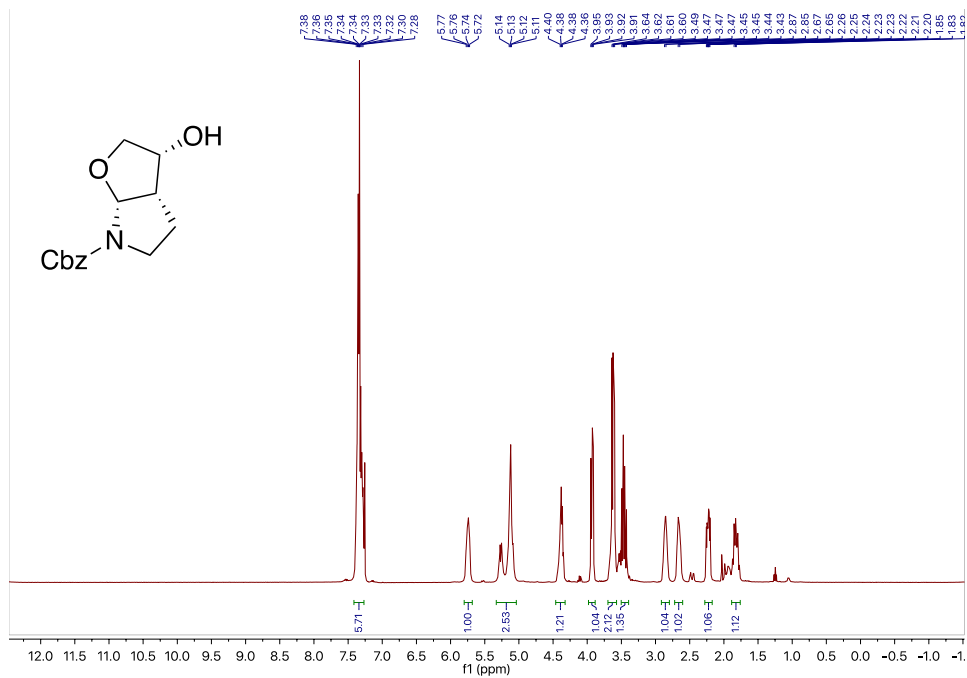


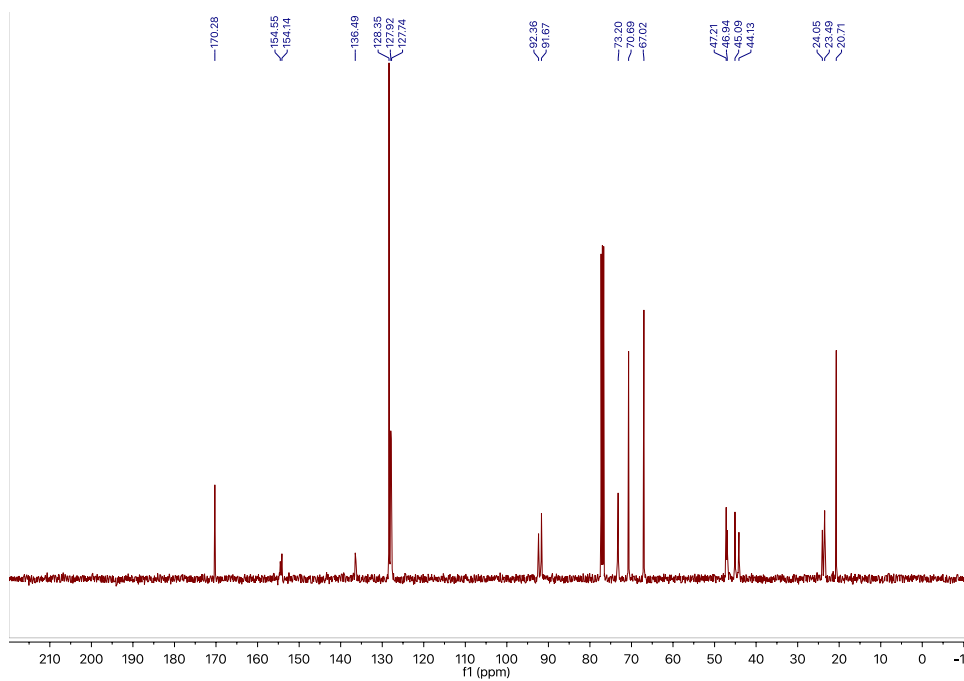
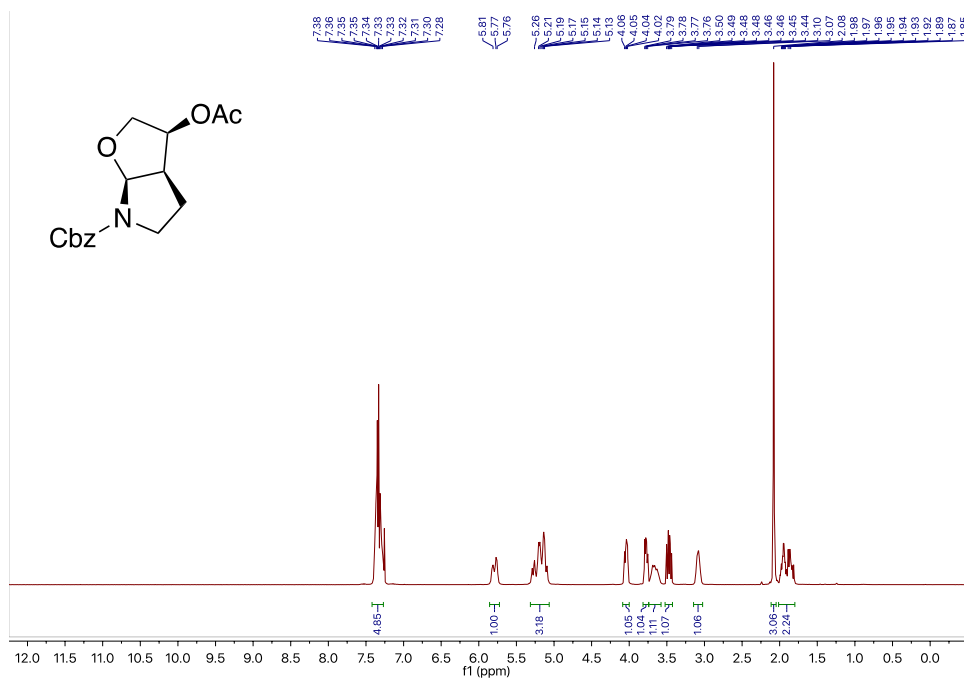


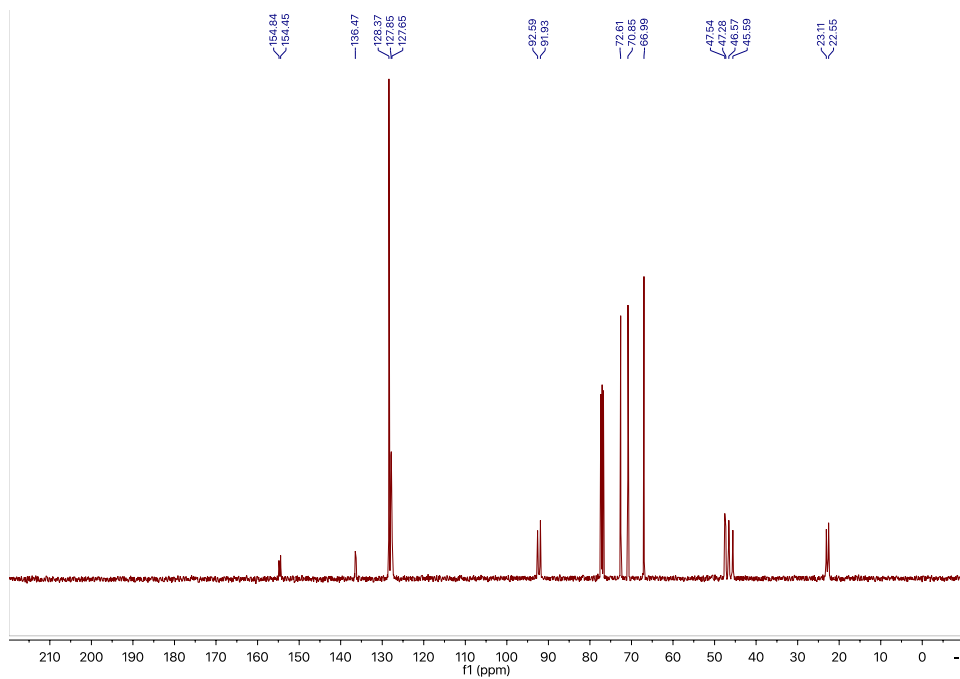
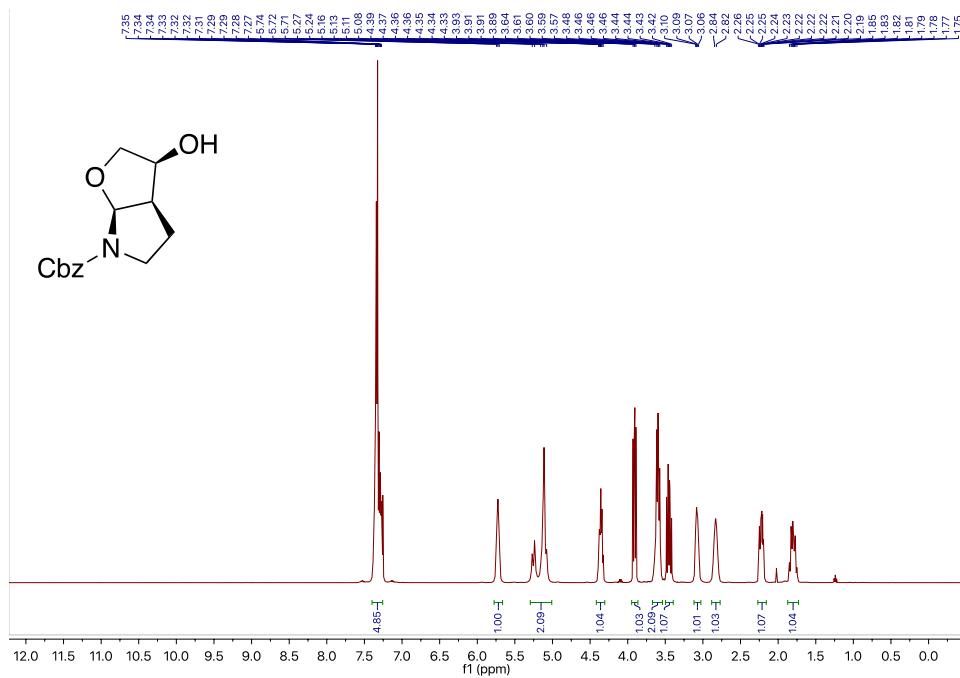


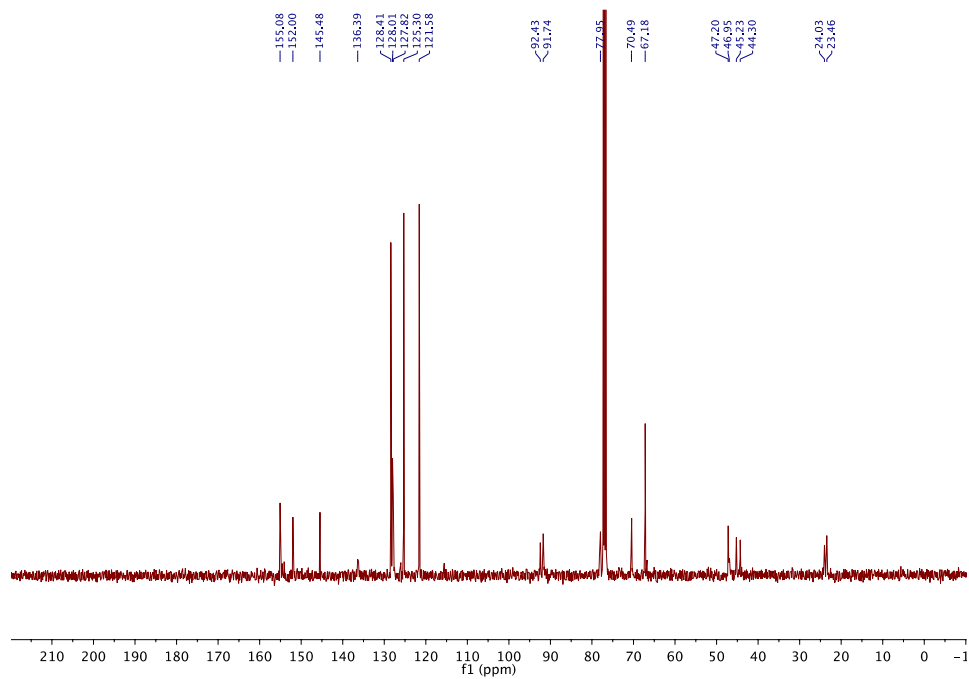
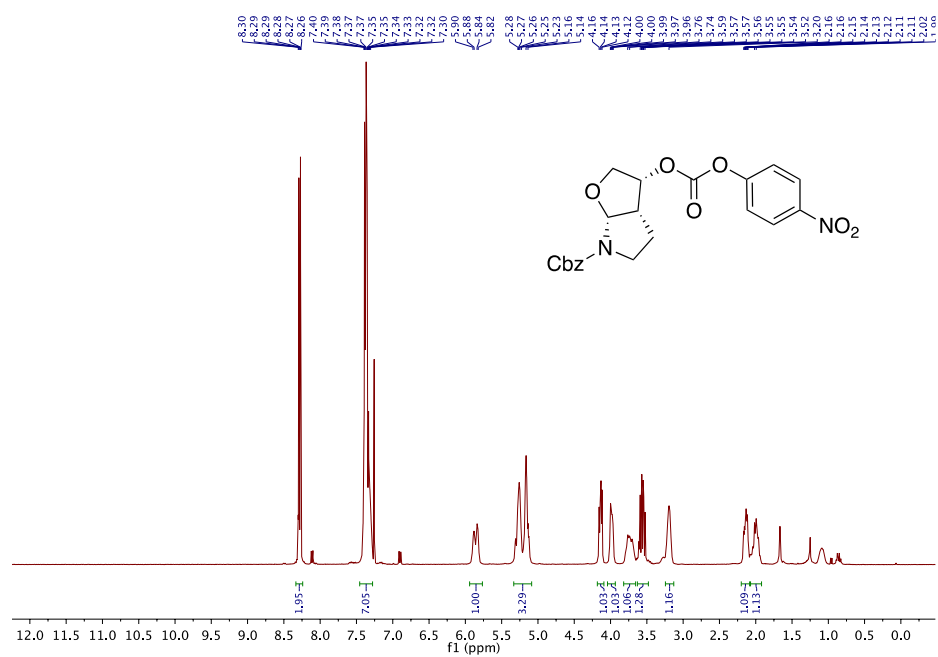


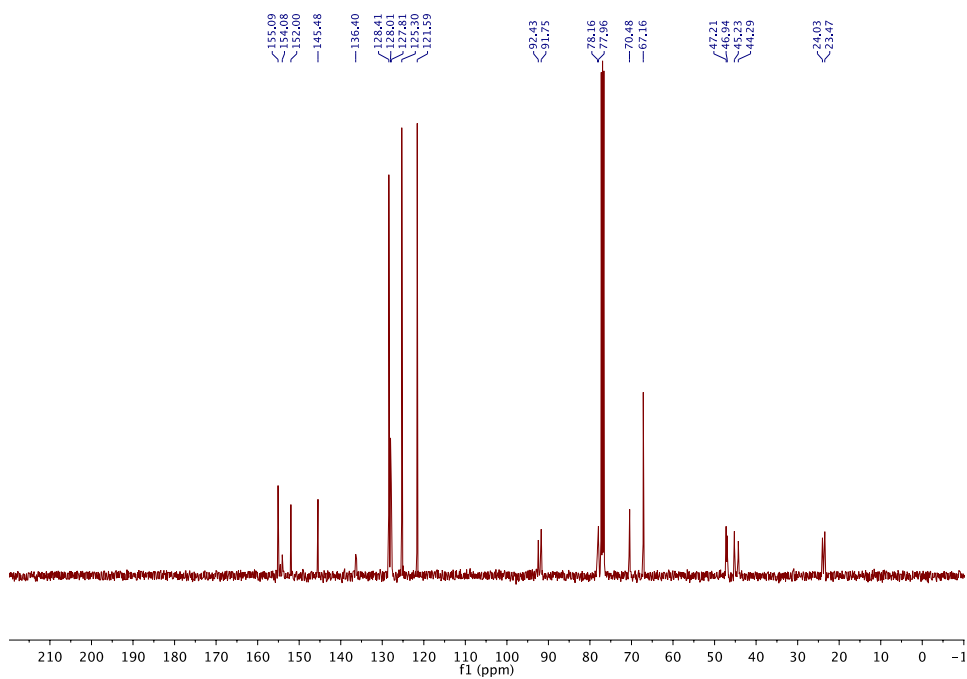
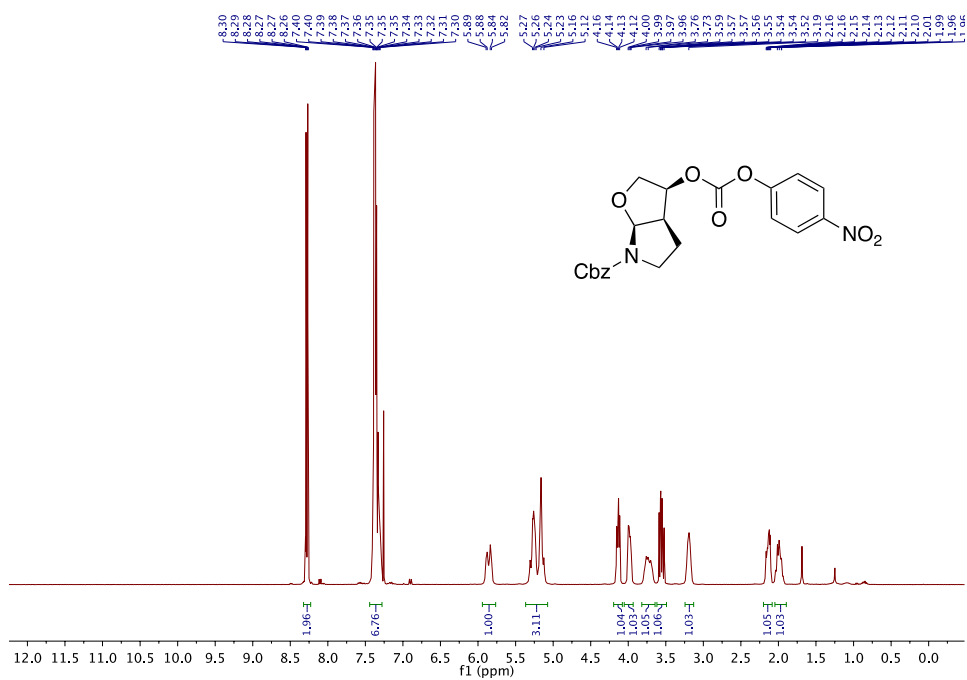


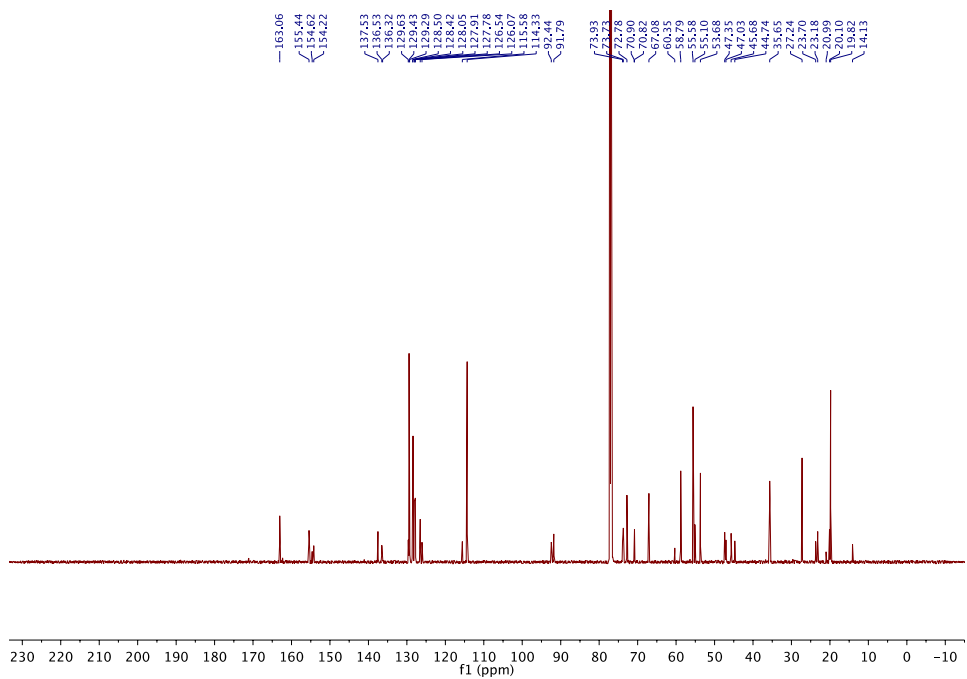
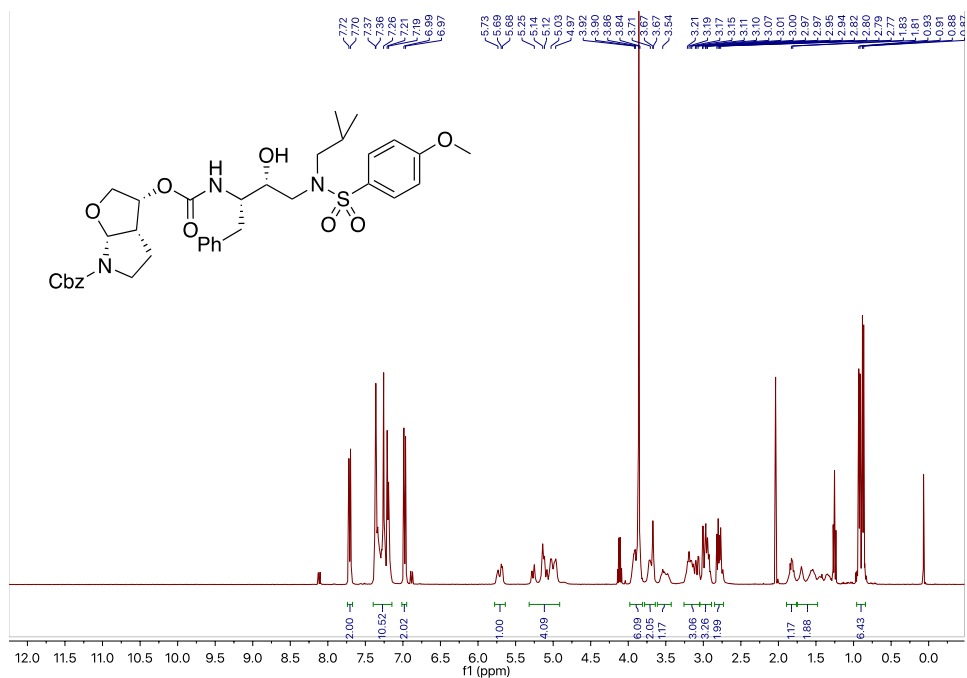


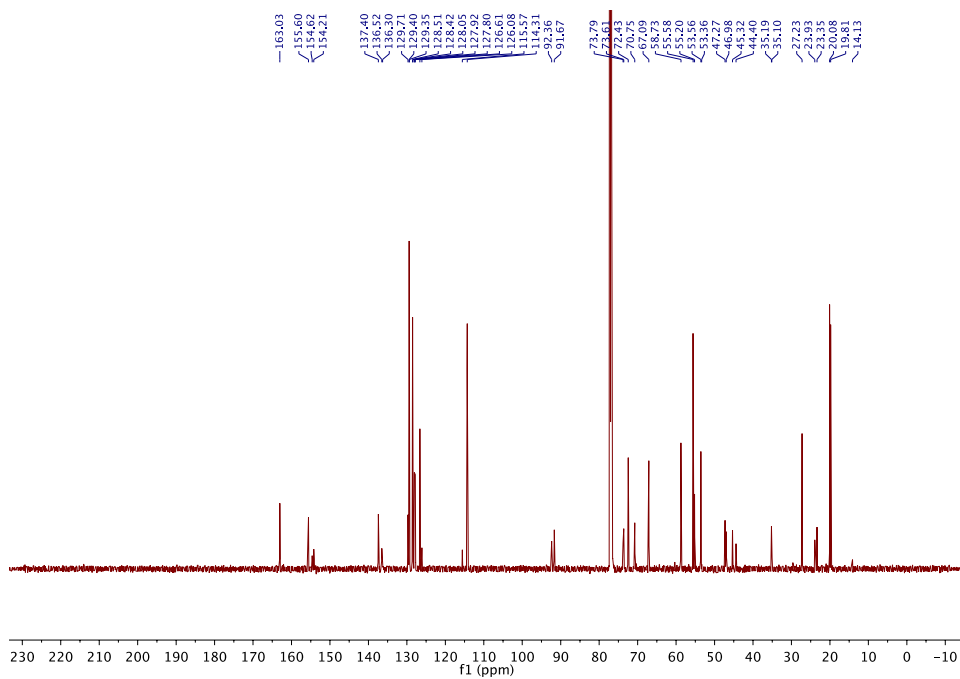
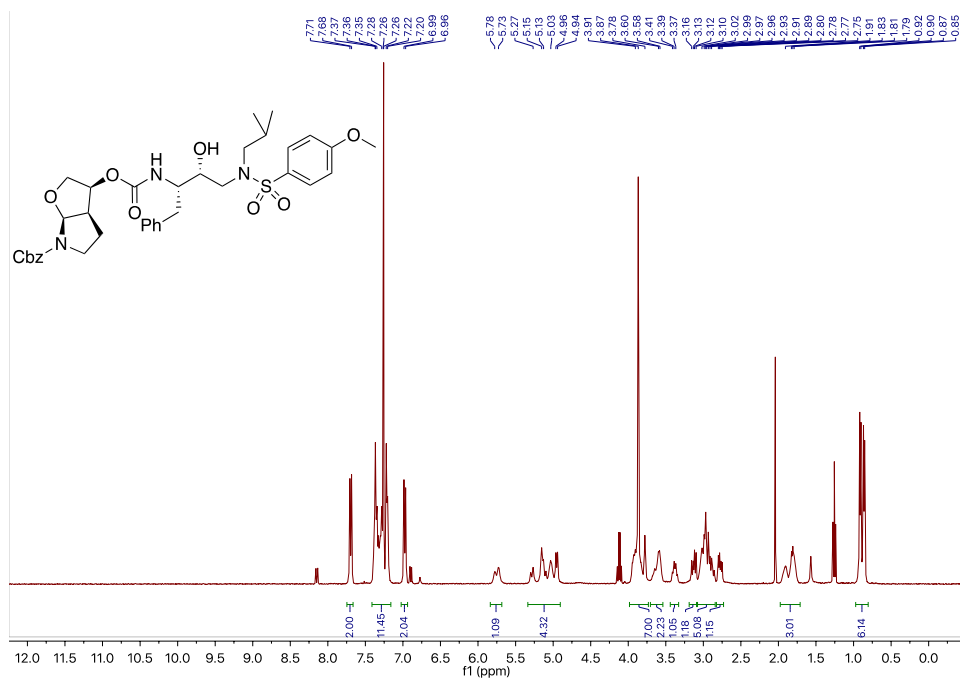


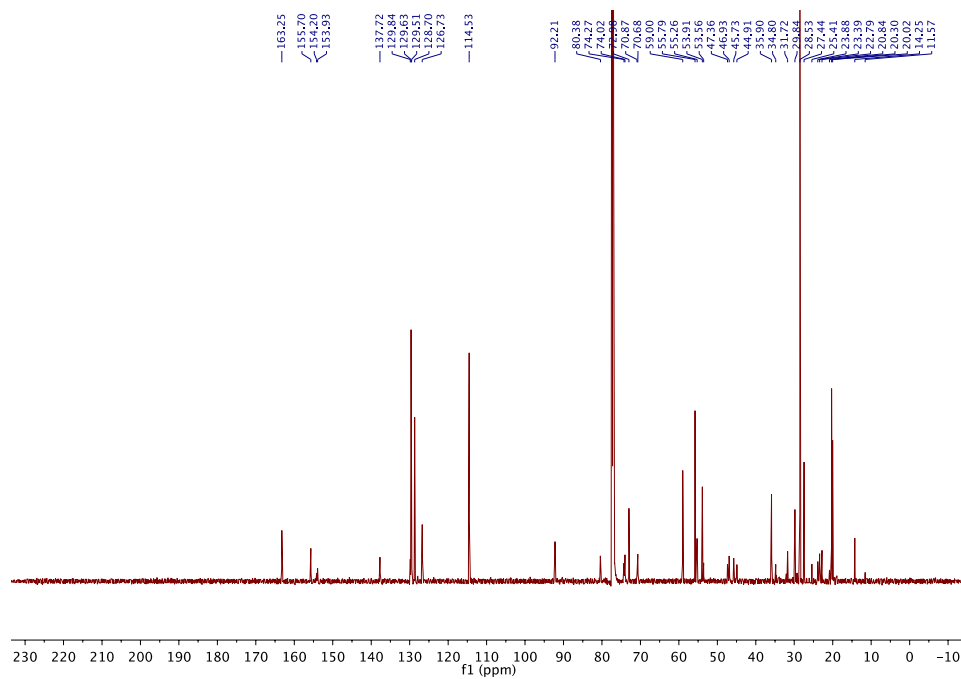
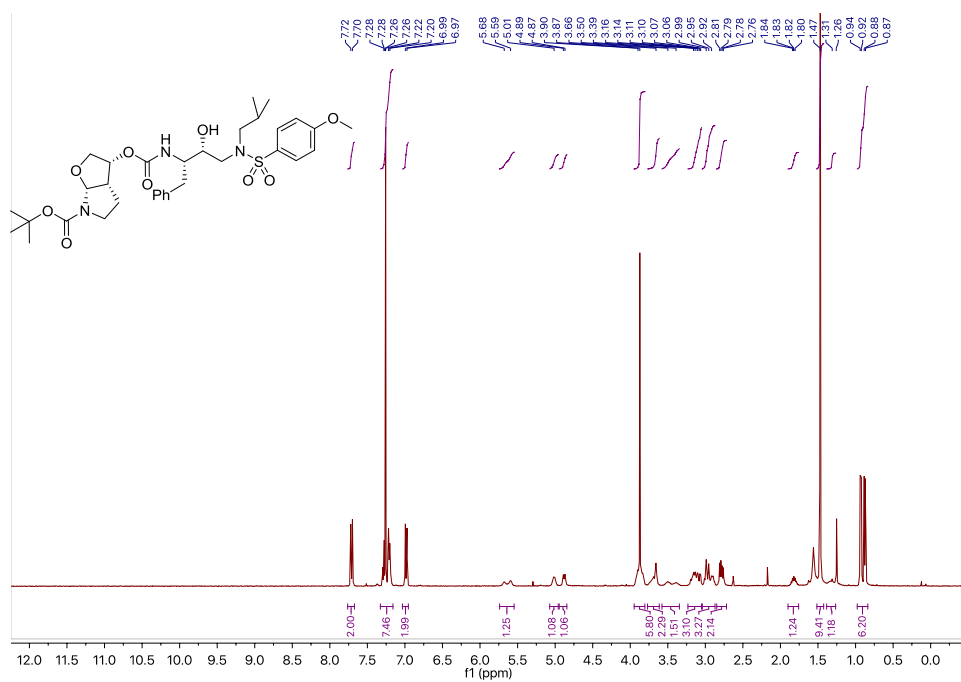


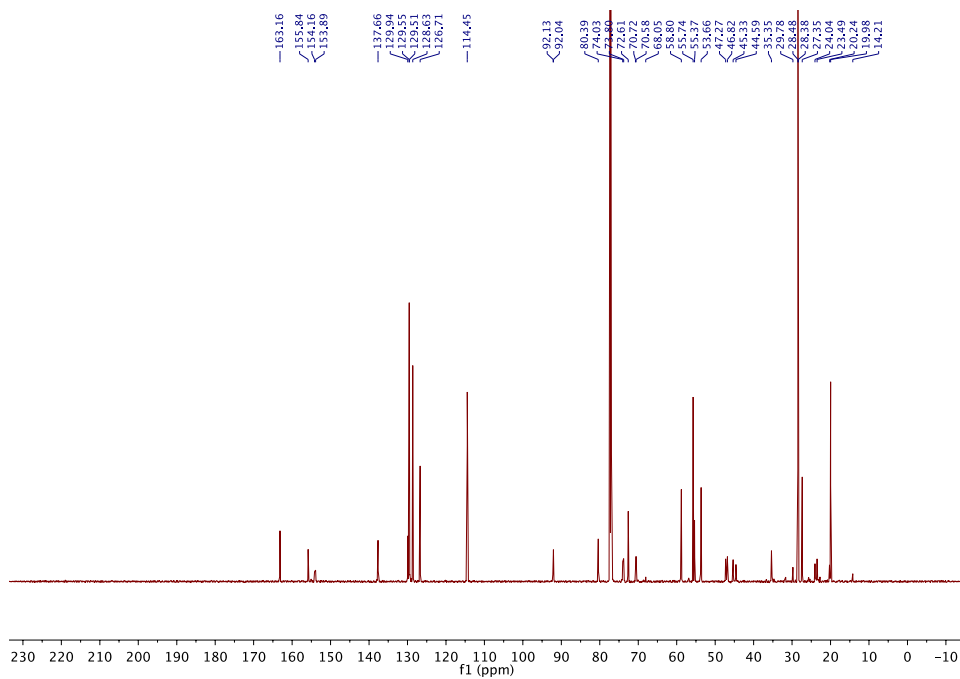
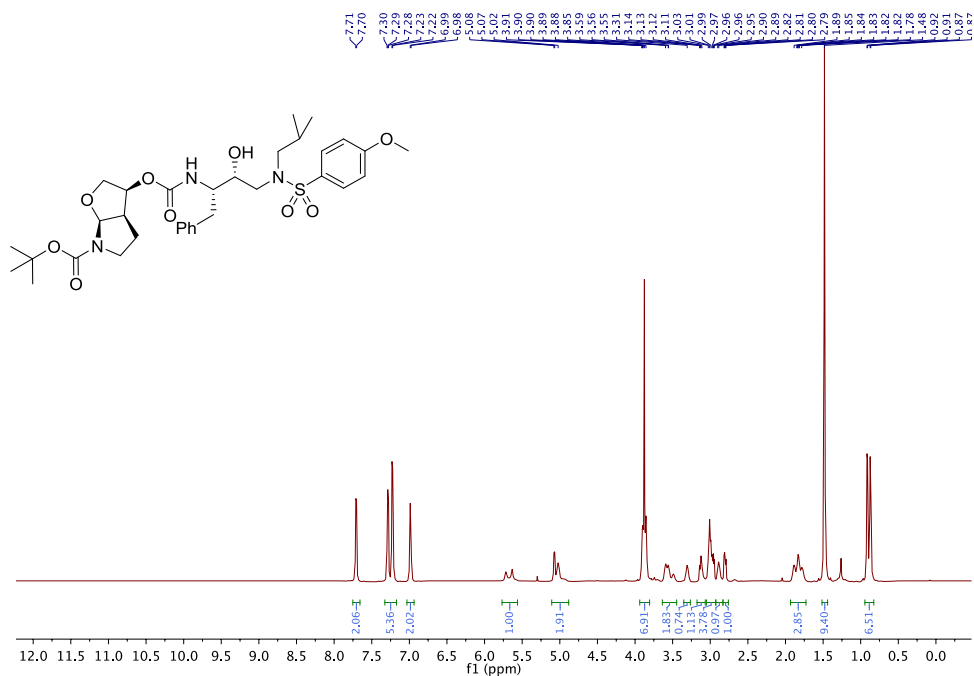


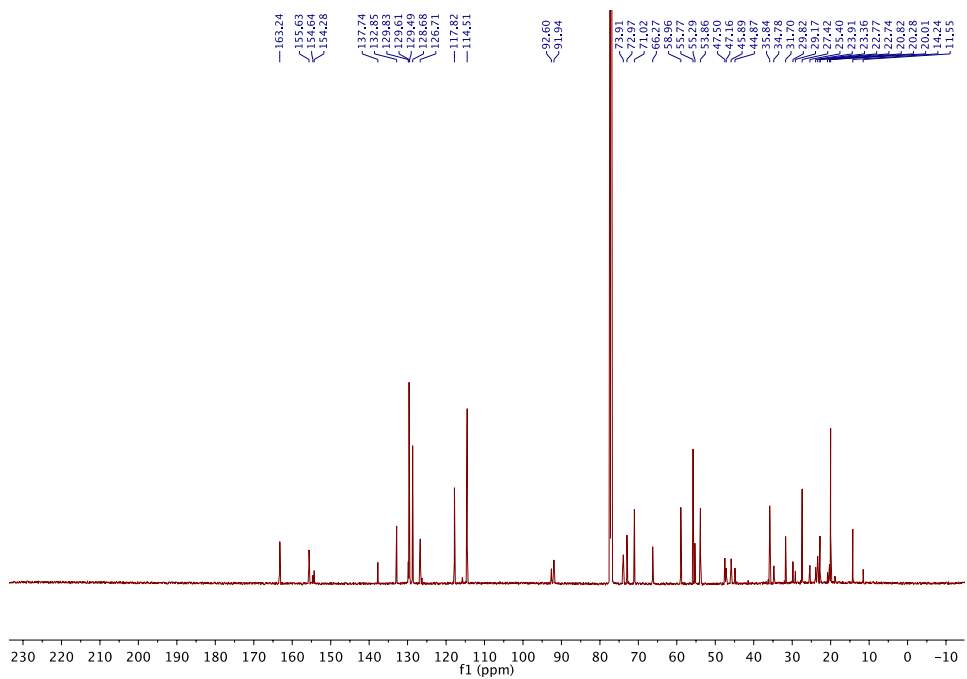


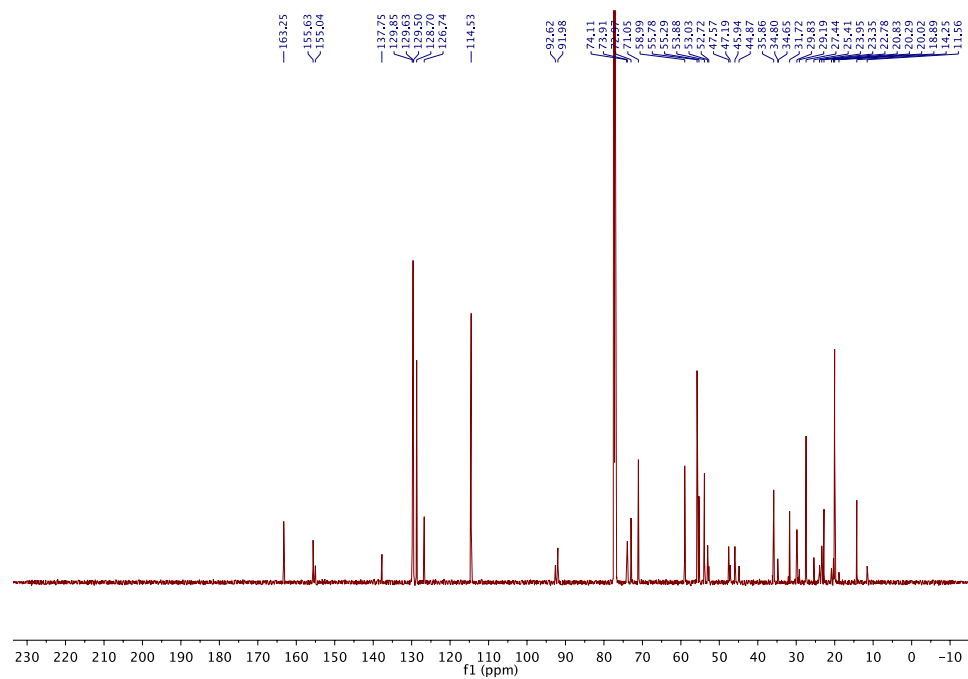
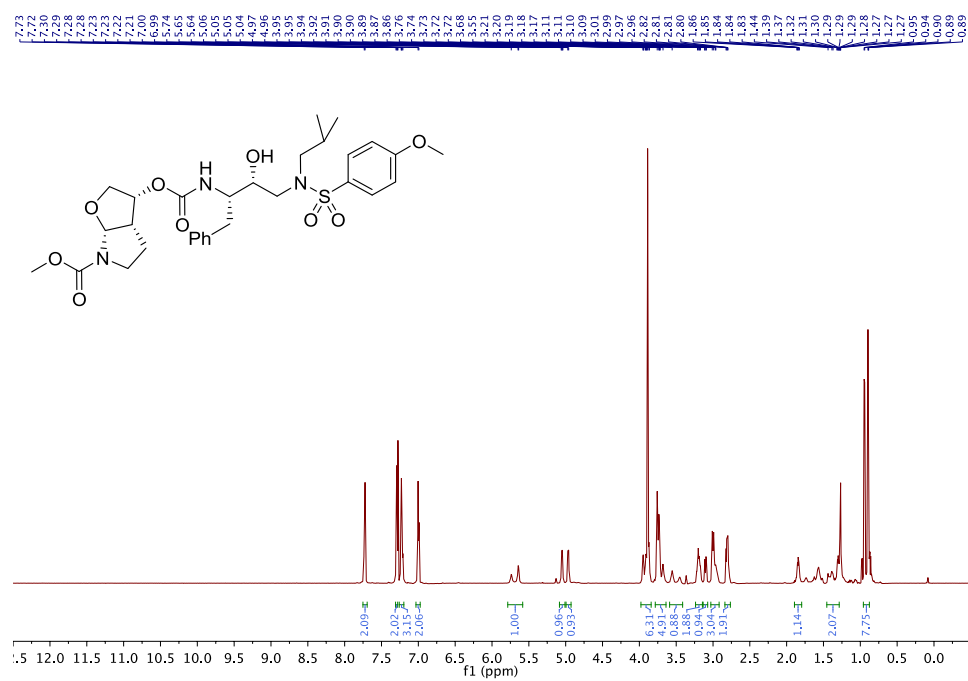


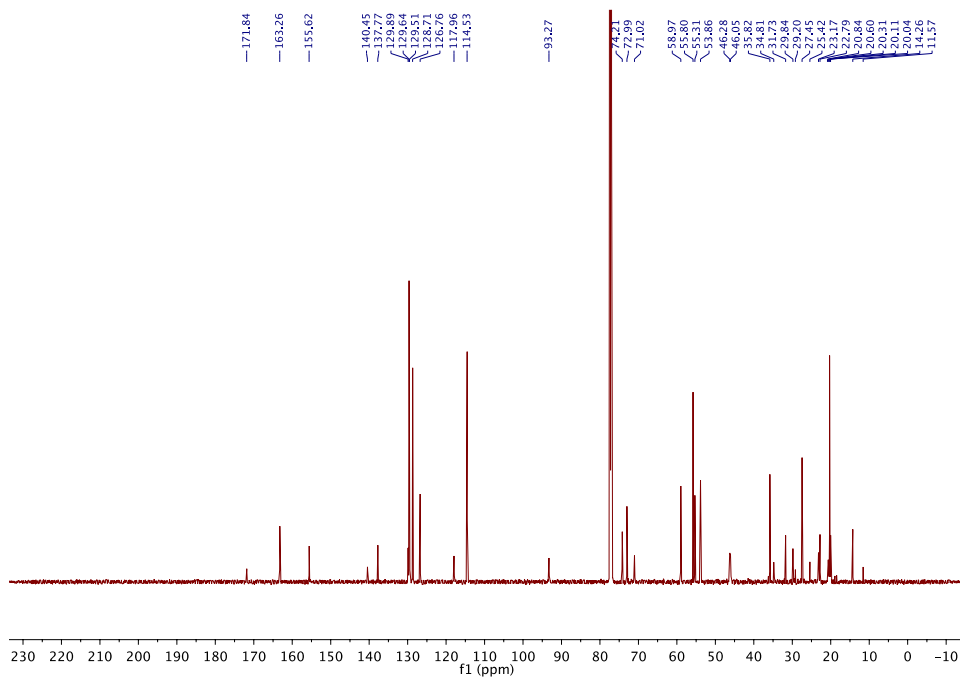
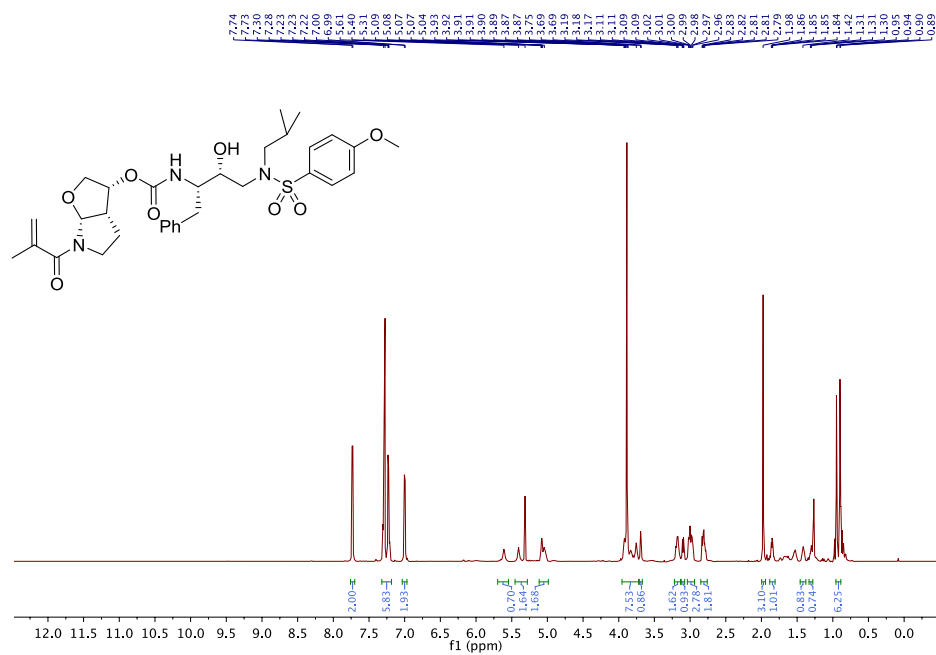


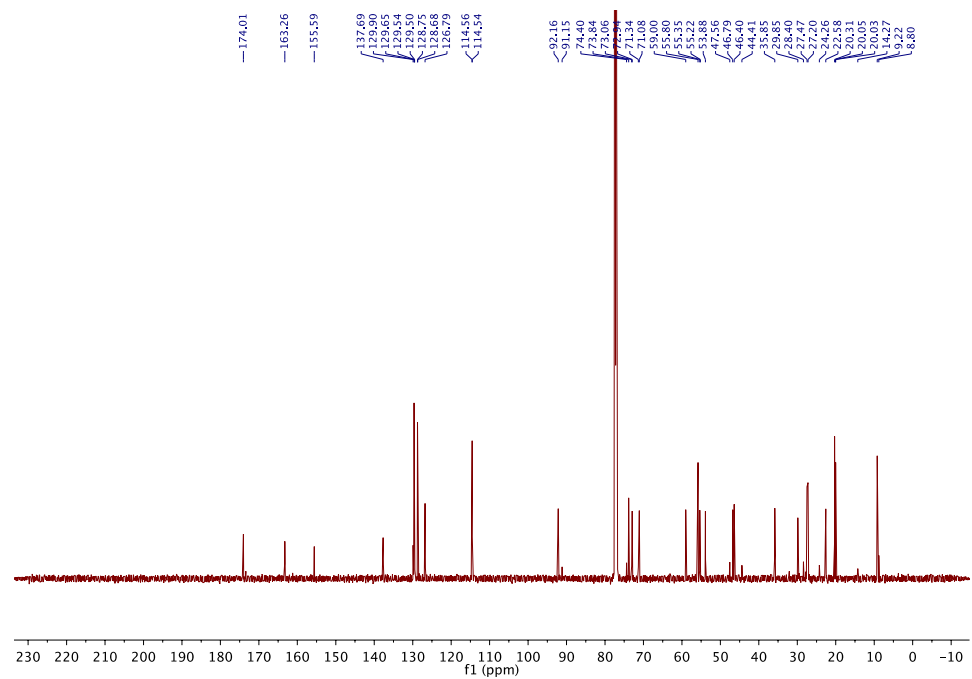
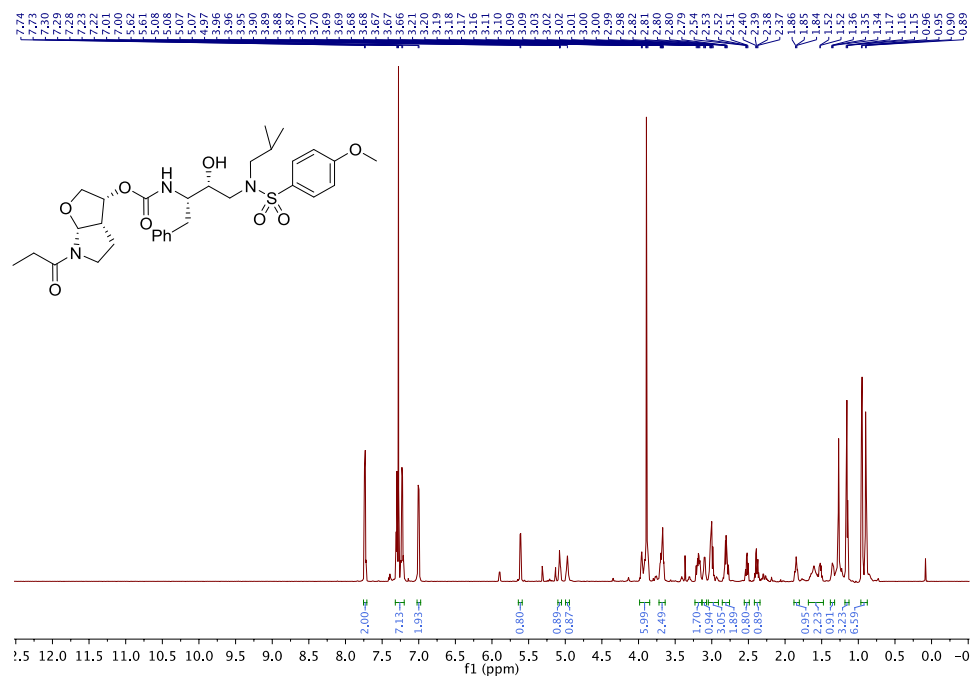


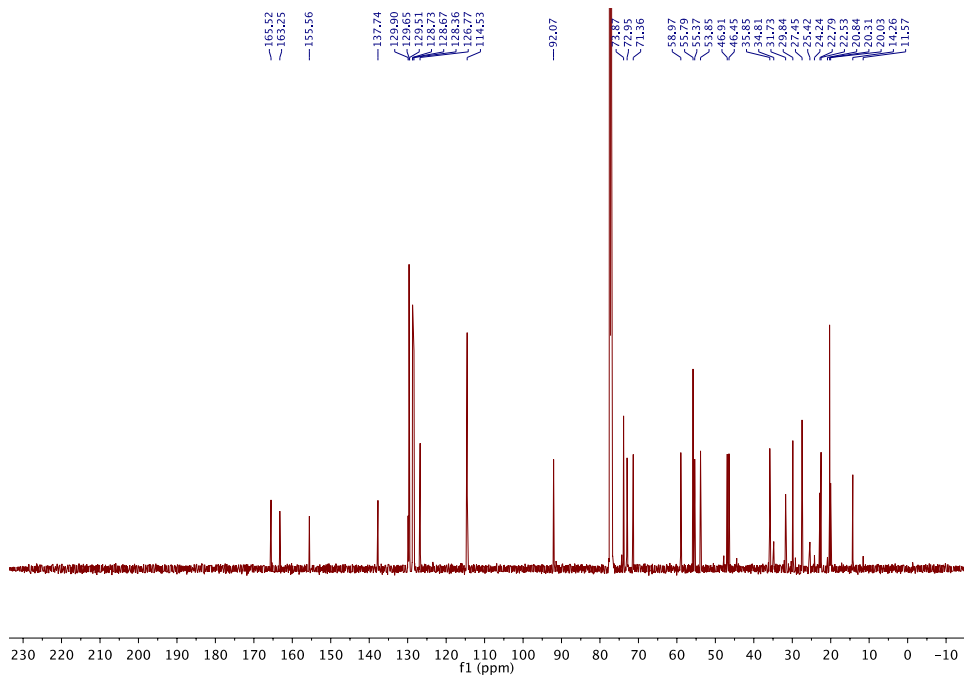
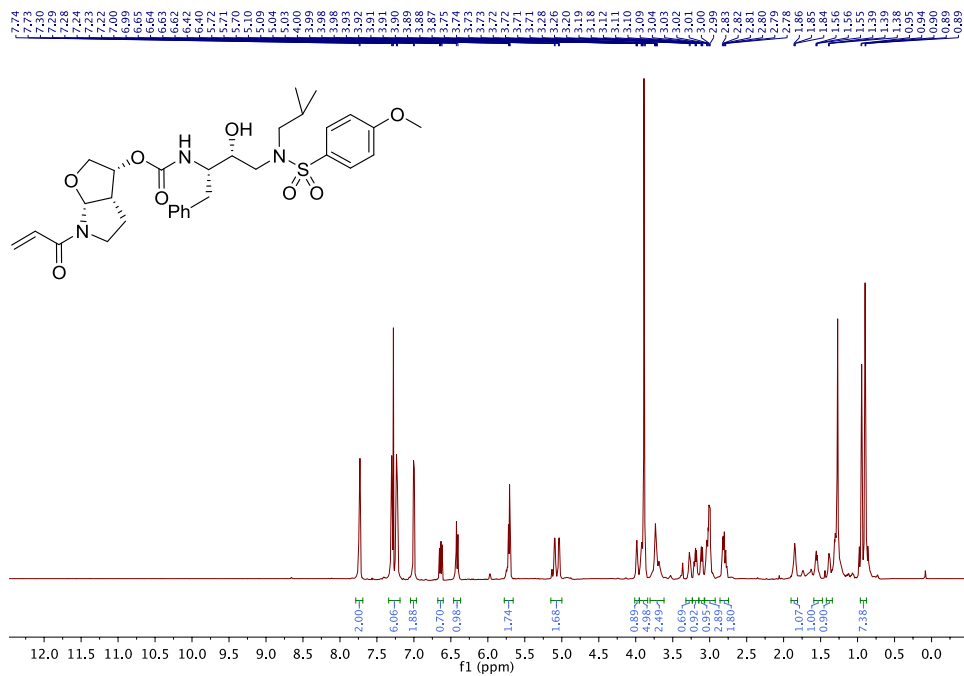


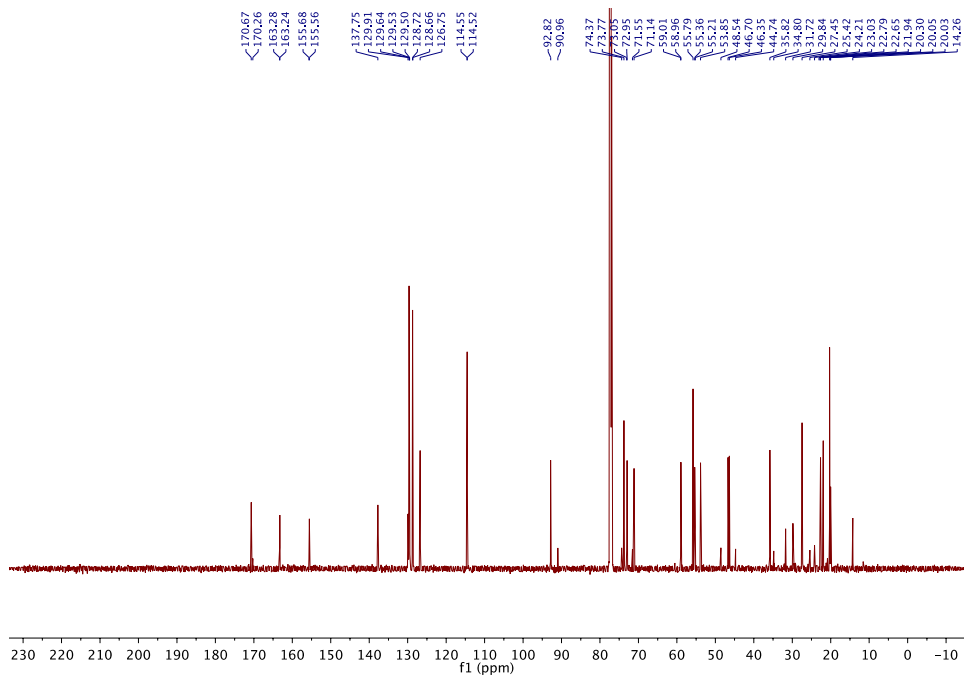
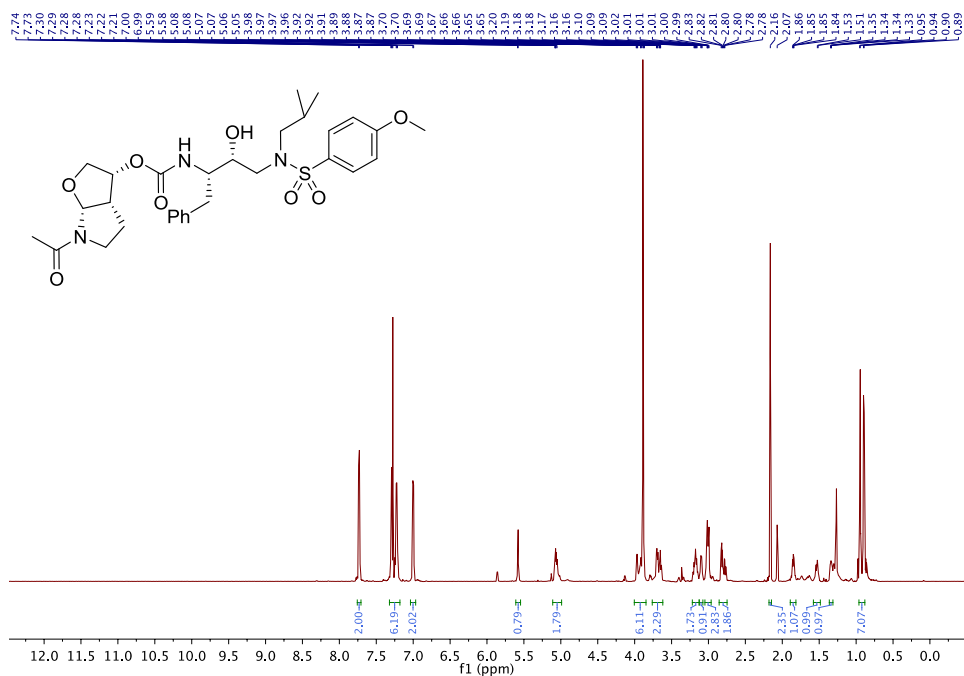


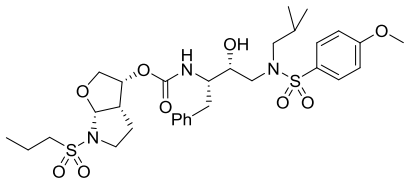


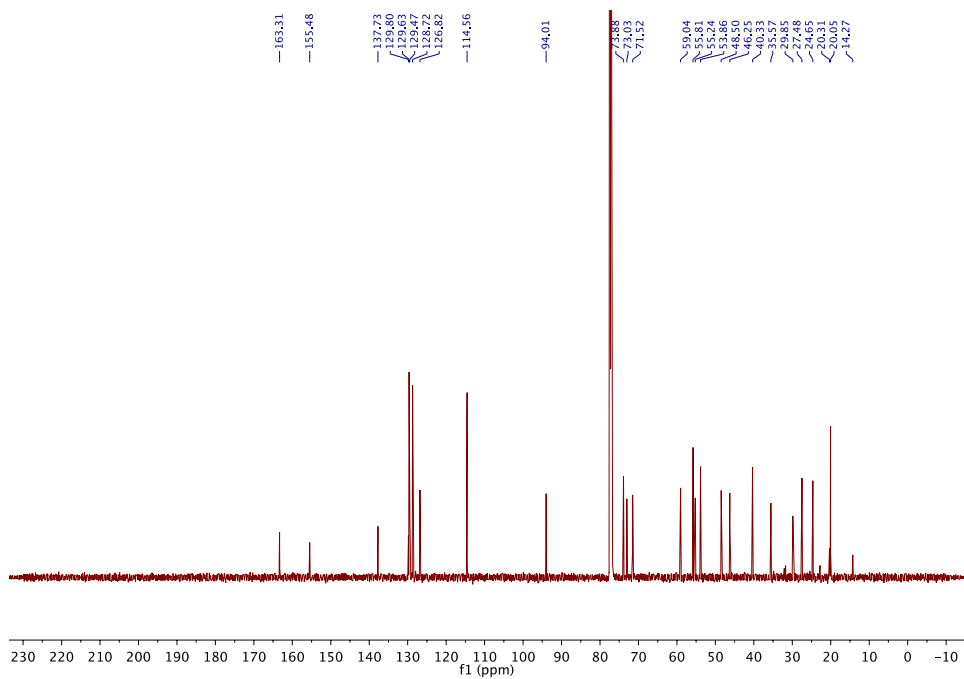
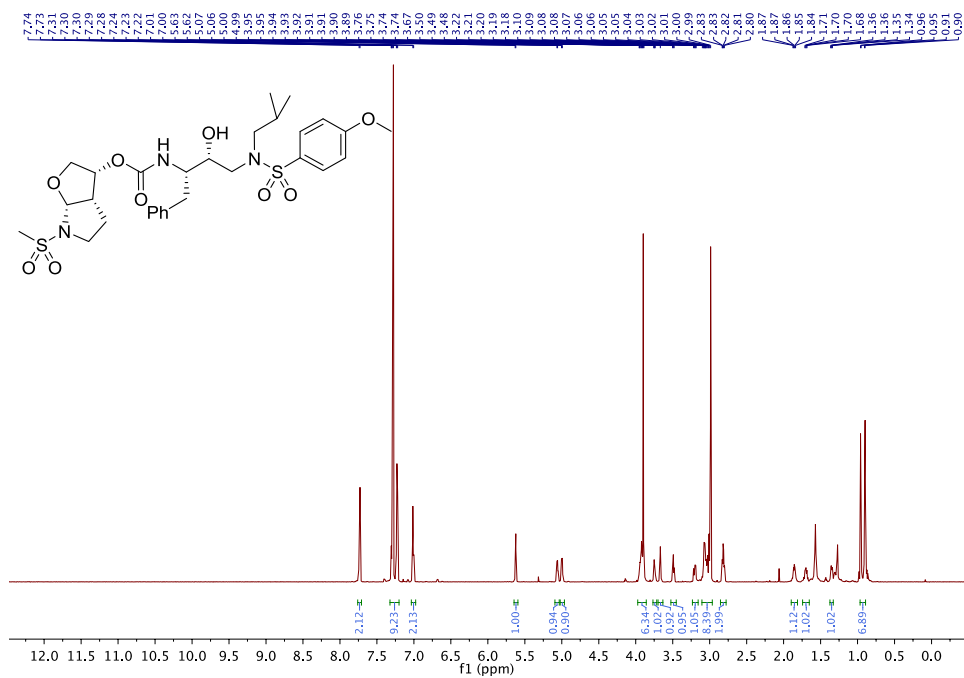


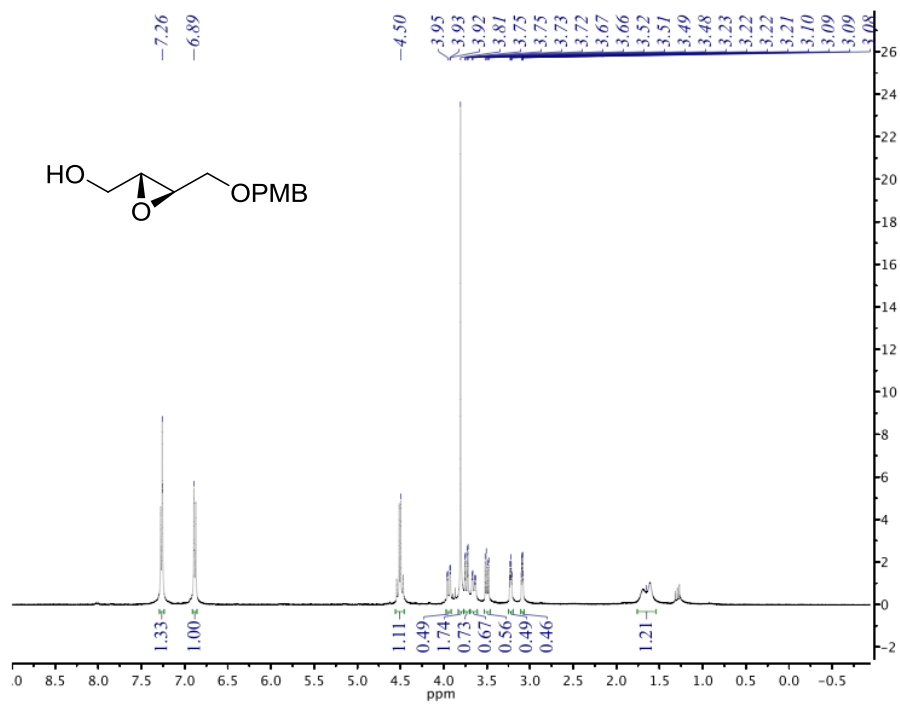
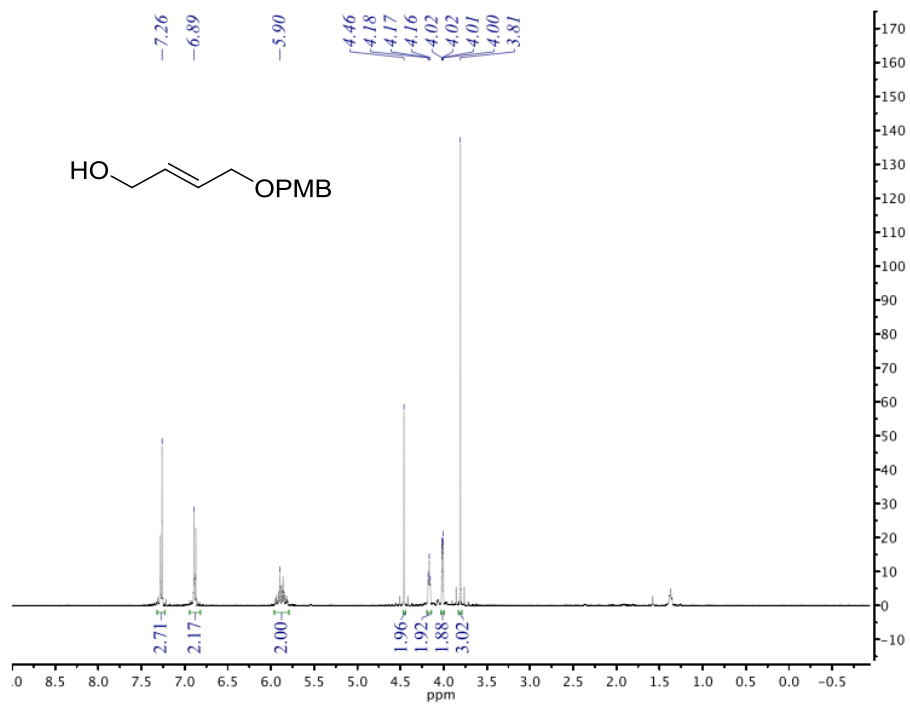


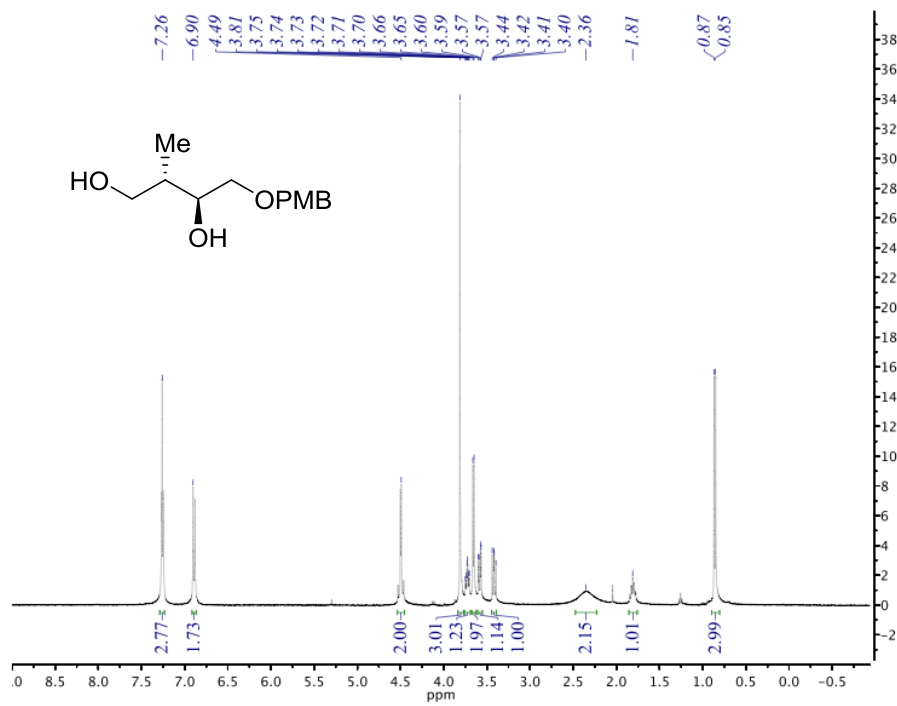


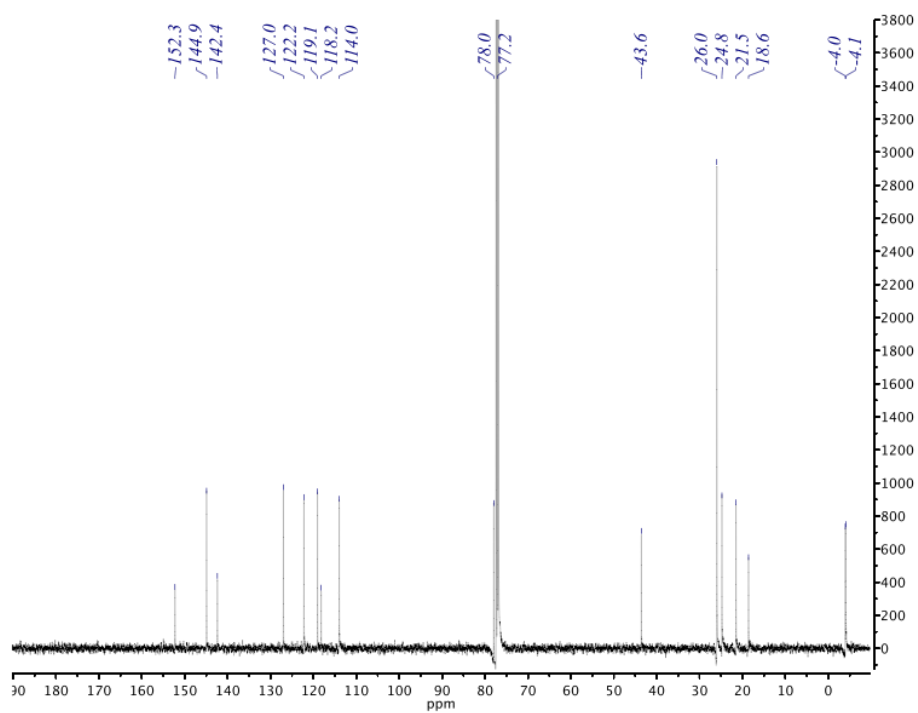
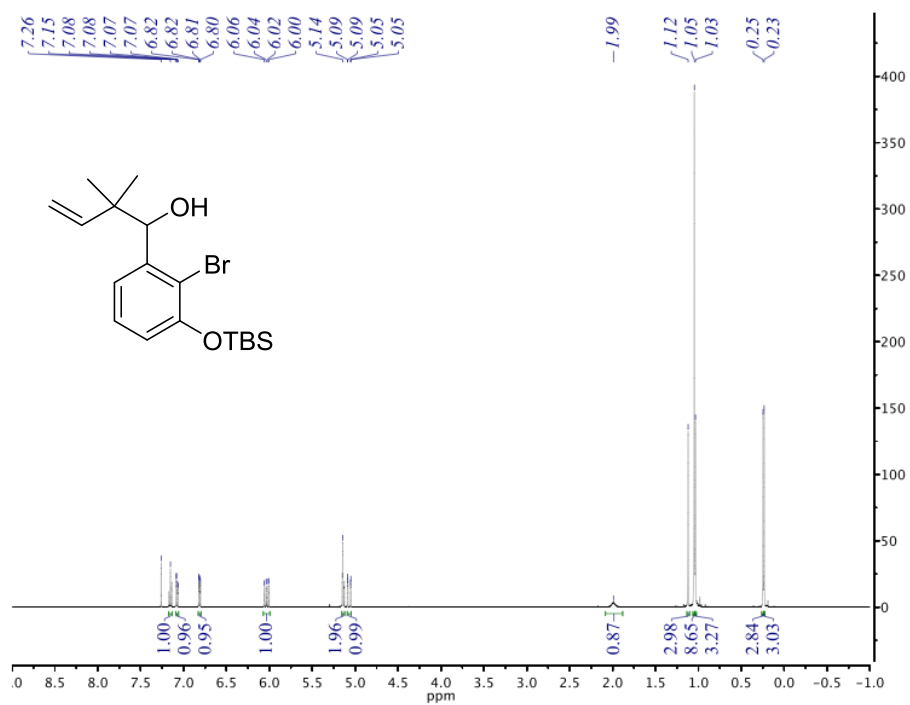


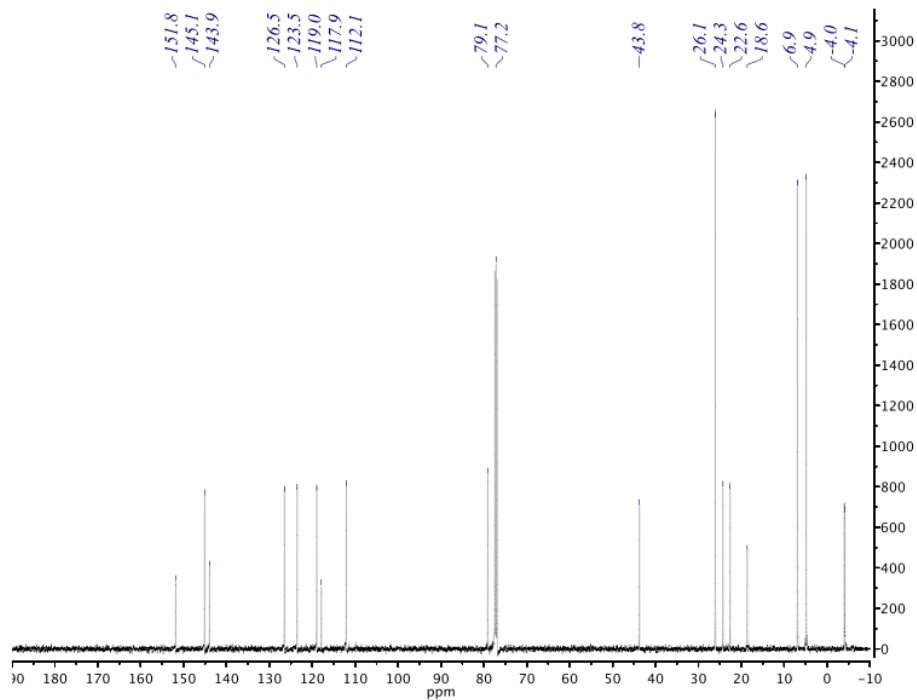
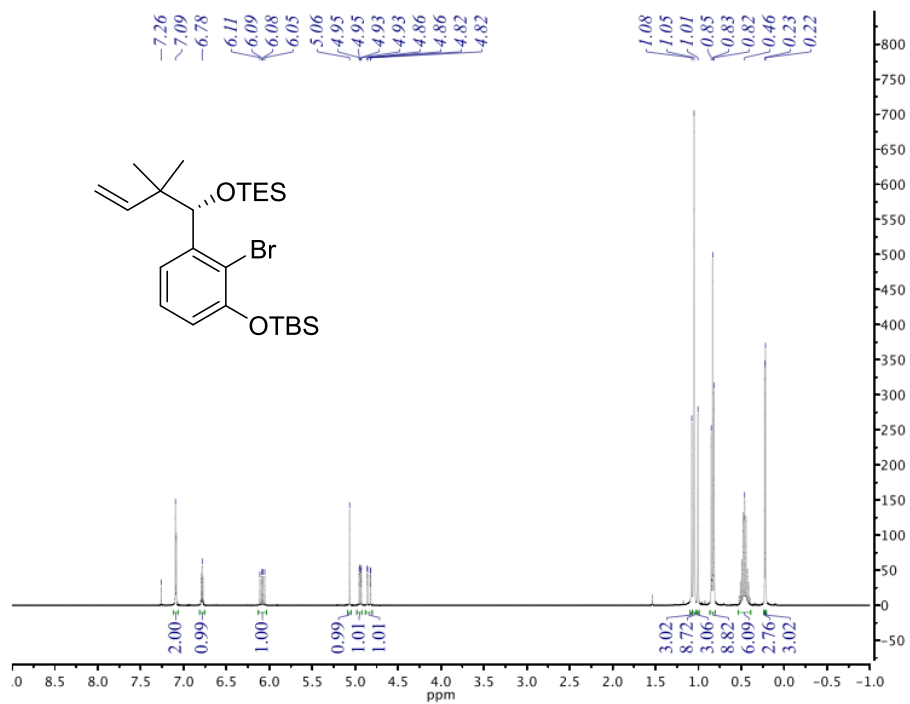


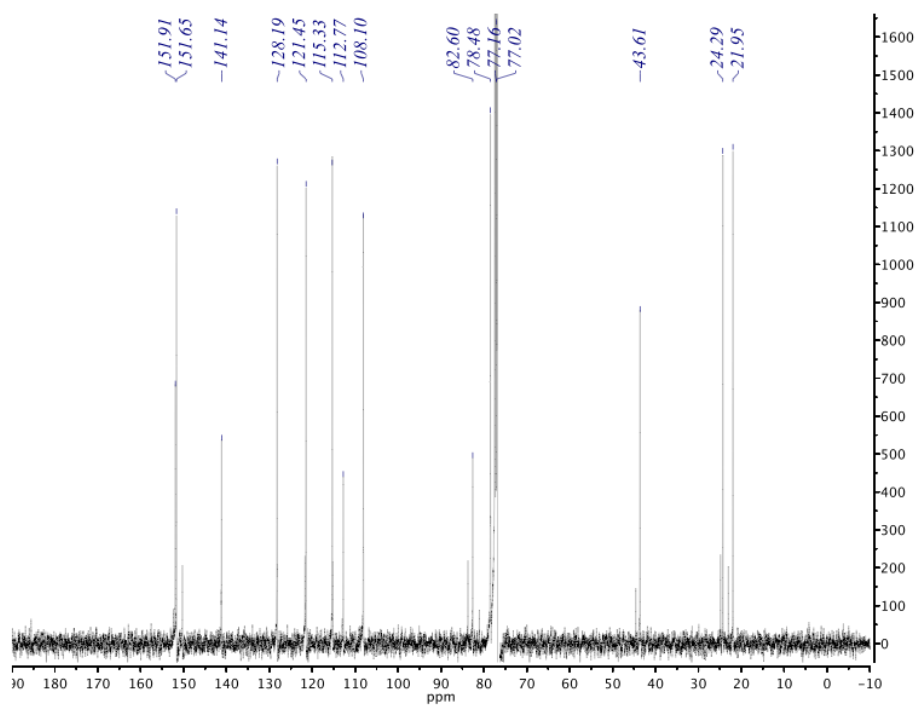
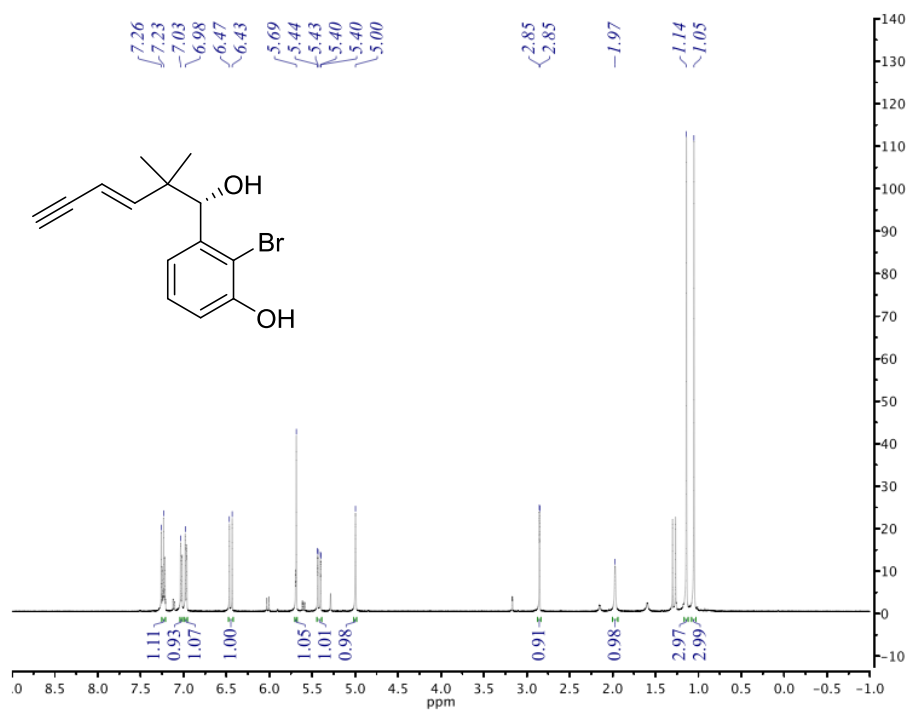


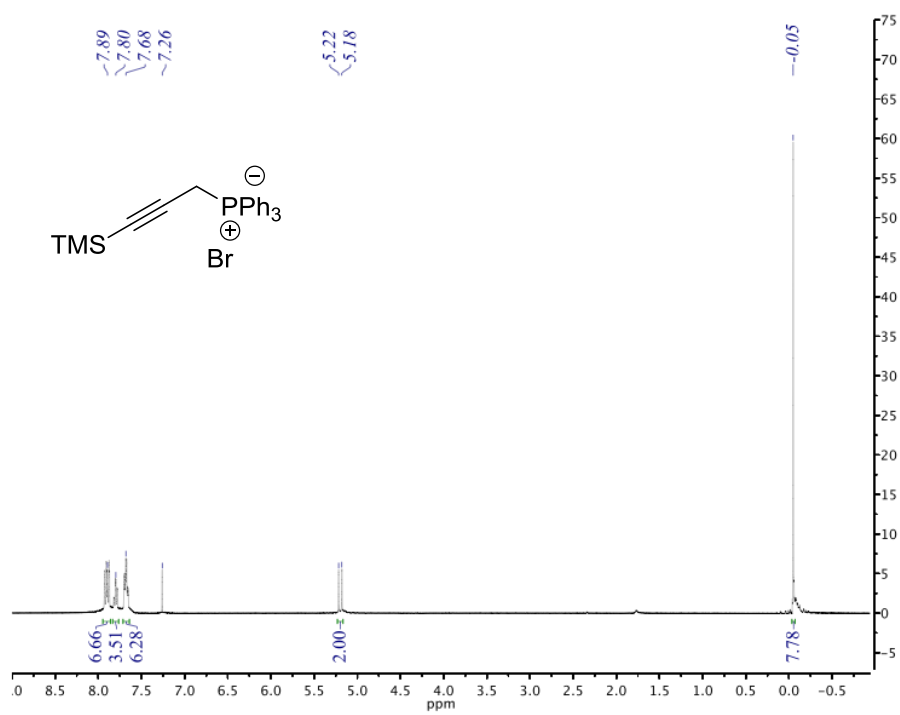




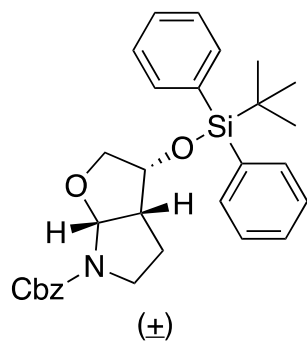
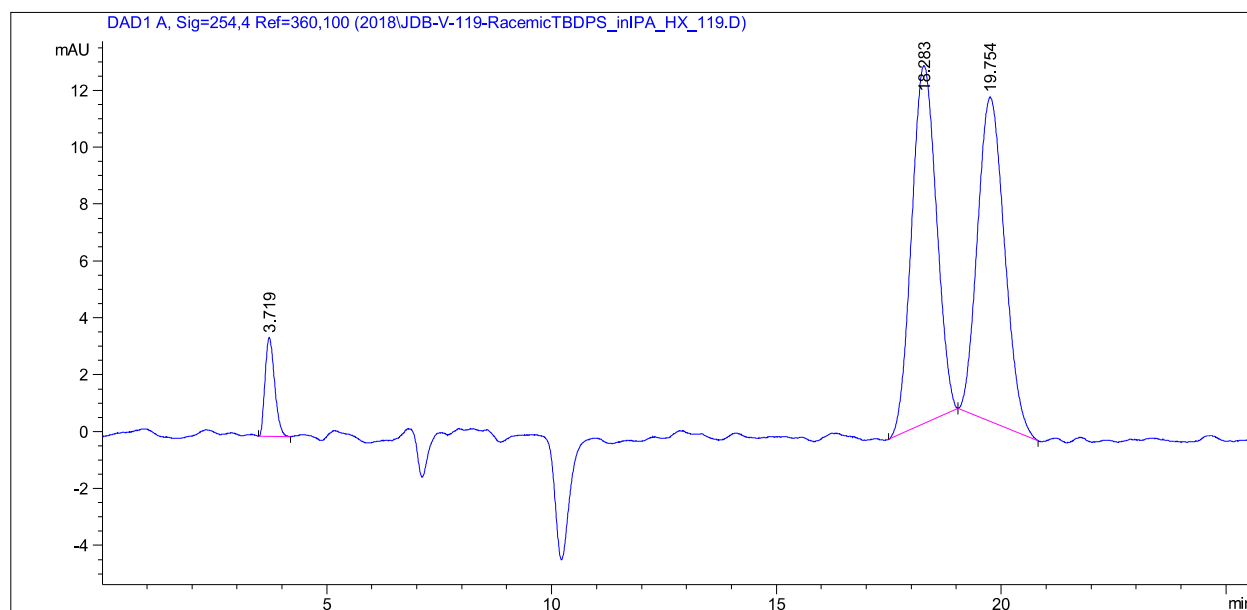








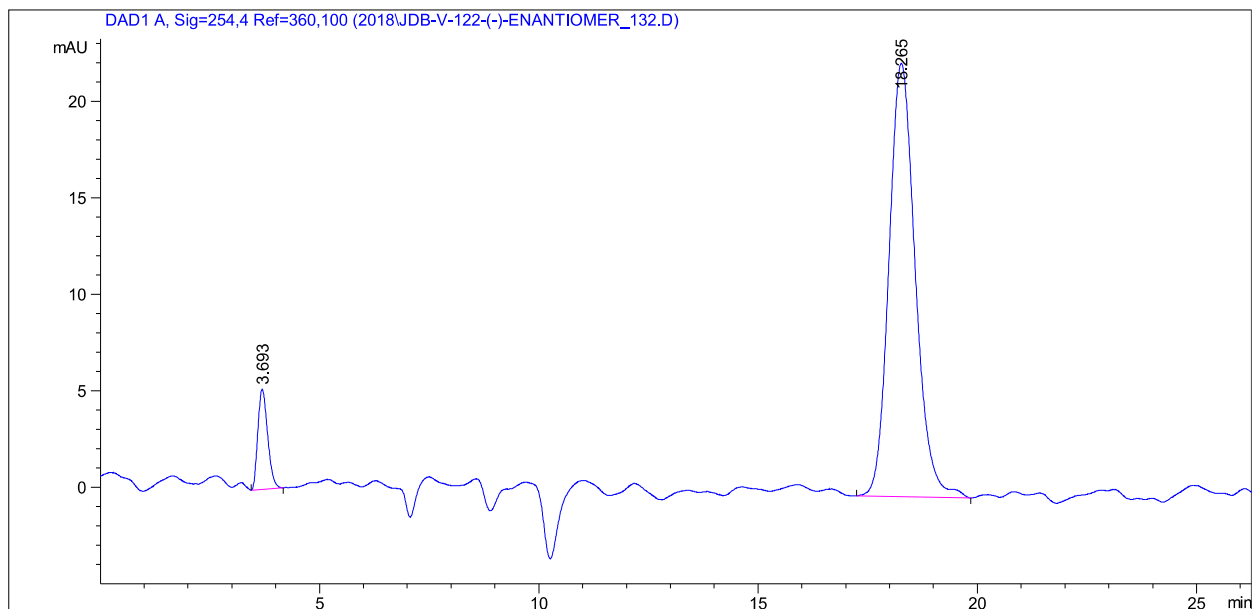
APPENDIX B: HPLC ANALYSIS OF LIPASE RESOLUTION



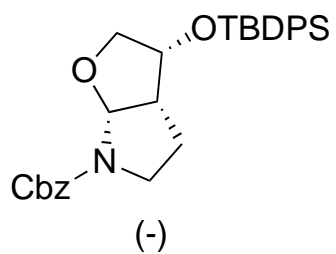
Signal 1: DAD1 A, Sig=254, 4 Ref=360, 100

Peak #	Retention Time [min]	Type	Width [min]	Area [mAU*s]	Height [mAU]	Area %
1	3.675	BB	0.2125	22.60342	1.56501	2.3191
2	18.226	BB	0.5723	476.35641	12.39609	48.8730
3	19.710	BB	0.6305	475.72269	11.22348	48.8080

Totals : 974.68252 25.18458

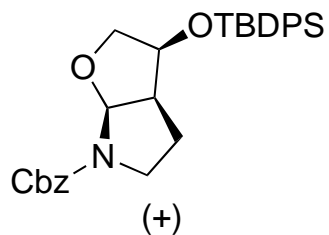
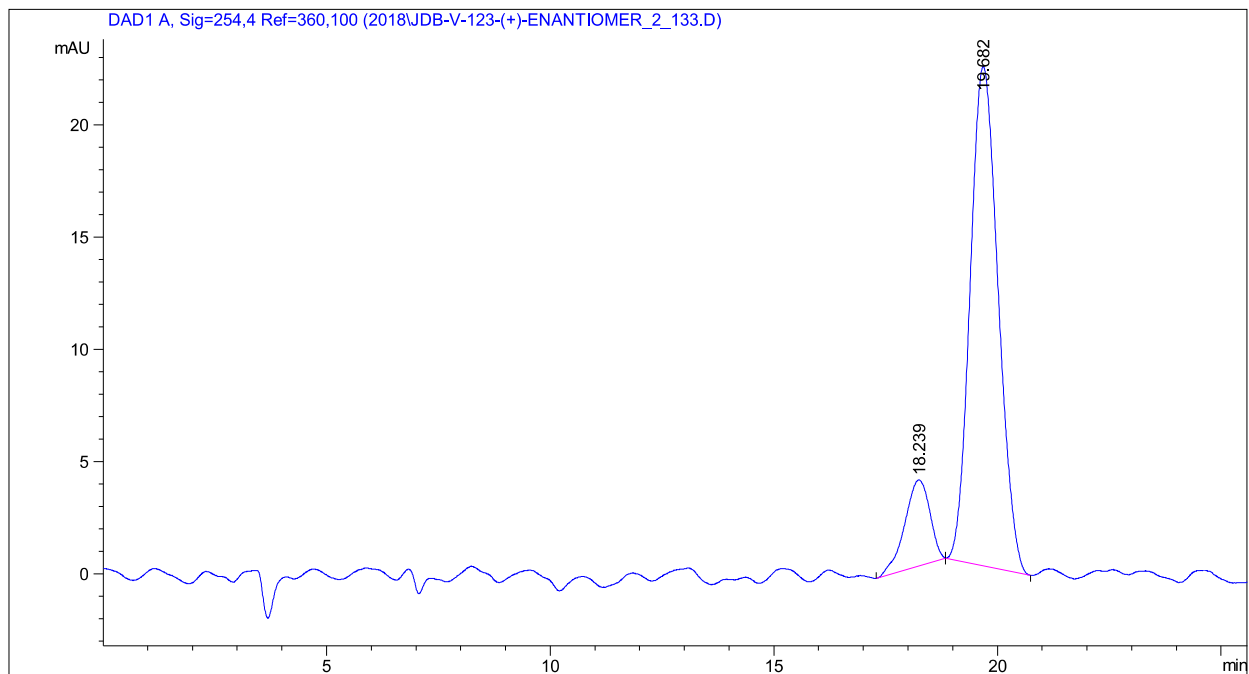


Signal 1: DAD1 A, Sig=254, 4 Ref=360, 100



Peak #	Ret Time [min]	Type	Width [min]	Area [mAU*s]	Height [mAU]	Area %
1	3.693	BB	0.2420	80.83189	5.18130	7.9373
2	18.265	BB	0.6329	937.55017	22.46679	92.0627

Total : 1018.38206 27.64809



Signal 1: DAD1 A, Sig=254, 4 Ref=360, 100

Peak #	Ret Time [min]	Type	Width [min]	Area [mAU*s]	Height [mAU]	Area %
1	18.239	BB	0.5106	150.13605	3.83639	13.4592
2	19.682	BB	0.6685	965.35626	22.23782	86.5408

Total s : 1115.49231 26.07421

REFERENCES

- (1) Poiesz, B. J.; Ruscetti, F. W.; Gazdar, A. F.; Bunn, P. A.; Minna, J. D.; Gallo, R. C. Detection and Isolation of Type C Retrovirus Particles from Fresh and Cultured Lymphocytes of a Patient with Cutaneous T-Cell Lymphoma. *Proceedings of the National Academy of Sciences* **1980**, 77 (12), 7415–7419.
- (2) Poiesz, B. J.; Ruscetti, F. W.; Reitz, M. S.; Kalyanaraman, V. S.; Gallo, R. C. Isolation of a New Type C Retrovirus (HTLV) in Primary Uncultured Cells of a Patient with Sézary T-Cell Leukaemia. *Nature* **1981**, 294 (5838), 268–271.
- (3) Centers for Disease Control (CDC). Kaposi's Sarcoma and Pneumocystis Pneumonia among Homosexual Men--New York City and California. *MMWR Morb. Mortal. Wkly. Rep.* **1981**, 30 (25), 305–308.
- (4) Hymes, K. B.; Cheung, T.; Greene, J. B.; Prose, N. S.; Marcus, A.; Ballard, H.; William, D. C.; Laubenstein, L. J. Kaposi's Sarcoma in Homosexual Men-a Report of Eight Cases. *Lancet* **1981**, 2 (8247), 598–600.
- (5) Centers for Disease Control (CDC). Update on Acquired Immune Deficiency Syndrome (AIDS)--United States. *MMWR Morb. Mortal. Wkly. Rep.* **1982**, 31 (37), 507–508, 513–514.
- (6) Barré-Sinoussi, F.; Chermann, J. C.; Rey, F.; Nugeyre, M. T.; Chamaret, S.; Gruest, J.; Dauguet, C.; Axler-Blin, C.; Vézinet-Brun, F.; Rouzioux, C.; Rozenbaum, W.; Montagnier, L. Isolation of a T-Lymphotropic Retrovirus from a Patient at Risk for Acquired Immune Deficiency Syndrome (AIDS). *Science* **1983**, 220 (4599), 868–871.
- (7) Gallo, R. C.; Salahuddin, S. Z.; Popovic, M.; Shearer, G. M.; Kaplan, M.; Haynes, B. F.; Palker, T. J.; Redfield, R.; Oleske, J.; Safai, B. Frequent Detection and Isolation of Cytopathic Retroviruses (HTLV-III) from Patients with AIDS and at Risk for AIDS. *Science* **1984**, 224 (4648), 500–503.
- (8) Case, K. Nomenclature: Human Immunodeficiency Virus. *Ann. Intern. Med.* **1986**, 105 (1), 133.
- (9) Nyamweya, S.; Hegedus, A.; Jaye, A.; Rowland-Jones, S.; Flanagan, K. L.; Macallan, D. C. Comparing HIV-1 and HIV-2 Infection: Lessons for Viral Immunopathogenesis. *Rev. Med. Virol.* **2013**, 23 (4), 221–240.
- (10) Motomura, K.; Chen, J.; Hu, W.-S. Genetic Recombination between Human Immunodeficiency Virus Type 1 (HIV-1) and HIV-2, Two Distinct Human Lentiviruses. *J Virol* **2008**, 82 (4), 1923–1933.
- (11) Pérez-Losada, M.; Arenas, M.; Galán, J. C.; Palero, F.; González-Candelas, F. Recombination in Viruses: Mechanisms, Methods of Study, and Evolutionary Consequences. *Infection, Genetics and Evolution* **2015**, 30, 296–307.

- (12) Gao, F.; Bailes, E.; Robertson, D. L.; Chen, Y.; Rodenburg, C. M.; Michael, S. F.; Cummins, L. B.; Arthur, L. O.; Peeters, M.; Shaw, G. M.; Sharp, P. M.; Hahn, B. H. Origin of HIV-1 in the Chimpanzee Pan Troglodytes Troglodytes. *Nature* **1999**, 397 (6718), 436–441.
- (13) Hirsch, V. M.; Olmsted, R. A.; Murphey-Corb, M.; Purcell, R. H.; Johnson, P. R. An African Primate Lentivirus (SIVsm) Closely Related to HIV-2. *Nature* **1989**, 339 (6223), 389–392.
- (14) Shaw, G. M.; Hunter, E. HIV Transmission. *Cold Spring Harb Perspect Med* **2012**, 2 (11).
- (15) Belyakov, I. M.; Berzofsky, J. A. Immunobiology of Mucosal HIV Infection and the Basis for Development of a New Generation of Mucosal AIDS Vaccines. *Immunity* **2004**, 20 (3), 247–253.
- (16) Sierra, S.; Kupfer, B.; Kaiser, R. Basics of the Virology of HIV-1 and Its Replication. *J. Clin. Virol.* **2005**, 34 (4), 233–244.
- (17) Cummins, N. W.; Badley, A. D. Making Sense of How HIV Kills Infected CD4 T Cells: Implications for HIV Cure. *Mol Cell Ther* **2014**, 2.
- (18) Al-Jabri, A. A. How Does HIV-1 Infect a Susceptible Human Cell? *J Sci Res Med Sci* **2003**, 5 (1–2), 31–44.
- (19) Blumenthal, R.; Durell, S.; Viard, M. HIV Entry and Envelope Glycoprotein-Mediated Fusion. *J Biol Chem* **2012**, 287 (49), 40841–40849.
- (20) Lobritz, M. A.; Ratcliff, A. N.; Arts, E. J. HIV-1 Entry, Inhibitors, and Resistance. *Viruses* **2010**, 2 (5), 1069–1105.
- (21) Human Immunodeficiency Virus (HIV). *Transfus Med Hemother* **2016**, 43 (3), 203–222.
- (22) Fanales-Belasio, E.; Raimondo, M.; Suligoi, B.; Buttò, S. HIV Virology and Pathogenetic Mechanisms of Infection: A Brief Overview. *Ann. Ist. Super. Sanita* **2010**, 46 (1), 5–14.
- (23) Wilen, C. B.; Tilton, J. C.; Doms, R. W. HIV: Cell Binding and Entry. *Cold Spring Harb Perspect Med* **2012**, 2 (8).
- (24) Horwitz, J. P.; Chua, J.; Noel, M. Nucleosides. V. The Monomesylates of 1-(2'-Deoxy- β -D-Lyxofuranosyl)Thymine1,2. *J. Org. Chem.* **1964**, 29 (7), 2076–2078.
- (25) Broder, S. The Development of Antiretroviral Therapy and Its Impact on the HIV-1/AIDS Pandemic. *Antiviral Res.* **2010**, 85 (1), 1–18.
- (26) Hammer, S. M.; Katzenstein, D. A.; Hughes, M. D.; Gundacker, H.; Schooley, R. T.; Haubrich, R. H.; Henry, W. K.; Lederman, M. M.; Phair, J. P.; Niu, M.; Hirsch, M. S.; Merigan, T. C. A Trial Comparing Nucleoside Monotherapy with Combination Therapy in HIV-Infected Adults with CD4 Cell Counts from 200 to 500 per Cubic Millimeter. AIDS Clinical Trials Group Study 175 Study Team. *N. Engl. J. Med.* **1996**, 335 (15), 1081–1090.

- (27) Schooley, R. T.; Ramirez-Ronda, C.; Lange, J. M.; Cooper, D. A.; Lavelle, J.; Lefkowitz, L.; Moore, M.; Larder, B. A.; St Clair, M.; Mulder, J. W.; McKinnis, R.; Pennington, K. N.; Harrigan, P. R.; Kinghorn, I.; Steel, H.; Rooney, J. F. Virologic and Immunologic Benefits of Initial Combination Therapy with Zidovudine and Zalcitabine or Didanosine Compared with Zidovudine Monotherapy. Wellcome Resistance Study Collaborative Group. *J. Infect. Dis.* **1996**, *173* (6), 1354–1366.
- (28) Ghosh, A. K.; Osswald, H. L.; Prato, G. Recent Progress in the Development of HIV-1 Protease Inhibitors for the Treatment of HIV/AIDS. *J. Med. Chem.* **2016**, *59* (11), 5172–5208.
- (29) Qian, K.; Morris-Natschke, S. L.; Lee, K.-H. HIV Entry Inhibitors and Their Potential in HIV Therapy. *Medicinal Research Reviews* **2009**, *29* (2), 369–393.
- (30) Henrich, T. J.; Kuritzkes, D. R. HIV-1 Entry Inhibitors: Recent Development and Clinical Use. *Curr Opin Virol* **2013**, *3* (1), 51–57.
- (31) Fung, H. B.; Guo, Y. Enfuvirtide: A Fusion Inhibitor for the Treatment of HIV Infection. *Clin Ther* **2004**, *26* (3), 352–378.
- (32) Tomaras, G. D.; Greenberg, M. L. Mechanisms for HIV-1 Entry: Current Strategies to Interfere with This Step. *Current Infectious Disease Reports* **2001**, *3* (1), 93–99.
- (33) Wild, C.; Greenwell, T.; Matthews, T. A Synthetic Peptide from HIV-1 Gp41 Is a Potent Inhibitor of Virus-Mediated Cell-Cell Fusion. *AIDS Res. Hum. Retroviruses* **1993**, *9* (11), 1051–1053.
- (34) Rad, T. M.; Saghaie, L.; Fassihi, A. HIV-1 Entry Inhibitors: A Review of Experimental and Computational Studies. *Chemistry & Biodiversity* **2018**, *15* (10), e1800159.
- (35) Castonguay, L. A.; Weng, Y.; Adolfsen, W.; Di Salvo, J.; Kilburn, R.; Caldwell, C. G.; Daugherty, B. L.; Finke, P. E.; Hale, J. J.; Lynch, C. L.; Mills, S. G.; MacCoss, M.; Springer, M. S.; DeMartino, J. A. Binding of 2-Aryl-4-(Piperidin-1-Yl)Butanamines and 1,3,4-Trisubstituted Pyrrolidines to Human CCR5: A Molecular Modeling-Guided Mutagenesis Study of the Binding Pocket. *Biochemistry* **2003**, *42* (6), 1544–1550.
- (36) Dorr, P.; Westby, M.; Dobbs, S.; Griffin, P.; Irvine, B.; Macartney, M.; Mori, J.; Rickett, G.; Smith-Burchnell, C.; Napier, C.; Webster, R.; Armour, D.; Price, D.; Stammen, B.; Wood, A.; Perros, M. Maraviroc (UK-427,857), a Potent, Orally Bioavailable, and Selective Small-Molecule Inhibitor of Chemokine Receptor CCR5 with Broad-Spectrum Anti-Human Immunodeficiency Virus Type 1 Activity. *Antimicrob Agents Chemother* **2005**, *49* (11), 4721–4732.
- (37) Chung, S.; Miller, J. T.; Lapkouski, M.; Tian, L.; Yang, W.; Le Grice, S. F. J. Examining the Role of the HIV-1 Reverse Transcriptase P51 Subunit in Positioning and Hydrolysis of RNA/DNA Hybrids. *J Biol Chem* **2013**, *288* (22), 16177–16184.

- (38) Nanni, R. G.; Ding, J.; Jacobo-Molina, A.; Hughes, S. H.; Arnold, E. Review of HIV-1 Reverse Transcriptase Three-Dimensional Structure: Implications for Drug Design. *Perspectives in Drug Discovery and Design* **1993**, *1* (1), 129–150.
- (39) Sarafianos, S. G.; Marchand, B.; Das, K.; Himmel, D. M.; Parniak, M. A.; Hughes, S. H.; Arnold, E. Structure and Function of HIV-1 Reverse Transcriptase: Molecular Mechanisms of Polymerization and Inhibition. *J. Mol. Biol.* **2009**, *385* (3), 693–713.
- (40) Huang, H.; Chopra, R.; Verdine, G. L.; Harrison, S. C. Structure of a Covalently Trapped Catalytic Complex of HIV-1 Reverse Transcriptase: Implications for Drug Resistance. *Science* **1998**, *282* (5394), 1669–1675.
- (41) Kati, W. M.; Johnson, K. A.; Jerva, L. F.; Anderson, K. S. Mechanism and Fidelity of HIV Reverse Transcriptase. *J. Biol. Chem.* **1992**, *267* (36), 25988–25997.
- (42) Jonckheere, H.; Anné, J.; De Clercq, E. The HIV-1 Reverse Transcription (RT) Process as Target for RT Inhibitors. *Med Res Rev* **2000**, *20* (2), 129–154.
- (43) Larder, B. A.; Purifoy, D. J. M.; Powell, K. L.; Darby, G. Site-Specific Mutagenesis of AIDS Virus Reverse Transcriptase. *Nature* **1987**, *327* (6124), 716–717.
- (44) Steitz, T. A. A Mechanism for All Polymerases. *Nature* **1998**, *391* (6664), 231–232.
- (45) Rungrotmongkol, T.; Nunthaboot, N.; Aruksakunwong, O.; Hannongbua, S. HIV-1 Reverse Transcriptase – Computational Studies on the Polymerase Active Site. In *Encyclopedia of Biophysics*; Roberts, G. C. K., Ed.; Springer: Berlin, Heidelberg, 2013; pp 989–992.
- (46) Davies, J. F.; Hostomska, Z.; Hostomsky, Z.; Jordan, S. R.; Matthews, D. A. Crystal Structure of the Ribonuclease H Domain of HIV-1 Reverse Transcriptase. *Science* **1991**, *252* (5002), 88–95.
- (47) Schultz, S. J.; Champoux, J. J. RNase H Activity: Structure, Specificity, and Function in Reverse Transcription. *Virus research* **2008**, *134* (1–2), 86.
- (48) Stein, D. S.; Moore, K. H. P. Phosphorylation of Nucleoside Analog Antiretrovirals: A Review for Clinicians. *Pharmacotherapy: The Journal of Human Pharmacology and Drug Therapy* **2001**, *21* (1), 11–34.
- (49) Otto, M. J. New Nucleoside Reverse Transcriptase Inhibitors for the Treatment of HIV Infections. *Current Opinion in Pharmacology* **2004**, *4* (5), 431–436.
- (50) De Clercq, E. Chapter Nine - The Nucleoside Reverse Transcriptase Inhibitors, Nonnucleoside Reverse Transcriptase Inhibitors, and Protease Inhibitors in the Treatment of HIV Infections (AIDS). In *Advances in Pharmacology*; De Clercq, E., Ed.; Antiviral Agents; Academic Press, 2013; Vol. 67, pp 317–358.

- (51) Shirvani, P.; Fassihi, A.; Saghaie, L. Recent Advances in the Design and Development of Non-Nucleoside Reverse Transcriptase Inhibitor Scaffolds. *ChemMedChem* **2019**, *14* (1), 52–77.
- (52) Zhuang, C.; Pannecouque, C.; De Clercq, E.; Chen, F. Development of Non-Nucleoside Reverse Transcriptase Inhibitors (NNRTIs): Our Past Twenty Years. *Acta Pharmaceutica Sinica B* **2019**.
- (53) Namasivayam, V.; Vanangamudi, M.; Kramer, V. G.; Kurup, S.; Zhan, P.; Liu, X.; Kongsted, J.; Byrareddy, S. N. The Journey of HIV-1 Non-Nucleoside Reverse Transcriptase Inhibitors (NNRTIs) from Lab to Clinic. *J. Med. Chem.* **2019**, *62* (10), 4851–4883.
- (54) Zheng, R.; Jenkins, T. M.; Craigie, R. Zinc Folds the N-Terminal Domain of HIV-1 Integrase, Promotes Multimerization, and Enhances Catalytic Activity. *Proc Natl Acad Sci U S A* **1996**, *93* (24), 13659–13664.
- (55) Hajimahdi, Z.; Zarghi, A. Progress in HIV-1 Integrase Inhibitors: A Review of Their Chemical Structure Diversity. *Iran J Pharm Res* **2016**, *15* (4), 595–628.
- (56) Di Santo, R. Inhibiting the HIV Integration Process: Past, Present, and the Future. *J. Med. Chem.* **2014**, *57* (3), 539–566.
- (57) Craigie, R. The Molecular Biology of HIV Integrase. *Future Virol* **2012**, *7* (7), 679–686.
- (58) Li, B.-W.; Zhang, F.-H.; Serrao, E.; Chen, H.; Sanchez, T. W.; Yang, L.-M.; Neamati, N.; Zheng, Y.-T.; Wang, H.; Long, Y.-Q. Design and Discovery of Flavonoid-Based HIV-1 Integrase Inhibitors Targeting Both the Active Site and the Interaction with LEDGF/P75. *Bioorganic & Medicinal Chemistry* **2014**, *22* (12), 3146–3158.
- (59) Poeschla, E. M. Integrase, LEDGF/P75 and HIV Replication. *Cell. Mol. Life Sci.* **2008**, *65* (9), 1403–1424.
- (60) Craigie, R. HIV Integrase, a Brief Overview from Chemistry to Therapeutics. *J. Biol. Chem.* **2001**, *276* (26), 23213–23216.
- (61) Yang, W.; Lee, J. Y.; Nowotny, M. Making and Breaking Nucleic Acids: Two-Mg²⁺-Ion Catalysis and Substrate Specificity. *Mol. Cell* **2006**, *22* (1), 5–13.
- (62) Steitz, T. A.; Steitz, J. A. A General Two-Metal-Ion Mechanism for Catalytic RNA. *Proc Natl Acad Sci U S A* **1993**, *90* (14), 6498–6502.
- (63) Mouscadet, J.-F.; Tchertanov, L. Raltegravir: Molecular Basis of Its Mechanism of Action. *Eur J Med Res* **2009**, *14* (Suppl 3), 5–16.
- (64) Shimura, K.; Kodama, E. N. Elvitegravir: A New HIV Integrase Inhibitor. *Antivir Chem Chemother* **2009**, *20* (2), 79–85.

- (65) Yadav, G.; Kumar, P.; Kumar, Y.; Singh, P. K. Dolutegravir, Second Generation Integrase Inhibitor: A New Hope for HIV Patient. *European Journal of Molecular & Clinical Medicine* **2018**, 5 (1), 20–29.
- (66) Louis, J. M.; Nashed, N. T.; Parris, K. D.; Kimmel, A. R.; Jerina, D. M. Kinetics and Mechanism of Autoprocessing of Human Immunodeficiency Virus Type 1 Protease from an Analog of the Gag-Pol Polyprotein. *Proc Natl Acad Sci U S A* **1994**, 91 (17), 7970–7974.
- (67) Weber, I. T.; Agniswamy, J. HIV-1 Protease: Structural Perspectives on Drug Resistance. *Viruses* **2009**, 1 (3), 1110–1136.
- (68) Wondrak, E. M.; Nashed, N. T.; Haber, M. T.; Jerina, D. M.; Louis, J. M. A Transient Precursor of the HIV-1 Protease ISOLATION, CHARACTERIZATION, AND KINETICS OF MATURATION. *J. Biol. Chem.* **1996**, 271 (8), 4477–4481.
- (69) Wlodawer, A.; Miller, M.; Jaskólski, M.; Sathyanarayana, B. K.; Baldwin, E.; Weber, I. T.; Selk, L. M.; Clawson, L.; Schneider, J.; Kent, S. B. H. Conserved Folding in Retroviral Proteases: Crystal Structure of a Synthetic HIV-1 Protease. *Science* **1989**, 245 (4918), 616–621.
- (70) Brik, A.; Wong, C.-H. HIV-1 Protease: Mechanism and Drug Discovery. *Organic & Biomolecular Chemistry* **2003**, 1 (1), 5–14.
- (71) Greenlee, W. J.; Siegl, P. K. S. Chapter 7. Angiotensin / Renin Modulators. In *Annual Reports in Medicinal Chemistry*; Bristol, J. A., Ed.; Academic Press, 1992; Vol. 27, pp 59–68.
- (72) Roberts, N. A.; Martin, J. A.; Kinchington, D.; Broadhurst, A. V.; Craig, J. C.; Duncan, I. B.; Galpin, S. A.; Handa, B. K.; Kay, J.; Kröhn, A. Rational Design of Peptide-Based HIV Proteinase Inhibitors. *Science* **1990**, 248 (4953), 358–361.
- (73) Krohn, A.; Redshaw, S.; Ritchie, J. C.; Graves, B. J.; Hatada, M. H. Novel Binding Mode of Highly Potent HIV-Proteinase Inhibitors Incorporating the (R)-Hydroxyethylamine Isostere. *J. Med. Chem.* **1991**, 34 (11), 3340–3342.
- (74) Lyle, T. A. 7.12 - Ribonucleic Acid Viruses: Antivirals for Human Immunodeficiency Virus. In *Comprehensive Medicinal Chemistry II*; Taylor, J. B., Trigg, D. J., Eds.; Elsevier: Oxford, 2007; pp 329–371.
- (75) Tie, Y.; Kovalevsky, A. Y.; Boross, P.; Wang, Y.-F.; Ghosh, A. K.; Tozser, J.; Harrison, R. W.; Weber, I. T. Atomic Resolution Crystal Structures of HIV-1 Protease and Mutants V82A and I84V with Saquinavir. *Proteins: Structure, Function, and Bioinformatics* **2007**, 67 (1), 232–242.
- (76) Erickson, J.; Neidhart, D. J.; VanDrie, J.; Kempf, D. J.; Wang, X. C.; Norbeck, D. W.; Plattner, J. J.; Rittenhouse, J. W.; Turon, M.; Wideburg, N. Design, Activity, and 2.8 Å Crystal Structure of a C2 Symmetric Inhibitor Complexed to HIV-1 Protease. *Science* **1990**, 249 (4968), 527–533.

- (77) Kempf, D. J.; Sham, H. L.; Marsh, K. C.; Flentge, C. A.; Betebenner, D.; Green, B. E.; McDonald, E.; Vasavanonda, S.; Saldivar, A.; Wideburg, N. E.; Kati, W. M.; Ruiz, L.; Zhao, C.; Fino, L.; Patterson, J.; Molla, A.; Plattner, J. J.; Norbeck, D. W. Discovery of Ritonavir, a Potent Inhibitor of HIV Protease with High Oral Bioavailability and Clinical Efficacy. *J. Med. Chem.* **1998**, *41* (4), 602–617.
- (78) Marastoni, M.; Bazzaro, M.; Bortolotti, F.; Salvadori, S.; Tomatis, R. Symmetry-Based Inhibitors of HIV-1 Protease. Design, Synthesis and Preliminary Structure-Activity Studies of Acylated 2,3-Diamino-1-Hydroxypropanes and 2,4 Diamino-1-Hydroxybutanes. *Eur J Med Chem* **1999**, *34* (7–8), 651–657.
- (79) Kempf, D. J.; Marsh, K. C.; Denissen, J. F.; McDonald, E.; Vasavanonda, S.; Flentge, C. A.; Green, B. E.; Fino, L.; Park, C. H.; Kong, X. P. ABT-538 Is a Potent Inhibitor of Human Immunodeficiency Virus Protease and Has High Oral Bioavailability in Humans. *Proc. Natl. Acad. Sci. U.S.A.* **1995**, *92* (7), 2484–2488.
- (80) Kumar, G. N.; Rodrigues, A. D.; Buko, A. M.; Denissen, J. F. Cytochrome P450-Mediated Metabolism of the HIV-1 Protease Inhibitor Ritonavir (ABT-538) in Human Liver Microsomes. *J. Pharmacol. Exp. Ther.* **1996**, *277* (1), 423–431.
- (81) Koudriakova, T.; Iatsimirskaia, E.; Utkin, I.; Gangl, E.; Vouros, P.; Storozhuk, E.; Orza, D.; Marinina, J.; Gerber, N. Metabolism of the Human Immunodeficiency Virus Protease Inhibitors Indinavir and Ritonavir by Human Intestinal Microsomes and Expressed Cytochrome P4503A4/3A5: Mechanism-Based Inactivation of Cytochrome P4503A by Ritonavir. *Drug Metab. Dispos.* **1998**, *26* (6), 552–561.
- (82) Sevrioukova, I. F.; Poulos, T. L. Structure and Mechanism of the Complex between Cytochrome P4503A4 and Ritonavir. *Proc. Natl. Acad. Sci. U.S.A.* **2010**, *107* (43), 18422–18427.
- (83) deSolms, S. J.; Giuliani, E. A.; Guare, J. P.; Vacca, J. P.; Sanders, W. M.; Graham, S. L.; Wiggins, J. M.; Darke, P. L.; Sigal, I. S.; Zugay, J. A. Design and Synthesis of HIV Protease Inhibitors. Variations of the Carboxy Terminus of the HIV Protease Inhibitor L-682,679. *J. Med. Chem.* **1991**, *34* (9), 2852–2857.
- (84) Lyle, T. A.; Wiscount, C. M.; Guare, J. P.; Thompson, W. J.; Anderson, P. S.; Darke, P. L.; Zugay, Z. A.; Emini, E. A.; Schleif, W. A.; Quintero, J. C. Benzocycloalkyl Amines as Novel C-Termini for HIV Protease Inhibitors. *J. Med. Chem.* **1991**, *34* (3), 1228–1230.
- (85) Dorsey, B. D.; Levin, R. B.; McDaniel, S. L.; Vacca, J. P.; Guare, J. P.; Darke, P. L.; Zugay, J. A.; Emini, E. A.; Schleif, W. A.; Quintero, J. C. L-735,524: The Design of a Potent and Orally Bioavailable HIV Protease Inhibitor. *J. Med. Chem.* **1994**, *37* (21), 3443–3451.
- (86) Vacca, J. P.; Dorsey, B. D.; Schleif, W. A.; Levin, R. B.; McDaniel, S. L.; Darke, P. L.; Zugay, J.; Quintero, J. C.; Blahy, O. M.; Roth, E. L-735,524: An Orally Bioavailable Human Immunodeficiency Virus Type 1 Protease Inhibitor. *Proc. Natl. Acad. Sci. U.S.A.* **1994**, *91* (9), 4096–4100.

- (87) Varney, M. D.; Appelt, K.; Kalish, V.; Reddy, M. R.; Tatlock, J.; Palmer, C. L.; Romines, W. H.; Wu, B.-W.; Musick, L. Crystal-Structure-Based Design and Synthesis of Novel C-Terminal Inhibitors of HIV Protease. *J. Med. Chem.* **1994**, *37* (15), 2274–2284.
- (88) Gehlhaar, D. K.; Moerder, K. E.; Zichi, D.; Sherman, C. J.; Ogden, R. C.; Freer, S. T. De Novo Design of Enzyme Inhibitors by Monte Carlo Ligand Generation. *J. Med. Chem.* **1995**, *38* (3), 466–472.
- (89) Kaldor, S. W.; Hammond, M.; Dressman, B. A.; Fritz, J. E.; Crowell, T. A.; Hermann, R. A. New Dipeptide Isosteres Useful for the Inhibition of HIV-1 Protease. *Bioorganic & Medicinal Chemistry Letters* **1994**, *4* (11), 1385–1390.
- (90) Kaldor, S. W.; Appelt, K.; Fritz, J. E.; Hammond, M.; Crowell, T. A.; Baxter, A. J.; Hatch, S. D.; Wiskerchen, M.; Muesing, M. A. A Systematic Study of P1–P3 Spanning Sidechains for the Inhibition of HIV-1 Protease. *Bioorganic & Medicinal Chemistry Letters* **1995**, *5* (7), 715–720.
- (91) Kalish, V. J.; Tatlock, J. H.; Davies, J. F.; Kaldor, S. W.; Dressman, B. A.; Reich, S.; Pino, M.; Nyugen, D.; Appelt, K.; Musick, L.; Wu, B. Structure-Based Drug Design of Nonpeptidic P2 Substituents for HIV-1 Protease Inhibitors. *Bioorganic & Medicinal Chemistry Letters* **1995**, *5* (7), 727–732.
- (92) Kaldor, S. W.; Kalish, V. J.; Davies, J. F.; Shetty, B. V.; Fritz, J. E.; Appelt, K.; Burgess, J. A.; Campanale, K. M.; Chirgadze, N. Y.; Clawson, D. K.; Dressman, B. A.; Hatch, S. D.; Khalil, D. A.; Kosa, M. B.; Lubbehusen, P. P.; Muesing, M. A.; Patick, A. K.; Reich, S. H.; Su, K. S.; Tatlock, J. H. Viracept (Nelfinavir Mesylate, AG1343): A Potent, Orally Bioavailable Inhibitor of HIV-1 Protease. *J. Med. Chem.* **1997**, *40* (24), 3979–3985.
- (93) Kim, E. E.; Baker, C. T.; Dwyer, M. D.; Murcko, M. A.; Rao, B. G.; Tung, R. D.; Navia, M. A. Crystal Structure of HIV-1 Protease in Complex with VX-478, a Potent and Orally Bioavailable Inhibitor of the Enzyme. *J. Am. Chem. Soc.* **1995**, *117* (3), 1181–1182.
- (94) Kempf, D. J.; Marsh, K. C.; Paul, D. A.; Knigge, M. F.; Norbeck, D. W.; Kohlbrenner, W. E.; Codacovi, L.; Vasavanonda, S.; Bryant, P.; Wang, X. C. Antiviral and Pharmacokinetic Properties of C2 Symmetric Inhibitors of the Human Immunodeficiency Virus Type 1 Protease. *Antimicrob. Agents Chemother.* **1991**, *35* (11), 2209–2214.
- (95) Sham, H. L.; Kempf, D. J.; Molla, A.; Marsh, K. C.; Kumar, G. N.; Chen, C. M.; Kati, W.; Stewart, K.; Lal, R.; Hsu, A.; Betebenner, D.; Korneyeva, M.; Vasavanonda, S.; McDonald, E.; Saldivar, A.; Wideburg, N.; Chen, X.; Niu, P.; Park, C.; Jayanti, V.; Grabowski, B.; Granneman, G. R.; Sun, E.; Japour, A. J.; Leonard, J. M.; Plattner, J. J.; Norbeck, D. W. ABT-378, a Highly Potent Inhibitor of the Human Immunodeficiency Virus Protease. *Antimicrob. Agents Chemother.* **1998**, *42* (12), 3218–3224.
- (96) Fässler, A.; Rösel, J.; Grüther, M.; Tintelnot-Blomley, M.; Atteri, E.; Bold, G.; Lang, M. Novel Pseudosymmetric Inhibitors of HIV-1 Protease. *Bioorganic & Medicinal Chemistry Letters* **1993**, *3* (12), 2837–2842.

- (97) Priestle, J. P.; Fässler, A.; Rösel, J.; Tintelnot-Blomley, M.; Strop, P.; Grütter, M. G. Comparative Analysis of the X-Ray Structures of HIV-1 and HIV-2 Proteases in Complex with CGP 53820, a Novel Pseudosymmetric Inhibitor. *Structure* **1995**, *3* (4), 381–389.
- (98) Fässler, A.; Bold, G.; Capraro, H.-G.; Cozens, R.; Mestan, J.; Poncioni, B.; Rösel, J.; Tintelnot-Blomley, M.; Lang, M. Aza-Peptide Analogs as Potent Human Immunodeficiency Virus Type-1 Protease Inhibitors with Oral Bioavailability. *J. Med. Chem.* **1996**, *39* (16), 3203–3216.
- (99) Bold, G.; Fässler, A.; Capraro, H.-G.; Cozens, R.; Klimkait, T.; Lazdins, J.; Mestan, J.; Poncioni, B.; Rösel, J.; Stover, D.; Tintelnot-Blomley, M.; Acemoglu, F.; Beck, W.; Boss, E.; Eschbach, M.; Hürlimann, T.; Masso, E.; Roussel, S.; Ucci-Stoll, K.; Wyss, D.; Lang, M. New Aza-Dipeptide Analogues as Potent and Orally Absorbed HIV-1 Protease Inhibitors: Candidates for Clinical Development. *J. Med. Chem.* **1998**, *41* (18), 3387–3401.
- (100) Clemente, J. C.; Coman, R. M.; Thiaville, M. M.; Janka, L. K.; Jeung, J. A.; Nukoolkarn, S.; Govindasamy, L.; Agbandje-McKenna, M.; McKenna, R.; Leelamanit, W.; Goodenow, M. M.; Dunn, B. M. Analysis of HIV-1 CRF_01 A/E Protease Inhibitor Resistance: Structural Determinants for Maintaining Sensitivity and Developing Resistance to Atazanavir. *Biochemistry* **2006**, *45* (17), 5468–5477.
- (101) Robinson, B. S.; Riccardi, K. A.; Gong, Y. F.; Guo, Q.; Stock, D. A.; Blair, W. S.; Terry, B. J.; Deminie, C. A.; Djang, F.; Colonno, R. J.; Lin, P. F. BMS-232632, a Highly Potent Human Immunodeficiency Virus Protease Inhibitor That Can Be Used in Combination with Other Available Antiretroviral Agents. *Antimicrob. Agents Chemother.* **2000**, *44* (8), 2093–2099.
- (102) Thaisrivongs, S.; Tomich, P. K.; Watenpaugh, K. D.; Chong, K.-T.; Howe, W. J.; Yang, C.-P.; Strohbach, J. W.; Turner, S. R.; McGrath, J. P. Structure-Based Design of HIV Protease Inhibitors: 4-Hydroxycoumarins and 4-Hydroxy-2-Pyrones as Non-Peptidic Inhibitors. *J. Med. Chem.* **1994**, *37* (20), 3200–3204.
- (103) Skulnick, H. I.; Johnson, P. D.; Howe, W. J.; Tomich, P. K.; Chong, K.-T.; Watenpaugh, K. D.; Janakiraman, M. N.; Dolak, L. A.; McGrath, J. P. Structure-Based Design of Sulfonamide-Substituted Non-Peptidic HIV Protease Inhibitors. *J. Med. Chem.* **1995**, *38* (26), 4968–4971.
- (104) Turner, S. R.; Strohbach, J. W.; Tommasi, R. A.; Aristoff, P. A.; Johnson, P. D.; Skulnick, H. I.; Dolak, L. A.; Seest, E. P.; Tomich, P. K.; Bohanon, M. J.; Horng, M.-M.; Lynn, J. C.; Chong, K.-T.; Hinshaw, R. R.; Watenpaugh, K. D.; Janakiraman, M. N.; Thaisrivongs, S. Tipranavir (PNU-140690): A Potent, Orally Bioavailable Nonpeptidic HIV Protease Inhibitor of the 5,6-Dihydro-4-Hydroxy-2-Pyrone Sulfonamide Class. *J. Med. Chem.* **1998**, *41* (18), 3467–3476.
- (105) Ghosh, A. K.; Ramu Sridhar, P.; Kumaragurubaran, N.; Koh, Y.; Weber, I. T.; Mitsuya, H. Bis-Tetrahydrofuran: A Privileged Ligand for Darunavir and a New Generation of HIV Protease Inhibitors That Combat Drug Resistance. *ChemMedChem* **2006**, *1* (9), 939–950.

- (106) Ghosh, A. K.; Thompson, W. J.; Holloway, M. K.; McKee, S. P.; Duong, T. T.; Lee, H. Y.; Munson, P. M.; Smith, A. M.; Wai, J. M.; Darke, P. L.; Zugay, J. A.; Emini, E. A.; Schleif, W. A.; Huff, J. R.; Anderson, P. S. Potent HIV Protease Inhibitors: The Development of Tetrahydrofuranylglycines as Novel P2-Ligands and Pyrazine Amides as P3-Ligands. *J. Med. Chem.* **1993**, *36* (16), 2300–2310.
- (107) Ghosh, A. K.; Thompson, W. J.; McKee, S. P.; Duong, T. T.; Lyle, T. A.; Chen, J. C.; Darke, P. L.; Zugay, J. A.; Emini, E. A. 3-Tetrahydrofuran and Pyran Urethanes as High-Affinity P2-Ligands for HIV-1 Protease Inhibitors. *J. Med. Chem.* **1993**, *36* (2), 292–294.
- (108) Ghosh, A. K.; Chen, Y. Synthesis and Optical Resolution of High Affinity P2-Ligands for HIV-1 Protease Inhibitors. *Tetrahedron Letters* **1995**, *36* (4), 505–508.
- (109) Ghosh, A. K.; Kincaid, J. F.; Walters, D. E.; Chen, Y.; Chaudhuri, N. C.; Thompson, W. J.; Culberson, C.; Fitzgerald, P. M. D.; Lee, H. Y.; McKee, S. P.; Munson, P. M.; Duong, T. T.; Darke, P. L.; Zugay, J. A.; Schleif, W. A.; Axel, M. G.; Lin, J.; Huff, J. R. Nonpeptidal P2 Ligands for HIV Protease Inhibitors: Structure-Based Design, Synthesis, and Biological Evaluation. *J. Med. Chem.* **1996**, *39* (17), 3278–3290.
- (110) Ghosh, A. K.; Anderson, D. D.; Weber, I. T.; Mitsuya, H. Enhancing Protein Backbone Binding--a Fruitful Concept for Combating Drug-Resistant HIV. *Angew. Chem. Int. Ed. Engl.* **2012**, *51* (8), 1778–1802.
- (111) Ghosh, A. K.; Kincaid, J. F.; Cho, W.; Walters, D. E.; Krishnan, K.; Hussain, K. A.; Koo, Y.; Cho, H.; Rudall, C.; Holland, L.; Buthod, J. Potent HIV Protease Inhibitors Incorporating High-Affinity P2-Ligands and (R)-(Hydroxyethylamino)Sulfonamide Isostere. *Bioorganic & Medicinal Chemistry Letters* **1998**, *8* (6), 687–690.
- (112) Yoshimura, K.; Kato, R.; Kavlick, M. F.; Nguyen, A.; Maroun, V.; Maeda, K.; Hussain, K. A.; Ghosh, A. K.; Gulnik, S. V.; Erickson, J. W.; Mitsuya, H. A Potent Human Immunodeficiency Virus Type 1 Protease Inhibitor, UIC-94003 (TMC-126), and Selection of a Novel (A28S) Mutation in the Protease Active Site. *J. Virol.* **2002**, *76* (3), 1349–1358.
- (113) Ghosh, A. K.; Chapsal, B. D.; Weber, I. T.; Mitsuya, H. Design of HIV Protease Inhibitors Targeting Protein Backbone: An Effective Strategy for Combating Drug Resistance. *Acc. Chem. Res.* **2008**, *41* (1), 78–86.
- (114) Hayashi, H.; Takamune, N.; Nirasawa, T.; Aoki, M.; Morishita, Y.; Das, D.; Koh, Y.; Ghosh, A. K.; Misumi, S.; Mitsuya, H. Dimerization of HIV-1 Protease Occurs through Two Steps Relating to the Mechanism of Protease Dimerization Inhibition by Darunavir. *Proc. Natl. Acad. Sci. U.S.A.* **2014**, *111* (33), 12234–12239.
- (115) Roberts, J. D.; Bebenek, K.; Kunkel, T. A. The Accuracy of Reverse Transcriptase from HIV-1. *Science* **1988**, *242* (4882), 1171–1173.
- (116) Coffin, J. M. HIV Population Dynamics in Vivo: Implications for Genetic Variation, Pathogenesis, and Therapy. *Science* **1995**, *267* (5197), 483–489.

- (117) Todd, M. J.; Luque, I.; Velázquez-Campoy, A.; Freire, E. Thermodynamic Basis of Resistance to HIV-1 Protease Inhibition: Calorimetric Analysis of the V82F/I84V Active Site Resistant Mutant. *Biochemistry* **2000**, *39* (39), 11876–11883.
- (118) Hong, L.; Zhang, X. C.; Hartsuck, J. A.; Tang, J. Crystal Structure of an in Vivo HIV-1 Protease Mutant in Complex with Saquinavir: Insights into the Mechanisms of Drug Resistance. *Protein Sci.* **2000**, *9* (10), 1898–1904.
- (119) Laco, G. S.; Schalk-Hihi, C.; Lubkowski, J.; Morris, G.; Zdanov, A.; Olson, A.; Elder, J. H.; Wlodawer, A.; Gustchina, A. Crystal Structures of the Inactive D30N Mutant of Feline Immunodeficiency Virus Protease Complexed with a Substrate and an Inhibitor,. *Biochemistry* **1997**, *36* (35), 10696–10708.
- (120) Zhang, H.; Wang, Y.-F.; Shen, C.-H.; Agniswamy, J.; Rao, K. V.; Xu, C.-X.; Ghosh, A. K.; Harrison, R. W.; Weber, I. T. Novel P2 Tris-Tetrahydrofuran Group in Antiviral Compound 1 (GRL-0519) Fills the S2 Binding Pocket of Selected Mutants of HIV-1 Protease. *J. Med. Chem.* **2013**, *56* (3), 1074–1083.
- (121) Ghosh, A. K.; Xu, C.-X.; Rao, K. V.; Baldrige, A.; Agniswamy, J.; Wang, Y.-F.; Weber, I. T.; Aoki, M.; Miguel, S. G. P.; Amano, M.; Mitsuya, H. Probing Multidrug-Resistance and Protein-Ligand Interactions with Oxatricyclic Designed Ligands in HIV-1 Protease Inhibitors. *ChemMedChem* **2010**, *5* (11), 1850–1854.
- (122) Ghosh, A. K.; Parham, G. L.; Martyr, C. D.; Nyalapatla, P. R.; Osswald, H. L.; Agniswamy, J.; Wang, Y.-F.; Amano, M.; Weber, I. T.; Mitsuya, H. Highly Potent HIV-1 Protease Inhibitors with Novel Tricyclic P2 Ligands: Design, Synthesis, and Protein–Ligand X-Ray Studies. *J. Med. Chem.* **2013**, *56* (17), 6792–6802.
- (123) Norton Matos, M.; Afonso, C. A. M.; Batey, R. A. Synthesis of Substituted Pyrrolidines and Piperidines from Endocyclic Enamine Derivatives. Synthesis of (±)-Laburnamine. *Tetrahedron* **2005**, *61* (5), 1221–1244.
- (124) Design of HIV-1 Protease Inhibitors with Amino-bis-tetrahydrofuran Derivatives as P2-Ligands to Enhance Backbone-Binding Interactions: Synthesis, Biological Evaluation, and Protein–Ligand X-ray Studies | Journal of Medicinal Chemistry
- (125) Ghosh, A. K.; Williams, J. N.; Ho, R. Y.; Simpson, H. M.; Hattori, S.; Hayashi, H.; Agniswamy, J.; Wang, Y.-F.; Weber, I. T.; Mitsuya, H. Design and Synthesis of Potent HIV-1 Protease Inhibitors Containing Bicyclic Oxazolidinone Scaffold as the P2 Ligands: Structure–Activity Studies and Biological and X-Ray Structural Studies. *J. Med. Chem.* **2018**, *61* (21), 9722–9737.
- (126) Ghosh, A. K.; Chapsal, B. D.; Baldrige, A.; Steffey, M. P.; Walters, D. E.; Koh, Y.; Amano, M.; Mitsuya, H. Design and Synthesis of Potent HIV-1 Protease Inhibitors Incorporating Hexahydrofuopyranol-Derived High Affinity P2 Ligands: Structure–Activity Studies and Biological Evaluation. *J. Med. Chem.* **2011**, *54* (2), 622–634.

- (127) Jiménez, C. Marine Natural Products in Medicinal Chemistry. *ACS Med. Chem. Lett.* **2018**, 9 (10), 959–961.
- (128) Yñíguez-Gutierrez, A. E.; Bachmann, B. O. Fixing the Unfixable: The Art of Optimizing Natural Products for Human Medicine. *J. Med. Chem.* **2019**, 62 (18), 8412–8428.
- (129) Fleming, A. On the Antibacterial Action of Cultures of a *Penicillium*, with Special Reference to Their Use in the Isolation of *B. Influenzæ*. *Br J Exp Pathol* **1929**, 10 (3), 226–236.
- (130) Raynor, B. D. Penicillin and Ampicillin. *Primary Care Update for OB/GYNS* **1997**, 4 (4), 147–152.
- (131) Cragg, G. M.; Pezzuto, J. M. Natural Products as a Vital Source for the Discovery of Cancer Chemotherapeutic and Chemopreventive Agents. *Med Princ Pract* **2016**, 25 Suppl 2, 41–59.
- (132) Pham, C.-D.; Hartmann, R.; Böhrer, P.; Stork, B.; Wesselborg, S.; Lin, W.; Lai, D.; Proksch, P. Callyspongiolide, a Cytotoxic Macrolide from the Marine Sponge *Callyspongia* Sp. *Org. Lett.* **2014**, 16 (1), 266–269.
- (133) Prota, A. E.; Bargsten, K.; Northcote, P. T.; Marsh, M.; Altmann, K.-H.; Miller, J. H.; Díaz, J. F.; Steinmetz, M. O. Structural Basis of Microtubule Stabilization by Laulimalide and Peloruside A. *Angew. Chem. Int. Ed. Engl.* **2014**, 53 (6), 1621–1625.
- (134) Kavallaris, M. Microtubules and Resistance to Tubulin-Binding Agents. *Nat. Rev. Cancer* **2010**, 10 (3), 194–204.
- (135) Zhou, J.; Gao, B.; Xu, Z.; Ye, T. Total Synthesis and Stereochemical Assignment of Callyspongiolide. *J. Am. Chem. Soc.* **2016**, 138 (22), 6948–6951.
- (136) Ghosh, A. K.; Kassekert, L. A. Enantioselective Synthesis of Both Epimers at C-21 in the Proposed Structure of Cytotoxic Macrolide Callyspongiolide. *Org. Lett.* **2016**, 18 (13), 3274–3277.
- (137) Ghosh, A. K.; Kassekert, L. A.; Bungard, J. D. Enantioselective Total Synthesis and Structural Assignment of Callyspongiolide. *Org. Biomol. Chem.* **2016**, 14 (48), 11357–11370.
- (138) Crimmins, M. T.; DeBaillie, A. C. Enantioselective Total Synthesis of Bistramide A. *J. Am. Chem. Soc.* **2006**, 128 (15), 4936–4937.
- (139) Nicolaou, K. C.; Adsool, V. A.; Hale, C. R. H. An Expedient Procedure for the Oxidative Cleavage of Olefinic Bonds with $\text{PhI}(\text{OAc})_2$, NMO, and Catalytic OsO_4 . *Org. Lett.* **2010**, 12 (7), 1552–1555.

VITA

Joseph Bungard was born in Chesterfield, VA, and raised in the nearby county of Powhatan, VA. It was during his Junior year of high school when he was first introduced to chemistry by Mrs. Thomas. Following a year of AP chemistry and high school graduation, he decided to continue to pursue an education in the field of science at Virginia Commonwealth University in the fall of 2010. After a semester of majoring in Chemical Engineering, he became more interested in the fundamentals of chemistry. His desire to apply his scientific knowledge to the lab setting as an undergraduate researcher was made possible under the direction of Dr. Matthew C. T. Hartman. It was in Hartman's lab where he was exposed to synthetic organic techniques and applications in medicinal chemistry. Specifically, he worked on synthesizing dihydrophenanthrene linkers as potential drug delivery systems. After graduating VCU in the spring of 2014, he decided to gain industry experience at Afton Chemical in Richmond, VA. It wasn't long until he realized his true passion for research and discovery. Following a year sabbatical from academia, his fascination of research led him to Purdue University to begin his graduate work. While at Purdue, he joined the group of Professor Arun K. Ghosh in the fall of 2015 and began research in organic synthesis and medicinal chemistry. After graduating from Purdue, Joseph will begin his Postdoctoral Career under the guidance of Professor Craig Lindsley at Vanderbilt University.

PUBLICATIONS

1. Ghosh, A. K.; Kassekert, L. A.; Bungard, J. D., Enantioselective Total Synthesis and Structural Assignment of Callyspongiolide. *Org. Biomol. Chem.* **2016**, 14, 11357.